Title
Novel Analytical Methods for Examining Biomolecular Complexes Using Electrospray Ionization Mass Spectrometry

Author
Flick, Tawnya Grace

Publication Date
2012

Peer reviewed|Thesis/dissertation

Novel Analytical Methods for Examining Biomolecular Complexes Using Electrospray Ionization Mass Spectrometry

by

Tawnya Grace Flick

A dissertation submitted in partial satisfaction of the

requirements for the degree of

Doctor of Philosophy

in

Chemistry

in the

Graduate Division

of the

University of California, Berkeley

Committee in charge:

Professor Evan R. Williams, Chair

Professor Kristie A. Boering

Professor Robert Glaeser

Fall 2012

Novel Analytical Methods for Examining

Biomolecular Complexes Using Electrospray Ionization Mass Spectrometry

by

Tawnya Grace Flick

Abstract

Novel Analytical Methods for Examining

Biomolecular Complexes Using Electrospray Ionization Mass Spectrometry

by

Tawnya Grace Flick

Doctor of Philosophy in Chemistry

University of California, Berkeley

Prof. Evan R. Williams, Chair

Several analytical strategies and investigations are presented in this dissertation to improve the quantification, sensitivity, and structural information that can be obtained for gaseous biomolecular ions in electrospray ionization (ESI) mass spectrometry (MS) experiments. Internal or external standards are commonly employed to quantify molecules in complex mixtures because molecular ion abundances cannot be directly related to the concentration of the molecules in solution. A new standard-free quantitation method is used to obtain the relative concentrations of components in a mixture using the abundances of large, nonspecific clusters formed by ESI. Large non-covalent clusters overcome differences in ionization efficiencies between molecules, and are representative of the solution-phase mixture. The sensitivity in MS experiments can be significantly lowered by the presence of high concentrations of salts in the ESI solution because nonspecific ion adduction to biomolecules distributes ion signal into different forms with various numbers of adducts. Studies here demonstrate the extent of both sodium ion and acid molecule adduction to proteins are inversely related, and both depend significantly on the proton affinity of the anion in the ESI solution. Several solution-phase additives that contain anions with low proton affinity values are shown to effectively desalt protein ions generated by ESI, which should result in improved detection limits, more accurate mass measurements, and improved tandem MS sensitivity. Additionally, a solution-phase additive ($HClO_4$) is discovered that can be used to count the number of basic sites accurately in peptides and proteins based on the number of $HClO_4$ adducts to low charge states. High charge states of peptides and proteins can be readily formed by ESI of aqueous solutions that contain trivalent metal ions, and fragmentation of these trivalent metal ion-peptide or protein complexes by electron capture dissociation can be used to increase the structural information obtained from these experiments. Metal ion-biomolecule interactions are ubiquitous in nature where they play a role in many biological processes. Here, nonspecific metal ion

adduction to protein cation and anions is shown to result in more compact conformations compared to the bare protein ion, likely a result of salt-bridge interactions between the metal ion and the biomolecule.

TABLE OF CONTENTS

Acknowledgements

I would like to thank my advisor, Professor Evan R. Williams, for giving me the opportunity to be in his group, and become a part of mass spectrometry research. Evan has taught me so much about mass spectrometry, and particularly how valuable it is to communicate your results effectively to your peers. I would also like to thank other members of the group who have contributed to my time here, such as Dr. William A. Donald, Dr. Ryan D. Leib, Dr. Jeremy T. O'Brien, and Dr. James S. Prell.

I would also like to thank many people who supported me outside of the research environment. In instances of self-doubt, my husband, Jacob, continues to motivate and inspire me to work towards excellence both in my career and personal life. I would also like to thank my daughter, Ailee, who inspires me every day with her smile. Finally, I would like to thank my mother, Teresa Rehberg. Her consistency, dedication and hard work in both her career and personal life will always inspire me towards excellence.

CHAPTER 1

1.1 Biological Mass Spectrometry

The structure and functions of biomolecules are largely dictated by their non-covalent interactions with other molecules. For instance, proteins can interact with other proteins, peptides, metal ions, small molecules, and nucleic acids.[1] These interactions are responsible for much of the complex chemical processes in life, such as cell division, cell signaling, ion transport, and homeostasis. A number of established solution-phase techniques are commonly employed to study non-covalent biomolecular interactions, including optical spectroscopy, nuclear magnetic resonance, light scattering, and differential scanning calorimetry. The detailed study of these systems in the condensed phase can be challenging, due to the high concentrations required for many techniques and signal contributions from bulk solvent, counter-ions, and contaminants. Non-covalent biomolecular complexes can also be generated in the gas-phase, and information about these systems can be rapidly obtained using mass spectrometry with minimal sample requirements.[2-4] Mass spectrometric techniques have been used to obtain information complementary to results from more common solution-phase techniques, including information about complex stoichiometry,[5,6] binding energies,[7,8] and biomolecule conformation.[9,10]

The advantages of mass spectrometry (MS) in biochemical analysis continue to make it an important tool, including high sensitivity, specificity, and speed.[11,12] MS enables the gas-phase separation of molecules based on their mass-to-charge ratio, m/z, which allows for rapid analysis and compound identification of complex mixtures. For example, Marshall and coworkers could identify up to 20,000 compounds in petroleum samples with a mass measuring accuracy of ~400 ppb.[13] Molecular weight measurements can be made using less than femtomoles of sample,[2-4] making detection of minor components in a complex mixture possible. MS has been used to identify and locate post-translational modifications,[14,15] identify active sites,[16,17] and identify drug candidates from screens of combinatorial libraries.[18,19] MS has also enabled top down and bottom up proteomics for the analysis of the complete complement of proteins in a cell.[20,21]

Methods developed over the last several years have greatly extended the utility of MS in analyzing large biomolecular complexes. Two ionization methods, electrospray ionization (ESI) and matrix assisted laser desorption ionization (MALDI), have enabled the production of intact gas-phase ions and clusters of high molecular weight. With ESI, gaseous multiply-charged molecules can be formed directly from solution, which is a significant advantage for the analysis of large molecules and noncovalent complexes with MS. The multiple charging of analytes by ESI results in m/z values of large molecules that are within a range where all mass spectrometers operate at higher resolution.[22,23] Gas-phase biomolecular ions as large as 110 MDa and intact nano-machineries as complex as the entire ribosome of *E. coli*[24,25] or whole virus particles[26,27] have been produced using ESI and analyzed with MS.

Current techniques and combined methodologies have greatly increased the analytical capabilities of MS by characterizing additional molecular properties other than mass. Since the number of possible elemental compositions at a given nominal mass increases with molecular size, obtaining the exact elemental composition of larger molecules directly from mass alone can be challenging.[28,29] Without some compositional information known, the mass limit for unambiguously determining the amino acid composition is ~500-600 Da, which cannot be overcome by instrumental or methodological improvements. Also, exact mass measurements do not provide any information about molecular conformation. Elemental composition and molecular structure can be further elucidated using many different gas-phase techniques, including, but not limited to, tandem mass spectrometry,[30-32] ion mobility spectrometry (IMS),[33,34] and noncovalent modification of the analyte of interest.[35-37] These techniques have greatly extended the utility of mass spectrometry in analyzing larger biomolecules with specific gas-phase conformations.

1.2 Electrospray Ionization

The ions investigated in all of the experiments conducted here were generated by ESI. ESI is an ionization technique that can generate gas-phase ions from solution with very little fragmentation, and therefore has greatly extended the utility of mass spectrometry as a tool to study large biomolecular complexes. In ESI, a solution containing the analyte of interest is passed, at atmospheric pressure, through a small diameter capillary. An electric field is produced by applying a potential difference of 0.5-3 kV between the solution and the entrance to the mass spectrometer. The effect of the electric field as the solution emerges from the tip is to generate a spray of highly charged droplets in the form of a taylor cone. These droplets are unstable at ambient pressure and evaporate solvent molecules until the surface tension of the droplet can no longer support the net charge at the droplet surface. Lord Rayleigh predicted that the maximum number of charges, $z_r e$, that a droplet can sustain prior to fission occurring is given by eq. 1:

$$z_r e = 8\pi(\varepsilon_o \gamma R^3)^{1/2} \quad (1)$$

where z_r is the unit charge limit, e is the elementary charge, ε_o is the permittivity of the surrounding media, γ is the surface tension and R is the radius of the droplet. Once the Coulombic repulsion between the charges at the droplet surface exceeds the surface tension, the droplet undergoes Rayleigh fission. Droplet fission typically occurs within ~20% of the Rayleigh limit, and each discharge event results in the loss of 10 – 30% of the charge and 0.3 – 2% of the mass of the parent droplet. In general, ions are likely formed by a combination of fission cycles forming smaller and smaller droplets, solvent evaporation, and possibly ion desorption out of highly charged droplets.

There is still no clear consensus on the mechanism by which solute ions are finally formed from the charged droplets generated by ESI. There are two major theories that explain the final production of gas-phase ions: the charge residue model (CRM)[38] and the ion evaporation model (IEM).[39] The CRM suggests that electrospray droplets undergo several evaporation and fission cycles until progeny droplets are formed that contain on average one analyte of interest.[38] The ion is finally formed when the remaining solvent molecules evaporate and the charge is transferred to the analyte.[38] The IEM, based on the work by Iribarne and Thomson, assumes that when a droplet reaches a certain radius, the electric field becomes so great that ions desorb off the surface of the droplet.[39] Several studies have reported that the number of charges observed on various large ions formed by ESI is approximately equal to the Rayleigh limiting charge of solvent droplets of the same size as the analyte.[40,41] This result provides evidence that large ions are formed by the CRM and not the IEM, since these ions could not acquire this many charges if they were to desorb off the surface at this droplet size.[40,41] Recently, Hogan and coworkers proposed that the number of charges on a macromolecule is determined by the emission of small charge carriers from macromolecule-containing nanodroplets, and that, after solvent evaporation, the remaining charge is transferred to the macromolecule.[42,43] However, limited experimental data has been reported in support of this model.

1.2.1 Factors that Affect Charging of Peptides and Proteins. Multiple charging of intact biomolecular ions by ESI is analytically advantageous because of improved mass spectrometer performance at lower m/z values and the increase in tandem MS efficiency for higher ion charge states.[22,44] Increasing analyte charge also increases the sensitivity of mass spectrometers where the signal is proportional to charge, such as orbitrap and Fourier-transform ion cyclotron resonance (FT-ICR) instruments.[22,23] Due to these advantages, the factors that influence analyte charge in ESI have been extensively studied, as well as how they can be altered to increase analyte charge.[41,45-52]

Several factors are known to influence the extent of analyte charging in ESI, including analyte conformation,[46-48] solvent and analyte basicity,[41,49,50] instrumental factors,[45] and solvent surface tension,[41,51] but the exact contribution of each of these factors is not well understood. A narrow charge state distribution centered at high m/z is often formed from solutions where a protein has retained its native structure, whereas a broad charge state distribution and higher charge states are formed from solutions when the protein is denatured.[46-48] This effect can be largely attributed to reduced coulombic repulsion and increased accessibility to basic sites on a protein with an elongated conformation compared to a more compact structure. The solution-phase denaturation of proteins as a result of heating or acidifying the bulk ESI solution can be monitored by ESI-MS from shifts in the charge state distribution towards higher charge.[47] Addition of compounds with high gas-phase basicities into the ESI solution shifts the charge state distribution of proteins and peptides towards lower charge due to proton transfer, with the degree of charge reduction correlating well with the gas-phase

basicity of the additive.[49] Charge reduction of analytes can also be achieved by increasing the number of collisions in the electrospray interface.[53]

An effective method to enhance the charging observed for many biomolecules is the use of supercharging reagents, such as *m*-nitrobenzyl alcohol (*m*-NBA).[41,51,54-69] Supercharging reagents have high boiling points and the concentrations of these reagents increases as ESI droplet evaporation occurs. The enhanced charging was originally demonstrated in denaturing solutions where addition of these reagents into solutions results in a substantial increase in surface tension as organic solvents preferentially evaporate. For instance, the surface tension of *m*-NBA (50 ± 5 mN/m) is higher than organic solvents like methanol (22.1 mN/m at 25˚C). This increase in surface tension allows a droplet of a particular size to maintain a higher charge density before reaching the Rayleigh limit (eq. 1), resulting in the formation of enhanced analyte charging, whether ions are formed by the charge residue or ion evaporation model. More recently, this supercharging method has been shown to be effective at increasing the charge states of protein and protein complex ions formed from native solutions,[51-65] even though addition of these reagents into aqueous solutions should effectively lower the droplet surface tension as ESI droplet evaporation occurs. Enrichment of the supercharging reagent affects many physical properties of the ESI droplet, including the temperature and propensities to proton transfer, etc. Results from circular dichroism spectroscopy[61,64] and hydrogen deuterium-exchange MS[62,64] indicate the supercharging reagents do not affect protein conformation at the low concentrations typically used in the initial solutions, but can cause chemical and/or thermal denaturation of the protein in the ESI droplet as the concentration of these reagents is increased.[58,60-64] Proteins that have lost some or all of their native structures can carry away more charge and the charge enhancement from the denaturing effect is greater than the effect of the lower surface tension.[60]

The charge states of proteins can also be increased from unbuffered aqueous solutions by introducing acid vapor into the drying gas.[70] The acid vapor lowers the pH of the ESI droplets, resulting in acid denaturation of the protein and higher ion charge states in the mass spectrum.[70] For example, addition of HCl acid vapor into the drying gas resulted in an increase in the maximum charge state of cytochrome *c* formed from aqueous solutions by 10 and a 6.5 shift in the average charge state compared to when no acid vapor is added.[70] An electrothermal supercharging method was recently introduced to generate high charge state protein ions from buffered ammonium bicarbonate solutions in which the protein has a native structure prior to ESI droplet formation.[71] This method can be used to obtain mass spectra for proteins resembling those from denatured solutions, where the maximum extent of charging can exceed the number of basic sites, by simply increasing the electrospray voltage.[71] In chapter 7 and 8, addition of trivalent metal ions to aqueous solutions containing peptides and proteins results in an increase in the average and maximum ion charge states that can be formed by ESI as a result of trivalent metal ion adduction to the biomolecules during ion formation, and these ions are used to increase the structural information that can be obtained in electron capture dissociation experiments.

1.3 Quantitation with ESI-MS.

The ability to accurately and rapidly measure concentrations of substances in complex mixtures is a key challenge in ESI-MS. Manufactured solid dosage forms of small molecules can result in low levels of impurities that stem from unreacted starting materials, degradation products, or products from competing side reactions.[72,73] Since these impurities may have unintended side effects, they must be quantified, structurally identified, and shown to be biologically inert.[72,73] In proteomics, protein modifications and/or the upregulation of protein expression can be biomarkers for disease.[15,21] Since mass spectrometry is commonly utilized to identify components in a mixture, it is advantageous to be able to quantify the concentration of these substances simultaneously.[15,21]

A significant limitation when using ESI-MS for mixture analysis is that quantitative information about how much of each component is present in solution cannot be determined directly from ion abundances in the mass spectrum. The ionization efficiency of a molecule depends on many factors, including their surface activity or hydrophobicities,[45,74-76] concentration,[76,77] gas-phase basicity,[49,78] and the ionization efficiency of other components in the solution.[50,78] For instance, the ESI intensity of tetraalkylammonium halides increases by over an order of magnitude when the hydrophobic chain length increases from methyl to butyl, a result attributed to the surface activities of these ions.[45] Ion abundances depend significantly on the solution composition or pH. For example, addition of basic solvents and additives to solutions containing proteins and peptides results in lower charge state ions centered at high m/z and reduced ion signal,[49,78] whereas ESI of proteins from a denaturing solution results in a broad charge state distribution at lower m/z, which can result in ion abundances that depend on m/z-dependent detection biases.[46,48]

Due to these factors, quantitation by ESI-MS is typically performed using an internal or external standard that closely mimics the physical properties of the analyte. The most robust quantitation is performed using an internal standard that is an isotopically labeled form of the analyte,[21,79-83] and are commonly employed in the analysis of small molecules in the pharmaceutical industry.[82,83] Internal standards, such as isotope-coded affinity tags[80] and stable isotope labeling with amino acids in cell cultures,[81] are commonly used in proteomics to obtain information about relative gene expression. In chapters 2 and 3, a new standard-free quantitation method is used to obtain solution mole percentages of components in a mixture by the abundances of large, nonspecific clusters in the mass spectrum without using either an internal or external standard.[76,84-86] This method is used to quantify amino acids and a dipeptide using serine as a clustering agent, which has a tendency to form homochiral clusters with specific conformations,[87,88] and to determine the dosage of over-the-counter and prescription drugs, such as Tamiflu.[76,84-86]

1.4 Nonspecific Ion-Biomolecule Interactions.

1.4.1 Hofmeister Series. Ions can affect the stability, solubility, and function of proteins through nonspecific interactions. In 1888, Franz Hofmeister observed that various metal salts at molar concentrations had different propensities to precipitate hen-egg albumin from aqueous solution,[89,90] and the same ordering of ions based on this "salting-out" property was found to be reproducible for a variety of other biomolecules. The following general order was observed for cations and anions:

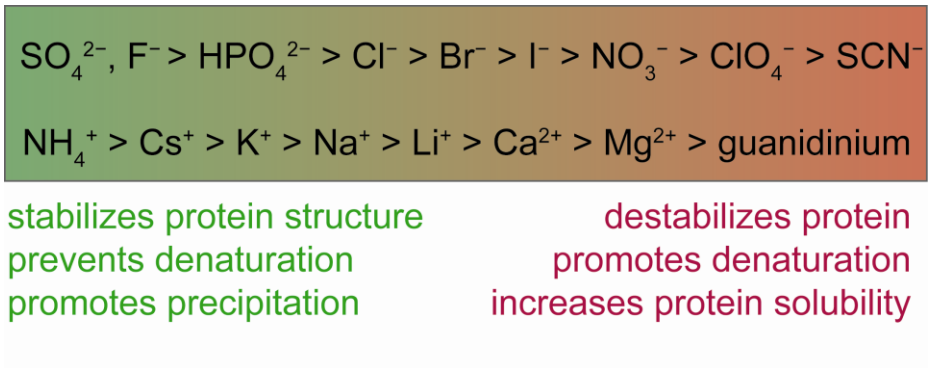

Scheme 1.1 Hofmeister Ion Series

Ions to the left of the series, referred to as kosmotropes, decrease protein solubility by stabilizing the native protein conformations. Ions at the right of the series are called chaotropes, and they increase protein solubility by destabilizing native conformations. Numerous studies over the last 122 year have observed this trend, and the Hofmeister series has been correlated well with many ionic properties, including ionic radii,[91,92] polarizabilities,[92] solvation free energies,[91-93] viscosity coefficients,[93] surface tension of aqueous solutions,[94,95] and elution times from Sephadex G10 columns.[96,97] The precise ordering of the ions depends substantially on the type of experiment and salts and biomolecules used, and anions generally have a greater effect than cations. It has also been observed that there is a reverse ordering of the ions when the isoelectric point (pI) of the protein is several units greater than the pH of the protein.[92,98]

Despite numerous studies using many different methods, the exact origin of the Hofmeister series is still widely debated. It is thought that both ion-water and ion-biomolecule interactions play significant roles in the source of the Hofmeister phenomena, but it is not well established the extent to which each of these factors contribute. The extent to which ions can order water has been a subject of much debate. Recently, both femtosecond pump-probe spectroscopy of aqueous salt solutions[99] and sum-frequency generation spectroscopy of aqueous solutions containing both salts and polymers[100] indicate that individual ions do not order water significantly beyond the first solvation shell.[101] In striking contrast, infrared photodissociation experiments on ions in aqueous nanodrops have shown that the sulfate dianion order water molecules well past the first and second solvation shell, and that long-range patterning of water occurs for many different ions to various extents.[102]

Although nonspecific ion adduction to proteins is common with ESI and MALDI, there are no direct studies of the Hofmeister effect on ion-protein interactions in the gas-phase using ESI-MS until this recent work. Colussi and coworkers measured ESI mass spectra of solutions containing mixtures of equimolar amounts of sodium salts of monovalent anions and found that the relative abundances of the anions correlated well with both the ionic radii and solvation energies, two properties that have previously been related to the Hofmeister series.[91] In chapter 4, we report that addition of eleven different sodium salts with various Hofmeister anions to aqueous solutions results in different extents of nonspecific sodium and acid molecule adduction to protein ions generated by ESI.[103] The extent of sodium and acid molecule adduction to multiply charged protein ions is inversely related and depends strongly on the proton affinity (PA) of the anion, and does not directly follow the Hofmeister series, suggesting that direct protein-ion interactions may not play a significant role in the observed effect of anions on protein structure in solution.[103]

1.4.2 Reducing Nonspecific Ion Adduction to Proteins. Nonspecific ion adduction to proteins is often considered a nuisance in the analysis of biomolecules because it often results in severe ion suppression.[77,78,104-108] The adverse effects of some salts can be especially challenging for some biological samples that require essential salts or high ionic strength to assemble and maintain their functional forms in solution. Even millimolar concentrations of salts in the sample matrix can result in severe ion suppression in ESI.[106] For instance, addition of 10 mM CsCl to aqueous solutions containing 1 μM lysozyme resulted in a 330-fold reduction in protein ion abundance.[106]

Several approaches have been developed that make it possible to more readily analyze samples with high salt concentrations. Salts, such as sodium chloride, are often removed prior to MS analysis using a variety of techniques, such as dialysis[109] or liquid chromatography,[110] to reduce adduction and improve ion formation by ESI. However, removal of salts prior to ESI-MS analysis can adversely effect the structure of many proteins and effect the specific binding of protein complexes.[105,111] McLuckey and coworkers demonstrated that sodium adduction to gaseous proteins can be significantly reduced when the solution pH is ~3 units less than the pI of the protein in positive-mode ESI-MS.[112] Addition of molar quantities of ammonium acetate to ESI protein-containing solutions with high salt concentrations can reduce sodium adduction to proteins and can be used to improve the mass measuring accuracy of large protein complexes where adducts to molecular ions are not resolved.[104,105] For example, addition of 7 M ammonium acetate to aqueous solutions that contain 20 mM NaCl and 10 μM ubiquitin resulted in an ~11-fold increase in the signal-to-noise ratio for the protein ions.[104] It was proposed that this effect is a result of the precipitation of Na^+ and Cl^- from solution within the evaporating electrospray droplets, due to the low solubility of sodium acetate and ammonium chloride compared to ammonium acetate, prior to the formation of gas-phase protein ions.[104]

Recently, it has been shown that several anions, such as tartrate and citrate, can substantially reduce the extent of nonspecific metal ion adduction to protein ions formed by ESI.[113] Konnermann and coworkers found that the extent of nonspecific calcium adduction to proteins was reduced when calcium tartrate was added to ESI solutions compared to calcium acetate and calcium chloride, and suggested that tartrate acts as a solution-phase chelator of calcium.[113] Gas-phase ion/ion reactions between DNA anions and several chelating anions, such as citrate, in a dual nanospray source have also been shown to significantly decrease the extent of nonspecific metal ion adduction to anions.[114] Interestingly, ammonium citrate or tartrate have also been shown to reduce nonspecific adduction to oligonucleotide and protein ions formed by MALDI when added directly to the sample matrix.[115,116] In chapter 6, several solution-phase additives, including ammonium citrate and ammonium tartrate, that contain anions with low PA are shown to effectively desalt gaseous protein ions formed by ESI.

1.5 Specific Ion-Biomolecule Interactions.

Additional information about peptide or protein sequence or higher-order structure can be obtained by combining mass measurements with covalent or noncovalent modifications at specific residues in a protein or peptide. Many amino acids can be chemically modified selectively, such as conversion of lysine to homoarginine[117] and cysteine thiol to thialamine.[118] Modifications of specific residues can provide constraints on possible amino acid compositions when accurate mass is insufficient to unambiguously identify the peptide.[119] For example, a cysteine modification using an alkylating reagent that contains chlorine can be used to determine the number of cysteine residue in a peptide sequence based on the distinctive isotope distribution of chlorine.[119] The number of cysteine residues in a peptide sequence constrains the possible amino acid composition, which increases the effectiveness of the accurate mass measurement approach.[119]

These covalent labeling methods can also map protein structure and interactions by measuring the differential reactivity of different side chains.[37] Much like H/D exchange, the reactivity of amino acids depends largely on the accessibility of the side chain to the reagent and the inherent reactivity of the chemical modifier and the side chain.[37] In comparison to H/D exchange measurements, the possibility of back-exchange and scrambling are virtually nonexistent with covalent labeling reagents.[37] Due to the size of covalent modifications, however, protein structure is more likely to be altered by the modification compared to when deuterium is used to probe structure.[37] Coupled with mass spectrometry, covalent labeling has been used to probe protein surface topology and determine protein interactions.[37]

Specific noncovalent adduction has also been used to obtain information about the composition or surface accessibility of specific residues on proteins.[120,121] In gas-phase ion/molecule reactions, adduction of acidic molecules, such as HI, to various peptides and proteins occurs when the gas-phase acidity of the acid is less than or equal to ~330 kcal • mol^{-1}.[120,121] The number of basic sites (Arg, Lys, His, N-terminus)

on 20 of 21 oligopeptides was determined by the sum of the ion charge state and number of adducted HI molecules.[120] 18-crown-6 (18C6) was found to have a strong preference to bind to lysine residues in small peptides and proteins with minimal interaction to the protonated side chains of histidine, arginine, and the N-terminus.[122,123] The number of lysine residues can be unambiguously determined in small peptides, such as tetralysine, but cannot be determined in larger proteins, such as cytochrome *c*.[122,123] This result was attributed to the lack of accessibility of 18C6 to lysine residues in the interior of the protein.[122,123] Napthalene-disulfonic acid (NDS) and Cibacron Blue F3G-A (CCB) were either found to interact specifically with arginine and the N-terminus or all basic sites, respectively.[124,125] The maximum number of complex adducts in these experiments was found to equal the number of arginine residues plus the N-terminus for NDS and equal to all basic sites for CCB for small peptides and ubiquitin.[48,125] In chapter 6, it is demonstrated that the number of basic sites (Arg, His, Lys, and the N-terminus) in peptides and proteins can be accurately determined from the number of $HClO_4$ molecules adducted to lower charge state ions generated by ESI.[126] For 18 oligopeptides, the sum of the number of protons and the maximum number of $HClO_4$ acid molecules adducted to the lower charge state ions is equal to the number of basic sites on the proteins.[126]

1.6 Structural Information: Tandem Mass Spectrometry.

1.6.1 Fourier-Transform Ion Cyclotron Resonance Mass Spectrometry. In a uniform magnetic field directed along the *z*-axis, ions with a velocity component along the *x*- or *y*-axis will be confined in an orbit about the *z*-axis due to the Lorentz force of the magnetic field. The frequency of this orbit (ω_c) is inversely proportional to the mass-to-charge ratio (m/*z*) of the ion and directly proportional to the magnetic field strength (*B*), eq. 2.

$$\omega_c = \frac{zeB}{m} \qquad \text{(eq. 2)}$$

In FT-ICR, ions are trapped in ultrahigh vacuum (i.e., ~10^{-10} Torr) in an electrostatic potential well along the *z*-axis. To measure the *m*/*z* and abundance of trapped ions, an electrostatic waveform is applied to a set of opposing plates parallel to the *z*-axis to coherently excite the cyclotron motion of the ions until an image current can be measured on another set of opposing plates parallel to the *z*-axis. The transient signal of this image current is Fourier-transformed to yield the *m*/*z* and abundance of the trapped ions. Ions of a given *m*/*z* can also be selectively ejected from the ion cell by exciting their cyclotron motion until their radius exceeds the dimensions of the ion cell. Using these techniques, ions can be *m*/*z*-selected and stored in an FT-ICR ion cell for long periods of time before detection or ejection from the ion cell.

There are several advantages for using FT-ICR MS to study biomolecular ion structure. The sensitivity and mass accuracy of FT-ICR MS both increase with increasing magnetic field strength, making it possible to perform exact mass measurements on less than femtomoles of sample with accuracies of less than ~400 ppb. If a broadband RF sweep is used for ion excitation, all ions with a given frequency (m/z) range can be excited and subsequently detected, thus making multichannel detection possible. Since ions can be stored in an ion cell for long periods of time, tandem sequences of ion isolation, activation, excitation, and detection events can be performed relatively easily, making FT-ICR highly advantageous for gas-phase experiments with many steps. FT-ICR MS is also often used for tandem MS^n experiments because of its superior resolution and mass measuring accuracy, which greatly aids in the identification of resulting fragment ions.

1.6.2 Electron Capture Dissociation. Peptide and protein sequencing by tandem mass spectrometry is widely used to identify the primary sequence of these molecules and identify sites of post-translational modifications. Information about the conformation of an ion can be inferred from both the identity of the fragments, as well as kinetics and thermodynamics of the dissociation process. Dissociation by ion-electron recombination methods, such as in electron capture dissociation (ECD) where a free electron is captured by an ion, are important tools for the analysis of peptide and protein structure, because these techniques often preserve labile covalent bonds and noncovalent interactions and provide extensive sequence coverage that is complementary to more traditional "slow-heating" activation techniques, such as collision induced dissociation (CID).[14,30-32,127] In ECD, low-energy electrons are generated from a heated dispenser cathode within the ion cell and are allowed to react with the trapped precursor ion on the millisecond time scale. The fragmentation of peptides upon electron capture typically occurs at N-C_α peptide bonds to form c and $z^\bullet$ fragments.[30,127] Some researchers have proposed that ECD is a "non-ergodic" process, such that statistical redistribution of the energy gained upon electron capture does not occur before the reduced peptide fragments.[30-32] Others have proposed that electron capture occurs near the N-C_α peptide bond, which subsequently becomes very weak in the resulting radical species, and that ECD does involve statistical energy redistribution.[127]

For larger proteins, greater sequence coverage is often obtained from high charge state protein ions formed by ESI from denaturing solutions that have more elongated conformations compared to low charge states formed from native solutions.[30,31,128-132] However, denaturation of the protein prior to MS analysis makes it impossible to investigate native protein structure and protein complex stoichiometry directly by MS. Several approaches have been developed to enhance the sequence information obtained from ECD experiments of protein ions formed in native mass spectrometry. Activation of the reduced precursor formed by ECD of low charge state ions with IR laser irradiation or off-resonance CID results in enhanced sequence coverage for the protein, a result attributed to breaking noncovalent interactions holding

fragment ion together in the native protein strucutre.[133] ECD of high charge state protein ions generated by ESI from native solutions containing supercharging reagents results in enhanced sequence coverage compared to the highest charge state formed without these reagents.[62,134] In chapter 7, high charge state protein ions can be readily formed by ESI from aqueous solutions that contain 1.0 mM $LaCl_3$, where the protein has a native structure in solution. ECD of these ions results in comparable sequence coverage to that obtained for high charge state ions formed from denaturing solutions, and should reduce the need to denature ions prior to tandem MS analysis.

High charge state ions of small peptides also typically dissociate more readily in ion-electron recombination methods.[30,31,128-132] For example, at least 36% more unique peptides could be identified with an ion-electron recombination method than collisional dissociation methods for both tryptic and Lys-C peptides with charge states greater than two.[130] Several approaches have been developed to increase the structural information that can be obtained for small peptides or acidic molecules that would typically form singly charged ions by ESI. Zubarev and coworkers developed a new technique to overcome this limitation called electron detachment dissociation (EDD), where electronically excited radical cations, $(M+H)^{2+\bullet}$, are formed by irradiating trapped cations, $(M+H)^{+}$, with electrons that have more than 10 eV kinetic energy.[135] $(M+H)^{2+\bullet}$ dissociates through sidechain losses and backbone fragmentation.[135] EDD of small peptides and acidic molecules results in a substantial improvement in sequence coverage compared to that obtain from ECD results. For example, EDD of positively-charged dications of the Trp cage protein resulted in 100% sequence coverage, whereas only 26% sequence coverage is obtained from ECD. Electron capture induced dissociation (ECID) can also be used to generated excited radical cations or anions by transferring electrons from neutral alkali metal atoms, such as sodium and cesium, to cations and anions through high-energy collisions (100 keV). This technique can also be used to ionize neutral fragments that are formed by ECID through secondary collisions with the alkali metal atoms.

Complexation of a divalent metal ion (M_D) to a small peptide can result in divalent ions that can readily be dissociated by ion-electron recombination methods,[136-139] and complementary sequence information can often be obtained compared to that from the fully protonated molecular ions. Håkansson and coworkers found that ECD of $(\text{substance P} + H + M_D)^{3+}$, where M_D = different alkaline earth metal ions, Mn, Fe, or Zn, results in similar sequence coverage as that obtained from ECD of $(\text{substance P} + 3H)^{3+}$, and protonated *c* ions and complementary metal containing *z* ions are formed, which has been attributed to the metal ion binding close to the C-terminus.[137] In contrast, ECD of Co^{2+} and Ni^{2+}-bound peptides predominately cleaves C-terminal to methionine, the likely metal binding site, and lower sequence coverage than that from ECD of $(\text{substance P} + 3H)^{3+}$ is obtained.[137] In chapter 8, ECD of trivalent metal ion-peptide complexes results in enhanced sequence coverage and electron capture efficiency compared to ECD results for divalent metal ion-peptide complexes for small peptides. ECD results for larger peptides (MW > 1,000 Da) complexed to trivalent metal ions indicate that the metal ion binds specifically to acidic sites in the peptide.

1.7 Structural Information: Ion Mobility of Biomolecular Complexes.

In ion mobility spectrometry (IMS) experiments, gaseous ions are separated based on differences in the amount of time necessary for a static, weak electric field to pull them through a drift region containing an inert buffer gas, usually several Torr of helium or nitrogen. The electric field accelerates the ions through the drift region, while collisions with inert, gas molecules slow the mobility of the ion. In general, larger ions have more collisions, and therefore take longer to reach the end of the drift region. The average collision cross section of an ion can be directly related to their mobility in these experiments. If the cross sections are different enough and the resolution of the IMS instrument allows, distinct conformations of an ion can be detected.

Applications of ion mobility have increased dramatically since the commercial availability of travelling wave ion mobility spectrometry (TWIMS) coupled to a time-of-flight (TOF) mass spectrometer. In TWIMS, a wave of amplitude V is applied to a set of adjacent lenses and moved along the axis of the drift region at a velocity (*v*). Some ions are able to traverse the drift region at the velocity of the wave, whereas other fall behind, resulting in a drift separation. Unlike static drift tube measurements, the collision cross section of an ion can only be determined by calibrating drift times for ions of interest against those measured for ions with known cross section values. Recently, cross section measurements for a large set of biomolecular ions have been determined,[140] making the cross section calibration over a wider range of cross sections possible.

TWIMS or IMS is increasingly coupled with MS in order to reduce mass spectral complexity and interrogate ion structures. With TWIMS or IMS as an orthogonal separation to MS, the species of interest can be separated from chemical noise, isobaric compounds, and different compound classes. TWIMS has been used to evaluate the gas-phase conformations of peptides,[141,142] proteins,[141,143-145] multi-protein complexes,[143-145] and even intact viruses,[146,147] and these conformations are often related to their solution-phase structures. TWIMS MS was recently used to determine that the collision cross section (ccs)[145] of a sickle hemoglobin tetramer is greater than that of normal hemoglobin, consistent with their X-ray crystal structures.[145] IMS MS has also been extensively used to reveal the structures of early oligomeric intermediates of amyloid-β and other fibril forming peptides in amyloid fibril formation, which has been difficult to obtain with more traditional structural biology techniques. In chapter 9, the gas-phase conformations of protein cation and anions adducted nonspecifically with various metal ions are shown to be more compact than the conformation of the non-metallated protein ion with more compact conformations observed for metal ions with higher charge. However, a specific ion-protein interaction that results in a more elongated conformation is shown, indication that specific solution-phase structures can be preserved in the gas-phase when formed by ESI.

1.8 References

(1) Crivici, A.; Ikura, M. *Annu. Rev. Biophys. Biomolec. Struct.* **1995**, *24*, 85-116.
(2) Valaskovic, G. A.; Kelleher, N. L.; Little, D. P.; Aaserud, D. J.; McLafferty, F. W. *Anal. Chem.* **1995**, *67*, 3802-3805.
(3) Valaskovic, G. A.; Kelleher, N. L.; McLafferty, F. W. *Science* **1996**, *273*, 1199-1202.
(4) Belov, M. E.; Gorshkov, M. V.; Udseth, H. R.; Anderson, G. A.; Smith, R. D. *Anal. Chem.* **2000**, *72*, 2271-2279.
(5) Sharon, M.; Robinson, C. V. In *Annual Review of Biochemistry*; Annual Reviews: Palo Alto, 2007; Vol. 76, pp 167-193.
(6) Loo, J. A. *Mass Spectrom. Rev.* **1997**, *16*, 1-23.
(7) Kapur, A.; Beck, J. L.; Brown, S. E.; Dixon, N. E.; Sheil, M. M. *Protein Sci.* **2002**, *11*, 147-157.
(8) Daneshfar, R.; Kitova, E. N.; Klassen, J. S. *J. Am. Chem. Soc.* **2004**, *126*, 4786-4787.
(9) Wang, L. T.; Lane, L. C.; Smith, D. L. *Protein Sci.* **2001**, *10*, 1234-1243.
(10) van Duijn, E.; Simmons, D. A.; van den Heuvel, R. H. H.; Bakkes, P. J.; van Heerikhuizen, H.; Heeren, R. M. A.; Robinson, C. V.; van der Vies, S. M.; Heck, A. J. R. *J. Am. Chem. Soc.* **2006**, *128*, 4694-4702.
(11) Haskins, N. J.; Eckers, C.; Organ, A. J.; Dunk, M. F.; Winger, B. E. *Rapid Commun. Mass Spectrom.* **1995**, *9*, 1027-1030.
(12) Bowers, M. T.; Marshall, A. G.; McLafferty, F. W. *J. Phys. Chem.* **1996**, *100*, 12897-12910.
(13) McKenna, A. M.; Purcell, J. M.; Rodgers, R. P.; Marshall, A. G. *Energy Fuels* **2010**, *24*, 2929-2938.
(14) Mann, M.; Jensen, O. N. *Nat. Biotechnol.* **2003**, *21*, 255-261.
(15) Freitas, M. A.; Sklenar, A. R.; Parthun, M. R. *J. Cell. Biochem.* **2004**, *92*, 691-700.
(16) Wang, F.; Li, W. Q.; Emmett, M. R.; Hendrickson, C. L.; Marshall, A. G.; Zhang, Y. L.; Wu, L.; Zhang, Z. Y. *Biochemistry* **1998**, *37*, 15289-15299.
(17) Sun, Y. P.; Bauer, M. D.; Lu, W. P. *J. Mass Spectrom.* **1998**, *33*, 1009-1016.
(18) Chu, Y. H.; Dunayevskiy, Y. M.; Kirby, D. P.; Vouros, P.; Karger, B. L. *J. Am. Chem. Soc.* **1996**, *118*, 7827-7835.
(19) Eldridge, G. R.; Vervoort, H. C.; Lee, C. M.; Cremin, P. A.; Williams, C. T.; Hart, S. M.; Goering, M. G.; O'Neil-Johnson, M.; Zeng, L. *Anal. Chem.* **2002**, *74*, 3963-3971.
(20) Petyuk, V. A.; Qian, W. J.; Hinault, C.; Gritsenko, M. A.; Singhal, M.; Monroe, M. E.; Camp, D. G.; Kulkarni, R. N.; Smith, R. D. *J. Proteome Res.* **2008**, *7*, 3114-3126.
(21) Bantscheff, M.; Schirle, M.; Sweetman, G.; Rick, J.; Kuster, B. *Anal. Bioanal. Chem.* **2007**, *389*, 1017-1031.

(22) Marshall, A. G.; Hendrickson, C. L. In *Annual Review of Analytical Chemistry*; Annual Reviews: Palo Alto, 2008; Vol. 1, pp 579-599.
(23) Perry, R. H.; Cooks, R. G.; Noll, R. J. *Mass Spectrom. Rev.* **2008**, *27*, 661-699.
(24) Rostom, A. A.; Fucini, P.; Benjamin, D. R.; Juenemann, R.; Nierhaus, K. H.; Hartl, F. U.; Dobson, C. M.; Robinson, C. V. *Proc. Natl. Acad. Sci. U. S. A.* **2000**, *97*, 5185-5190.
(25) Benjamin, D. R.; Robinson, C. V.; Hendrick, J. P.; Hartl, F. U.; Dobson, C. M. *Proc. Natl. Acad. Sci. U. S. A.* **1998**, *95*, 7391-7395.
(26) Bacher, G.; Szymanski, W. W.; Kaufman, S. L.; Zollner, P.; Blaas, D.; Allmaier, G. *J. Mass Spectrom.* **2001**, *36*, 1038-1052.
(27) van den Heuvel, R. H.; Heck, A. J. R. *Curr. Opin. Chem. Biol.* **2004**, *8*, 519-526.
(28) He, F.; Emmett, M. R.; Hakansson, K.; Hendrickson, C. L.; Marshall, A. G. *J. Proteome Res.* **2004**, *3*, 61-67.
(29) Zubarev, R. A.; Hakansson, P.; Sundqvist, B. *Anal. Chem.* **1996**, *68*, 4060-4063.
(30) Zubarev, R. A.; Horn, D. M.; Fridriksson, E. K.; Kelleher, N. L.; Kruger, N. A.; Lewis, M. A.; Carpenter, B. K.; McLafferty, F. W. *Anal. Chem.* **2000**, *72*, 563-573.
(31) Zubarev, R. A.; Kelleher, N. L.; McLafferty, F. W. *J. Am. Chem. Soc.* **1998**, *120*, 3265-3266.
(32) Cooper, H. J.; Hakansson, K.; Marshall, A. G. *Mass Spectrom. Rev.* **2005**, *24*, 201-222.
(33) Clemmer, D. E.; Jarrold, M. F. *J. Mass Spectrom.* **1997**, *32*, 577-592.
(34) Clemmer, D. E.; Hudgins, R. R.; Jarrold, M. F. *J. Am. Chem. Soc.* **1995**, *117*, 10141-10142.
(35) Miranker, A.; Robinson, C. V.; Radford, S. E.; Aplin, R. T.; Dobson, C. M. *Science* **1993**, *262*, 896-900.
(36) Konermann, L.; Simmons, D. A. *Mass Spectrom. Rev.* **2003**, *22*, 1-26.
(37) Mendoza, V. L.; Vachet, R. W. *Mass Spectrom. Rev.* **2009**, *28*, 785-815.
(38) Dole, M.; Mack, L. L.; Hines, R. L. *J. Chem. Phys.* **1968**, *49*, 2240-&.
(39) Iribarne, J. V.; Thomson, B. A. *J. Chem. Phys.* **1976**, *64*, 2287-2294.
(40) de la Mora, J. F. *Anal. Chim. Acta* **2000**, *406*, 93-104.
(41) Iavarone, A. T.; Williams, E. R. *J. Am. Chem. Soc.* **2003**, *125*, 2319-2327.
(42) Hogan, C. J.; Carroll, J. A.; Rohrs, H. W.; Biswas, P.; Gross, M. L. *J. Am. Chem. Soc.* **2008**, *130*, 6926-+.
(43) Hogan, C. J.; Carroll, J. A.; Rohrs, H. W.; Biswas, P.; Gross, M. L. *Anal. Chem.* **2009**, *81*, 369-377.
(44) Loo, J. A.; Quinn, J. P.; Ryu, S. I.; Henry, K. D.; Senko, M. W.; McLafferty, F. W. *Proc. Natl. Acad. Sci. U. S. A.* **1992**, *89*, 286-289.
(45) Fenn, J. B. *J. Am. Soc. Mass Spectrom.* **1993**, *4*, 524-535.
(46) Loo, J. A.; Loo, R. R. O.; Udseth, H. R.; Edmonds, C. G.; Smith, R. D. *Rapid Commun. Mass Spectrom.* **1991**, *5*, 101-105.
(47) Chowdhury, S. K.; Katta, V.; Chait, B. T. *J. Am. Chem. Soc.* **1990**, *112*, 9012-9013.

(48) Konermann, L.; Douglas, D. J. *J. Am. Soc. Mass Spectrom.* **1998**, *9*, 1248-1254.
(49) Iavarone, A. T.; Jurchen, J. C.; Williams, E. R. *J. Am. Soc. Mass Spectrom.* **2000**, *11*, 976-985.
(50) Wang, G. D.; Cole, R. B. *J. Am. Soc. Mass Spectrom.* **1996**, *7*, 1050-1058.
(51) Iavarone, A. T.; Jurchen, J. C.; Williams, E. R. *Anal. Chem.* **2001**, *73*, 1455-1460.
(52) Fenn, J. B.; Mann, M.; Meng, C. K.; Wong, S. F.; Whitehouse, C. M. *Science* **1989**, *246*, 64-71.
(53) Thomson, B. A. *J. Am. Soc. Mass Spectrom.* **1997**, *8*, 1053-1058.
(54) Lomeli, S. H.; Yin, S.; Loo, R. R. O.; Loo, J. A. *J. Am. Soc. Mass Spectrom.* **2009**, *20*, 593-596.
(55) Lomeli, S. H.; Peng, I. X.; Yin, S.; Loo, R. R. O.; Loo, J. A. *J. Am. Soc. Mass Spectrom.* **2010**, *21*, 127-131.
(56) Iavarone, A. T.; Jurchen, J. C.; Williams, E. R. *Anal. Chem.* **2001**, *73*, 1455-1460.
(57) Iavarone, A. T.; Williams, E. R. *Int. J. Mass Spectrom.* **2002**, *219*, 63-72.
(58) Sterling, H. J.; Williams, E. R. *J. Am. Soc. Mass Spectrom.* **2009**, *20*, 1933-1943.
(59) Sterling, H. J.; Kintzer, A. F.; Feld, G. K.; Cassou, C. A.; Krantz, B. A.; Williams, E. R. *J. Am. Soc. Mass Spectrom.* **2012**, *23*, 191-200.
(60) Sterling, H. J.; Cassou, C. A.; Trnka, M. J.; Burlingame, A. L.; Krantz, B. A.; Williams, E. R. *Phys. Chem. Chem. Phys.* **2011**, *13*, 18288-18296.
(61) Sterling, H. J.; Daly, M. P.; Feld, G. K.; Thoren, K. L.; Kintzer, A. F.; Krantz, B. A.; Williams, E. R. *J. Am. Soc. Mass Spectrom.* **2010**, *21*, 1762-1774.
(62) Sterling, H. J.; Williams, E. R. *Anal. Chem.* **2010**, *82*, 9050-9057.
(63) Sterling, H. J.; Kintzer, A. F.; Feld, G. K.; Cassou, C. A.; Krantz, B. A.; Williams, E. R. *J. Am. Soc. Mass Spectrom.*, *23*, 191-200.
(64) Sterling, H. J.; Prell, J. S.; Cassou, C. A.; Williams, E. R. *J. Am. Soc. Mass Spectrom.* **2011**, *22*, 1178-1186.
(65) Grimm, R. L.; Beauchamp, J. L. *J. Phys. Chem. A* **2010**, *114*, 1411-1419.
(66) Douglass, K. A.; Venter, A. R. *J. Am. Soc. Mass Spectrom.* **2012**, *23*, 489-497.
(67) Hogan, C. J.; Loo, R. R. O.; Loo, J. A.; de la Moraa, J. F. *Phys. Chem. Chem. Phys.* **2010**, *12*, 13476-13483.
(68) Sze, S. K.; Ge, Y.; Oh, H.; McLafferty, F. W. *Proc. Natl. Acad. Sci. U. S. A.* **2002**, *99*, 1774-1779.
(69) Sheng, Y.; Loo, J. A. *Int. J. Mass Spectrom.* **2011**, *300*, 118-122122.
(70) Kharlamova, A.; Prentice, B. M.; Huang, T. Y.; McLuckey, S. A. *Anal. Chem.*, *82*, 7422-7429.
(71) Sterling, H. J.; Cassou, C. A.; Susa, A. C.; Williams, E. R. *Anal. Chem.* **2012**, *84*, 3795-3801.
(72) Gorog, S. *J. Pharm. Biomed. Anal.* **2008**, *48*, 247-253.
(73) Basak, A. K.; Raw, A. S.; Al Hakim, A. H.; Furness, S.; Samaan, N. I.; Gill, D. S.; Patel, H. B.; Powers, R. F.; Yu, L. *Adv. Drug Deliv. Rev.* **2007**, *59*, 64-72.

(74) Cech, N. B.; Enke, C. G. *Anal. Chem.* **2000**, *72*, 2717-2723.
(75) Cech, N. B.; Enke, C. G. *Anal. Chem.* **2001**, *73*, 4632-4639.
(76) Leib, R. D.; Flick, T. G.; Williams, E. R. *Anal. Chem.* **2009**, *81*, 3965-3972.
(77) Tang, L.; Kebarle, P. *Anal. Chem.* **1993**, *65*, 3654-3668.
(78) Pan, P.; McLuckey, S. A. *Anal. Chem.* **2003**, *75*, 5468-5474.
(79) Marshall, J.; Franks, J.; Abell, I.; Tye, C. *J. Anal. At. Spectrom.* **1991**, *6*, 145-150.
(80) Gygi, S. P.; Rist, B.; Gerber, S. A.; Turecek, F.; Gelb, M. H.; Aebersold, R. *Nat. Biotechnol.* **1999**, *17*, 994-999.
(81) Ong, S. E.; Blagoev, B.; Kratchmarova, I.; Kristensen, D. B.; Steen, H.; Pandey, A.; Mann, M. *Mol. Cell. Proteomics* **2002**, *1*, 376-386.
(82) Hopfgartner, G.; Bourgogne, E. *Mass Spectrom. Rev.* **2003**, *22*, 195-214.
(83) Gros, M.; Petrovic, M.; Barcelo, D. *Talanta* **2006**, *70*, 678-690.
(84) Flick, T. G.; Leib, R. D.; Williams, E. R. *Anal. Chem.* **2009**, *81*, 8434-8440.
(85) Flick, T. G.; Leib, R. D.; Williams, E. R. *Anal. Chem.* **2010**, *82*, 1179-1182.
(86) Leib, R. D.; Williams, E. R. *J. Am. Soc. Mass Spectrom.* **2011**, *22*, 624-632.
(87) Cooks, R. G.; Zhang, D. X.; Koch, K. J.; Gozzo, F. C.; Eberlin, M. N. *Anal. Chem.* **2001**, *73*, 3646-3655.
(88) Counterman, A. E.; Clemmer, D. E. *J. Phys. Chem. B* **2001**, *105*, 8092-8096.
(89) Hofmeister, F. *Naunyn-Schmiedeberg's Arch. Pharmacol.* **1888**, *25*, 1-30.
(90) Kunz, W.; Henle, J.; Ninham, B. W. *Curr. Opin. Colloid Interface Sci.* **2004**, *9*, 19-37.
(91) Cheng, J.; Vecitis, C. D.; Hoffmann, M. R.; Colussi, A. J. *J. Phys. Chem. B* **2006**, *110*, 25598-25602.
(92) Zhang, Y. J.; Cremer, P. S. *Proc. Natl. Acad. Sci. U. S. A.* **2009**, *106*, 15249-15253.
(93) Hribar, B.; Southall, N. T.; Vlachy, V.; Dill, K. A. *J. Am. Chem. Soc.* **2002**, *124*, 12302-12311.
(94) Cho, Y. H.; Zhang, Y. J.; Christensen, T.; Sagle, L. B.; Chilkoti, A.; Cremer, P. S. *J. Phys. Chem. B* **2008**, *112*, 13765-13771.
(95) Zhang, Y.; Furyk, S.; Sagle, L. B.; Cho, Y.; Bergbreiter, D. E.; Cremer, P. S. *J. Phys. Chem. C* **2007**, *111*, 8916-8924.
(96) Collins, K. D. *Methods* **2004**, *34*, 300-311.
(97) Washabaugh, M. W.; Collins, K. D. *J. Biol. Chem.* **1986**, *261*, 2477-2485.
(98) Bostrom, M.; Tavares, F. W.; Finet, S.; Skouri-Panet, F.; Tardieu, A.; Ninham, B. W. *Biophys. Chem.* **2005**, *117*, 217-224.
(99) Omta, A. W.; Kropman, M. F.; Woutersen, S.; Bakker, H. J. *Science* **2003**, *301*, 347-349.
(100) Chen, X.; Yang, T.; Kataoka, S.; Cremer, P. S. *J. Am. Chem. Soc.* **2007**, *129*, 12272-12279.
(101) O'Brien, J. T.; Prell, J. S.; Bush, M. F.; Williams, E. R. *J. Am. Chem. Soc.* **2010**, *132*, 8248-+.

(102) Prell, J. S.; O'Brien, J. T.; Williams, E. R. *J. Am. Chem. Soc.* **2011**, *133*, 4810-4818.
(103) Flick, T. G.; Merenbloom, S. I.; Williams, E. R. *J. Am. Soc. Mass Spectrom.* **2011**, *22*, 1968-1977.
(104) Iavarone, A. T.; Udekwu, O. A.; Williams, E. R. *Anal. Chem.* **2004**, *76*, 3944-3950.
(105) Sterling, H. J.; Batchelor, J. D.; Wemmer, D. E.; Williams, E. R. *J. Am. Soc. Mass Spectrom.* **2010**, *21*, 1045-1049.
(106) Wang, G. D.; Cole, R. B. *Anal. Chem.* **1994**, *66*, 3702-3708.
(107) Juraschek, R.; Dulcks, T.; Karas, M. *J. Am. Soc. Mass Spectrom.* **1999**, *10*, 300-308.
(108) Mirza, U. A.; Chait, B. T. *Anal. Chem.* **1994**, *66*, 2898-2904.
(109) Liu, C. L.; Wu, Q. Y.; Harms, A. C.; Smith, R. D. *Anal. Chem.* **1996**, *68*, 3295-3299.
(110) Ikonomou, M. G.; Blades, A. T.; Kebarle, P. *Anal. Chem.* **1990**, *62*, 957-967.
(111) Hernandez, H.; Robinson, C. V. *Nat. Protoc.* **2007**, *2*, 715-726.
(112) Pan, P.; Gunawardena, H. P.; Xia, Y.; McLuckey, S. A. *Anal. Chem.* **2004**, *76*, 1165-1174.
(113) Pan, J. X.; Xu, K.; Yang, X. D.; Choy, W. Y.; Konermann, L. *Anal. Chem.* **2009**, *81*, 5008-5015.
(114) Turner, K. B.; Monti, S. A.; Fabris, D. *J. Am. Chem. Soc.* **2008**, *130*, 13353-13363.
(115) Currie, G. J.; Yates, J. R. *J. Am. Soc. Mass Spectrom.* **1993**, *4*, 955-963.
(116) Zhu, Y. F.; Taranenko, N. I.; Allman, S. L.; Martin, S. A.; Chen, C. H. *Rapid Commun. Mass Spectrom.* **1996**, *10*, 1591-1596.
(117) Geschwind, II; Li, C. H. *Biochimica Et Biophysica Acta* **1957**, *25*, 171-178.
(118) Itano, H. A.; Robinson, E. A. *J. Biol. Chem.* **1972**, *247*, 4819-&.
(119) Conrads, T. P.; Anderson, G. A.; Veenstra, T. D.; Pasa-Tolic, L.; Smith, R. D. *Anal. Chem.* **2000**, *72*, 3349-3354.
(120) Stephenson, J. L.; McLuckey, S. A. *Anal. Chem.* **1997**, *69*, 281-285.
(121) Stephenson, J. L.; McLuckey, S. A. *J. Am. Chem. Soc.* **1997**, *119*, 1688-1696.
(122) Julian, R. R.; Beauchamp, J. L. *J. Am. Soc. Mass Spectrom.* **2002**, *13*, 493-498.
(123) Ly, T.; Julian, R. R. *J. Am. Soc. Mass Spectrom.* **2006**, *17*, 1209-1215.
(124) Friess, S. D.; Daniel, J. M.; Hartmann, R.; Zenobi, R. *Int. J. Mass Spectrom.* **2002**, *219*, 269-281.
(125) Salih, B.; Zenobi, R. *Anal. Chem.* **1998**, *70*, 1536-1543.
(126) Flick, T. G.; Merenbloom, S. I.; Williams, E. R. *Anal. Chem.* **2011**, *83*, 2210-2214.
(127) Turecek, F. *J. Am. Chem. Soc.* **2003**, *125*, 5954-5963.
(128) Breuker, K.; Oh, H. B.; Lin, C.; Carpenter, B. K.; McLafferty, F. W. *Proc. Natl. Acad. Sci. U. S. A.* **2004**, *101*, 14011-14016.
(129) Breuker, K.; Oh, H. B.; Horn, D. M.; Cerda, B. A.; McLafferty, F. W. *J. Am. Chem. Soc.* **2002**, *124*, 6407-6420.

(130) Good, D. M.; Wirtala, M.; McAlister, G. C.; Coon, J. J. *Mol. Cell. Proteomics* **2007**, *6*, 1942-1951.
(131) Oh, H.; Breuker, K.; Sze, S. K.; Ge, Y.; Carpenter, B. K.; McLafferty, F. W. *Proc. Natl. Acad. Sci. U. S. A.* **2002**, *99*, 15863-15868.
(132) McLafferty, F. W.; Horn, D. M.; Breuker, K.; Ge, Y.; Lewis, M. A.; Cerda, B.; Zubarev, R. A.; Carpenter, B. K. *J. Am. Soc. Mass Spectrom.* **2001**, *12*, 245-249.
(133) Horn, D. M.; Ge, Y.; McLafferty, F. W. *Anal. Chem.* **2000**, *72*, 4778-4784.
(134) Yin, S.; Loo, J. A. *Int. J. Mass Spectrom.*, *300*, 118-122.
(135) Yang, J.; Mo, J. J.; Adamson, J. T.; Hakansson, K. *Anal. Chem.* **2005**, *77*, 1876-1882.
(136) Fung, Y. M. E.; Liu, H. C.; Chan, T. W. D. *J. Am. Soc. Mass Spectrom.* **2006**, *17*, 757-771.
(137) Liu, H. C.; Hakansson, K. *J. Am. Soc. Mass Spectrom.* **2006**, *17*, 1731-1741.
(138) Adamson, J. T.; Hakansson, K. *Anal. Chem.* **2007**, *79*, 2901-2910.
(139) Chen, X. F.; Chan, W. Y. K.; Wong, P. S.; Yeung, H. S.; Chan, T. W. D. *J. Am. Soc. Mass Spectrom.* **2011**, *22*, 233-244.
(140) Bush, M. F.; Hall, Z.; Giles, K.; Hoyes, J.; Robinson, C. V.; Ruotolo, B. T. *Anal. Chem.* **2010**, *82*, 9557-9565.
(141) Pringle, S. D.; Giles, K.; Wildgoose, J. L.; Williams, J. P.; Slade, S. E.; Thalassinos, K.; Bateman, R. H.; Bowers, M. T.; Scrivens, J. H. *Int. J. Mass Spectrom.* **2007**, *261*, 1-12.
(142) Thalassinos, K.; Grabenauer, M.; Slade, S. E.; Hilton, G. R.; Bowers, M. T.; Scrivens, J. H. *Anal. Chem.* **2009**, *81*, 248-254.
(143) Uetrecht, C.; Rose, R. J.; van Duijn, E.; Lorenzen, K.; Heck, A. J. R. *Chem. Soc. Rev.* **2010**, *39*, 1633-1655.
(144) Kaddis, C. S.; Lomeli, S. H.; Yin, S.; Berhane, B.; Apostol, M. I.; Kickhoefer, V. A.; Rome, L. H.; Loo, J. A. *J. Am. Soc. Mass Spectrom.* **2007**, *18*, 1206-1216.
(145) Scarff, C. A.; Patel, V. J.; Thalassinos, K.; Scrivens, J. H. *J. Am. Soc. Mass Spectrom.* **2009**, *20*, 625-631.
(146) Thomas, J. J.; Bothner, B.; Traina, J.; Benner, W. H.; Siuzdak, G. *Spectr.-Int. J.* **2004**, *18*, 31-36.
(147) Bothner, B.; Siuzdak, G. *Chembiochem* **2004**, *5*, 258-260.

CHAPTER 2

Standard-Free Quantitation of Mixtures using Clusters Formed by Electrospray Mass Spectrometry

2.1 Introduction

Mass spectrometry (MS) has many advantages for analyzing complex mixtures, including high sensitivity, specificity and speed.[1] In combination with electrospray ionization (ESI), non-volatile and thermally labile molecules can be readily ionized directly from solution and mass analyzed, making ESI-MS a powerful detection method when coupled with liquid chromatography or electrophoresis.[1-3] Elemental composition can be obtained from exact mass measurements,[4] and unknown molecular ions can be identified and structurally characterized using tandem mass spectrometry in which a precursor of interest is isolated, typically dissociated, and the resulting fragments mass analyzed.[5,6]

A limitation of ESI-MS for mixture analysis is the difficulty of obtaining quantitative information about how much of each component is present in a solution mixture directly from ion abundances in the mass spectrum. Ionization efficiencies of molecules in a mixture can differ significantly as a result of many factors, including their surface activities or hydrophobicities, molecular basicity and conformation.[7-22] The matrix or other solutes present in solution can either enhance or reduce the ion abundance of some analytes.[23-26] Instrumental parameters or mass-dependent ion transmission and detection can also affect relative ion abundances.[27-29] Because of these and other factors, quantitation with ESI-MS is typically done with internal standards. Molecules with similar physical properties to the analyte of interest as well as analyte molecules that have been isotopically labeled can be used as standards.[30-34] Quantitation using internal standards is common in small molecule analysis, such as in pharmaceutical chemistry, where characterization of therapeutics and related impurities from unreacted starting materials, synthetic intermediates, and degradation products is necessary to ensure the quality, efficacy and safety of drugs.[35,36] Internal standards, such as isotope-coded affinity tags[30,31] and stable isotope labeling with amino acids in cell cultures,[32,33] are commonly used in proteomics to obtain information about relative gene expression.[30-33]

A new standard-free quantitation method to obtain solution molar fractions using the abundances of cluster ions formed by ESI was recently introduced.[37] The composition of clusters formed from peptide-containing solutions approached that in the bulk solution with increasing cluster sizes. From the abundances of clusters containing ~15 or more peptide molecules, the solution composition could be determined to within ~20% or better even in cases where the ionization/detection efficiency of the individual molecules differed by over an order of magnitude.[37] This method has the advantages that reasonably accurate quantitative information can be obtained directly from an ESI

mass spectrum without using either an internal or external standard, the components do not need to be identified, and effects of instrument or detector mass bias are significantly reduced. This method can greatly reduce the time and effort necessary to obtain quantitative information from mixtures.

A critical requirement to obtain quantitative information using this method is that clusters must form statistically, which appears to occur for large peptide clusters.[37] Clusters of small molecules often exhibit "magic" numbers, such as $H(H_2O)_{21}^+$,[38] which can either be due to the special stability of the specific cluster or instability of adjacent clusters. Protonated serine shows a strong propensity to form magic numbers and the protonated octamer is especially stable.[12,39-59] Protonated serine octamer is often the most abundant ion observed in a mass spectrum of serine and is readily formed by ESI,[12,39-47] sonic spray[48-50] and even by thermal sublimation.[51-53] The protonated octamer also has a strong homochiral preference, which has led some to suggest that serine may have played a role in the origin of homochirality in living systems.[39-42,53] The structure of the protonated octamer has been investigated by H/D exchange,[54-56] ion mobility,[42,43,48] infrared photodissociation spectroscopy,[57] and quantum chemical calculations,[39,41,43] from which evidence for at least two different forms of the octamer have been deduced.

Although protonated serine octamer is homochirally selective, doubly protonated octamer and clusters with 9 – 10 serine molecules show a heterochiral preference.[44,58] Higher-order octameric clusters, e.g., $[16Ser + 2H]^{2+}$, $[24Ser + 3H]^{3+}$, have also been reported to have slightly enhanced abundances and it has been suggested that the serine octamer is a building block in their assembly.[39,42] Results from ion mobility experiments indicate that large clusters with as many as 500+ serine molecules form tightly packed spherical structures.[48]

Because of the strong preference of serine to form "magic" numbers and clusters that show strong chiral preferences, serine-containing solutions provide an excellent test of whether our standard-free cluster quantitation method is generally applicable because our method requires that the cluster composition is statistical and therefore representative of the solution-phase analyte concentrations. Here, we demonstrate that large serine clusters formed by ESI from solutions containing serine as a major component incorporate aliphatic, basic, and acidic amino acids statistically. Although the protonated octamer effectively excludes a dipeptide and threonine of the opposite chirality, these molecules are incorporated into larger clusters statistically. From the abundances of the larger clusters, the solution-phase percent molar fractions can be determined with better than 10% accuracy. These results indicate that our method should be broadly applicable to a wide range of analytes.

2.2 Experimental

2.2.1 Sample Preparation. L-serine, L-lysine, L-leucine, L-threonine, L-glutamic acid, D-threonine, and diglycine were purchased from Sigma-Aldrich, Co. (St. Louis, MO). Stock solutions for each analyte were prepared at 12 mM in water and all mixed analyte solutions were prepared to a final total concentration of 3 mM in water

using these stock solutions. The minor component was incorporated into L-serine solutions at a % mole fraction ranging from 0.03% to 24%.

2.2.2 Mass Spectrometry. Experiments were performed on a 9.4 T Fourier-transform ion cyclotron resonance mass spectrometer with an external ESI source that is described elsewhere.[60] Ions are formed by ESI from borosilicate capillaries that are pulled so that the tips have a ~2 μm inner diameter (model P-87 capillary puller, Sutter Instruments, Novato, CA). The capillary is loaded with a small volume (~2-10 μL) of analyte solution, and a platinum wire is inserted into the solution and grounded. A new capillary was used for each solution to avoid sample contamination. The borosilicate capillary is positioned ~2 mm away from the source inlet capillary and a potential of -800 to -1200 V is applied to this inlet capillary. Ions are accumulated in an external hexapole ion trap for 1.5 s and subsequently are injected into the cell. Nitrogen gas introduced through a piezoelectric valve to a cell pressure of ~1 × 10^{-6} Torr is used to enhance ion trapping, and three hexapole injections are used prior to detection. Three mass spectra of 50 coadded scans were acquired at three different DC offset values between 4.5-6.3 V for each analyte to take into account the affect of this parameter on relative ion abundances in the mass spectrum. Error bars for data obtained from the protonated molecular ions, protonated octamer, and larger cluster abundances ($n \geq 32$) correspond to the standard deviation from the average value obtained from the mass spectra at three DC offset voltages.

2.3 Results and Discussion

2.3.1 Solute Concentration from Cluster Ion Abundances. For clusters that are formed statistically from the molecules in solution and for which the ionization efficiency is not influenced by their composition, the solution-phase concentration of various analytes that are incorporated into these clusters can be determined from the cluster abundances. The percent molar fraction of a minor component, F_m%, can be obtained by using a weighted average (eq.1):

$$D = \frac{V_d \times F_m \times C}{(1 - F_m)} \times MW \qquad \text{eq. 1}$$

where I is the abundance of each observed cluster consisting of n total molecules with h molecules of the minor fraction component. For example, if two clusters consisting of 40 molecules are formed, one a homogenous cluster containing 40 molecules of component **A** and the other a heterogeneous cluster containing 39 molecules of **A** and one molecule of **B**, and the normalized abundances of these clusters are 100 and 15, respectively, then the percent molar fraction (F_m%) of **B** is ((15 × (1/40))/(15 + 100.0)) × 100 = 0.33%. Solute concentration can also be obtained from cluster abundances using a binomial expansion, but the weighted average method is more accurate for larger cluster sizes when the signal-to-noise ratio is low.[37]

In these experiments, relative ion abundances depend on a number of instrumental parameters. For example, the DC potential applied to the external

hexapole used to store ions prior to injecting them into the cell can be varied to preferentially introduce higher *m*/*z* ions. To take this effect into account, mass spectra were acquired at three different DC offset voltages and the percent molar fractions determined from the ion abundances were averaged for these three spectra. The significantly higher error bars in the protonated molecular ion data compared to those for the large cluster ($n \geq 32$) data reflect the larger effect this parameter has at lower *m*/*z*.

2.3.2 L-Threonine in L-Serine. The side chain of threonine has an additional methylene group compared to that of serine, but this minor structural difference results in dramatically different ionization efficiencies for these two amino acids with ESI. A representative ESI mass spectrum of a solution containing 1% L-threonine with 99% L-serine at a total amino acid concentration of 3 mM is shown in Figure 1. The abundance of protonated L-threonine is 3.9% that of L-serine. Thus, the relative abundance of protonated L-threonine is nearly 4 times greater than its corresponding solution concentration. Preferential ionization of threonine over serine has been reported previously[43] and could be due to increased surface activity or hydrophobicity owing to the extra methylene group or a slightly higher proton affinity.[61] Other factors, including solution concentration, instrumental parameters, ion transmission and detection efficiency, can also play a significant role in the relative abundances of ions observed in ESI mass spectra.[7-11,13-29] Differences in ionization efficiency and contributions from these other factors make it difficult to obtain solution concentrations directly from molecular ion abundances without using standards.

In addition to the protonated molecular ions, both homogenous clusters of L-serine and heterogeneous clusters that have incorporated L-threonine are observed (Figure 1). Large clusters are often formed from concentrated solutions[40,43,62] and the abundances of these clusters can be increased by changing several instrumental parameters, including both the ion accumulation time and dc offset potential of the external hexapole that is used to accumulate ions prior to injection into the ion cell.[37] In these experiments, clusters consisting of as many as 91 amino acids were observed.

Percent molar fractions are obtained from the cluster abundances as a function of cluster size assuming statistical incorporation of the amino acids. Date from this mass spectrum (and mass spectra at two additional DC offset potentials) are shown in Figure 2a. For clusters with $n < 10$, the molar fraction of L-threonine obtained from the gas-phase cluster data is higher than that in solution (dashed line in Figure 2a). This could be due to the higher ionization efficiency of L-threonine, which has a larger effect on smaller clusters or it could be due to preferential incorporation of L-threonine at small cluster sizes. The general trend with cluster size suggests that the higher ionization efficiency of L-threonine may be more important for these clusters. For the larger clusters ($n \geq 32$), the calculated molar fraction of L-threonine does not change significantly with cluster size. An average molar fraction of L-threonine determined from the $n = 32 – 89$ cluster abundances is 0.88% ± 0.10%, which is close to the solution-phase value of 1.0%. This indicates that any differences in ionization/detection efficiency or effects of preferential incorporation of L-threonine into these larger clusters are minor. The abundances of these larger clusters gradually decrease with increasing size and no “magic” numbers are observed, consistent with nonspecific aggregation.

The weighting of these data either by their respective abundances or cluster sizes results in a negligible change in the percent molar fraction determined. The molar fraction of L-threonine determined just from octameric clusters is 1.6% ± 0.5%, indicating that the octamer can readily incorporate L-threonine as previously reported.[43,45,53]

These data were obtained as a function of the % molar fraction of L-threonine ranging from 0.05% to 20%. The L-threonine molar fraction determined from the abundances of clusters with $n \geq 32$ is shown in Figure 2b. These data are linear over nearly three orders of magnitude change in solution molar fraction and have a slope of 1.02 ($r^2 = 0.999$). This slope is close to the ideal slope of 1.00 indicating that the relative molar fractions can be determined from the cluster abundances with about 2% accuracy. In contrast, the slope for the molar fraction calculated from the abundances of the protonated monomer is 3.75 ($r^2 = 0.993$) indicating that preferential ionization of protonated L-threonine occurs consistently over this range of solution concentration. Data for the octamer has a slope of 1.41 ($r^2 = 0.994$), consistent with either preferential ionization of the heterogeneous octamer or preferential incorporation of L-threonine into the L-serine octamer. These data suggest that L-threonine does not significantly disrupt the structure of the octamer.

2.3.3 D-Threonine in L-Serine. Because of the strong propensity of serine octamers to form homochiral clusters, the effects of the chirality of an impurity molecule on incorporation into serine clusters, including the octamer, were investigated. Partial ESI mass spectra of 5.0% L-threonine and D-threonine in L-serine are shown in Figure 3a and 3b, respectively. Protonated homochiral serine octamer is most abundant, but protonated octamers that contain 1–3 L-threonine molecules but only 1–2 D-threonine octamers are also observed. The abundances of the heterogeneous octamer clusters containing L-threonine are significantly higher than those containing D-threonine indicating that the L-serine octamer has a clear preference for incorporating threonine that has the same chirality.

The measured % molar fraction of D-threonine as a function of cluster size for the 5.0% solution is shown in Figure 4a. As with L-threonine, the % molar fraction of D-threonine calculated from the very smallest clusters is higher than the solution value. In contrast, data for the octamer clearly show that D-threonine is excluded. For the larger clusters ($n \geq 32$), no chiral preference is apparent and the measured molar fraction calculated for these clusters is 5.5% ± 1.0%, consistent with the solution-phase molar fraction of 5.0%. Previously, it has been suggested that the octamer may be the building blocks for $[16Ser+2H]^{2+}$ and $[24Ser+3H]^{3+}$ due to their enhanced abundance compared to neighboring clusters of the same charge state, but this effect is significantly lower than for the octamer.[39,42] Interestingly, no significant chiral preference is observed for higher-order clusters with integer multiples of the octamer (n = 16, 24, 32, 40, etc.), indicating that octamers are not simply the building blocks for these higher-order clusters.

The measured % mole fraction of D-threonine in L-serine obtained from the protonated molecular ions, the octamer cluster, and clusters with $n \geq 32$ as a function of solution molar fraction from 0.05% to 20% are shown in Figure 4b. These data are linear and have slopes of 3.01 ($r^2 = 0.957$), 0.38 ($r^2 = 0.992$), and 1.05 ($r^2 = 0.999$),

respectively. Protonated D-threonine is preferentially ionized, but the low value for the octamer clearly indicates that it is significantly excluded. However, D-threonine is incorporated statistically into the larger clusters.

2.3.4 L-Leucine in L-Serine. To determine the effect of incorporation of an amino acid with an aliphatic side chain, ESI mass spectra were obtained from solutions consisting of 0.03% to 18% L-leucine in L-serine and the measured % molar fraction obtained from these data are shown in Figure 5. L-leucine is preferentially ionized at all concentrations, consistent with its higher surface activity or hydrophobicity, but this effect is greatest for a solution containing 0.17% L-leucine. At this concentration, the abundance of protonated L-leucine is 10.8% that of protonated L-serine indicating that protonated L-leucine is preferentially ionized/detected by factor of 54. The strong dependence of protonated L-leucine abundance on the solution composition illustrates the challenges of relating the abundance of protonated ions to their corresponding concentrations in solution.

In contrast, the measured % molar fraction for both the octamer and clusters with $n \geq 32$ are linear over this range of concentration with slopes of 0.90 ($r^2 = 0.993$) and 1.03 ($r^2 = 0.997$), respectively. This indicates that there is a slight propensity for the octamer to exclude L-leucine, but incorporation of L-leucine into the larger clusters is statistical.

2.3.5 L-Lysine in L-Serine. To determine the effect of incorporation of a basic amino acid, ESI mass spectra were obtained from solutions consisting of 0.04% to 18% L-lysine in L-serine and the measured % molar fraction obtained as a function of cluster size for the 4.3% solution molar fraction is shown in Figure 6a. Protonated L-lysine is 21-fold more abundant than protonated L-serine despite its much lower solution-phase concentration, likely owing to its significantly higher basicity. The difference in ionization efficiency depends on the relative molar fraction (Figure 6b) but L-lysine is more readily ionized and detected by as much as a factor of 460 over L-serine. However, incorporation of even a single L-lysine molecule into small serine clusters can greatly reduce this difference in ionization efficiency for the clusters (Figure 6a).

Results for both the octamer and higher-order clusters ($n \geq 32$) are shown in Figure 6b. These data can be fit with lines with slopes of 0.11 ($r^2 = 0.997$) and 0.93 ($r^2 = 1.00$), respectively. Thus, the L-serine octamer efficiently excludes L-lysine from these clusters whereas L-lysine is incorporated statistically into the larger clusters (within 7%) and effects of this incorporation on the ionization/detection efficiency of these clusters are small.

2.3.6 L-Glutamic Acid in L-Serine. As is the case for L-leucine and L-lysine, protonated L-glutamic acid is preferentially ionized and detected in ESI mass spectra when the molar fraction of L-glutamic acid is between 0.05% and 24%, and the relative ionization efficiency depends strongly on concentration. The proton affinity of L-glutamic acid is higher than that of L-serine[61] owing to the ability of the side-chain oxygen atoms to solvate the charge in glutamic acid,[63] and the higher proton affinity of L-glutamic acid is the likely origin of the significantly higher ionization efficiency. This effect, as well as any effects of specific clustering, becomes negligible at larger cluster size (Figure 7a).

Data for the octamer and larger clusters ($n \geq 32$) as a function of solution molar fraction can be fit to lines with slopes of 0.40 ($r^2 = 0.991$) and 0.90 ($r^2 = 0.999$) (Figure 7b). As was the case for L-lysine, the octamer preferentially excludes L-glutamic acid but incorporation of this amino acid into the larger clusters approaches the statistical value within 10%.

2.3.7 GlyGly in Serine. To determine the effects of incorporation of a small peptide into serine clusters, ESI mass spectra of diglycine at % molar fractions between 0.05% and 5.0% were obtained and these data are summarized in Figure 8. Protonated diglycine is preferentially ionized over protonated L-serine at all concentrations, consistent with its higher surface activity or hydrophobicity, but the ionization efficiency depends on the % molar fraction. At 0.05% molar fraction, diglycine is preferentially ionized/detected by a factor of 93 over L-serine. In contrast, the protonated octamer and larger cluster ($n \geq 32$) data can be fit to lines with slopes of 0.01 ($r^2 = 0.898$), and 1.01 ($r^2 = 0.999$), respectively. The much higher discrimination of the octamer for the dipeptide vs. the amino acids investigated indicates that this dipeptide causes a greater disruption of the very stable octamer structure. In striking contrast, the larger serine clusters can incorporate this dipeptide readily and the % molar fraction determined from the larger cluster data is within 1% of the solution-phase % molar fraction.

2.4 Conclusions

Quantifying the relative concentrations of components in solution using ESI mass spectrometry is challenging owing to many different factors that affect relative ionization/detection efficiencies, including molecular structure, matrix effects, instrumental parameters, etc. A newly introduced standard-free quantitation method, which uses the abundances of larger molecular clusters formed by ESI to obtain relative solution-phase molar fractions,[37] was investigated using L-serine as a major component. Serine has a strong propensity to form “magic” number clusters that show either homo- or heterochiral preferences and is a rigorous test of this method, which requires that impurity molecules are incorporated statistically and do not influence the ionization/detection efficiency of larger clusters. Incorporation of aliphatic, basic and acidic amino acids, and a dipeptide, into larger serine clusters is statistical and the abundances of these clusters reflect the solution-phase molar fractions with better than 10% accuracy over nearly three orders of magnitude in concentration. By comparison, some of the protonated molecular ions in these mixtures were ionized/detected up to a factor of 460 more efficiently than protonated serine under these experimental conditions. The octamer effectively included some amino acids but excluded others. Although the octamer is chirally selective, higher-order serine clusters incorporated threonine molecules of the opposite chirality statistically. The results obtained from amino acids that have significantly different physical properties using serine that has by far the highest propensity to form “magic” number clusters of any of the amino acids suggest that this standard-free quantitation method should be generally applicable to a broad range of analytes.

Although not as accurate or as generally applicable as methods that employ internal standards, this standard-free quantitation method has the advantages that reasonably accurate quantitative information can rapidly be obtained directly from an

ESI mass spectrum with no prior knowledge of the composition or the identity of the impurity molecules necessary, making it applicable to a wide range of analytical problems. This method also significantly reduces effects of instrument or detector mass bias, but does require high resolution in order to identify the charge states and compositions of larger clusters. This standard-free cluster quantitation method may be particularly useful in molecular synthesis because unreacted starting materials, intermediates, degraded or modified catalysts or unintended products of side reactions could be quantified directly from an ESI mass spectrum. This method would be especially advantageous when some of the reaction products are unknown or when appropriate standards are not readily available. Absolute concentrations of each individual component could be obtained by spiking the solutions with a known concentration of a clustering agent, such as serine, at relatively high concentrations like those used here. From the relative molar fractions of each component determined from the abundances of larger clusters, the absolute concentration of each component could be obtained. The sensitivity and accuracy of this method could be improved on trapping mass spectrometers by selectively introducing higher m/z ions into the ion cell. The m/z of clusters generally increases with cluster size[62] making it possible to selectively introduce larger clusters that should have compositions more representative of analyte concentrations in solution. The abundances of larger clusters could also be increased by using other ionization methods, such as sonic spray.[48] It is likely that other molecules that have an even greater propensity to form large clusters could be identified and different agents with physical properties matching those of molecules suspected to be present in mixtures of unknowns could be used.

The statistical incorporation of analytes into the larger clusters suggests that these clusters are formed by solvent evaporation from larger droplets whose composition reflects that of the original bulk solution, i.e., a charge residue mechanism.[7-12] Solvent evaporation from a droplet formed by ESI would increase the concentration of the analytes and ultimately, the resulting charged clusters formed from the nonvolatile analytes should reflect the original solution-phase composition.

2.5 References

(1) Bowers, M. T.; Marshall, A. G.; McLafferty, F. W. *J. Phys. Chem.* **1996**, *100*, 12897-12910.
(2) Aebersold, R.; Mann, M. *Nature* **2003**, *422*, 198-207.
(3) Valaskovic, G. A.; Kelleher, N. L.; McLafferty, F. W. *Science* **1996**, *273*, 1199-1202.
(4) Kim, S.; Rodgers, R. P.; Marshall, A. G. *Int. J. Mass Spectrom.* **2006**, *251*, 260-265.
(5) Kelleher, N. L.; Lin, H. Y.; Valaskovic, G. A.; Aaserud, D. J.; Fridriksson, E. K.; McLafferty, F. W. *J. Am. Chem. Soc.* **1999**, *121*, 806-812.
(6) Sleno, L.; Volmer, D. A. *J. Mass Spectrom.* **2004**, *39*, 1091-1112.
(7) Fenn, J. B. *J. Am. Soc. Mass Spectrom.* **1993**, *4*, 524-535.
(8) Cech, N. B.; Enke, C. G. *Mass Spectrom. Rev.* **2001**, *20*, 362-387.
(9) Kebarle, P. *J. Mass Spectrom.* **2000**, *35*, 804-817.
(10) Iavarone, A. T.; Williams, E. R. *J. Am. Chem. Soc.* **2003**, *125*, 2319-2327.
(11) Cole, R. B. *J. Mass Spectrom.* **2000**, *35*, 763-772.
(12) Spencer, E. A. C.; Ly, T.; Julian, R. R. *Int. J. Mass Spectrom.* **2008**, *270*, 166-172.
(13) Hogan, C. J.; Carroll, J. A.; Rohrs, H. W.; Biswas, P.; Gross, M. L. *J. Am. Chem. Soc.* **2008**, *130*, 6926-6927.
(14) Cech, N. B.; Enke, C. G. *Anal. Chem.* **2000**, *72*, 2717-2723.
(15) Cech, N. B.; Enke, C. G. *Anal. Chem.* **2001**, *73*, 4632-4639.
(16) Cheng, J.; Vecitis, C. D.; Hoffmann, M. R.; Colussi, A. J. *J. Phys. Chem. B* **2006**, *110*, 25598-25602.
(17) Tang, L.; Kebarle, P. *Anal. Chem.* **1993**, *65*, 3654-3668.
(18) Amad, M. H.; Cech, N. B.; Jackson, G. S.; Enke, C. G. *J. Mass Spectrom.* **2000**, *35*, 784-789.
(19) Iavarone, A. T.; Jurchen, J. C.; Williams, E. R. *J. Am. Soc. Mass Spectrom.* **2000**, *11*, 976-985.
(20) Grandori, R. *J. Mass Spectrom.* **2003**, *38*, 11-15.
(21) Konermann, L.; Douglas, D. J. *Biochemistry* **1997**, *36*, 12296-12302.
(22) Kuprowski, M. C.; Boys, B. L.; Konermann, L. *J. Am. Soc. Mass Spectrom.* **2007**, *18*, 1279-1285.
(23) Pan, P.; McLuckey, S. A. *Anal. Chem.* **2003**, *75*, 5468-5474.
(24) King, R.; Bonfiglio, R.; Fernandez-Metzler, C.; Miller-Stein, C.; Olah, T. *J. Am. Soc. Mass Spectrom.* **2000**, *11*, 942-950.
(25) Iavarone, A. T.; Jurchen, J. C.; Williams, E. R. *Anal. Chem.* **2001**, *73*, 1455-1460.
(26) Iavarone, A. T.; Udekwu, O. A.; Williams, E. R. *Anal. Chem.* **2004**, *76*, 3944-3950.
(27) Belov, M. E.; Nikolaev, E. N.; Harkewicz, R.; Masselon, C. D.; Alving, K.; Smith, R. D. *Int. J. Mass Spectrom.* **2001**, *208*, 205-225.
(28) Marshall, A. G.; Hendrickson, C. L.; Jackson, G. S. *Mass Spectrom. Rev.* **1998**, *17*, 1-35.

(29) Page, J. S.; Kelly, R. T.; Tang, K.; Smith, R. D. *J. Am. Soc. Mass Spectrom.* **2007**, *18*, 1582-1590.
(30) Gygi, S. P.; Rist, B.; Gerber, S. A.; Tureček, F.; Gelb, M. H.; Aebersold, R. *Nature Biotech.* **1999**, *17*, 994-999.
(31) Han, D. K.; Eng, J.; Zhou, H. L.; Aebersold, R. *Nature Biotech.* **2001**, *19*, 946-951.
(32) Ishihama, Y.; Sato, T.; Tabata, T.; Miyamoto, N.; Sagane, K.; Nagasu, T.; Oda, Y. *Nature Biotech.* **2005**, *23*, 617-621.
(33) Ong, S. E.; Kratchmarova, I.; Mann, M. *J. Proteome Res.* **2003**, *2*, 173-181.
(34) Havliš, J.; Shevchenko, A. *Anal. Chem.* **2004**, *76*, 3029-3036.
(35) Görög, S. *Anal. Bioanal. Chem.* **2003**, *377*, 852-862.
(36) Görög, S. *J. Pharm. Biomed. Anal.* **2008**, *48*, 247-253.
(37) Leib, R. D.; Flick, T. G.; Williams, E. R. *Anal. Chem.* **2009**, *81*, 3965-3972.
(38) Shi, Z.; Ford, J. V.; Wei, S.; Castleman Jr., A. W. *J. Chem. Phys.* **1993**, *99*, 8009-8015.
(39) Koch, K. J.; Gozzo, F. C.; Zhang, D. X.; Eberlin, M. N.; Cooks, R. G. *Chem. Commun.* **2001**, 1854-1855.
(40) Cooks, R. G.; Zhang, D. X.; Koch, K. J.; Gozzo, F. C.; Eberlin, M. N. *Anal. Chem.* **2001**, *73*, 3646-3655.
(41) Hodyss, R.; Julian, R. R.; Beauchamp, J. L. *Chirality* **2001**, *13*, 703-706.
(42) Counterman, A. E.; Clemmer, D. E. *J. Phys. Chem. B* **2001**, *105*, 8092-8096.
(43) Julian, R. R.; Hodyss, R.; Kinnear, B.; Jarrold, M. F.; Beauchamp, J. L. *J. Phys. Chem. B* **2002**, *106*, 1219-1228.
(44) Julian, R. R.; Myung, S.; Clemmer, D. E. *J. Am. Chem. Soc.* **2004**, *126*, 4110-4111.
(45) Concina, B.; Hvelplund, P.; Nielsen, A. B.; Nielsen, S. B.; Rangama, J.; Liu, B.; Tomita, S. *J. Am. Soc. Mass Spectrom.* **2006**, *17*, 275-279.
(46) Nanita, S. C.; Cooks, R. G. *Angew. Chem. Int. Ed.* **2006**, *45*, 554-569.
(47) Nemes, P.; Schlosser, G.; Vekey, K. *J. Mass Spectrom.* **2005**, *40*, 43-49.
(48) Myung, S.; Julian, R. R.; Nanita, S. C.; Cooks, R. G.; Clemmer, D. E. *J. Phys. Chem. B* **2004**, *108*, 6105-6111.
(49) Nanita, S. C.; Sokol, E.; Cooks, R. G. *J. Am. Soc. Mass Spectrom.* **2007**, *18*, 856-868.
(50) Takats, Z.; Nanita, S. C.; Cooks, R. G.; Schlosser, G.; Vekey, K. *Anal. Chem.* **2003**, *75*, 1514-1523.
(51) Perry, R. H.; Wu, C. P.; Nefliu, M.; Cooks, R. G. *Chem. Commun.* **2007**, 1071-1073.
(52) Takats, Z.; Cooks, R. G. *Chem. Commun.* **2004**, 444-445.
(53) Yang, P. X.; Xu, R. F.; Nanita, S. C.; Cooks, R. G. *J. Am. Chem. Soc.* **2006**, *128*, 17074-17086.
(54) Mazurek, U.; Geller, O.; Lifshitz, C.; McFarland, M. A.; Marshall, A. G.; Reuben, B. G. *J. Phys. Chem. A* **2005**, *109*, 2107-2112.
(55) Mazurek, U.; Engeser, M.; Lifshitz, C. *Int. J. Mass Spectrom.* **2006**, *249*, 473-476.

(56) Takats, Z.; Nanita, S. C.; Schlosser, G.; Vekey, K.; Cooks, R. G. *Anal. Chem.* **2003**, *75*, 6147-6154.
(57) Kong, X. L.; Tsai, I. A.; Sabu, S.; Han, C. C.; Lee, Y. T.; Chang, H. C.; Tu, S. Y.; Kung, A. H.; Wu, C. C. *Angew. Chem. Int. Ed.* **2006**, *45*, 4130-4134.
(58) Julian, R. R.; Myung, S.; Clemmer, D. E. *J. Phys. Chem. B* **2005**, *109*, 440-444.
(59) Schalley, C. A.; Weis, P. *Int. J. Mass Spectrom.* **2002**, *221*, 9-19.
(60) Jurchen, J. C.; Williams, E. R. *J. Am. Chem. Soc.* **2003**, *125*, 2817-2826.
(61) Bleiholder, C.; Suhai, S.; Paizs, B. *J. Am. Soc. Mass Spectrom.* **2006**, *17*, 1275-1281.
(62) Jurchen, J. C.; Garcia, D. E.; Williams, E. R. *J. Am. Soc. Mass Spectrom.* **2003**, *14*, 1373-1386.
(63) O'Brien, J. T.; Prell, J. S.; Steill, J. D.; Oomens, J.; Williams, E. R. *J. Phys. Chem. A* **2008**, *112*, 10823-10830.

2.6 Figures

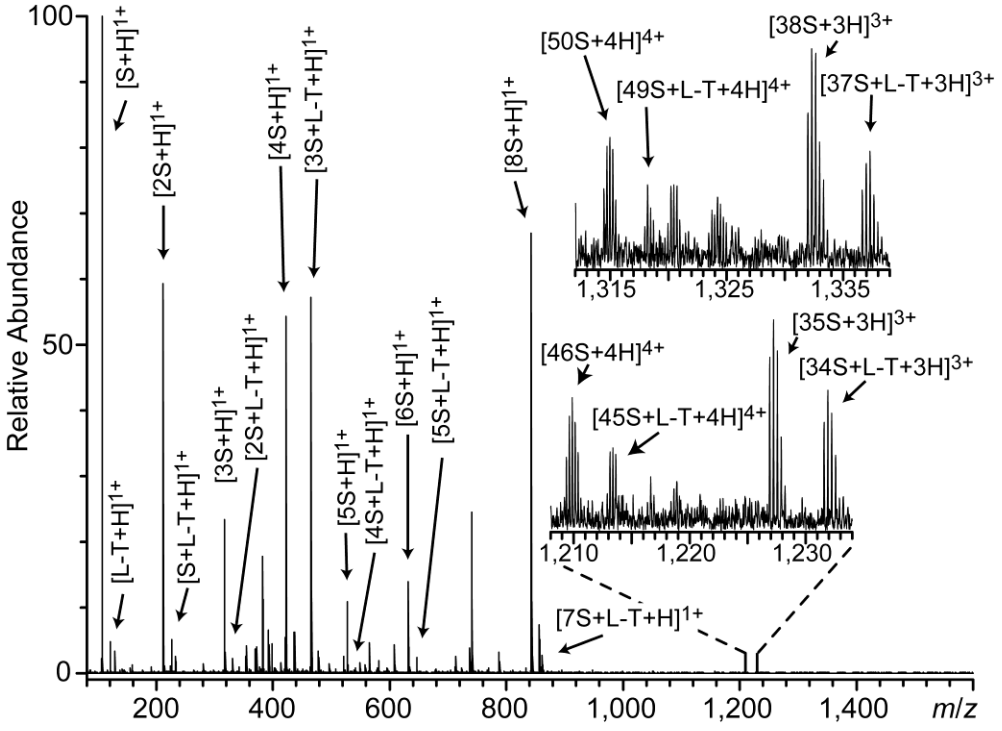

Figure 2.1. ESI mass spectrum of a solution containing 1.0% molar fraction of L-threonine in L-serine (3.0 mM total peptide concentration) with some regions of the spectra with large molecular clusters inset.

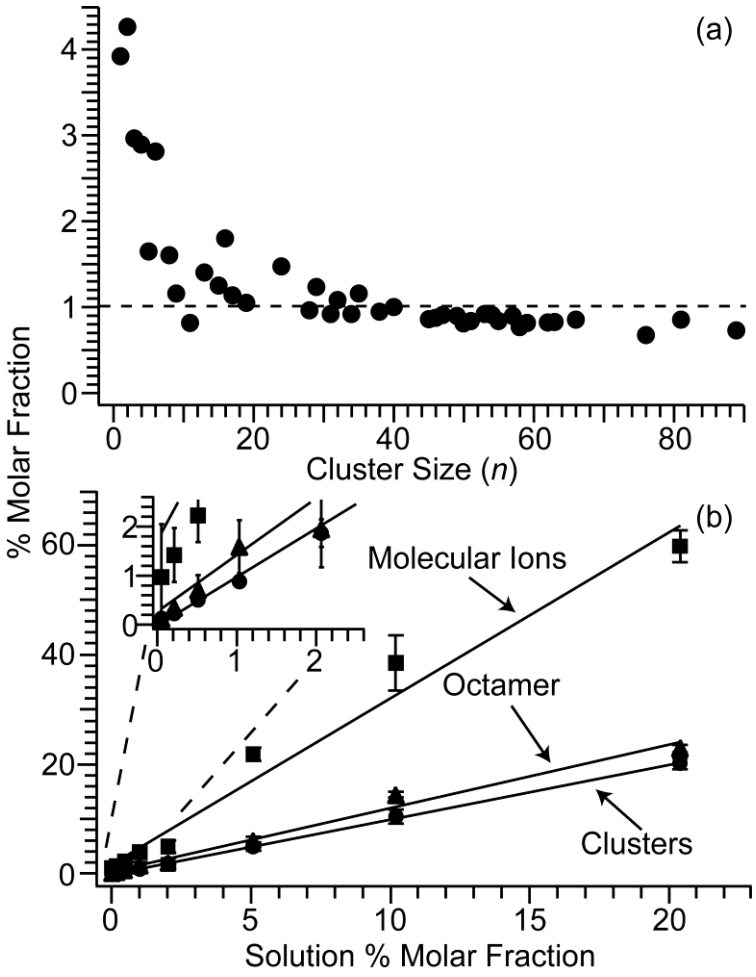

Figure 2.2. (a) Percent molar fractions calculated from the cluster ion abundances assuming statistical incorporation and identical ionization efficiencies obtained from ESI mass spectra of a 1.0% molar fraction of L-threonine in L-serine (3.0 mM total peptide) as a function of cluster size, *n*. The dashed line corresponds to the solution % molar fraction. (b) Percent molar fractions of L-threonine in L-serine obtained from the protonated molecular ions (squares), from protonated octamer (triangles), and from cluster abundances for $n \geq 32$ (circles) as a function of the solution % molar fraction. These data are linear with slopes of 3.75, 1.41, and 1.02 for the protonated molecular ions, protonated octamer, and clusters with $n \geq 32$, respectively. Error bars correspond to a standard deviation of three spectra acquired at dc offset voltages of 4.5, 4.8, and 5.2 V.

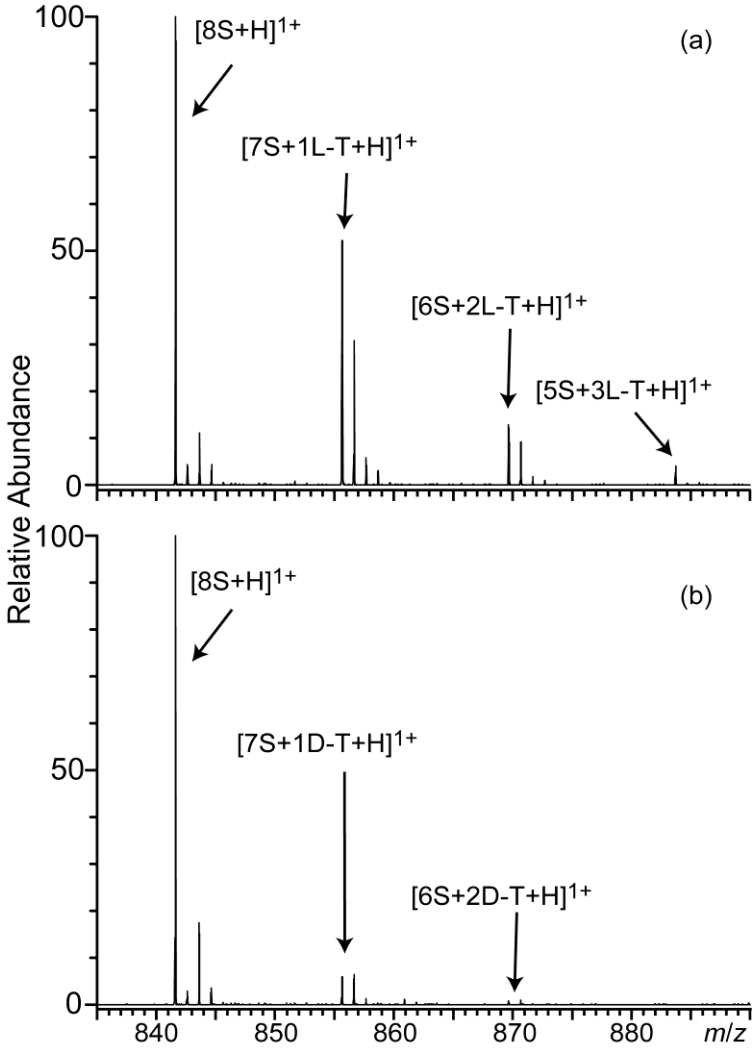

Figure 2.3. Partial ESI mass spectra of solutions containing 5.0% molar fraction of L-threonine (top) and D-threonine (bottom) in L-serine (3.0 mM total peptide concentration) showing homogeneous and heterogenous clusters of protonated octamer.

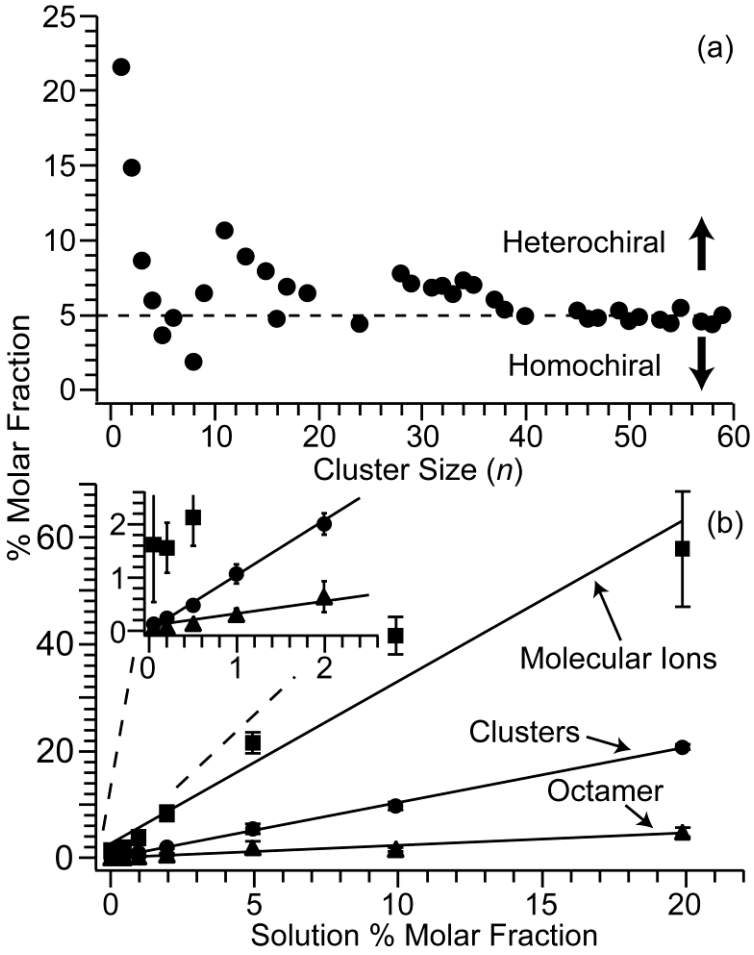

Figure 2.4. (a) Percent molar fractions calculated from cluster ion abundances obtained from ESI mass spectra of a 5.0% molar fraction of D-threonine with L-serine (3.0 mM total peptide concentration) as a function of cluster size, *n*. The dashed line corresponds to the % molar fraction in solution. (b) Percent molar fractions of D-threonine in L-serine calculated from the protonated molecular ions (squares), from protonated octamers (triangles), and from cluster abundances for $n \geq 32$ as a function of the solution % molar fraction. These data are linear with slopes of 3.01, 0.38, and 1.05 for the protonated molecular ions, protonated octamers, and cluster abundances for $n \geq 32$, respectively.

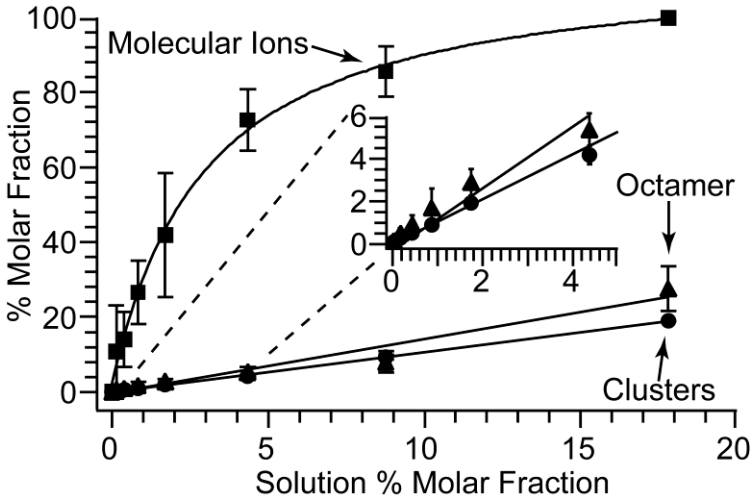

Figure 2.5. Percent molar fractions of L-leucine in L-serine obtained from the protonated molecular ions (squares), from protonated octamers (triangles), and from cluster abundances for $n \geq 32$ (circles) as a function of the solution % molar fraction. The data from protonated octamers and cluster abundances for $n \geq 32$ are linear with slopes of 0.90 and 1.03, respectively. Data for the molecular ions are non-linear and at the 0.17% molar fraction, L-leucine is preferentially ionized/detected by a factor of 63 over L-serine.

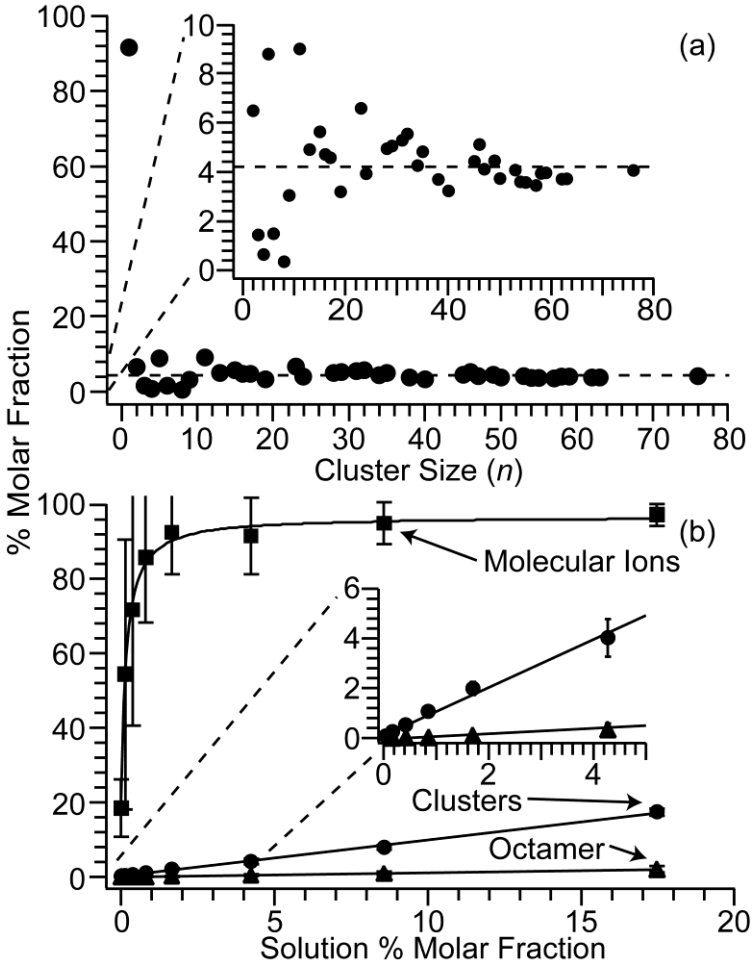

Figure 2.6. (a) Percent molar fractions calculated from cluster ion abundances obtained from ESI mass spectra of a 4.3% molar fraction of L-lysine with L-serine (3.0 mM total peptide concentration) as a function of cluster size, *n*. The dashed line corresponds to the % molar fraction in solution. (b) Percent molar fractions of L-lysine in L-serine calculated from the protonated molecular ions (squares), from protonated octamers (triangles), and from cluster ion abundances (circles) for $n \geq 32$ as a function of the % molar fraction in solution. Data for the protonated octamers and larger clusters ($n \geq 32$) are linear with slopes of 0.11 and 0.93, respectively. Data for the molecular ions are non-linear and at 0.04% molar fraction, L-lysine is preferentially ionized/detected by a factor of 460 over L-serine.

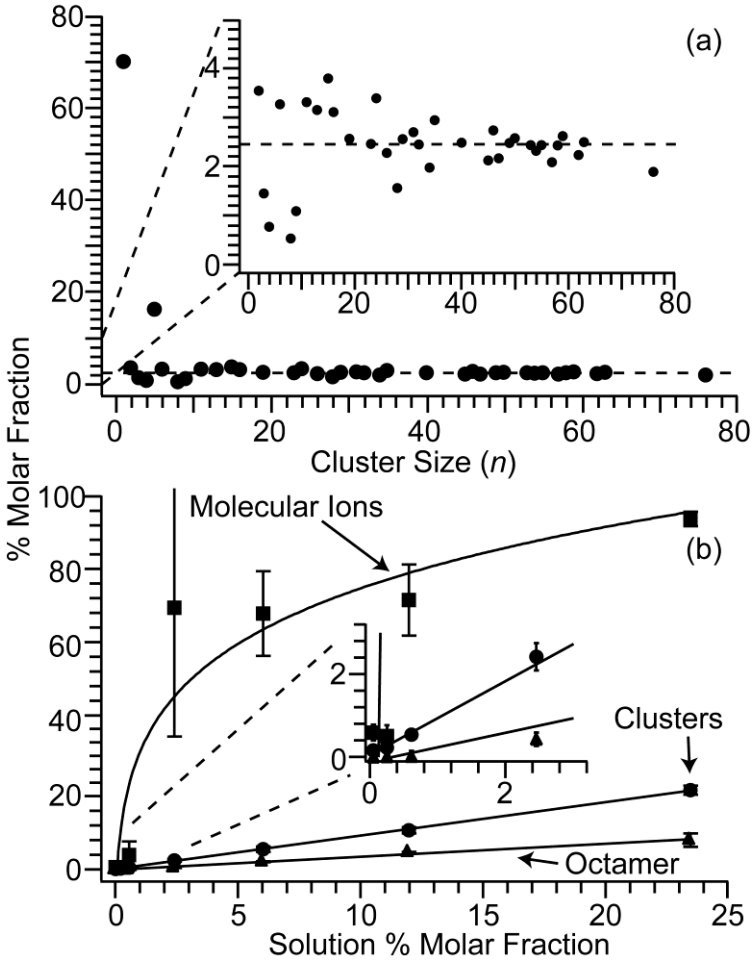

Figure 2.7. (a) Percent molar fractions calculated from cluster ion abundances obtained from ESI mass spectra of a 2.5% molar fraction of L-glutamic acid with L-serine (3.0 mM total peptide concentration) as a function of cluster size, *n*. The dashed line corresponds to the % molar fraction in solution. (b) Percent molar fractions of L-glutamic acid in L-serine calculated from the protonated molecular ions (squares), from protonated octamers (triangles), and from cluster ion abundances (circles) for $n \geq 32$ as a function of the % molar fraction in solution. Data for the protonated octamers and larger clusters ($n \geq 32$) are linear with slopes of 0.40 and 0.90, respectively. Data for the molecular ions are non-linear and at 2.5% molar fraction, L-glutamic acid is preferentially ionized/detected by a factor of 29 over L-serine.

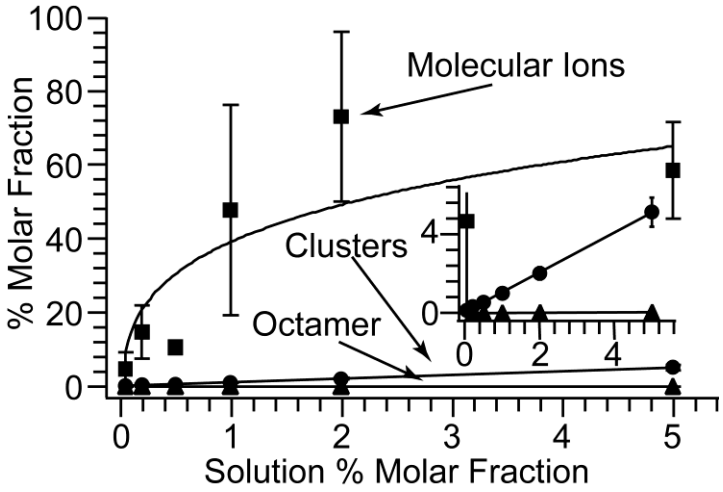

Figure 2.8. Percent molar fractions of Gly-Gly in L-serine obtained from the protonated molecular ions (squares), from protonated octamers (triangles), and from cluster abundances for $n \geq 32$ as a function of the solution % molar fraction. The data from protonated octamers and cluster abundances $n \geq 32$ are linear with slopes of 0.01 and 1.01, respectively. Data for the molecular ions are non-linear and at 0.05% molar fraction, diglycine is preferentially ionized/detected by a factor of 93 over L-serine.

CHAPTER 3

Direct Standard-Free Quantitation of Tamiflu and Other Pharmaceutical Tablets Using Clustering Agents with Electrospray Ionization Mass Spectrometry

(This chapter is reproduced with permission from Flick, T.G.; Leib, R.D.; Williams, E.R. *Anal. Chem.* **2009**, *81*, 8434-8440.

3.1 Introduction

Accurate and rapid quantitation of small molecules in pharmaceutical mixtures is critical to the entire drug development process[1-2] and is important for identifying counterfeit or substandard pharmaceutical drugs.[3-7] The high demand and cost and limited availability of many pharmaceutical drugs used to treat major diseases provide incentives to produce counterfeit drugs and motivate the low quality production of the active ingredient once a drug is no longer under patent protection.[3-7] The individuals most at risk of exposure to counterfeit or substandard drugs are from impoverished countries.[3-7] It is estimated that between 6% and 15% of all medicines are counterfeit,[7-8] and it is thought counterfeit medicines can exceed 50% in Asia and Africa.[7] Substances used to adulterate pharmaceutical drugs can include highly toxic substances, leading to unnecessary mortality, which lowers public confidence in legitimate medicines.[3-7] Counterfeit drugs can also lead to drug resistance due to extended exposure to low dosages of active ingredients without physical improvement; this is particularly harmful for patients who require therapy programs for AIDS and malaria.[3] Currently, Tamiflu is in short supply as countries gather stockpiles of the drug in fear of the H1N1 flu pandemic, which could lead to an increase in counterfeit tablets.[9] Counterfeit drugs can potentially be identified either by visual inspection or by the absence of an active ingredient. However, counterfeit drugs that pass visual inspection but contain the active ingredient at substantially lower levels can be more challenging to identify if suitable standards are not available. Therefore, new analytical methods that increase the speed and accessibility with which quantitative information can be obtained to meet increasing analytical demands are important.

Mass spectrometry (MS) has several advantages for analyzing pharmaceutical components in complex mixtures, including high sensitivity, selectivity, and speed.[2] With electrospray ionization (ESI), a wide range of thermally labile molecules can be ionized and information about elemental composition and structure can be obtained from exact mass and tandem MS measurements.[10-11] The abundances of ions in ESI mass spectra depend on many factors. Molecules that are more basic, or that have high surface activities or hydrophobicities, are more readily ionized,[12-16] and the ionization efficiency depends on the analyte conformation and concentration and the solution composition or matrix as well.[17-20] Mass-dependent ion transmission and detection also affect the measured ion abundances.[16] Because of these and other factors, obtaining quantitative information about the concentrations of analytes in solution directly from the corresponding ion abundances in the mass spectrum is

challenging without the use of standards, such as isotopically labeled molecules or molecules that have structures or properties similar to those of the analytes of interest.[21]

A new standard-free quantitation method to obtain the relative solution-phase concentrations of components in a mixture using the abundances of clusters formed by ESI was recently introduced.[22-23] The composition of large, nonspecific clusters can reflect the solution-phase composition, and differences in ionization/detection and transmission efficiencies are significantly reduced. Using this method, solution-phase mole fractions can be obtained with better than 10-20% accuracy even in cases where the ionization/detection efficiency of the individual components differed by up to a factor of 460.[23] This quantitation method has several important advantages, including that no conventional reference standard is required, the components in the mixtures do not need to be identified, and effects of instrument and detector mass bias are significantly reduced. Although not as accurate as methods that use standards, this method provides reasonable quantitative information about mixtures with very little time and effort. Here, we demonstrate this standard-free quantitation method for the analysis of the pharmaceutical over-the-counter and prescription drug formulations Tamiflu, Sudafed, and Dramamine directly without conventional standards or chromatographic separations.

3.2 Experimental

Experiments were performed on a 9.4 T Fourier-transform ion cyclotron resonance mass spectrometer described elsewhere.[24] Tamiflu, Sudafed Sinus and Allergy, and Dramamine (generic) tablets were dissolved in water to a final concentration of 10 mM for at least one of their active ingredients, sonicated for 30-60 min. and filtered (0.45 μm). The filtrate was spiked into solutions containing 10 mM of L-phenylalanine, L-tryptophan, L-serine, or prednisone to a calculated % mole fraction for the active ingredient between 0.2% and 2.3%. A low % mole fraction was used to reduce the effects of sodium from the tablets on cluster adduction, which unnecessarily congests the mass spectral data. These clustering agents were chosen because they are inexpensive and readily available and the three amino acids are known to form clusters.[25] Multiple ESI mass spectra of each of these solutions were obtained using conditions described previously (see also the Supporting Information).[22-23]

3.3 Results and Discussion

3.3.1 ESI Mass Spectra of Dissolved Tablets. Active ingredients in pharmaceutical tablets are expected to be water-soluble, and ESI mass spectra of filtered aqueous solutions in which tablets of Tamiflu, Sudafed, and Dramamine were individually dissolved have ions corresponding to their active ingredients (Figure 3.1). Protonated oseltamivir, the only active ingredient in Tamiflu (30 mg), is the predominant ion in the mass spectrum. Both protonated phenylephrine and chlorpheniramine, the two active ingredients in Sudafed at 10 and 4 mg, respectively, are formed, but the abundances of these ions do not reflect the relative dosages of these molecules in the tablet. The mole ratio of these active ingredients is ~12:1

(phenylephrine:chlorpheniramine) in the tablet, but the relative ion abundance is ~1:4. For Dramamine, which contains 50 mg of dimenhydrinate, a salt of diphenhydramine and 8-chlorotheophylline, the mass spectrum contains sodiated diphenhydramine, but no 8-chlorotheophylline is observed. Although the active ingredients in each of these tablets can be readily identified by ESI-MS, except in the case of Dramamine, for which only one salt component forms a positive ion, the concentration of these ingredients cannot be deduced from these mass spectral data alone.

3.3.2 Tablet Dosage from Cluster Ion Abundances. The concentration of the active ingredient in each of these tablets can be obtained by adding a known concentration of a clustering agent to these solutions. If clusters formed with this added agent incorporate the drug molecules nonspecifically and ionization/detection efficiencies do not depend significantly on the cluster composition, then the % mole fraction, F_m (%), of the drug in the solution can be obtained from the abundances and composition of the clusters using a weighted average:

$$F_m\% = \frac{\sum_h A_h \frac{h}{n}}{\sum_h A_h} \times 100$$

Equation 1.

where A is the abundance of each observed cluster consisting of n total molecules with h molecules of the minor fraction component.[22-23]

3.3.3 Tamiflu. An ESI mass spectrum of a solution containing Tamiflu and L-tryptophan in which the calculated % mole fraction of the active ingredient, oseltamivir, is 1.3% is shown in Figure 3.2a. In this spectrum, the relative abundance of protonated oseltamivir is ~1.6× greater than that of protonated L-tryptophan, indicating that oseltamivir has a 160× greater ionization/detection efficiency under these conditions. In addition to the protonated molecules, homogenous L-tryptophan clusters and heterogeneous clusters containing both L-tryptophan and oseltamivir are observed. From the abundances of these clusters, the % mole fraction of oseltamivir can be determined assuming that this molecule incorporates statistically into L-tryptophan clusters. These data as a function of cluster size are shown in Figure 3.2b. For clusters containing fewer than 10 molecules, the values are higher than the solution-phase value, which indicates that either the smaller clusters containing oseltamivir are more readily ionized or that oseltamivir is preferentially incorporated into these smaller clusters. Both the significantly higher ionization efficiency of oseltamivir and the trend in these data with increasing cluster size suggest that this is an effect of ionization efficiency. The average % mole fraction determined from the larger clusters ($n \geq 20$) is 1.4 ± 0.6%, from which a dosage in the original tablet of 32 ± 13 mg of oseltamivir is obtained. This value is 7% higher than the actual value of 30 mg in the Tamiflu tablet.

Similar results were obtained using L-phenylalanine and prednisone as clustering agents. Measured % mole fractions of 1.2 ± 0.4% and 1.3 ± 0.2% were obtained from clusters with $n \geq 20$ and $n \geq 13$ for L-phenylalanine and prednisone, respectively (Figure 3.3), from which oseltamivir dosages in the Tamiflu tablet of 28 ± 9 and 35 ± 6 mg were

obtained. L-serine was also evaluated as a clustering agent,[23] but remarkably, no higher order clusters were observed. This is likely the result of the much higher ionization efficiency of the minor constituent oseltamivir compared to L-serine.

3.3.4 Sudafed. An ESI mass spectrum of a solution containing Sudafed and L-tryptophan is shown in Figure 3.4a. The abundances of protonated molecules of the two active ingredients phenylephrine and chlorpheniramine are 52% and 44% of protonated L-tryptophan, despite the ~100× higher concentration of L-tryptophan, indicating that both active ingredients are preferentially ionized/detected. Clusters consisting of up to 39 molecules are also observed. Although protonated chlorpheniramine is formed by ESI, the intact salt chlorpheniramine maleate incorporates into the L-tryptophan clusters. The % mole fraction determined from the cluster abundances as a function of the cluster size are shown in parts b and c of Figure 3.4 for phenylephrine and chlorpheniramine maleate, respectively. The values for the smallest clusters are too high, likely a result of preferential ionization of clusters that contain the more readily ionized molecules at small sizes. However, these values approach the solution-phase values at larger clusters sizes, indicating that incorporation into these larger clusters is statistical and that differences in ionization efficiencies are greatly reduced. A % mole fraction calculated from the higher order clusters ($n \geq 21$) results in values of 1.1 ± 0.4% and 0.45 ± 0.15% for these respective active ingredients. From these values, the measured dosages obtained from the Sudafed tablet that contains 10 mg of phenylephrine hydrochloride and 4 mg of chlorpheniramine maleate are 8.7 ± 2.9 and 7.0 ± 2.3 mg, respectively.

Similar results were obtained using L-phenylalanine and prednisone as clustering agents. For L-phenyalanine, dosages of 7.5 ± 1.9 and 6.3 ± 1.6 mg were obtained for phenylephrine hydrochloride and chlorpheniramine maleate, respectively, from clusters with $n \geq 11$. From prednisone clusters with 10 or more molecules, values of 12.4 ± 3.4 and 7.2 ± 1.2 mg were obtained for these respective ingredients. For all three clustering agents, the value obtained for chlorpheniramine maleate is slightly higher than the actual value and these data are remarkably self-consistent. These results indicate that some preferential incorporation of this active ingredient into all of these clusters may occur, or the higher ionization efficiency of chlorpheniramine has a similar effect on these clusters irrespective of the clustering agent. No higher order clusters were observed with L-serine as a clustering agent, likely due to the significantly lower ionization efficiency of L-serine compared to the two active ingredients.

3.3.5 Dramamine. The % mole fraction obtained as a function of the cluster size for dimenhydrinate using L-tryptophan and L-phenylalanine as clustering agents are shown in parts a and b of Figure 3.5, respectively. In these solutions, the % mole fraction of dimenhydrinate is 1.1% and 1.0%, respectively. Dimenhydrinate is preferentially ionized over both of these clustering agents, and the smaller clusters appear to reflect this preferential ionization efficiency. However, the % mole fractions obtained for clusters with 10 or more molecules are remarkably constant, indicating that this effect is negligible for these larger clusters. Using data obtained from higher-order clusters ($n \geq 20$), % mole fractions of 1.2 ± 0.3% and 1.2 ± 0.4% are obtained with L-tryptophan and L-phenylalanine, respectively. From these respective values, dosages

of 56 ± 14 and 59 ± 18 mg are obtained. These values are slightly higher than the actual value of 50 mg of dimenhydrinate. As was the case for the solutions containing the other drugs, no clusters were observed with L-serine.

3.4 Conclusions

The dosage of active ingredients in several pharmaceutical tablets can be obtained without conventional standards or separation of the active ingredients from salts and other inactive ingredients by adding a clustering agent to filtered solutions containing dissolved tablets and obtaining the % mole fraction from the abundance and composition of large clusters. Internal calibrants are often considered to be the "gold standard" of quantitation, but analysis with external standards is routinely used even though in some cases they might not be as accurate. There are trade-offs between ease-of-use and accuracy. This method is not as accurate or precise as methods that use conventional standards. This standard-free quantitation method has the advantages that it is fast, simple, and applicable to solutions containing unknown compounds or to solutions containing compounds where suitable standards may not be readily available, such as schedule I or II controlled substances or new designer drugs that have not been previously identified. This method does require enough resolution to separate clusters with different chemical compositions, including salt adducts, and the resolution required will depend on the complexity of the sample. Sufficient resolution for these analyses could also be obtained with orbitrap or high-resolution time-of-flight mass spectrometers. The relatively poor precision in these initial studies can be attributed to the relatively low S/N ratio for the larger clusters owing to the low concentration of the active ingredient used. Higher concentrations were not used because of potential mass interferences owing to salt adduction from the inactive ingredients, which complicate the mass spectra. If these salts were removed prior to analysis, higher concentrations could be used, which should greatly improve the precision of these measurements. A separation was not used here because oseltamivir phosphate, the active ingredient in Tamiflu, is a prescription drug and is not readily available in pure form, but the label claim is expected to be sufficiently accurate to demonstrate the potential of this standard-free quantitation method. Tryptophan, phenylalanine, and prednisone were found to be suitable clustering agents, although serine and small peptides were ineffective, perhaps because of their significantly different physical properties, including lower ionization efficiency or larger differences in molecular weight compared to the drugs of interest. Further investigations into molecular properties that enhance formation of large, nonspecific clusters could improve the accuracy and would be advantageous to making this standard-free quantitation method a rapid and reasonably accurate method to obtain quantitative information directly from a wide range of analytes.

3.5 References

(1) Görög, S. *J. Pharm. Biomed. Anal.* **2008,** *48*, 247-253.
(2) Lee, M. S.; Kerns, E. H. *Mass Spectrom. Rev.* **1999,** *18*, 187-279.
(3) Newton, P. N.; Green, M. D.; Fernandez, F. M.; Day, N. P. J.; White, N. J. *Lancet Infect. Dis.* **2006,** *6*, 602-613.
(4) Land, T. *Nature* **1992,** *355*, 192-192.
(5) Seiter, A. *Clin. Pharmacol. Ther.* **2009,** *85*, 576-578.
(6) Ye, H.; Hill, J.; Kauffman, J.; Gryniewicz, C.; Han, X. *Anal. Biochem.* **2008,** *379*, 182-191.
(7) Cockburn, R.; Newton, P. N.; Agyarko, E. K.; Akunyili, D.; White, N. J. *PLoS Med.* **2005,** *2*, 302-308.
(8) World Health Organization. *WHO Drug Information*; Geneva, Switzerland, 2009.
(9) Joseph-Charles, J.; Geneste, C.; Laborde-Kummer, E.; Gheyouche, R.; Boudis, H.; Dubost, J. P. *J. Pharm. Biomed. Anal.* **2007,** *44*, 1008-1013.
(10) Kim, S.; Rodgers, R. P.; Marshall, A. G. *Int. J. Mass Spectrom.* **2006,** *251*, 260-265.
(11) Kelleher, N. L.; Lin, H. Y.; Valaskovic, G. A.; Aaserud, D. J.; Fridriksson, E. K.; McLafferty, F. W. *J. Am. Chem. Soc.* **1999,** *121*, 806-812.
(12) Cech, N. B.; Enke, C. G. *Anal. Chem.* **2000,** *72*, 2717-2723.
(13) Cech, N. B.; Enke, C. G. *Anal. Chem.* **2001,** *73*, 4632-4639.
(14) Cheng, J.; Vecitis, C. D.; Hoffmann, M. R.; Colussi, A. J. *J. Phys. Chem. B* **2006,** *110*, 25598-25602.
(15) Kuprowski, M. C.; Boys, B. L.; Konermann, L. *J. Am. Soc. Mass Spectrom.* **2007,** *18*, 1279-1285.
(16) Page, J. S.; Kelly, R. T.; Tang, K.; Smith, R. D. *J. Am. Soc. Mass Spectrom.* **2007,** *18*, 1582-1590.
(17) Pan, P.; McLuckey, S. A. *Anal. Chem.* **2003,** *75*, 5468-5474.
(18) Iavarone, A. T.; Udekwu, O. A.; Williams, E. R. *Anal. Chem.* **2004,** *76*, 3944-3950.
(19) Iavarone, A. T.; Williams, E. R. *J. Am. Chem. Soc.* **2003,** *125*, 2319-2327.
(20) King, R.; Bonfiglio, R.; Fernandez-Metzler, C.; Miller-Stein, C.; Olah, T. *J. Am. Soc. Mass Spectrom.* **2000,** *11*, 942-950.
(21) Sleno, L.; Volmer, D. A. *Rapid Commun. Mass Spectrom.* **2005,** *19*, 1928-1936.
(22) Leib, R. D.; Flick, T. G.; Williams, E. R. *Anal. Chem.* **2009,** *81*, 3965-3972.
(23) Flick, T. G.; Leib, R. D.; Williams, E. R. *Anal. Chem.* **2009,** *81*, 8434-8440.
(24) Jurchen, J. C.; Williams, E. R. *J. Am. Chem. Soc.* **2003,** *125*, 2817-2826.
(25) Takats, Z.; Nanita, S. C.; Cooks, R. G.; Schlosser, G.; Vekey, K. *Anal. Chem.* **2003,** *75*, 1514-1523.

3.6 Figures

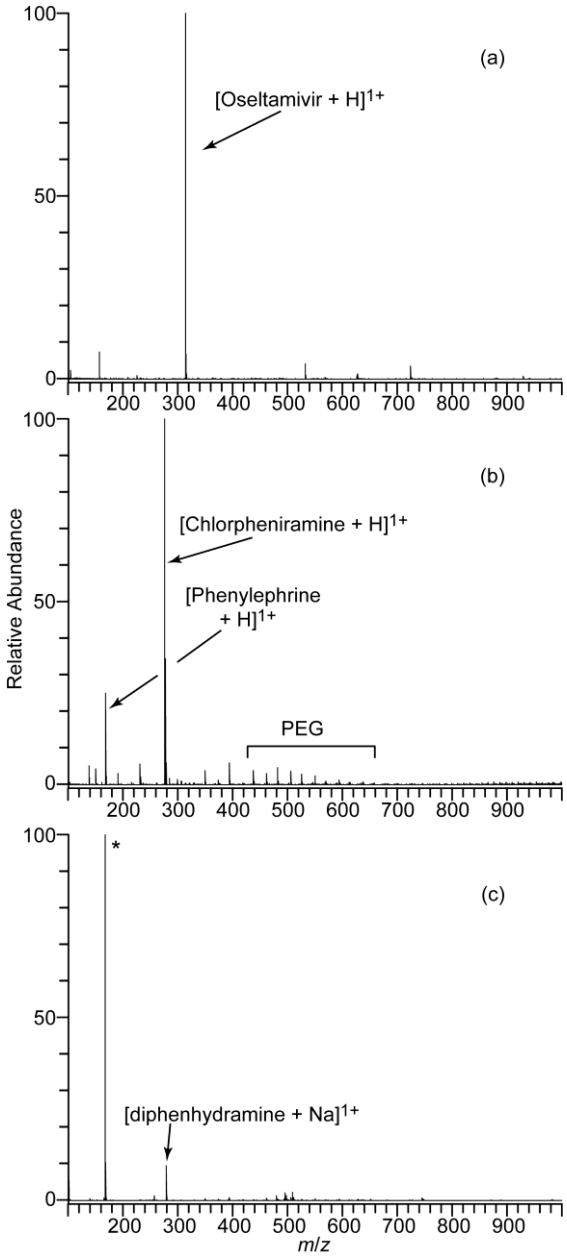

Figure 3.1. Electrospray mass spectra of aqueous solutions containing dissolved and filtered (a) Tamiflu® (30 mg oseltamivir) (b) Sudafed® (10 mg Phenylephrine HCL and 4 mg chlorpheniramine maleate) and (c) Dramamine® (50 mg dimenhydrinate). * indicates an unidentified ion at *m*/*z* 165. PEG is polyethylene glycol.

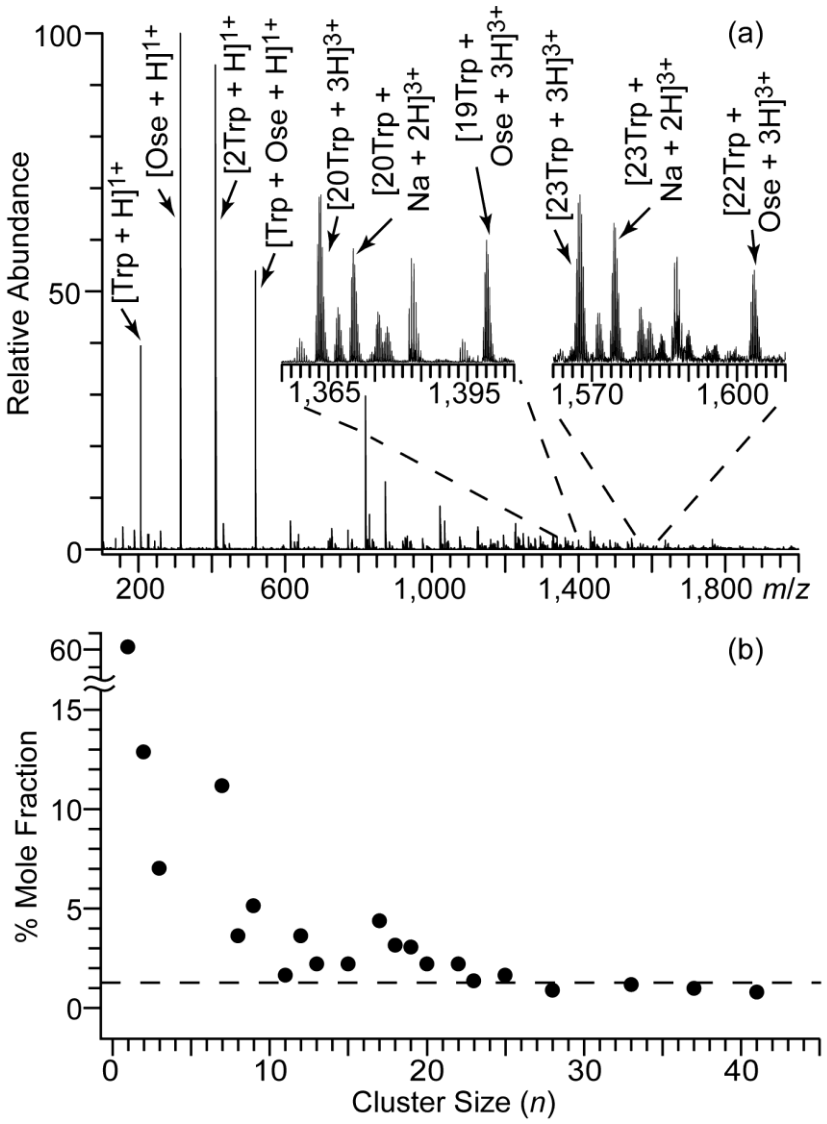

Figure 3.2. (a) ESI mass spectrum of a solution containing 1.3% mole fraction of oseltamivir (Ose) from a Tamiflu tablet preparation in L-tryptophan (10 mM total concentration) with some regions of the spectra with large molecular clusters inset. (b) Percent mole fractions calculated from protonated molecule and cluster ion abundances obtained from three ESI mass spectra of 1.3% mole fraction oseltamivir from a Tamiflu tablet preparation as a function of cluster size, *n*. The dashed line corresponds to the % mole fraction in solution.

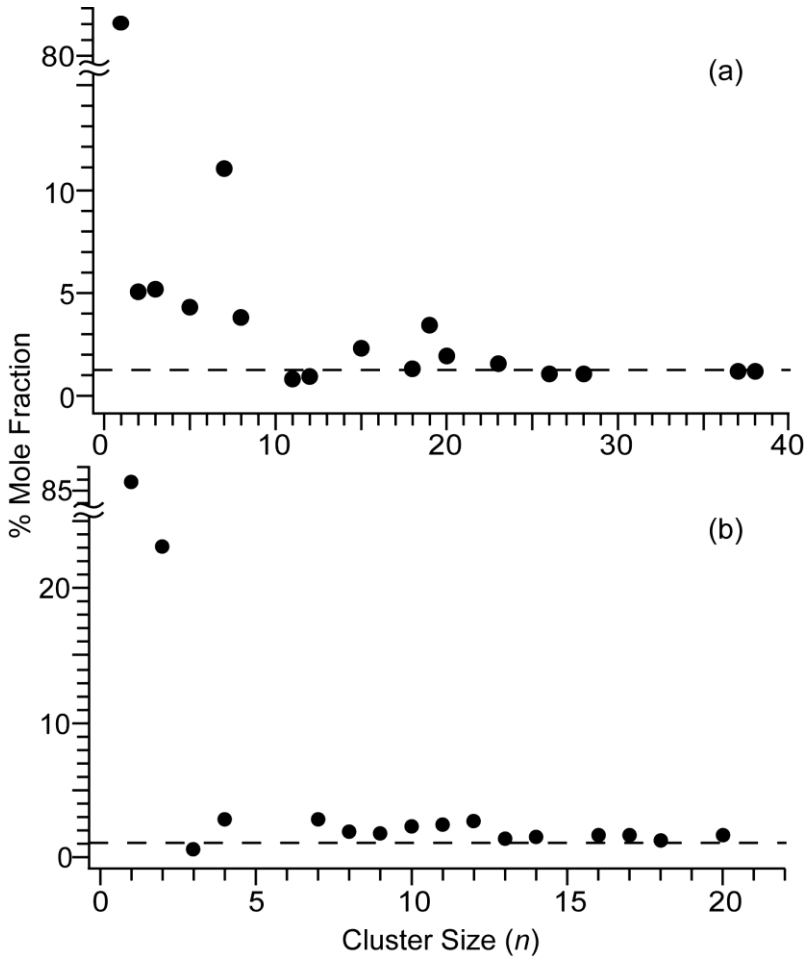

Figure 3.3. Percent mole fractions calculated from protonated molecule and cluster ion abundances obtained from three ESI mass spectra of a 1.3% and 1.0 % mole fraction of oseltamivir from a Tamiflu® tablet preparation in (a) L-phenylalanine and (b) prednisone, respectively.

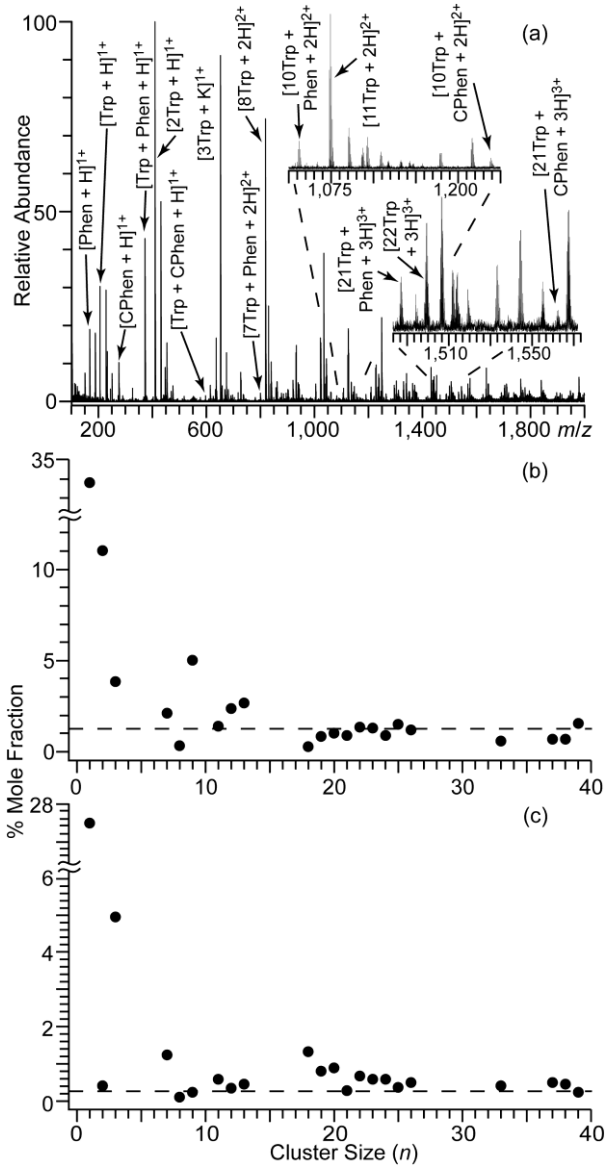

Figure 3.4. (a) ESI mass spectrum of a solution containing 1.3% mole fraction phenylephrine hydrochloride (Phen) and 0.3% of chlorpheniramine maleate (CPhen) from a Sudafed tablet preparation in L-tryptophan (10 mM total concentration) with some regions of the spectra with large molecular clusters inset. Percent mole fractions calculated from protonated molecule and cluster ion abundances obtained from three ESI mass spectra with L-tryptophan for (b) 1.3% mole fraction Phen and (c) 0.3% mole fraction CPhen as a function of cluster size, *n*. The dashed line corresponds to the % mole fraction in solution.

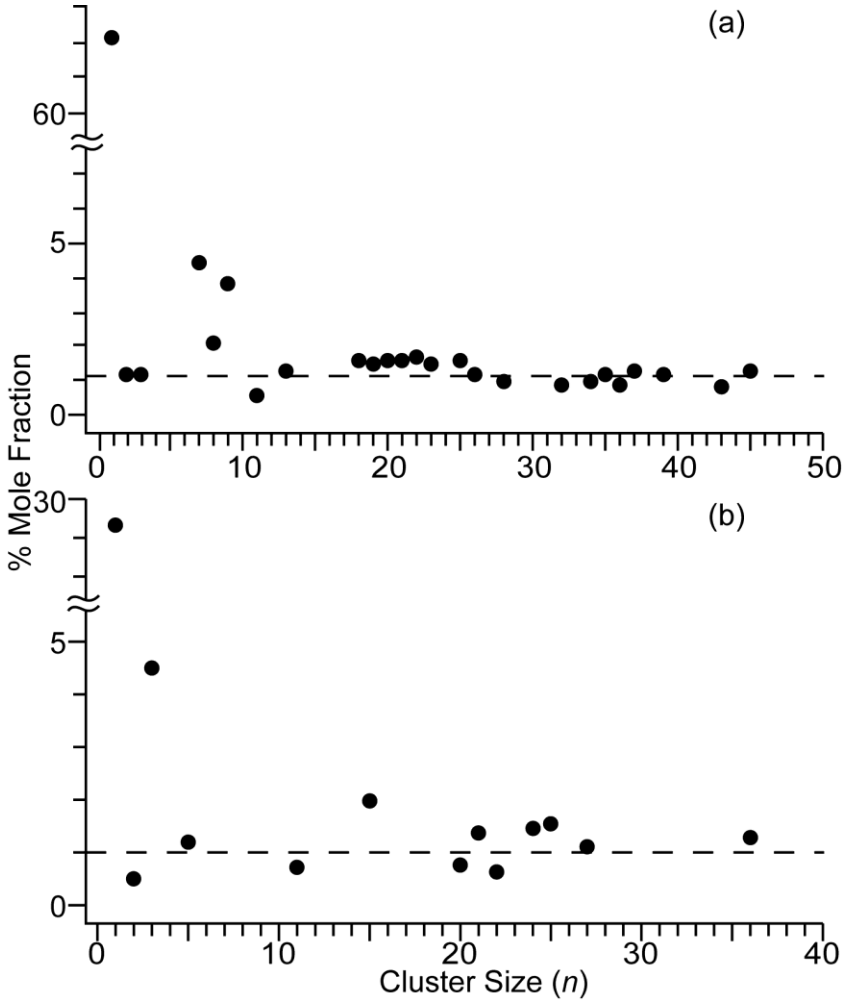

Figure 3.5. Percent mole fractions calculated from protonated molecule and cluster ion abundances obtained from three ESI mass spectra of 1.1% and 1.0% dimenhydrinate from a Dramamine tablet preparation in (a) L-tryptophan and (b) L-phenylalanine, respectively, as a function of cluster size, *n*. The dashed line corresponds to the % mole fraction in solution.

CHAPTER 4

Anion Effects on Sodium Ion and Acid Molecule Adduction to Protein Ions in Electrospray Ionization Mass Spectrometry

4.1 Introduction

Ion-protein interactions are ubiquitous in nature where they play a role in many biological functions. Some membrane proteins form channels in cell walls to selectively transport certain ions into and out of the cytoplasm.[1-3] Perhaps the best known examples are the sodium and potassium ion channels, which combine to create the action potentials necessary for the function of the nervous system.[1,2] Other channels specific to the transport of calcium and chloride ions contribute to the cardiac action potentials.[2,3] Proteins with EF-hand motifs, such as calmodulin and troponin-C, bind calcium ions in order to regulate functions such as inflammation, metabolism, skeletal- and smooth-muscle contraction, and memory.[4,5] Protein-metal ion interactions have also been implicated in the misfolding and subsequent aggregation of proteins resulting in the formation of plaques and fibrils in both prion-based[6-8] and Alzheimer's diseases.[9,10] Both metal chelators and redistribution of metals within the brain are actively pursued as potential treatments for Alzheimer's disease.[9,10]

In addition to specific ion-protein interactions, ions can also affect the stability, solubility, and function of proteins through nonspecific interactions. Nearly 125 years ago, Franz Hofmeister first published his findings on how different ions affect protein solubility, resulting in an ordering of ions based on their propensity to stabilize or destabilize protein structure:[11,12]

$$F^- \approx COOH^- \approx SO_4^{2-} > Cl^- > Br^- > NO_2^- > I^- > ClO_4^- > SCN^-$$

Ions towards the left of this series (kosmotropes) stabilize proteins and cause them to precipitate, whereas ions to the right of the series (chaotropes) destabilize proteins and make them more soluble in aqueous solutions. Hofmeister effects correlate well with many ionic properties, including ionic radii,[13,14] polarizabilities,[14] solvation free energies,[13-15] viscosity coefficients,[15] surface tension of aqueous solutions,[16,17] and elution times from Sephadex-G10 columns.[18] The effect of ions on protein stability is known to vary both with isoelectric point (pI) of the protein and pH of solution,[14,19,20] and anions generally have a larger effect than cations.

Despite numerous studies using many different methods, the origins of these phenomena are still widely debated. Evidence supporting both direct ion-protein interactions as well as ion-induced water ordering has been reported,[13-27] but the relative importance of these effects is not well understood. Results from time-resolved

spectroscopy experiments indicate that sulfate, a strong kosmotrope, does not affect the reorientation time of water molecules beyond the first solvation shell,[26] which has been interpreted as evidence that ion-induced water ordering does not play a significant role in the Hofmeister effect. However, recent infrared photodissociation studies of gaseous hydrated sulfate indicate that this anion can pattern the structure of water well past the second solvation shell.[25] Additional recent evidence suggests that many different ions can affect the structure of water past the first and even second solvent shell to various extents.[27]

Ion adduction to proteins often occurs with both electrospray ionization (ESI)[28-37] and matrix assisted laser desorption/ionization (MALDI).[37-40] Signal suppression in ESI can occur even when low concentrations of many salts are present,[33-37,41,42] and extensive sodium adduction to both proteins and DNA frequently occurs.[31-35,42] Salts are often removed by dialysis or using liquid chromatography to reduce adduction and improve ion formation in ESI.[32,36,37] Sodium adduction in ESI depends on the pI of the protein and the pH of the solution and more adduction typically occurs for low charge state ions.[31,34] McLuckey and coworkers reported that sodium adduction to gaseous protein ions is the highest when the solution pH is several units or more greater than the pI of the protein, and can be significantly reduced when the solution pH is ~3 units lower than the pI in positive ion mode MS.[31] High concentrations of some additives, such as ammonium acetate, can reduce sodium adduction to proteins[34] and can be used to improve the mass measuring accuracy of large protein complexes where adducts to molecular ions are not resolved.[35] Konermann and coworkers found the extent of nonspecific calcium adduction to proteins was reduced when calcium tartrate was added to ESI solutions compared to calcium acetate and calcium chloride, and suggested that tartrate acts as a solution-phase chelator of calcium.[28] Gas-phase ion/ion reactions between DNA anions and several chelating ions, such as citrate, have also been shown to significantly reduce nonspecific metal ion adduction.[42]

Anion and acid molecule adduction to biological molecules has also been observed in both ESI and in MALDI MS.[29,30,38-40,43,44] Gas-phase reactions of protein cations with anions can result in acid molecule adduction for anions with proton affinities ~330 kcal/mol or lower,[45,46] and for reactions between protein ions and gaseous HI, the maximum number of HI adducts equals the number of basic sites less the number of protons.[46] Addition of 10 mM perchloric acid to ESI solutions containing peptides or proteins leads to extensive adduction of acid molecules and can be used to accurately determine the number of basic sites in the molecule.[29] A similar relationship between the number of basic sites and the maximum extent of adduction has been observed for some acids in MALDI.[38-40] The presence of anions in ESI solutions containing neutral oligosaccharides, which do not have a highly acidic group, can increase the absolute intensity of the deprotonated molecular ions. A significant increase in the abundance of $(M - H)^-$ was observed for anions that have a higher proton affinity than that of the sugar, which was attributed to proton transfer from the oligosaccharide to the anion being favored, whereas acid molecule adduction was observed when the proton affinity of the anion was less than that of the oligosaccharide.[43]

Despite the common occurrence of ion and molecule adduction in ESI and MALDI, there are no direct studies of the Hofmeister effect on anion-protein interactions using MS. Colussi and co-workers measured ESI mass spectra of solutions containing mixtures of equimolar amounts of the sodium salts of monovalent anions and found that the relative intensities of the anions correlated well with both the ionic radii and the solvation free energies, two properties that have previously been related to the Hofmeister series.[13] Here, the effects of anions on adduction of ions and molecules to proteins was investigated by adding millimolar concentrations of sodium salts of various anions to aqueous solutions from which protein ions are formed using ESI. Significant differences in the extents of both sodium and acid molecule adduction to the protein ions are observed. These differences do not correlate well with solution-phase properties but do correlate well with the proton affinity of the anion. These results suggest that direct ion-protein interactions may not play a significant role in the origin of the Hofmeister series.

4.2 Experimental

ESI mass spectra were acquired using a LTQ-orbitrap hybrid mass spectrometer (Thermo Electron, Bremen, Germany). Bovine ubiquitin, porcine insulin chain B, chicken egg white lysozyme, and equine cytochrome *c* were from Sigma Aldrich (St. Louis, MO) and dialyzed against 18.2 MΩ water (Milli-Q, Millipore, Billerica, MA) using Slide-A-Lyzer cartridges (Thermo Scientific) with a molecular weight cut-off of 3,500 Da (insulin chain B, ubiquitin) or 10,000 Da (lysozyme, cytochrome *c*). The sodium salts of F^- (≥ 99%), $COOH^-$ (≥ 99%), NO_2^- (≥ 97%), Cl^- (≥ 99.5%), SCN^- (≥ 98%), Br^- (≥ 99%), I^- (≥ 99.5%), SO_4^{2-} (≥ 99%), ClO_4^- (≥ 98%), PF_6^- (≥ 98%), and SbF_6^- (technical grade) were from Sigma Aldrich and were used without further purification. Solutions containing 10 μM protein and 1.0 mM of the salt were prepared by diluting aliquots of stock solutions in 18.2 MΩ water. The source region was heated to ~210 °C in order to generate consistent signal, resulting in an electrospray emitter temperature of ~180 °C. An autosampler delivered 15.0 μL injections of sample into the mass spectrometer at a flow rate of 50 $\mu L \bullet min^{-1}$ for a total analysis time of 7 minutes, including a wash step after each sample. The high flow rate was used to decrease the total sample analysis time.

4.3 Results and Discussion

4.3.1 Sodium and Acid Molecule Adduction. ESI mass spectra of proteins acquired from aqueous solutions with millimolar concentrations of sodium salts of F^-, $COOH^-$, NO_2^-, Cl^-, SCN^-, Br^-, I^-, SO_4^{2-}, ClO_4^-, PF_6^- and SbF_6^- show various extents of sodium and acid molecule adduction depending on the counterion of the sodium salt and to a lesser extent, the identity of the protein. For example, ESI mass spectra of aqueous solutions containing 10 μM ubiquitin and either 1.0 mM NaF or $NaSbF_6$ are shown in Figure 4.1a and 4.1b, respectively. With NaF, adduction of multiple sodium ions to the protein occurs, with a significantly greater extent of adduction observed for lower charge state ions, as has been reported previously.[31,34] For the 6+ charge state, the abundance of the single sodium adduct is ~70% that of the protonated molecular

ion, and adduction of up to 23 sodium ions, $(M - 17H + 23Na)^{6+}$, is observed. No HF adducts to any charge state are detected. In striking contrast, no additional sodium adduction occurs with 1.0 mM $NaSbF_6$ compared to that obtained when the protein is sprayed from an aqueous solution without salt added. However, extensive adduction of $HSbF_6$ occurs (Figure 4.1b). Acid molecule adduction to the 6+ and 11+ charge states accounts for approximately 61% and 13%, respectively, of the total ion abundance of each charge state, consistent with the greater extent of acid molecule adduction for lower charge state ions observed previously.[30,45]

A wide range of charge states were produced from these aqueous solutions owing to the high source temperature used. Proteins can denature at high temperatures, which results in a broader distribution of charge states centered at higher charge.[47] Because sodium ion and acid molecule adduction were most prevalent for lower charge states, a low charge state ion that was common to each protein for all salts examined was chosen to compare the various extents of adduction. For example, partial mass spectra showing the 6+ charge state of ubiquitin obtained from solutions containing (a) no added salt or 1.0 mM of (b) NaCl, (c) Na_2SO_4, (d) $NaClO_4$, or (e) $NaPF_6$ are shown in Figure 4.2. The percent adduction of sodium to the protonated molecular ion relative to that from an aqueous solution without salt added is 77%, 60%, 37%, and 0% for these respective salts. There is no adduction of HCl, but H_2SO_4, $HClO_4$, and HPF_6 adducts at 21%, 40%, and 58% of the total ion intensity for the 6+ charge state, respectively, are formed. Sodium adducts with one or more acid molecules attached are included in the total percent acid adduction reported. Although equimolar concentrations of sodium are added to the ESI solutions in the form of various salts, except for Na_2SO_4, the extent of both sodium and acid molecule adduction to ubiquitin 6+ is significantly different.

ESI mass spectra of aqueous solutions containing 10 μM lysozyme with 1.0 mM of the sodium salt of F^-, $COOH^-$, NO_2^-, Cl^-, SCN^-, Br^-, I^-, SO_4^{2-}, ClO_4^-, PF_6^-, or SbF_6^- were obtained under identical conditions. Lysozyme (pI = 11) has a significantly higher isoelectric point than ubiquitin (pI = 6.6). Figure 4.3 shows the 9+ charge state of lysozyme formed by ESI from aqueous solutions containing 10 μM protein with (a) no added salt or 1.0 mM of (b) NaF, (c) NaCl, (d) Na_2SO_4, (e) $NaClO_4$, or (f) $NaPF_6$. Sodium adduction to the protonated molecular ion is the greatest with NaF and NaCl with 41% and 31% adduction to the protonated molecular ion, respectively, whereas there is no adduction of HF or HCl. There is 24% less sodium adduction with Na_2SO_4 compared to NaCl, similar to the results for ubiquitin 6+. Minimal sodium adduction occurs with $NaClO_4$ and $NaPF_6$ (<2% and <1%, respectively). Adducts of H_2SO_4, $HClO_4$, and HPF_6 are observed, and account for approximately 77%, 87%, and 81% of the total ion intensity for the 9+ charge state.

Various extents of acid molecule and sodium adduction to either lysozyme 9+ or ubiquitin 6+ were observed from the addition of different sodium salts to ESI solutions containing either of these proteins. The percent sodium and acid molecule adduction were determined for the eleven sodium salts for ubiquitin 6+ (pI = 6.6), lysozyme 9+ (pI = 11), insulin chain B 2+ (pI = 6.9) and cytochrome *c* 9+ (pI = 10). Based on observations for all proteins, the general ordering of anions was:

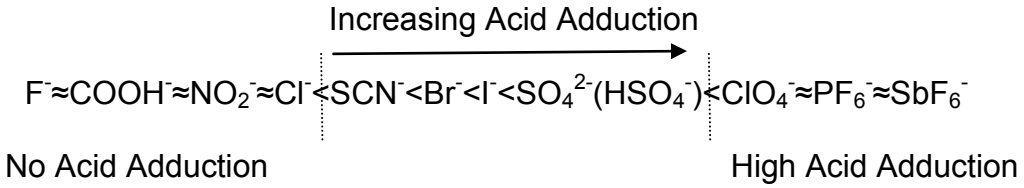

Sodium ion adduction was observed to be inversely related to the extent of acid molecule attachment; however, greater variation was observed at high levels of sodium ion adduction.

4.3.2 Adduction and Solution-phase Properties. The various extents of sodium and acid molecule adduction obtained when different anions are in these solutions were compared to common solution-phase properties. All the salts used here are soluble in water at 1.0 mM, but the salt concentration in the ESI droplet increases due to evaporation of water. Late in the droplet lifetime, the salts may reach their solubility limit and precipitate in the droplet, reducing the maximum number of potential adducts to the protein.[34] The percent sodium and acid molecule adduction to ubiquitin 6+ as a function of the solubility product constant (K_{sp}) of the sodium salt is shown in Figure 4.4a. NaI and $NaNO_2$ have similar K_{sp} values, but addition of $NaNO_2$ results in 22% greater sodium adduction than NaI even though the concentration of Na^+ in these solutions is the same. In contrast, the percent sodium adduction with NaSCN and NaBr differs by < 4% although their K_{sp} values differ by nearly three orders of magnitude. Extensive acid molecule adduction occurs for both H_2SO_4 (21%) and $HClO_4$ (40%), but the K_{sp} values of the sodium salts are two orders of magnitude different.

Addition of ammonium acetate at high levels can result in a significant decrease in the extent of sodium adduction to protein ions.[34,35] Although acetate can complex with sodium and precipitate out of solution at high concentrations, the percent sodium or acid molecule adduction to the protonated molecular ion does not correlate directly to the solubility of the sodium salt at the concentrations used here. Sodium adduction to ubiquitin 6+ is highest with NaF and NaCl, 84% and 77%, respectively, even though their solubilities differ by ×40. These data indicate that the extent of sodium and acid molecule adduction does not correlate well with the solubility of these sodium salts.

The percent acid molecule and sodium adduction for ubiquitin 6+ as a function of the pK_a of the acid of the corresponding anion is shown in Figure 4.4b. A similar level of sodium adduction to ubiquitin 6+ is observed with NaF and NaCl, 84% and 77%, respectively, even though HF is a weak acid (pK_a = 3.2) and HCl is a strong acid (pK_a = -8.0). HI and $HClO_4$ are both strong acids, with pK_a values of -11 and -10, respectively; however, the corresponding acid molecule adduction observed for these two anions are 3% and 40%, respectively. These data indicate the extent of acid molecule and sodium adduction does not correlate well with the pK_a of the protonated anion.

4.3.3 Adduction and Proton Affinity. The extent of acid molecule and sodium adduction were compared to the proton affinity (PA) of the anion (A^-). PA of A^- is the negative enthalpy change for the gas-phase reaction:

$$A^- + H^+ \longrightarrow AH \qquad PA(A^-) = -\Delta H_{rxn}$$

Results for ubiquitin 6+ and insulin chain B 2+ are shown in Figure 4.5a and 4.5b, respectively. SbF_6^- and HPF_6^- have the two lowest PA's of the anions studied here, and the highest levels of acid molecule attachment and the lowest levels of sodium adduction to the protonated molecular ions (<2% additional sodium adduction compared to that observed without salt addition) occurs for both the sodium salts of SbF_6^- and PF_6^-. NaF, which has the highest PA of the anions investigated, results in extensive sodium adduction, accounting for 84% and 39% of the total ion intensity for the 6+ and 2+ charge states of ubiquitin and insulin chain B, respectively. No HF adduction occurs with either protein. The extent of sodium ion and acid molecule adduction are inversely related, and are a strong function of the PA of the anion. The extent of sodium adduction increases and acid molecule adduction decreases as the PA of the anion increases across the range of ~280-360 kcal•mol^{-1}. No or minimal acid molecule adduction occurs for anions with a PA greater than that of NO_2^- (330 kcal•mol^{-1}). The transition between greater acid molecule adduction compared to sodium adduction occurs between 290-300 kcal•mol^{-1} for both ubiquitin 6+ and insulin chain B 2+, corresponding to the sodium salts of I^- and ClO_4^-. Acid molecule adduction increases from 3.2% to 40% and sodium adduction decreases from 44% to 37% with NaI and $NaClO_4$, respectively, for ubiquitin 6+. These data indicate that there is a significant change in the interaction between the anion and the protein that occurs for anions around the PA values where this transition between sodium ion and acid molecule adduction occurs.

Although 1.0 mM solutions of Na_2SO_4 have twice the concentration of Na^+ as 1.0 mM solutions of NaF, sodium adduction to ubiquitin 6+ is less for Na_2SO_4 (60%) than for NaF (84%). Adduction of H_2SO_4 to ubiquitin 6+ occurs, whereas no HF adduction is observed. The PA values of SO_4^{2-} and HSO_4^- are 441 and 312 kcal•mol^{-1}, respectively. The extents of sodium and acid molecule adduction observed for Na_2SO_4 indicates that HSO_4^- is most likely interacting with the protein. However, SO_4^{2-} is most prevalent at pH ~7. A 10^3 to 10^4 fold increase in acidity from the neutral bulk solution can occur in the ESI droplets as evaporation occurs, resulting in a pH of approximately 2.6 to 3.3.[48] The abundance of HSO_4^- increases from <0.001% to ~17% of the total sulfate ions in solution as the pH decreases from 7 to 2.6, consistent with our conclusion that this is the form of the anion that interacts with the protein.

The extent of protonation for each charge state changes significantly depending on how much sodium or acid molecule adduction occurs, because each sodium adduct typically replaces a proton and each acid molecule adduct adds a proton. The extent of protonation for ubiquitin 6+ and insulin chain B 2+, calculated as the average number of protons attached to these respective ions, as a function of the PA of the anion of the sodium salt are shown in Figure 4.5c and 4.5d, respectively, and these data are compared to the extent of protonation from aqueous solutions with no salt added (dashed lines in Figure 4.5c and 4.5d). Greater protonation occurs for anions with PA values < ~285 kcal•mol^{-1}, whereas less protonation occurs for anions with PA values > 287 kcal•mol^{-1}. One of the lowest extents of the protonation observed for ubiquitin 6+

and insulin chain B 2+ is 1.9 and 1.2, respectively, with NaF, the anion with the highest PA. These data indicate that the presence of the anion in the ESI solution directly affects the extent of protonation of the protein ions formed.

Similar results were obtained for lysozyme 9+ and cytochrome *c* 9+ (Figure 4.6a and 4.6b, respectively), two proteins with significantly higher isoelectric points than those of ubiquitin and insulin chain B. There is minimal sodium adduction and the greatest extent of acid molecule attachment to both proteins with $NaPF_6$ and $NaSbF_6$, the anions with the lowest PA values. Acid molecule adduction occurs for anions with a PA < 323 kcal • mol^{-1}. The sodium salt of F^-, which has the highest PA of the anions investigated, results in high levels of sodium adduction to the protonated molecular ion, 41% and 5.5% adduction to lysozyme 9+ and cytochrome *c* 9+, respectively, and no HF adduction occurs. Results from the eleven sodium salts for all four proteins evaluated indicate that the extent of sodium adduction increases and acid molecule attachment decreases with increasing PA of the anion.

The extent of protonation for lysozyme 9+ and cytochrome *c* 9+ as a function of the PA of the anion of each sodium salt is shown in Figures 4.6c and 4.6d, respectively. For anions with PA values greater than 315 kcal • mol^{-1}, the extent of protonation is slightly lower than that with no salt added (dashed line), but this value is significantly higher when the PA of the anion is less than ~315 kcal • mol^{-1}. The transition to higher extents of protonation occurs when acid molecule adduction on the protein is the most abundant and to lower extents of protonation when sodium adduction is most abundant and no acid molecule adduction occurs, indicating that these phenomena are related to the identity of the anion in the ESI solution.

The transition between sodium and acid molecule adduction is different for proteins with different isoelectric points. This transition occurs at PA values between 290-300 kcal • mol^{-1} for both ubiquitin 6+ (pI = 6.6) and insulin chain B 2+ (pI = 6.9) and at ~315 kcal • mol^{-1} for lysozyme 9+ (pI = 11) and cytochrome *c* 9+ (pI = 10). There is a sharper transition for lysozyme 9+ and cytochrome *c* 9+, but the transition is similar for proteins with similar isoelectric points, indicating that the number of acidic and basic sites in a protein is a factor in the extent of adduction.

4.3.4 Adduction Mechanism. There is an inverse correspondence between sodium and acid molecule adduction to these four proteins, which is a function of the PA of the anion. An anion can favorably interact with either basic or acidic sites in the protein via ionic interactions. For anions with a high PA (>~300 kcal • mol^{-1}), deprotonation of the acidic sites in the protein (Glu, Asp, and the C-terminus) by the anion can be favorable (Scheme 1). The PA of acetate is 348 kcal • mol^{-1}, and this value provides a rough estimate of the intrinsic PA of a carboxylate group in a protein, although the values of the latter depend on many additional factors, including inter- and intramolecular solvation and proximity of other charged residues. Deprotonation of acidic sites in the protein by the anion in the late stages of droplet evaporation makes possible strongly favorable interactions between the deprotonated site and sodium cations, consistent with the extensive sodium adduction to proteins observed for anions with high PA values.

Differences in the extent of calcium adduction to protein ions formed by ESI from solutions containing different calcium salts have been reported.[28] The extent of nonspecific calcium adduction to α-lactalbumin, β-lactoglobulin, calmodulin, and myoglobin was the greatest for calcium chloride and calcium acetate, and smallest for calcium tartrate.[28] These results were attributed to the ability of tartrate to sequester divalent metal cations during the final stages of the ESI droplet lifetime.[28] The PA's of chloride and acetate are 333 and 349 kcal • mol^{-1}, respectively, and nonspecific cation adduction would be predicted to be extensive from salts of these anions based on the trends observed here. The PA of the tartrate ion has not been reported, but adduction of tartrate to ubiquitin does occur (data not shown), indicating that the PA of this anion is lower than chloride and acetate. These results are consistent with the extent of nonspecific calcium adduction being a result of the PA of the anion as opposed to more specific complexation with the metal ion.

Anions with lower PA values can form ionic interactions with basic sites (Scheme 2) and adduction of anions to basic sites in peptides and proteins has been observed in both MALDI and ESI.[29,38-40] Addition of small amounts of perchloric acid to ESI solutions containing peptides and proteins results in adduction of $HClO_4$, and the maximum extent of adduction can be used to accurately determine the number of basic sites in these molecules.[29] Gaseous adduction of HI and other acids with PA ≤ ~330 kcal • mol^{-1} to proteins also occurs and can be related to the number of basic sites.[45,46] Dissociation of the adducted complex results in loss of the neutral acid, consistent with the much higher PA of the anion compared to the basic site.[29,46] The stabilities of these adducts increases with decreasing charge state,[29] so more adduction is typically observed for lower charge state ions.

4.4 Conclusions

Addition of anions at millimolar concentration as the sodium salt to ESI solutions containing proteins results in different extents of acid molecule and sodium ion adduction to the protein ions. The extents of acid molecule and sodium ion adduction are inversely related, and depend primarily on the gas-phase PA of the anion and do not correlate well with solution-phase properties. Although there is some similarity in anion ordering, the effect of the anion on acid molecule and sodium adduction to the protein is not directly correlated to the Hofmeister series, suggesting that ion-protein interactions may not contribute as much as ion-water interactions to the Hofmeister effect. Although this study is limited to sodium salts, this work can be extended to salts for other cations. Proteins with low affinity for metal ions often require millimolar metal concentrations to induce significant binding in solution. For example, β-lactoglobulin has a low affinity calcium binding site with a dissociation constant around 3 mM.[49] The use of salts with anions that have a relatively high PA, such as chloride and acetate salts, may result in substantial nonspecific adduction to these proteins in ESI experiments, making it difficult to detect a specific metal-protein interaction. Salts with low PA anions should suppress nonspecific metal adduction to proteins and may be useful additives to ESI solutions in experiments aimed at measuring such low affinity specific metal ion binding sites.

4.5 References

(1) MacKinnon, R. *Angew. Chem.-Int. Edit.* **2004**, *43*, 4265-4277.
(2) Catterall, W. A. *Annu. Rev. Biochem.* **1995**, *64*, 493-531.
(3) Hiraoka, M.; Kawano, S.; Hirano, Y.; Furukawa, T. *Cardiovasc. Res.* **1998**, *40*, 23-33.
(4) Crivici, A.; Ikura, M. *Annu. Rev. Biophys. Biomolec. Struct.* **1995**, *24*, 85-116.
(5) Ogawa, Y. *J. Biochem.* **1985**, *97*, 1011-1023.
(6) Jackson, G. S.; Murray, I.; Hosszu, L. L. P.; Gibbs, N.; Waltho, J. P.; Clarke, A. R.; Collinge, J. *Proc. Natl. Acad. Sci. U. S. A.* **2001**, *98*, 8531-8535.
(7) Lehmann, S. *Curr. Opin. Chem. Biol.* **2002**, *6*, 187-192.
(8) Wong, B. S.; Chen, S. G.; Colucci, M.; Xie, Z. L.; Pan, T.; Liu, T.; Li, R. L.; Gambetti, P.; Sy, M. S.; Brown, D. R. *J. Neurochem.* **2001**, *78*, 1400-1408.
(9) Duce, J. A.; Bush, A. I. *Prog. Neurobiol.* **2010**, *92*, 1-18.
(10) Bush, A. I. *Trends Neurosci.* **2003**, *26*, 207-214.
(11) Hofmeister, F. *Arch. Exp. Pathol. Pharmakol.* **1888**, *24*, 247-260.
(12) Kunz, W.; Henle, J.; Ninham, B. W. *Curr. Opin. Colloid Interface Sci.* **2004**, *9*, 19-37.
(13) Cheng, J.; Vecitis, C. D.; Hoffmann, M. R.; Colussi, A. J. *J. Phys. Chem. B* **2006**, *110*, 25598-25602.
(14) Zhang, Y. J.; Cremer, P. S. *Proc. Natl. Acad. Sci. U. S. A.* **2009**, *106*, 15249-15253.
(15) Hribar, B.; Southall, N. T.; Vlachy, V.; Dill, K. A. *J. Am. Chem. Soc.* **2002**, *124*, 12302-12311.
(16) Cho, Y. H.; Zhang, Y. J.; Christensen, T.; Sagle, L. B.; Chilkoti, A.; Cremer, P. S. *J. Phys. Chem. B* **2008**, *112*, 13765-13771.
(17) Zhang, Y.; Furyk, S.; Sagle, L. B.; Cho, Y.; Bergbreiter, D. E.; Cremer, P. S. *J. Phys. Chem. C* **2007**, *111*, 8916-8924.
(18) Washabaugh, M. W.; Collins, K. D. *J. Biol. Chem.* **1986**, *261*, 2477-2485.
(19) Bostrom, M.; Tavares, F. W.; Finet, S.; Skouri-Panet, F.; Tardieu, A.; Ninham, B. W. *Biophys. Chem.* **2005**, *117*, 217-224.
(20) Finet, S.; Skouri-Panet, F.; Casselyn, M.; Bonnete, F.; Tardieu, A. *Curr. Opin. Colloid Interface Sci.* **2004**, *9*, 112-116.
(21) Uejio, J. S.; Schwartz, C. P.; Duffin, A. M.; Drisdell, W. S.; Cohen, R. C.; Saykally, R. J. *Proc. Natl. Acad. Sci. U. S. A.* **2008**, *105*, 6809-6812.
(22) Smith, J. D.; Saykally, R. J.; Geissler, P. L. *J. Am. Chem. Soc.* **2007**, *129*, 13847-13856.
(23) Freire, M. G.; Neves, C.; Silva, A. M. S.; Santos, L.; Marrucho, I. M.; Rebelo, L. P. N.; Shah, J. K.; Maginn, E. J.; Coutinho, J. A. P. *J. Phys. Chem. B* **2010**, *114*, 2004-2014.
(24) Chen, X.; Yang, T.; Kataoka, S.; Cremer, P. S. *J. Am. Chem. Soc.* **2007**, *129*, 12272-12279.
(25) O'Brien, J. T.; Prell, J. S.; Bush, M. F.; Williams, E. R. *J. Am. Chem. Soc.* **2010**, *132*, 8248-8249.

(26) Omta, A. W.; Kropman, M. F.; Woutersen, S.; Bakker, H. J. *Science* **2003**, *301*, 347-349.
(27) Prell, J. S.; O'Brien, J. T.; Williams, E. R. *J. Am. Chem. Soc.* **2011**, *133*, 4810-4818.
(28) Pan, J. X.; Xu, K.; Yang, X. D.; Choy, W. Y.; Konermann, L. *Anal. Chem.* **2009**, *81*, 5008-5015.
(29) Flick, T. G.; Merenbloom, S. I.; Williams, E. R. *Anal. Chem.* **2011**, *83*, 2210-2214.
(30) Chowdhury, S. K.; Katta, V.; Beavis, R. C.; Chait, B. T. *J. Am. Soc. Mass Spectrom.* **1990**, *1*, 382-388.
(31) Pan, P.; Gunawardena, H. P.; Xia, Y.; McLuckey, S. A. *Anal. Chem.* **2004**, *76*, 1165-1174.
(32) Liu, C. L.; Wu, Q. Y.; Harms, A. C.; Smith, R. D. *Anal. Chem.* **1996**, *68*, 3295-3299.
(33) Pan, P.; McLuckey, S. A. *Anal. Chem.* **2003**, *75*, 5468-5474.
(34) Iavarone, A. T.; Udekwu, O. A.; Williams, E. R. *Anal. Chem.* **2004**, *76*, 3944-3950.
(35) Sterling, H. J.; Batchelor, J. D.; Wemmer, D. E.; Williams, E. R. *J. Am. Soc. Mass Spectrom.* **2010**, *21*, 1045-1049.
(36) Bauer, K. H.; Knepper, T. P.; Maes, A.; Schatz, V.; Voihsel, M. *J. Chromatogr. A* **1999**, *837*, 117-128.
(37) Dalluge, J. J. *Fresenius J. Anal. Chem.* **2000**, *366*, 701-711.
(38) Friess, S. D.; Daniel, J. M.; Hartmann, R.; Zenobi, R. *Int. J. Mass Spectrom.* **2002**, *219*, 269-281.
(39) Friess, S. D.; Zenobi, R. *J. Am. Soc. Mass Spectrom.* **2001**, *12*, 810-818.
(40) Salih, B.; Zenobi, R. *Anal. Chem.* **1998**, *70*, 1536-1543.
(41) Wang, G. D.; Cole, R. B. *Anal. Chem.* **1994**, *66*, 3702-3708.
(42) Turner, K. B.; Monti, S. A.; Fabris, D. *J. Am. Chem. Soc.* **2008**, *130*, 13353-13363.
(43) Jiang, Y. J.; Cole, R. B. *J. Am. Soc. Mass Spectrom.* **2005**, *16*, 60-70.
(44) Cai, Y.; Cole, R. B. *Anal. Chem.* **2002**, *74*, 985-991.
(45) Stephenson, J. L.; McLuckey, S. A. *J. Am. Chem. Soc.* **1997**, *119*, 1688-1696.
(46) Stephenson, J. L.; McLuckey, S. A. *Anal. Chem.* **1997**, *69*, 281-285.
(47) Leblanc, J. C. Y.; Beuchemin, D.; Siu, K. W. M.; Guevremont, R.; Berman, S. S. *Org. Mass Spectrom.* **1991**, *26*, 831-839.
(48) Gatlin, C. L.; Tureček, F. *Anal. Chem.* **1994**, *66*, 712-718.
(49) Simons, J.; Kosters, H. A.; Visschers, R. W.; de Jongh, H. H. J. *Arch. Biochem. Biophys.* **2002**, *406*, 143-152.

4.6 Figures

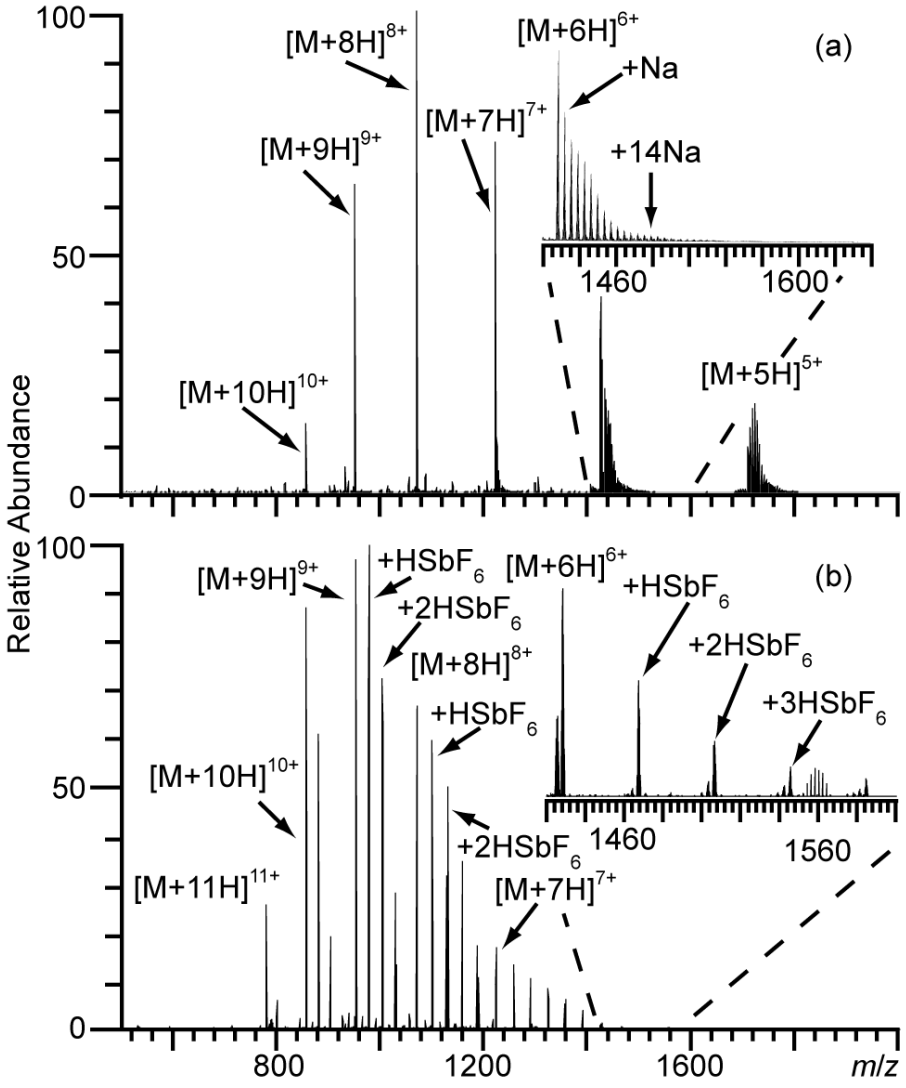

Figure 4.1. ESI mass spectra of aqueous solutions containing 10 μM ubiquitin and 1.0 mM (a) NaF or (b) $NaSbF_6$. Insets show various extents of sodium and acid molecule adduction to the 6+ charge state.

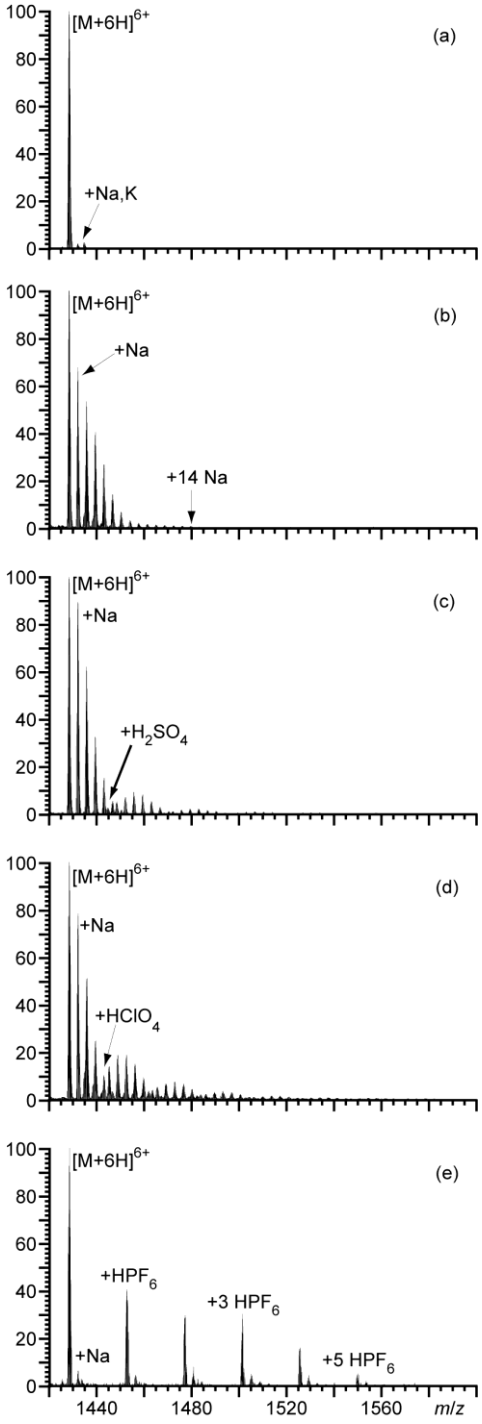

Figure 4.2. Partial ESI mass spectra showing the 6+ charge state of ubiquitin obtained from aqueous solutions containing 10 μM ubiquitin and (a) no added salt and 1.0 mM of the following salts: (b) NaCl, (c) Na_2SO_4, (d) $NaClO_4$, or (e) $NaPF_6$

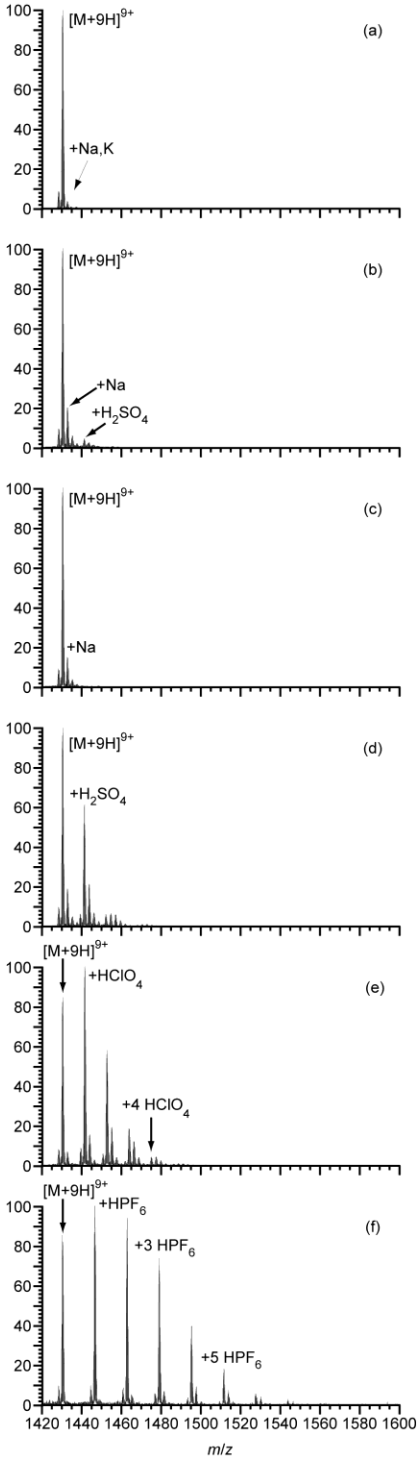

Figure 4.3. Partial ESI mass spectra showing the 9+ charge state of lysozyme obtained from aqueous solutions containing 10 μM lysozyme and (a) no added salt and 1.0 mM of each of the following salts: (b) NaF, (c) NaCl, (d) Na_2SO_4, (e) $NaClO_4$, or (f) $NaPF_6$.

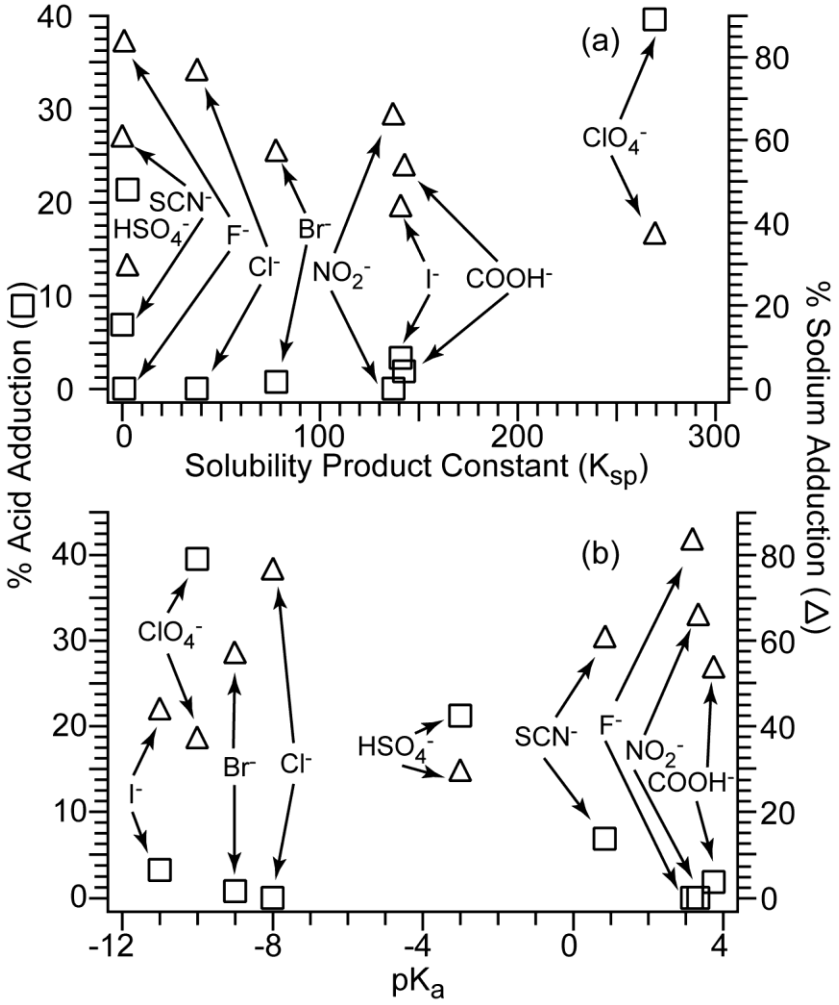

Figure 4.4. Percent acid molecule (squares) and sodium adduction (triangles) to ubiquitin 6+ as a function of (a) K_{sp} of the respective sodium salts or (b) pK_a of the acid of the corresponding anion obtained from 10 μM of ubquitin with 1.0 mM of NaF, NaCl, NaCOOH, $NaNO_2$, NaBr, NaSCN, NaI, Na_2SO_4 or $NaClO_4$.

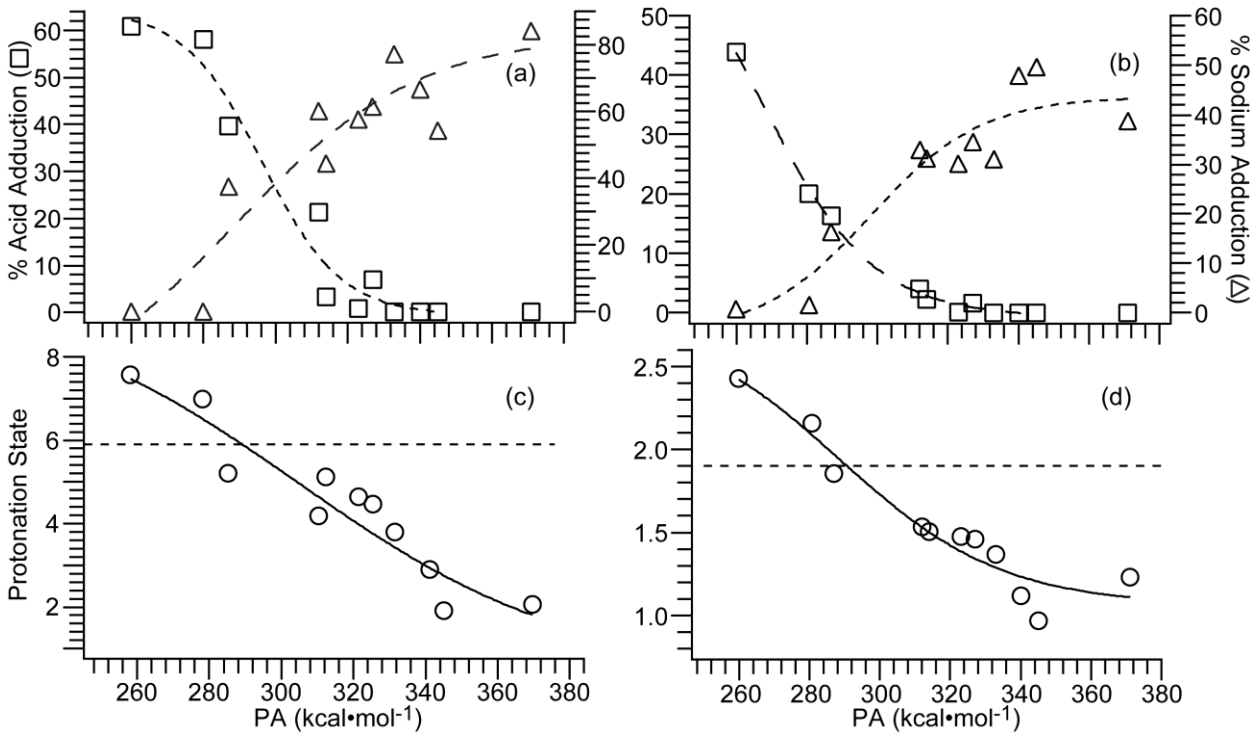

Figure 4.5. Percent acid molecule (squares) and sodium adduction (triangles) to (a) ubiquitin 6+ or (b) insulin chain B 2+ as a function of the proton affinity, PA (kcal • mol^{-1}), of the respective anion calculated from ESI mass spectra obtained from solutions containing 10 μM protein with 1.0 mM of NaF, NaCl, NaCOOH, $NaNO_2$, NaBr, NaSCN, NaI, Na_2SO_4, $NaClO_4$, $NaPF_6$, or $NaSbF_6$. The extent of protonation of (c) ubiquitin 6+ and (d) insulin chain B 2+ as a function of the PA of the anion from the sodium salts. The dashed line corresponds to the extent of protonation of the protein from ESI solutions with no salt added.

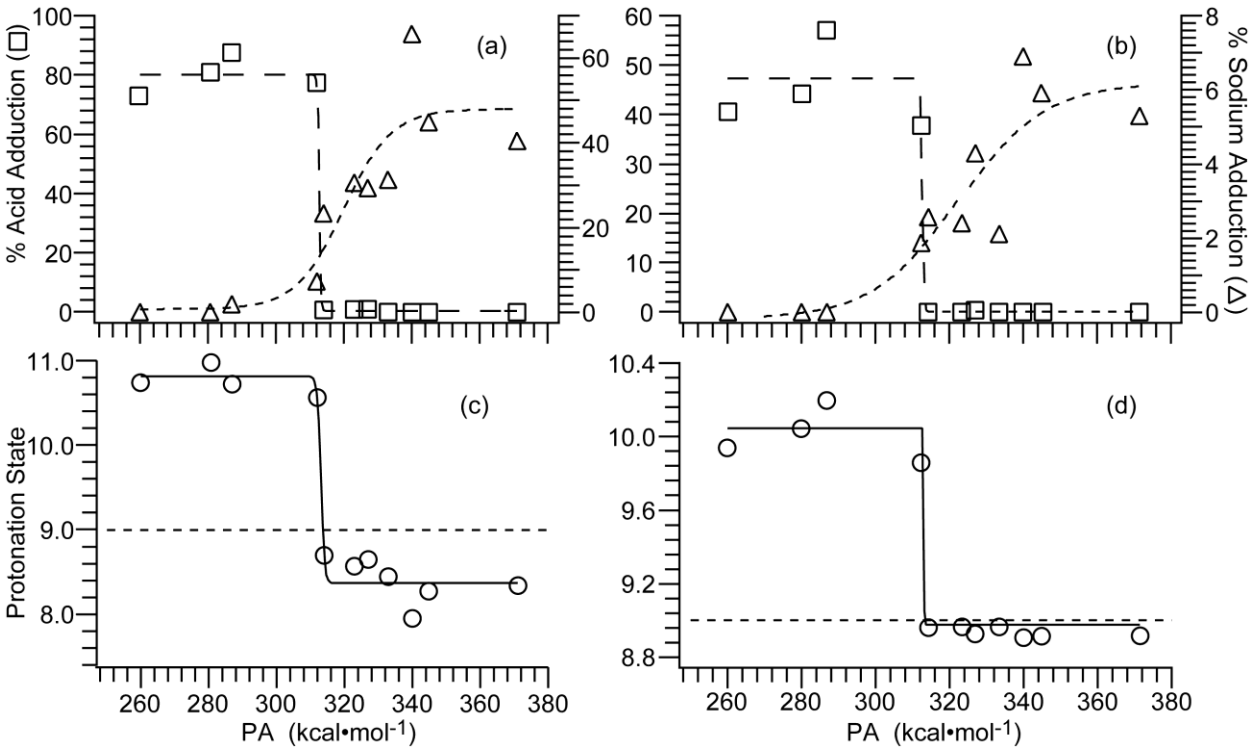

Figure 4.6. Percent acid molecule (squares) and sodium adduction (triangles) to (a) lysozyme 9+ and (b) cytochrome *c* 9+ as a function of the proton affinity, PA (kcal • mol^{-1}), of the anion calculated from ESI mass spectra of solutions containing 10 μM protein with 1.0 mM of NaF, NaCl, NaCOOH, $NaNO_2$, NaBr, NaSCN, NaI, Na_2SO_4, $NaClO_4$, $NaPF_6$, or $NaSbF_6$. The extent of protonation of (c) lysozyme 9+ and (d) cytochrome *c* 9+ as a function of the PA of the anion from the sodium salts. The dashed line corresponds to the extent of protonation of the protein from ESI solutions with no salt added.

Scheme 1.

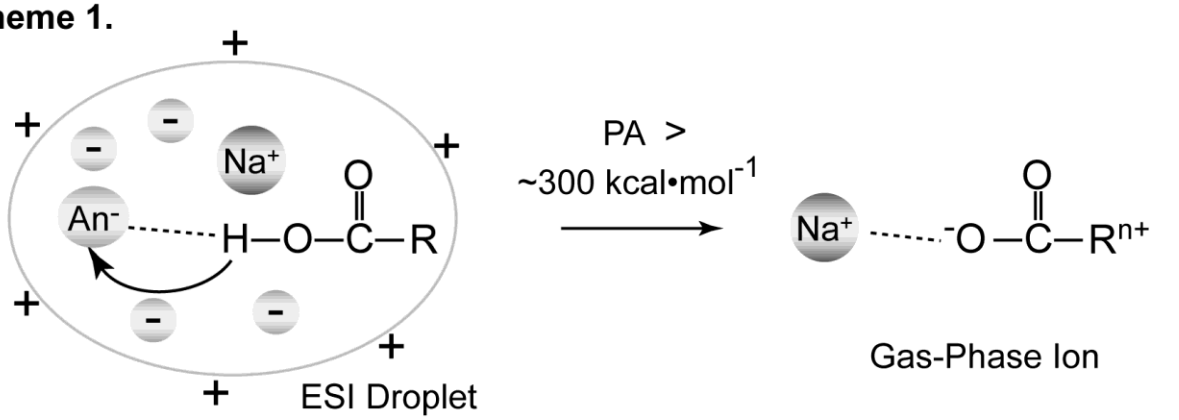

Scheme 2.

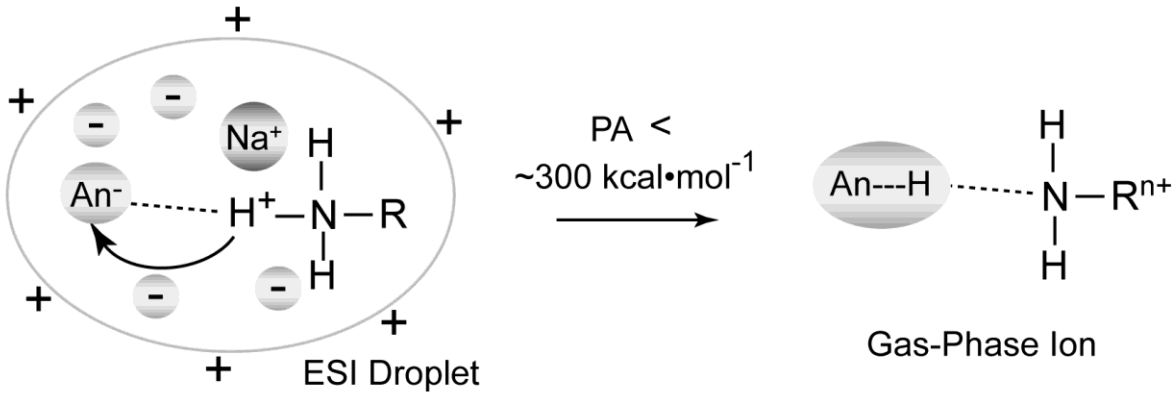

CHAPTER 5

A Simple and Robust Method for Determining the Number of Basic Sites in Peptides and Proteins using Electrospray Ionization Mass Spectrometry

5.1 Introduction

Accurate molecular weights of a wide range of molecules, even those present in complex mixtures[1-9] or at trace levels,[3,4] can be obtained using mass spectrometry. Information about elemental composition can be determined from isotope ratios or from exact mass measurements.[1-13] Marshall and coworkers were able to assign unique elemental compositions for up to 20,000 compounds in petroleum samples with a mass measuring accuracy of ~400 ppb.[2] Because the possible elemental compositions at a given nominal mass increases rapidly with molecular size, obtaining the elemental composition of larger molecules with just accurate mass measurements alone becomes more challenging.

Because biopolymers are comprised of a limited set of molecular sub-units, the number of possible elemental compositions in a given *m*/*z* range are constrained. More than 99% of peptides with a nominal mass of 1,000 Da can be excluded with a mass measuring accuracy of ± 1 ppm.[12] However, even with an unequivocal elemental composition of a peptide, an unambiguous amino acid composition cannot always be obtained because different combinations of amino acids can have the same elemental composition. The mass limit for unambiguously determining the amino acid composition of a peptide by accurate mass measurements alone is ~500-600 Da.[12] For larger peptides and proteins for which the amino acid composition cannot be determined directly from mass alone, additional information that further restricts the possible compositions is needed.[7-9] The amino acid composition of peptides formed by proteolysis of intact proteins is limited both by the enzyme used and by the organism. The number of peptides formed by proteolysis that can be used to uniquely identify a protein increases with mass measuring accuracy and protein size assuming that the peptides are not post-translationally modified.[9] The percentage of unique tryptic peptides at ~2,000 Da formed by proteolysis of *C. elegans* proteins that can be identified increases from 5% to 60% at mass measuring accuracies of 10 and 0.1 ppm, respectively.[9]

Information about the amino acid composition of a peptide can also be obtained by modifying specific residues.[4-6,14,15] Many amino acids can be chemically modified selectively, such as conversion of lysine to homo-arginine[14] and cysteine thiol to thialamine.[15] Residue specific chemical modifications can provide constraints on the possible amino acid composition.[4-6] Cysteine modification using an alkylating reagent that contains chlorine has been used to determine the number of cysteine residues in a peptide based on the distinctive isotopic distributions of ions containing chlorine.[4]

Knowledge of the number of cysteine residues constrains the possible peptide composition, which increases the effectiveness of the accurate mass measurement approach.[4] For *C. elegans*, this additional constraint increases the number of unique tryptic peptides at ~2,000 Da that can be identified from 60% to 80% at a 0.1 ppm mass measuring accuracy.[9]

Noncovalent adduction has also been used to obtain information about the composition or surface accessibility of specific residues.[16-26] McLuckey and coworkers found that adduction of acidic molecules, such as HI and HBr, to various peptides and proteins can occur via gas-phase ion/molecule reactions when the gas phase acidity (ΔH_{acid}) of the acid is less than or equal to ~330 kcal • mol^{-1}.[16,17] Peptide and protein ions were reacted in an ion trap with HI until changes in the abundance of adducts were imperceptible, in some instances for up to 3 s,[16,17] and the sum of the ion charge state and the maximum number of adducted HI molecules was found to equal the number of basic sites on 20 of the 21 oligopeptides.[16] Adduction of acidic molecules to peptide and protein ions also occurs in matrix-assisted laser desorption ionization (MALDI)-MS.[23-26] For small peptides, the total number of protons and maximum number of adducted acid molecules of bis(trifluoromethylsulfonyl)imide was equal to the number of basic sites, but lower adduction was observed for proteins.[26] Different sulfonic acid molecules, such as napthalene-disulfonic acid (NDS) and Cibacron Blue F3G-A (CCB), can bind specifically to either arginine and the N-terminus, exclusively, or all basic sites, respectively.[23-25] The maximum number of adducts was equal to the number of arginine residues plus the N-terminus for NDS and all basic sites for CCB for small peptides and ubiquitin.[23-25]

Solution additives in ESI have been used to reduce effects of salts,[27,28] increase or decrease charge states,[29-31] and to obtain information about protein composition and structure.[18-22,32] Addition of 18-crown-6-ether to solutions containing peptides and proteins results in preferential adduction to lysine although some binding to histidine, arginine, and the N-terminus also occurs.[20-22] Information about the number of lysine residues can be obtained for small peptides, but not all lysine residues are adducted with larger proteins, a result that has been attributed to solvent inaccessible residues.[20-22] Dibenzo-30-crown-10 ether (DB30C10) also forms complexes with peptides containing arginine, but adduction of two DB30C10 molecules was not observed for a peptide with two arginine residues.[19]

Here, we demonstrate the number of basic sites on a peptide or protein can be accurately determined directly from an ESI mass spectrum by adding 10 mM of perchloric acid ($HClO_4$) to a solution containing these molecules. For the 18 peptides and proteins studied here with molecular weights between 0.5 and 18.3 kDa, the sum of the ion charge state and the number of $HClO_4$ molecules attached to lower charge states is equal to the number of basic residues and the N-terminus when unmodified.

5.2 Experimental

All peptides, proteins, and perchloric acid (70% v:v in water, 11.6 M) were obtained from Sigma Aldrich Chemical Co. (St. Louis, MO). Proteins with a molecular weight (MW) greater than 10 kDa were dialyzed against 18.2 MΩ water using Slide-A-Lyzer (Thermo Scientific) cartridges with a MW cutoff of 10 kDa. Final solutions for

electrospray were prepared at a concentration of 10 μM peptide or protein and 10 mM $HClO_4$ in water. ESI mass spectra were acquired using a LTQ-orbitrap hybrid mass spectrometer (Thermo Electron, Bremen, Germany) equipped with a liquid chromatography autosampler. 15.0 μL of sample was injected for each analysis. The sample plug was introduced into the mass spectrometer for ~30 s using 18.2 MΩ water at a flow rate of 50 $\mu L \bullet min^{-1}$. Mass spectra were acquired continuously, and two minutes of data were averaged for each spectrum.

Additional experiments, including collision activation, were performed using a Waters-Micromass Q-TOF Premier (Waters Corporation, Manchester, UK) equipped with a nanoESI source. A solution containing 10 μM ubiquitin and 10 mM $HClO_4$ in 18.2 MΩ water was introduced to the mass spectrometer through a pulled borosilicate nanoESI emitter with 1.2 kV applied via a platinum wire. The source was maintained at a temperature of 120 °C with a cone gas velocity of 170 $L \bullet hr^{-1}$. The sample and extraction cones were operated at voltages of 40 and 0 V, respectively. The collision cell gas velocity was 0.6 $mL \bullet min^{-1}$, and both the cell entrance and exit were operated at -5 V.

5.3 Results and Discussion

Addition of 10 mM $HClO_4$ to aqueous solutions containing either a peptide or protein results in various extents of adduction of $HClO_4$ to the protonated molecules. For example, an ESI mass spectrum of an aqueous solution containing 10 mM $HClO_4$ and 10 μM ubiquitin, which shows various extents of adduction of $HClO_4$ molecules to the different charge states of the protonated protein, is shown in Figure 5.1a. More $HClO_4$ adduction occurs for lower charge state ions, as has been reported previously for adducts of other ions and molecules.[27,33] The 4+ charge state is the lowest one observed for ubiqutin under these conditions, and up to nine $HClO_4$ molecules are adducted, resulting in $(ubiquitin + 4H + 9HClO_4)^{4+}$. The number of protons (4) plus maximum number of $HClO_4$ adducts (9) for the 4+ charge state is 13, which is equal to the number of basic sites on the protein (Arg, His, Lys, and the N-terminus). Similarly, the number of protons (5) and maximum number of $HClO_4$ adducts (8) observed for the 5+ charge state is 13. Interestingly, the abundances of $(ubiquitin + 4H + 9HClO_4)^{4+}$ and $(ubiquitin + 5H + 8HClO_4)^{5+}$ are significantly greater, by a factor of approximately 10 and 2, respectively, than other ions in the same charge state with different numbers of attached $HClO_4$ molecules. No further adduction of $HClO_4$ to $(ubiquitin + 4H)^{4+}$ and $(ubiquitin + 5H)^{5+}$ is observed beyond the ninth and eighth molecule, respectively, although additional adduction of $NaClO_4$ does occur. Non-specific adduction of salts and salt clusters to protein ions has been observed previously with ESI-MS.[27,34] That no more adducts of $HClO_4$ to the protein ion are observed suggests that there are no more favorable sites to which $HClO_4$ can bind. In contrast, the maximum number of protons and adducted $HClO_4$ molecules for the 6+ to 12+ charge states of ubiquitin is lower than the total number of basic sites. For these ions, the maximum number of protons plus $HClO_4$ adducts is 12. A 13+ charge state is formed in low abundance but no attachment of $HClO_4$ is observed.

Similar results were obtained for bovine cytochrome *c*. An ESI mass spectrum of an aqueous solution containing 10 μM bovine cytochrome *c* and 10 mM $HClO_4$ is shown in Figure 5.1b. The maximum number of $HClO_4$ adducts observed for the 6+, 7+, and 8+ charge states are 17, 16, and 15, respectively, corresponding to the number of protons plus maximum number of attached $HClO_4$ molecules of 23 for each of these ions. This value is equal to the combined total of 23 arginine, histidine, and lysine residues. The abundance of (cytochrome *c* + 6H + 17$HClO_4$)$^{6+}$ is ~5× greater than all the other adducts for this charge state, indicating that there are 17 favorable binding sites that are predominantly occupied. Similar results were obtained for equine cytochrome *c*, which has one additional basic residue. The maximum number of protons plus $HClO_4$ adducts for the lowest charge states (6+ and 7+) is 24, which is equal to the number of basic residues in this protein. Both bovine and equine cytochrome *c* are acetylated at the N-terminus, which apparently makes this site unfavorable for $HClO_4$ adduction. Acetylation of the N-terminus lowers the gas-phase basicity of this site which is the likely origin of the significantly lower affinity of this site for $HClO_4$ attachment. As was the case for ubiquitin, the number of protons plus the maximum number of $HClO_4$ adducts is lower than the number of basic sites for the higher (10+ to 18+) charge states.

For all the peptides and proteins investigated, the maximum number of observed $HClO_4$ adducts to the higher charge state ions were between 1 to 3 molecules lower than the number of basic sites, but this depends on instrument conditions (vide infra). Even with the relatively "harsh" source conditions used here, the sum of the number of protons and maximum number of $HClO_4$ adducts for the lowest charge states of the 18 peptides and proteins investigated is equal to the number of basic sites (Figure 5.2; slope and correlation coefficient equals 1.00).

For each peptide or protein except melittin, the abundance of the most extensively adducted ion was significantly greater, by at least a factor of 2, than other ions with the same charge state but with lower numbers of $HClO_4$ molecules attached. The high abundance indicates that all the available binding sites in these molecules have high affinity for $HClO_4$, and makes it possible to unambiguously identify the number of binding sites. In contrast, the abundance of the most highly adducted ion in MALDI experiments with NDS[23] and CCB[25] was lower than other ions for the same charge state, suggesting a lower affinity for these molecules to basic sites. For melittin, the lowest charge state is 2+, and a maximum of four $HClO_4$ molecules are observed to adduct to form (melittin + 2H + 4$HClO_4$)$^{2+}$ (Figure 5.3). Melittin has six basic sites including an unmodified N-terminus. Thus, the maximum number of protons plus adducts of $HClO_4$ for this ion is equal to the number of basic sites. But unlike the other peptides and proteins investigated, the relative intensity of (melittin + 2H + 4$HClO_4$)$^{2+}$ is ~3× less than that for (melittin + 2H + 3$HClO_4$)$^{2+}$. Four of the six basic residues in melittin are adjacent to one another, which may result in steric hindrance and a lowering of the binding affinity of the fourth $HClO_4$ molecule at these four adjacent sites.

The relative intensity of the most adducted ion decreases at lower $HClO_4$ concentrations indicating a significant excess of $HClO_4$ is required to provide an unambiguous determination of the number of basic sites on a protein. Under these

conditions, the optimum ratio of acid:protein was ~1000:1 to produce high intensities for the most adducted ions. At lower concentrations of acid, adduction was either incomplete (100:1) or not observed (10:1 and lower), whereas cluster ions became the most intense features in the mass spectra at higher (10000:1 and greater) acid concentrations.

To determine the extent to which the abundances of the adducts depend on instrumental conditions, a mass spectrum of an aqueous solution containing 10 μM ubiquitin and 10 mM $HClO_4$ was obtained using a nanoESI emitter (~25 nL/min flow rate) and a Q-TOF mass spectrometer (Figure 5.4a). A comparison of the mass spectra in Figure 5.1a and 5.4a, obtained from the same solution, but with two different instruments operated with significantly different source conditions, shows that although the charge state distributions can differ significantly, formation of the ion for which the maximum number of adducts plus the number of protons is equal to the number basic sites is remarkably robust for the low charge states. The abundances of these maximally adducted ions are much greater in the nanoESI spectrum (Figure 5.4a) where they are observed for all the charge states produced (4+ to 12+). The $(\text{ubiquitin} + 4H + 9HClO_4)^{4+}$ is the only 4+ ion observed in Figure 5.4a, and the $(\text{ubiquitin} + 5H + 8HClO_4)^{5+}$ is ~10× more intense than the $(\text{ubiquitin} + 5H + 7HClO_4)^{5+}$ in Figure 5.4a, compared to 2× in Figure 5.1a.

More highly charged ions are observed with the orbitrap for which high solution flow rates were used. The presence of $HClO_4$ at high concentration necessitated high source temperatures under these conditions to obtain consistent ion signal. Thermal denaturation can occur at high source temperatures and could explain the more abundant high charge states. In contrast, the flow rates with nanospray are many orders of magnitude lower, and more reproducible signals were obtained under “softer” source conditions. The higher charge states in Figure 5.4a are likely the result of denaturation owing to the solution pH ~2.

The significantly greater abundance of the maximally adducted ions with nanoESI and “soft” source conditions suggests that the absence of these ions for the higher charge states under “harsher” source conditions is the result of gas-phase dissociation of these adducts. The stabilities of these maximally adducted ions were investigated by measuring collisional activation spectra of mass selected $(\text{ubiquitin} + 4H + 9HClO_4)^{4+}$, $(\text{ubiquitin} + 7H + 6HClO_4)^{7+}$, and $(\text{ubiquitin} + 11H + 2HClO_4)^{11+}$ ions as a function of collision voltage. These ions dissociate by sequential loss of $HClO_4$ molecules, and the abundance of these precursor ions as a function of collision voltage is shown in Figure 5.4b. These data show a clear trend in decreasing ion stability with increasing charge state. The collision voltage necessary to dissociate half of the precursor occurs at ~8.0, 12, and 29 V for the $(\text{ubiquitin} + 11H + 2HClO_4)^{11+}$, $(\text{ubiquitin} + 7H + 6HClO_4)^{7+}$, and $(\text{ubiquitin} + 4H + 9HClO_4)^{4+}$ ions, respectively. These results indicate that ion activation in any region of the mass spectrometer should be minimized in order to best preserve the adducts for all charge states.

The inverse correspondence between $HClO_4$ adduction and protonation extent indicates that $HClO_4$ adduction occurs at basic sites by displacing a net proton and forming an ion pair. Previous results from gas-phase ion/molecule reactions indicate

that acid adduction to proteins and peptides occurs for acids with a ΔH_{acid} of 330 kcal • mol^{-1} or less,[17] consistent with our observation that adduction occurs for $HClO_4$ which has a ΔH_{acid} of 287 kcal • mol^{-1}.[35] Based on McLuckey's findings that HI adduction to peptide and protein ions can occur as a result of gas-phase ion/molecule reactions and the maximum number of these adducts plus the ion charge state is equal to the number of basic sites,[16] HI was added to solutions at a concentration of 10 mM for 10 of the 18 proteins to test whether HI was equally as effective as $HClO_4$ as a solution-phase additive for this analysis. The resulting ESI mass spectra show lower extents of adduction of HI compared to $HClO_4$. HI adducts may be more weakly bound to these ions than $HClO_4$, and may be lost more readily by gas-phase dissociation.

In separate experiments, the extents of sodium and acid molecule adduction to molecular ions formed by ESI from aqueous solutions individually containing 11 different sodium salts and four different proteins was investigated. Adduction depends strongly on the gas-phase acidity of the counter ion of the salt, with acid adduction observed for acids with $\Delta H_{acid} \leq 315$ kcal • mol^{-1}. Based on these results, $HSbF_6$ or HPF_6 may also be effective for determining the number of basic sites in a peptide or protein.

5.4 Conclusions

These results demonstrate that the number of basic sites (Arg, Lys, His, and unmodified N-terminus) in peptides and proteins can be accurately determined from the number of $HClO_4$ molecules adducted to lower charge state ions formed by ESI from solutions that contain millimolar concentrations of $HClO_4$. This method has the advantage that it is rapid, and no covalent modifications, proteolytic digestion, gas-phase ion/molecule reactions, instrumental or other experimental modifications are required to obtain the number of basic sites in a peptide or protein. Because adduction of $HClO_4$ results in a 100 Da increase, this method does not require high resolution measurements and can be performed on any mass spectrometer with an ESI source. Addition of $HClO_4$ does reduce the overall ion signal but by less than a factor of two in these experiments. Any post-translational modification to a basic site that reduces basicity will also likely reduce binding affinity of $HClO_4$ and these sites will not likely be detected by this method. However, the simplicity and accuracy of this method could make it useful for determining peptide composition from accurate mass measurements by providing an additional constraint that would reduce the mass accuracy required to uniquely determine the peptide composition. Conversely, this information could be used to extend the molecular weight range of this method to larger peptides. Even if used for trypic peptide analysis for which cleavages occur at Lys and Arg, this method provides additional information about the number of His residues or missed cleavages due to incomplete digestion or when Pro is on the C-terminal end of Lys or Arg. Because the elemental composition of the adducts are known, the *m*/*z* spacing between adducts could potentially be used as an internal mass calibrant to further increase the mass measuring accuracy in these experiments.

Determining the number of basic sites from $HClO_4$ adduction to low charge states is remarkably robust even when vastly different source conditions or instruments are used. Collisional activation of these maximally adducted ions results in sequential loss

of $HClO_4$ molecules and the stabilities of these adducts increase with decreasing charge state. Thus, adducts will be best preserved using "soft" source conditions and nanospray. To insure maximum reliability of this method, either instrumental conditions for which the sum of protons and maximum $HClO_4$ adducts is the same for all charge states should be found, or proteins with a known number of basic residues could be used to determine the extent to which these adducts are preserved under a given set of experimental conditions. Addition of $HClO_4$ to solutions prior to ESI as done here does increase mass spectral complexity owing to the formation of a large number of adducts. For more complex samples, this reagent could be added in either a split flow[36,37] or a dual spray[38] in order to alternately acquire spectra with and without the reagent to aid spectral interpretation.

5.5 References

(1) Hughey, C. A.; Rodgers, R. P.; Marshall, A. G. *Analytical Chemistry* **2002**, *74*, 4145-4149.
(2) McKenna, A. M.; Purcell, J. M.; Rodgers, R. P.; Marshall, A. G. *Energy & Fuels* **2010**, *24*, 2929-2938.
(3) Haskins, N. J.; Eckers, C.; Organ, A. J.; Dunk, M. F.; Winger, B. E. *Rapid Communications in Mass Spectrometry* **1995**, *9*, 1027-1030.
(4) Goodlett, D. R.; Bruce, J. E.; Anderson, G. A.; Rist, B.; Pasa-Tolic, L.; Fiehn, O.; Smith, R. D.; Aebersold, R. *Analytical Chemistry* **2000**, *72*, 1112-1118.
(5) Hernandez, H.; Niehauser, S.; Boltz, S. A.; Gawandi, V.; Phillips, R. S.; Amster, I. J. *Analytical Chemistry* **2006**, *78*, 3417-3423.
(6) Leitner, A.; Lindner, W. *Journal of Mass Spectrometry* **2003**, *38*, 891-899.
(7) Smith, R. D.; Anderson, G. A.; Lipton, M. S.; Pasa-Tolic, L.; Shen, Y. F.; Conrads, T. P.; Veenstra, T. D.; Udseth, H. R. *Proteomics* **2002**, *2*, 513-523.
(8) Smith, R. D.; Anderson, G. A.; Lipton, M. S.; Masselon, C.; Pasa-Tolic, L.; Shen, Y.; Udseth, H. R. *OMICS A Journal of Integrative Biology* **2002**, *6*, 61-90.
(9) Conrads, T. P.; Anderson, G. A.; Veenstra, T. D.; Pasa-Tolic, L.; Smith, R. D. *Analytical Chemistry* **2000**, *72*, 3349-3354.
(10) Rodgers, R. P.; Blumer, E. N.; Hendrickson, C. L.; Marshall, A. G. *J. Am. Soc. Mass Spectrom.* **2000**, *11*, 835-840.
(11) He, F.; Hendrickson, C. L.; Marshall, A. G. *Analytical Chemistry* **2001**, *73*, 647-650.
(12) Zubarev, R. A.; Hakansson, P.; Sundqvist, B. *Analytical Chemistry* **1996**, *68*, 4060-4063.
(13) Kim, S.; Rodgers, R. P.; Marshall, A. G. *International Journal of Mass Spectrometry* **2006**, *251*, 260-265.
(14) Kimmel, J. R. *Methods in Enzymology* **1967**, *11*, 584-589.
(15) Itano, H. A.; Robinson, E. A. *Journal of Biological Chemistry* **1972**, *247*, 4819-&.
(16) Stephenson, J. L.; McLuckey, S. A. *Analytical Chemistry* **1997**, *69*, 281-285.
(17) Stephenson, J. L.; McLuckey, S. A. *Journal of the American Chemical Society* **1997**, *119*, 1688-1696.
(18) Julian, R. R.; Beauchamp, J. L. *J. Am. Soc. Mass Spectrom.* **2004**, *15*, 616-624.
(19) Julian, R. R.; Akin, M.; May, J. A.; Stoltz, B. M.; Beauchamp, J. L. *International Journal of Mass Spectrometry* **2002**, *220*, 87-96.
(20) Julian, R. R.; Beauchamp, J. L. *International Journal of Mass Spectrometry* **2001**, *210*, 613-623.
(21) Ly, T.; Julian, R. R. *J. Am. Soc. Mass Spectrom.* **2006**, *17*, 1209-1215.
(22) Ly, T.; Julian, R. R. *J. Am. Soc. Mass Spectrom.* **2008**, *19*, 1663-1672.
(23) Friess, S. D.; Zenobi, R. *J. Am. Soc. Mass Spectrom.* **2001**, *12*, 810-818.
(24) Friess, S. D.; Daniel, J. M.; Hartmann, R.; Zenobi, R. *International Journal of Mass Spectrometry* **2002**, *219*, 269-281.
(25) Salih, B.; Zenobi, R. *Analytical Chemistry* **1998**, *70*, 1536-1543.
(26) Kruger, R.; Karas, M. *J. Am. Soc. Mass Spectrom.* **2002**, *13*, 1218-1226.

(27) Iavarone, A. T.; Udekwu, O. A.; Williams, E. R. *Analytical Chemistry* **2004**, *76*, 3944-3950.
(28) Pan, J. X.; Xu, K.; Yang, X. D.; Choy, W. Y.; Konermann, L. *Analytical Chemistry* **2009**, *81*, 5008-5015.
(29) Iavarone, A. T.; Jurchen, J. C.; Williams, E. R. *J. Am. Soc. Mass Spectrom.* **2000**, *11*, 976-985.
(30) Hogan, C. J.; Carroll, J. A.; Rohrs, H. W.; Biswas, P.; Gross, M. L. *Journal of the American Chemical Society* **2008**, *130*, 6926-+.
(31) Lavarone, A. T.; Williams, E. R. *J. Am. Chem. Soc.* **2003**, *125*, 2319-2327.
(32) Zhang, Z. Q.; Smith, D. L. *Protein Science* **1993**, *2*, 522-531.
(33) Pan, P.; Gunawardena, H. P.; Xia, Y.; McLuckey, S. A. *Analytical Chemistry* **2004**, *76*, 1165-1174.
(34) Juraschek, R.; Dulcks, T.; Karas, M. *J. Am. Soc. Mass Spectrom.* **1999**, *10*, 300-308.
(35) Marcus, Y. *J. Chem. Soc. Farad. Trans. I* **1987**, *83*, 339.
(36) Konermann, L.; Collings, B. A.; Douglas, D. J. *Biochemistry* **1997**, *36*, 5554-5559.
(37) Yang, H. J.; Smith, D. L. *Biochemistry* **1997**, *36*, 14992-14999.
(38) Xia, Y.; Liang, X. R.; McLuckey, S. A. *J. Am. Soc. Mass Spectrom.* **2005**, *16*, 1750-1756.

5.6 Figures

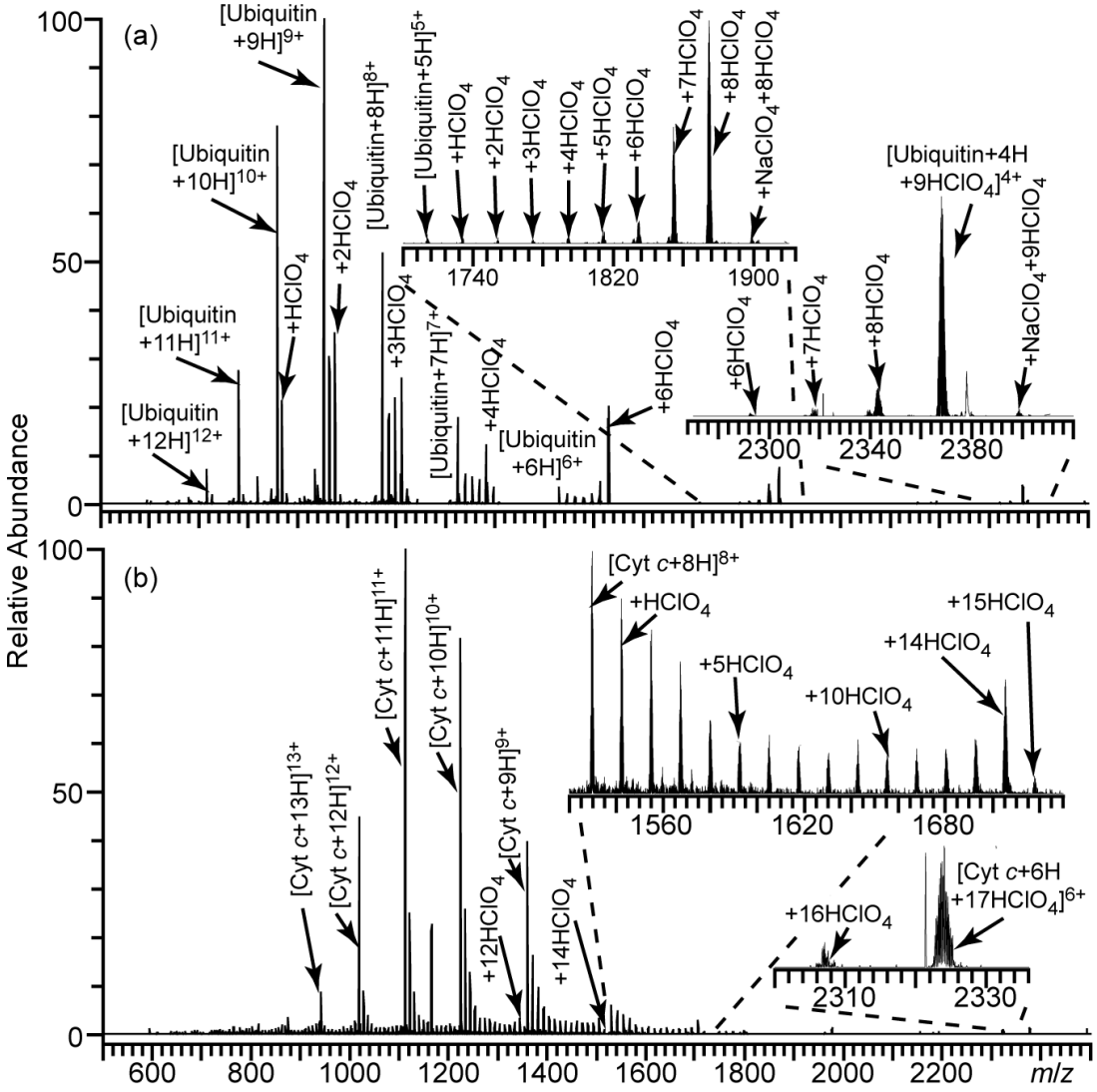

Figure 5.1. ESI mass spectra of solutions containing 10 mM $HClO_4$ and 10 μM (a) ubiquitin or (b) bovine cytochrome *c*. Insets show various extents of adduction of $HClO_4$ molecules to lower charge state ions.

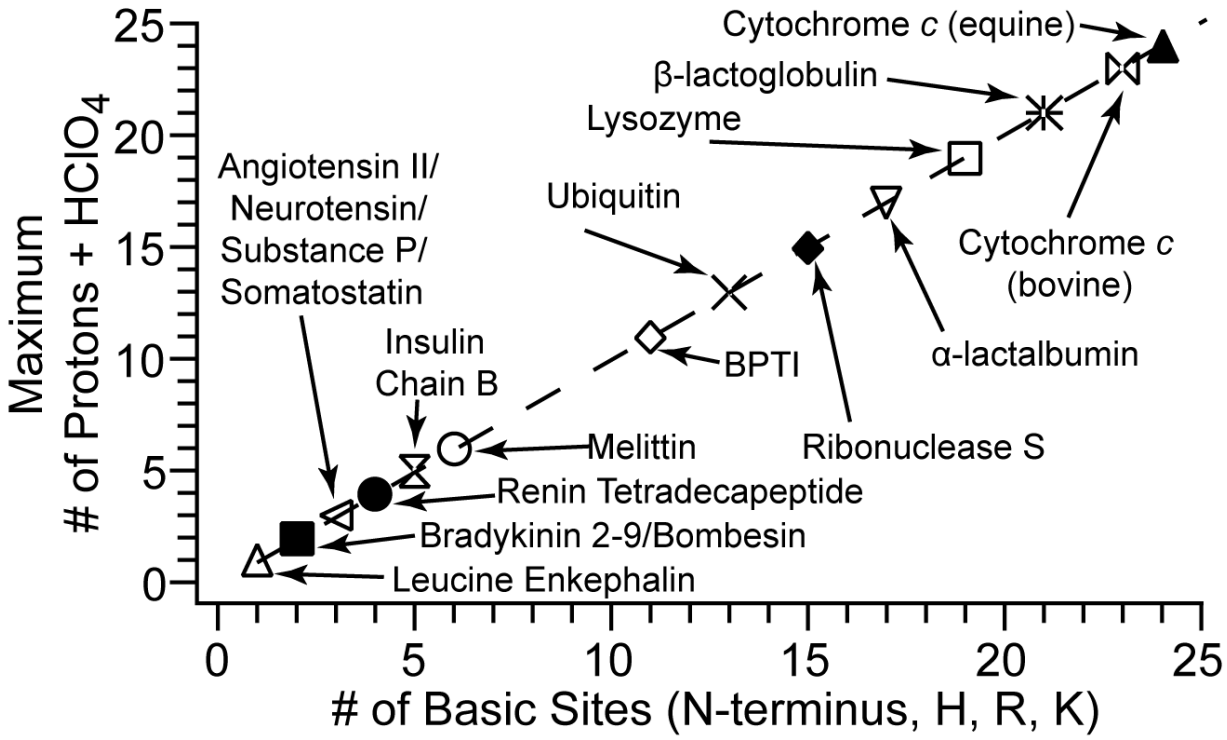

Figure 5.2. The sum of the number of protons and maximum number of $HClO_4$ molecules adducted to the lowest charge states formed by ESI from solutions containing 10 mM $HClO_4$ as a function of the number of basic sites (Arg, Lys, His, and unmodified N-terminus) for 18 peptides and proteins. These data are fit to a straight line (slope and correlation coefficient is equal to 1).

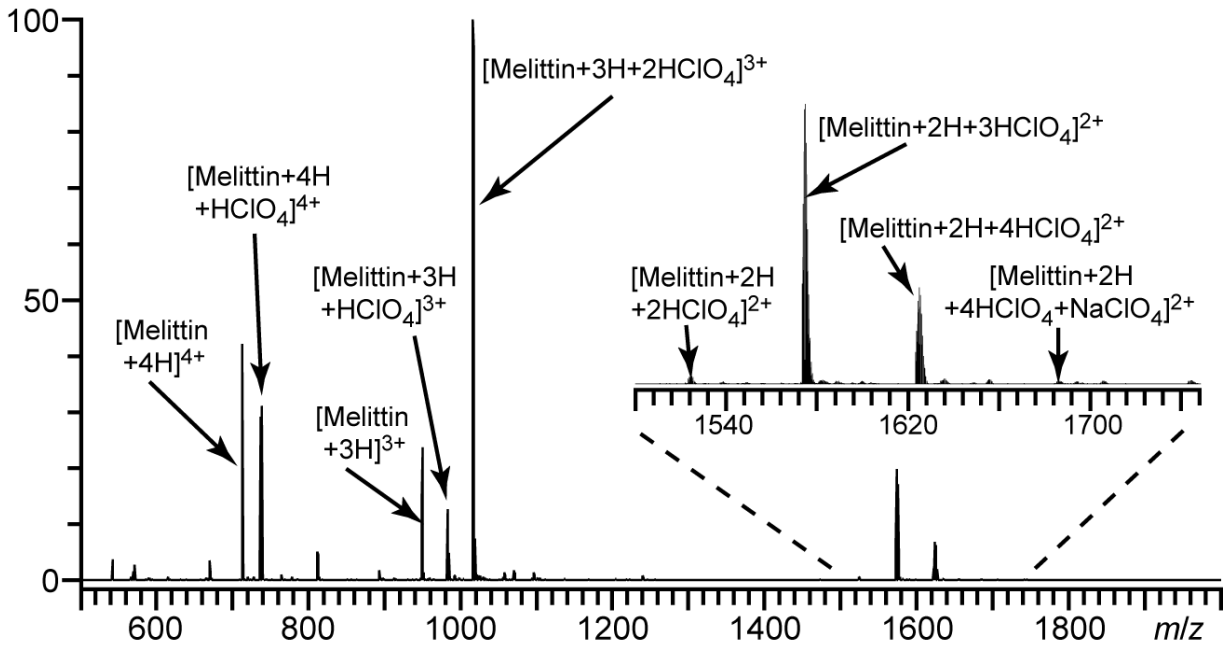

Figure 5.3. ESI mass spectrum of a solution containing 10 μM melittin and 10 mM $HClO_4$. Inset shows adduction of $HClO_4$ observed for the 2+ charge state.

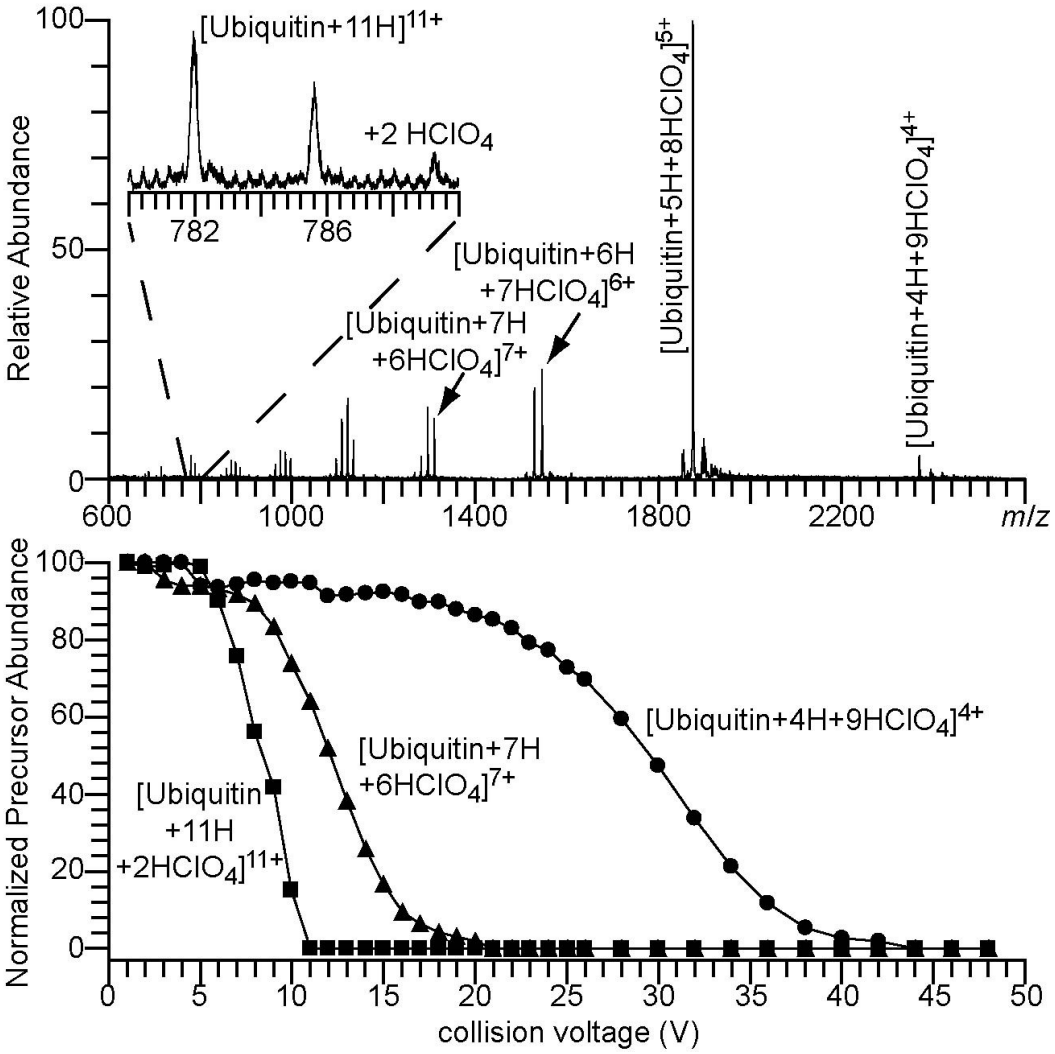

Figure 5.4. (a) A nanoESI mass spectrum of 10 μM ubiquitin and 10 mM $HClO_4$ acquired with a Q-TOF mass spectrometer, with inset showing adduction to the 11+ charge state, and (b) The normalized precursor abundance of mass-selected (ubiquitin + 11H + $2HClO_4$)$^{11+}$ (squares), (ubiquitin + 7H + $6HClO_4$)$^{7+}$ (triangles), and (ubiquitin + 4H + $9HClO_4$)$^{4+}$ (circles) ions as a function of collisional activation voltage.

CHAPTER 6

Solution Additives that Desalt Protein Ions in Native Mass Spectrometry

(This chapter is reproduced with permission from Flick, T.G.; Cassou, C.A.; Chang, T.M; Williams, E.R. This chapter was submitted to *Analytical Chemistry*.)

6.1 Introduction

Electrospray ionization (ESI) mass spectrometry (MS) is widely used to gently ionize and measure the masses of intact large molecules and complexes with high sensitivity (less than a femtomole of sample is possible).[1-13] However, the sensitivity of ESI-MS can be significantly lower when some salts, such as sodium chloride, are also present in the sample solution.[13-21] Even low millimolar concentrations of some metal ion salts can cause severe ion suppression and peak broadening due to cluster and adduct formation.[13-19] For example, addition of 10 mM CsCl to an aqueous solution containing 1 μM lysozyme resulted in a 330-fold reduction in protein ion abundance.[18] The adverse effects of some salts can be especially challenging for some biological samples that require essential salts or high ionic strength to assemble and maintain their functional forms in solution.[11-13]

There are several strategies to overcome the adverse effects of metal ion salts. The most common approach is to remove the salt from solution prior to ESI-MS, and this can be done using a variety of techniques, such as dialysis,[22,23] liquid chromatography,[23,24] and ion exchange.[25,26] However, removal of salts can also adversely affect the structures of some molecules and can affect binding of molecular complexes.[11-13] Sodium ion adduction in ESI depends on both the pI of the protein and the pH of the solution, and more adduction typically occurs for low charge state ions.[14-16] McLuckey and coworkers found that sodium adduction to gaseous positively charged protein ions can be significantly reduced when the solution pH is ~3 units lower than the pI of the protein.[15] High concentrations of ammonium acetate can reduce sodium adduction to protein ions and can be used to improve the mass measuring accuracy of large protein complexes where adducts to molecular ions are not resolved.[12-14] Addition of 7 M ammonium acetate to aqueous solutions containing 20 mM sodium chloride, and either cytochrome *c* or ubiquitin, resulted in a ~7- and ~11-fold improvement in signal-to-noise ratios (S/N) for the molecular ions of these respective proteins.[14]

Some anions, such as L-tartrate and citrate, can also reduce the extent of nonspecific metal ion adduction to biomolecules.[27-31] Konermann and coworkers found that nonspecific calcium adduction to proteins was significantly lower with calcium tartrate compared to calcium chloride or calcium acetate when these salts were added to the ESI solution, a result attributed to L-tartrate acting as a solution-phase chelator of calcium.[27] Gas-phase ion/ion reactions between DNA anions and several chelating ions, such as citrate, in a dual nanospray setup have also been shown to significantly reduce nonspecific metal ion adduction to DNA anions.[28] Metal ion adduction to oligonucleotides can also be reduced by adding acid vapors into the drying gas.[32]

Ions in solution can also affect the conformation and stability of protein and protein complex ions in the gas phase.[33-36] Attachment of acid molecules of select Hofmeister anions, ClO_4^-, I^-, and SO_4^{2-}, to ubiquitin, cytochrome *c*, and α-lactalbumin can induce compact conformations in the resulting gas-phase protein ions generated by ESI.[33] Ruotolo and coworkers found that anions with high gas-phase acidities, such as nitrate and chloride, bind to protein complexes in solution or during ESI and resulted in significant gas-phase stabilization of the protein complex ions.[34]

The extents of sodium ion and acid molecule adduction to positively charged protein ions formed by ESI from aqueous solutions that contain millimolar concentrations of sodium salts of various anions depend to a significant extent on the proton affinity (PA) of the anion.[37] The PA of an anion (A^-) is the negative enthalpy change for the gas-phase reaction:

$$A^- + H^+ \longrightarrow AH \qquad PA\ (A^-) = -\Delta H_{rxn}$$

For eleven sodium salts of anions that have PA values ranging from 260 to 371 kcal • mol^{-1}, the extent of sodium ion and acid molecule adduction to four proteins was inversely related. For anions with a high PA, deprotonation of acidic sites (Asp, Glu, and the C-terminus) can be favorable depending on the pI of the protein.[37] Deprotonation of acidic sites in the protein by the anion in the late stages of droplet evaporation makes possible strongly favorable interactions between the deprotonated site and sodium cations.[37] This results in little nonspecific sodium ion adduction to protein ions for anions with PA values below ~315 kcal • mol^{-1} and increasing adduction with increasing PA of the anion.[37] For anions with low PA values (< ~315 kcal • mol^{-1}), deprotonation of acidic sites is less favored, and acid molecule adduction to basic sites (Arg, Lys, His, N-terminus) occurs.[37] The number of basic sites in peptides and proteins can be accurately determined from the number of adducts.[37-39]

Here, we report that solution additives with anions that have low PA values can significantly reduce the extent of nonspecific sodium ion adduction and improve the abundances of gaseous protein and protein complex ions generated by ESI. Ammonium bromide and iodide are particularly effective at reducing nonspecific sodium adduction to protein ions at a significantly lower concentration than ammonium acetate, and acid molecule adduction, which depends on ion source conditions, is minimized.

6.2 Experimental

6.2.1 Mass Spectrometry. Mass spectra were acquired using either a LTQ-orbitrap mass spectrometer (Thermo Fisher Scientific, Waltham, MA, USA) or a 9.4 T Fourier-transform ion cyclotron resonance (FT-ICR) mass spectrometer equipped with an external ESI source that is described elsewhere.[40] Ions are generated by nanoESI from borosilicate capillaries that are pulled so that the tips have a ~2 μm inner diameter (model P-87 capillary puller, Sutter Instruments, Novato, CA). The capillary is loaded with a small volume (~2-10 μL) of analyte solution, and a platinum wire is inserted into the solution. The borosilicate capillary is positioned ~2 mm away from the source inlet capillary. Ions are generated by applying a potential difference of 800 to 1200 V

between the platinum wire and the inlet capillary. Total ion abundances can vary by a factor of up to five when different borosilicate capillaries are used. Due to the significant variability in the S/N between ESI capillaries, the average and standard deviation of the abundance of the protonated molecular ion and most abundant ion relative to the total ion abundance for each charge state are reported. To compare the effect of additives on absolute S/N, aqueous solutions containing 10 μM protein and 1.0 mM NaCl with or without an ammonium additive were analyzed using a single ESI capillary, which was washed between samples with water to reduce effects of cross contamination. This procedure was repeated using five different capillaries.

Bacillus amyloliquefaciens barstar and barnase were obtained by methods described previously.[41] Bovine ubiquitin, bovine cytochrome *c*, sodium chloride, ammonium acetate, ammonium bromide, ammonium iodide, ammonium tartrate, ammonium citrate, and $NaSbF_6$ were obtained from Sigma Aldrich (St. Louis, MO). The ammonium salt of SbF_6 is not commercially available, so $NaSbF_6$ was used instead.

6.2.2 Computational Chemistry. Initial geometries for the neutral and singly deprotonated forms of citric and L-tartaric acid were generated by a Monte Carlo conformational search using Macromodel 9.3 (Schrödinger, Inc., Portland, OR, U.S.A.). A selection of the low-energy conformers was used to create isomer geometries that represent different hydrogen bonding patterns, and geometry optimization at the B3LYP/6-31+G** level of theory was done using Q-Chem 4.0[42] (Q-Chem, Inc., Pittsburgh, PA, U.S.A). The geometries were further optimized with B3LYP/6-311++G** prior to vibrational frequency calculations at the same level of theory. Zero-point energies, enthalpy, and entropy corrections at 298 K were calculated using unscaled harmonic oscillator vibrational frequencies. Proton affinities and gas-phase basicities were calculated from $-\Delta H^{\circ}$ and $-\Delta G^{\circ}$, respectively, for the protonation of singly deprotonated citric and L-tartaric acid. These values were obtained from the lowest energy neutral and singly deprotonated structures (298 K).

6.3 Results and Discussion

6.3.1 Effects of Anions on Sodium Ion Adduction to Ubiquitin. The use of a new nanoESI capillary for each sample eliminates cross contamination of samples but makes it more challenging to accurately determine the extent to which various solution additives affect absolute signal owing primarily to the reproducibility of ion signal obtained from different capillaries. To determine how various additives affect ion signal, mass spectra of ubiquitin from solutions with and without different additives were obtained with a single ESI capillary that was cleaned prior to loading the capillary with a new sample, and this procedure was repeated using five different capillaries. The effects of the different additives on the relative abundances of both the fully protonated molecular ion and the most abundant ion relative to the total ion abundances of the 5+ and 6+ charge states of ubiquitin are given in Table 6.1, and representative ESI mass spectra obtained with a single ESI capillary that gave S/N values closest to the average of the five capillaries are shown in Figure 6.1.

ESI of an aqueous solution containing 1.0 mM NaCl and 10 μM ubiquitin results in molecular ions with extensive sodium ion adduction (Figure 6.1a). Both the 5+ and

6+ charge states have an average of six sodium ions adducted, and up to 17 sodium ions adduct to both charge states. Less than 3% of the total molecular ion abundance is from exclusively protonated molecular ions. The most abundant adducted form of the 5+ and 6+ ions account for only 11% and 13% of the total ion abundance for these respective charge states. Sodium ion adducts distribute the protein ion abundance into multiple cationized forms with various numbers of adducts, which lowers the S/N for each form of the protein ion in each charge state. With 1.0 M ammonium acetate added to this solution, the charge state distribution shifts to slightly higher charge, and less sodium ion adduction occurs, particularly to the higher charge state ion (Figure 6.1b). The average number of sodium ions adducted to the 5+ and 6+ charge states of ubiquitin is 4.8 and 1.3, respectively, and the fully protonated molecular ions account for approximately 28% of the total ion abundance.

A more substantial reduction in the extent of sodium ion adduction to ubiquitin occurs when either 25 mM ammonium bromide or ammonium iodide is added to solutions containing 1.0 mM NaCl (Figures 6.1c and 6.1d, respectively). With both ammonium additives, the charge state distribution is centered at the 6+, and the average number of sodium ions adducted to this charge state is 0.4. A more significant reduction in the average number of sodium ion adducts occurs to the 5+ charge state with ammonium bromide (0.4) compared to ammonium iodide (1.5), but both additives are significantly more effective at reducing sodium ion adduction to ubiquitin than ammonium acetate even when ammonium acetate is at a much higher concentration. With either ammonium iodide or ammonium bromide, the exclusively protonated molecular ions are the most abundant form of ubiquitin and account for 56% and 72% of the total ion abundance, respectively. With ammonium iodide, adduction of HI molecules occur, accounting for approximately 33% of the total ion abundance, whereas virtually no HBr adduction is observed under these conditions.

It was previously postulated that ammonium acetate reduces nonspecific sodium adduction to protein ions as a result of precipitation of sodium acetate in the ESI droplet as solvent preferentially evaporates and the salt is enriched.[14] However, the sodium salts of bromide and iodide are approximately a factor of 1.5 and 1.9 more soluble, respectively, than sodium acetate, indicating the effectiveness of bromide and iodide is not a result of the solubility of the sodium salts of these anions. The more significant reduction in sodium ion adducts with bromide and iodide compared to acetate is likely due to the 25 and 34 kcal • mol^{-1} lower PA values of these respective anions (PA of acetate = 348 kcal • mol^{-1}).[37] The lower PA values for iodide and bromide makes deprotonation of acidic sites on ubiquitin less favorable compared to acetate, thus fewer locations are available on the protein where sodium ions can adduct. HI adducts are observed, whereas no HBr adduction occurs, consistent with the 9 kcal • mol^{-1} lower PA of iodide compared to bromide.[37,37]

To determine the extent to which anions with even lower PA values can reduce sodium ion adduction, an ESI mass spectrum of ubiquitin was obtained from an aqueous solution containing 1.0 mM NaCl and 1.0 mM of the sodium salt of SbF_6^-, which has a PA value that is 88 kcal • mol^{-1} lower than that for acetate (Figure 6.1e). Only 1.0 mM $NaSbF_6$ was used because higher concentrations result in poor ubiquitin

ion abundance due to substantial formation of $Na^+(NaSbF_6)_n$ clusters. The charge state distribution is centered at 7+, and the average charge is ~2.8 charges higher than the solution without $NaSbF_6$. The average number of sodium ion adducts to the fully protonated 5+ to 8+ charge states is less than 0.3, and the exclusively protonated molecular ions account for 57% of the total ubiquitin ion abundance. This is the lowest sodium ion adduction observed for any of the additives investigated despite the factor of two higher concentration of sodium in this solution. As observed previously for salts with anions that have low PA values,[37,39] substantial $HSbF_6$ adduction occurs to ubiquitin ions, and accounts for approximately 33% of the total ubiquitin ion abundance.

To determine if the acid molecule adducts that occur with anions that have low PA values (i.e. $HSbF_6$ or HI) can be readily dissociated from ubiquitin using more energetic ion source conditions, ESI mass spectra of ubiquitin in aqueous solutions with 1.0 mM NaCl and 25 mM ammonium iodide or 1.0 mM $NaSbF_6$ were obtained on a LTQ-Orbitrap instrument using capillary temperatures of 100 ^oC or 300 ^oC (Figure 6.2). At 100 ^oC, minimal sodium ion adduction is observed to ubiquitin ions with either additive, but substantial HI or $HSbF_6$ adduction occurs. At 300 ^oC, HI adducts are eliminated without a significant increase (less than 1%) in the amount of sodium ion adduction to ubiquitin. An insignificant increase in the amount of sodium ion adduction is also observed at 300 ^oC with NaSbF, but only a small decrease (~14%) in the amount of $HSbF_6$ adduction to ubiquitin ions occurs compared to that at 100 ^oC, indicating that $HSbF_6$ adducts are more tightly bound to the protein ions than HI. However, $HSbF_6$ adducts can be readily removed by collisionally activating the ubiquitin ions after introduction into the mass spectrometer (Figure 6.3). These results indicate that the extent of acid molecule adduction that occurs to protein ions depends significantly on the ion source conditions, and acid molecule adducts can readily be dissociated from protein ions by activating the ion either in the source or after introduction into the mass spectrometer.

6.3.2 Effects of Anions on Sodium Adduction to Other Proteins and Complexes. Remarkably similar results on how anions affect the extent of sodium ion adduction to molecular ions of ubiquitin are obtained with cytochrome *c*. ESI of an aqueous solution containing 10 μM cytochrome *c* and 1.0 mM NaCl results in a charge state distribution centered at 7+ with an average and maximum number of 6.5 and 18 sodium ions adducted, respectively, to this ion. The fully protonated molecular ion is only 3% of the total ion abundance of the 7+ charge state. The most abundant form of the 7+ ions, $(M + 5H + 2Na)^{7+}$, is only 10% of the total ion abundance for this charge state, as a result of cytochrome *c* ion signal being distributed into multiple forms with various numbers of sodium adducts. Sodium adduction is lower for solutions with 1.0 mM NaCl and 1.0 M ammonium acetate, with an average and maximum number of sodium ion adducts of 3.4 and 9, respectively, to the 7+ charge state (Figure 6.4b). $(\text{cytochrome } c + 7H)^{7+}$ is significantly more abundant with ammonium acetate, accounting for 21% of the total ion abundance of this charge state. A dramatic reduction in sodium ion attachment occurs for solutions with 1.0 mM NaCl and 25 mM of either ammonium bromide or ammonium iodide (Figure 6.4c and 6.4d, respectively). The most abundant charge state is the 7+, and the average and maximum number of

sodium ion adducts is 0.5 and 3, respectively, with ammonium bromide and 0.8 and 5, respectively, with ammonium iodide. (cytochrome *c* + 7H)$^{7+}$ is the most abundant ion in the 7+ charge state with ammonium iodide or ammonium bromide, and accounts for 61% and 69% of the total ion abundance, respectively, for this charge state. For solutions with 1.0 mM NaCl and 1.0 mM $NaSbF_6$, the charge state distribution is shifted to higher charge, and the average number of sodium ion adducts to all charge states of cytochrome *c* is less than 0.3. There is more extensive adduction of $HSbF_6$ (78% of total ion abundance) to cytochrome *c* than ubiquitin, whereas less adduction of HI occurs (6% of total ion abundance). This indicates that the extent of molecular adduction depends on both the ion source conditions as well as the physical properties of the protein.

With large protein complexes, unresolved sodium and other metal ion adduction can result in significant broadening of charge states and an increase in the measured mass.[12] Adduction can be so extensive that charge states are unresolved, making mass measurements challenging. Buffer loading with ammonium acetate can be used in some instances to reduce the effect of adduction but can also affect the protein binding at high concentrations.[13,14] To determine whether the extent of sodium ion adduction to a protein complex can be reduced at a much lower additive concentration, ESI mass spectra of an aqueous solution of 5.0 μM barnase (bn) and 8.0 μM barstar (b*) containing 1.0 mM NaCl and either 1.0 M ammonium acetate (Figure 6.5) or 25 mM ammonium bromide (Figure 6.5b) were obtained. The charge states of the bn/b* complex range from 8+ to 10+ and b*, the excess reagent, is also observed with 6+ and 5+ charges. More adduction to the lower charge states of the bn/b* complex occurs. The average number of sodium ion adducts to the 8+ and 9+ charge states are 3.6 and 2.3, respectively, with 1.0 M ammonium acetate, whereas these respective values are 0.3 and 0.2 with 25 mM ammonium bromide. The abundance of the fully protonated bn/b* complex with 9+ charges is ~2-fold higher with ammonium bromide compared to ammonium acetate. These results indicate that ammonium bromide may be a useful additive to reduce the extent of sodium ion or other nonspecific metal ion adduction to protein complexes, as well as individual protein ions, formed by ESI from aqueous solutions with high ionic strength.

6.3.3 Effects of Salts on Absolute Ion Signal. To demonstrate the effect of different additives on absolute ion signal, the S/N for the protonated molecular ion and most abundant molecular ion of ubiquitin in the ESI mass spectra shown in Figure 6.1 is reported (Table 6.1, values in parentheses). With 1.0 mM NaCl, the total ion abundance of ubiquitin is poor, and the S/N of both the fully protonated molecular ion and the most abundant ion for each charge state are low. A low S/N of any single ion reduces the sensitivity with which tandem MS experiments can be made, and this is particularly a problem for the fully protonated molecular ion. With 1.0 mM ammonium acetate added to this solution, the S/N of the most abundant ion, (ubiquitin + 6H)$^{6+}$, increases by a factor of 4.4, but there is only a small increase (~6%) for the most abundant ion in the 5+ charge state. Both 25 mM ammonium iodide and ammonium bromide are more effective than ammonium acetate at shifting both ubiquitin 5+ and 6+ to the fully protonated form. The S/N of the most abundant ion, (ubiquitin + 6H)$^{6+}$,

increases by a factor of 30 and 66 with ammonium iodide and ammonium bromide, respectively, compared to that obtained without an ammonium additive, and there is a substantial increase (>37%) for the most abundant ion in the 5+ charge state as well. In addition, the absolute S/N for the most abundant ion of ubiquitin 5+ and 6+ is higher by more than a factor of 4.5 with either of these additives compared to that obtained with ammonium acetate. These results show that ammonium iodide or ammonium bromide can improve sensitivity by shifting ion abundance for a given charge state from many adducted forms into predominantly the fully protonated form.

6.3.4 Sodium Ion Adduction with Ammonium Citrate or Tartrate. Both citrate and L-tartrate were reported to reduce the extent of nonspecific Ca^{2+} binding to protein ions formed by ESI, an effect attributed to these anions chelating ability of Ca^{2+} in solution.[27] Ammonium salts of both anions also reduce metal ion adduction to protein and oligonucleotide ions formed by matrix assisted laser desorption/ionization (MALDI).[29-31] To determine if citrate or L-tartrate can be effective additives for reducing sodium adduction to protein ions as well, ESI mass spectra of ubiquitin from aqueous solutions containing 1.0 mM NaCl and 25 mM of either ammonium tartrate or citrate were obtained under identical conditions as those used for the other ammonium additives (Figures 6.1, 6.2, and 6.5), and these data are shown in Figure 6.6b and 6.6c, respectively. The charge state distribution is shifted slightly to higher charge and the extent of sodium ion adduction is significantly reduced compared to the solution with just 1.0 mM NaCl (Figure 6.6a). However, the fully protonated molecular ions of ubiquitin are 28% and 37% less abundant with ammonium tartrate and citrate compared to that observed with ammonium bromide. Substantial adduction of L-tartaric and citric acid to ubiquitin ions occurs and accounts for ~12% and 43% of the total ubiquitin ion abundance, respectively, whereas no HBr adducts occur. These results indicate that ammonium bromide is a better additive to reduce nonspecific adducts to protein ions compared to ammonium citrate or ammonium tartrate when relatively gentle ion source conditions are used.

In solution, neither citrate nor L-tartrate bind strongly to sodium ions (K_d ~ 1.6 and 2.0 M, respectively, for fully sodiated forms). This indicates that neither of these ions lowers the extent of sodium ion adduction to ubiquitin ions by sequestering Na^+ in solution by chelation. The pH of ESI droplets can increase as solvent evaporation occurs,[43] and the stability of the different forms of these anions depends on solvation. Previous results indicate that the extent of sodium ion and acid molecule adduction best correlates to the PA of the singly deprotonated form of the anions.[37] The PA and gas-phase basicity of the singly deprotonated citric or L-tartaric acid have not been previously reported, so these values were determined using computational chemistry.

The lowest energy structures of the neutral and singly deprotonated form of citric and L-tartaric acid are shown in Figure 6.7. Although only the structure of lowest energy for neutral citric and L-tartaric acid are shown, several other structures were found to be energetically competitive, and are shown in Figures 6.8 and 6.9, respectively. The most favorable deprotonation site on citric acid is at the central carboxylic acid (site 1), but deprotonation at the hydroxyl group (site 2) and terminal carboxylic acid (site 3) are only 2.2 and 3.2 kcal $\bullet$ mol^{-1} higher, respectively, in Gibbs

free energy. Deprotonation of L-tartaric acid at the carboxylic acid (site 1) is energetically favored compared to deprotonation at the hydroxyl group (site 2), which is calculated to be 9.0 kcal•mol^{-1} higher in Gibbs free energy. From the computed 298 K enthalpies of the lowest energy structures, the PA values for singly deprotonated citric and L-tartaric acid were computed at the B3LYP/6-311++G** level of theory to be 303 and 312 kcal•mol^{-1}, respectively, and the respective gas-phase basicity values were calculated to be 298 and 306 kcal•mol^{-1}. These results indicate that the effectiveness of ammonium tartrate and ammonium citrate in desalting gaseous protein ions is likely a result of the low PA of these anions, and not their ability to sequester sodium ions in solution prior to ion formation.

Extensive adduction of citric and L-tartaric acid occurs under the relatively gentle ion source conditions used in these experiments. Results presented here and from earlier studies[39] show that the extent of molecular adduction of acids to proteins can depend on ESI source conditions, and activation of these adducts through gas-phase collisions results in loss of the molecular acid.[39] Repeating these experiments using a Thermo LTQ-orbitrap mass spectrometer with more energetic source conditions (300 ^{o}C capillary temperature) results in a spectrum with a similar number of sodium adducts, but no citric or L-tartaric acid molecules attached (Figure 6.10). This indicates that the extent of molecular adduction, but not the amount of sodium ion adduction, observed in these experiments depends strongly on the extent to which the ions are activated in the ESI source or subsequently prior to mass analysis.

6.4 Conclusions

Sodium ion adduction to protein ions formed by ESI can adversely affect mass spectrometry measurements by reducing the overall ionization efficiency and distributing the existing ion abundance into many different adducted forms. Addition of some ammonium salts can reduce the amount of nonspecific sodium adduction to gaseous protein ions and significantly improve the ion abundance for proteins and protein complex ions formed by ESI. The effectiveness of these additives depends predominantly on the acidity of the anion. Ammonium bromide is particularly effective at lowering sodium adduction to gaseous protein ions without acid molecule adduction under relatively gentle source conditions. Anions, such as I^- and SbF_6^-, that have lower PA values than Br^- are also effective at reducing the extent of nonspecific sodium ion adduction, but attachment of the acid molecules can also occur. However, these molecular adducts can be readily dissociated from the protein ions by using harsher source conditions or by collisionally activating the ions after introduction into the mass spectrometer.

This method of desalting protein ions in native ESI is simple, very effective, requires no instrumental or other modifications, and can significantly increase the absolute abundances of the fully protonated forms of the molecular ions, which should result in improved detection limits, more accurate mass measurements, and improved tandem MS sensitivity. The method may be applicable to reducing interferences from nonspecific binding of many other metal ions as well. It may also be useful for measuring binding constants of proteins with low metal ion affinities by reducing the

extent of nonspecific adduction that can occur in ESI-MS. These additives may also be effective for desalting biomolecular ions formed by MALDI.

6.5 References

(1) Fenn, J. B.; Mann, M.; Meng, C. K.; Wong, S. F.; Whitehouse, C. M. *Science* **1989**, *246*, 64-71.
(2) Robinson, C. V.; Chung, E. W.; Kragelund, B. B.; Knudsen, J.; Aplin, R. T.; Poulsen, F. M.; Dobson, C. M. *J. Am. Chem. Soc.* **1996**, *118*, 8646-8653.
(3) Ruotolo, B. T.; Giles, K.; Campuzano, I.; Sandercock, A. M.; Bateman, R. H.; Robinson, C. V. *Science* **2005**, *310*, 1658-1661.
(4) Sterling, H. J.; Kintzer, A. F.; Feld, G. K.; Cassou, C. A.; Krantz, B. A.; Williams, E. R. *J. Am. Soc. Mass Spectrom.* **2012**, *23*, 191-200.
(5) Lazar, I. M.; Ramsey, R. S.; Sundberg, S.; Ramsey, J. M. *Anal. Chem.* **1999**, *71*, 3627-3631.
(6) Froehlich, T.; Arnold, G. J. *Methods in Mol. Biol* **2011**, *790*, 141-164.
(7) Valaskovic, G. A.; Kelleher, N. L.; McLafferty, F. W. *Science* **1996**, *273*, 1199-1202.
(8) Valaskovic, G. A.; Kelleher, N. L.; Little, D. P.; Aaserud, D. J.; McLafferty, F. W. *Anal. Chem.* **1995**, *67*, 3802-3805.
(9) Belov, M. E.; Gorshkov, M. V.; Udseth, H. R.; Anderson, G. A.; Smith, R. D. *Anal. Chem.* **2000**, *72*, 2271-2279.
(10) Emmett, M. R.; Caprioli, R. M. *J. Am. Soc. Mass Spectrom.* **1994**, *5*, 605-613.
(11) Cohen, S. L.; Ferredamare, A. R.; Burley, S. K.; Chait, B. T. *Protein Sci.* **1995**, *4*, 1088-1099.
(12) Hernandez, H.; Robinson, C. V. *Nat. Protoc.* **2007**, *2*, 715-726.
(13) Sterling, H. J.; Batchelor, J. D.; Wemmer, D. E.; Williams, E. R. *J. Am. Soc. Mass Spectrom.* **2010**, *21*, 1045-1049.
(14) Iavarone, A. T.; Udekwu, O. A.; Williams, E. R. *Anal. Chem.* **2004**, *76*, 3944-3950.
(15) Pan, P.; Gunawardena, H. P.; Xia, Y.; McLuckey, S. A. *Anal. Chem.* **2004**, *76*, 1165-1174.
(16) Pan, P.; McLuckey, S. A. *Anal. Chem.* **2003**, *75*, 5468-5474.
(17) Tang, L.; Kebarle, P. *Anal. Chem.* **1993**, *65*, 3654-3668.
(18) Wang, G. D.; Cole, R. B. *Anal. Chem.* **1994**, *66*, 3702-3708.
(19) Juraschek, R.; Dulcks, T.; Karas, M. *J. Am. Soc. Mass Spectrom.* **1999**, *10*, 300-308.
(20) Ikonomou, M. G.; Blades, A. T.; Kebarle, P. *Anal. Chem.* **1990**, *62*, 957-967.
(21) Mirza, U. A.; Chait, B. T. *Anal. Chem.* **1994**, *66*, 2898-2904.
(22) Liu, C. L.; Wu, Q. Y.; Harms, A. C.; Smith, R. D. *Anal. Chem.* **1996**, *68*, 3295-3299.
(23) Dalluge, J. J. *Fresenius J. Anal. Chem.* **2000**, *366*, 701-711.
(24) Bauer, K. H.; Knepper, T. P.; Maes, A.; Schatz, V.; Voihsel, M. *J. Chromatogr. A* **1999**, *837*, 117-128.
(25) Huber, C. G.; Buchmeiser, M. R. *Anal. Chem.* **1998**, *70*, 5288-5295.
(26) Jiang, Y.; Hofstadler, S. A. *Anal. Biochem.* **2003**, *316*, 50-57.
(27) Pan, J. X.; Xu, K.; Yang, X. D.; Choy, W. Y.; Konermann, L. *Anal. Chem.* **2009**, *81*, 5008-5015.

(28) Turner, K. B.; Monti, S. A.; Fabris, D. *J. Am. Chem. Soc.* **2008**, *130*, 13353-13363.
(29) Zhu, Y. F.; Taranenko, N. I.; Allman, S. L.; Martin, S. A.; Chen, C. H. *Rapid Commun. Mass Spectrom.* **1996**, *10*, 1591-1596.
(30) Currie, G. J.; Yates, J. R. *J. Am. Soc. Mass Spectrom.* **1993**, *4*, 955-963.
(31) Asara, J. M.; Allison, J. *J. Am. Soc. Mass Spectrom.* **1999**, *10*, 35-44.
(32) Kharlamova, A.; Prentice, B. M.; Huang, T. Y.; McLuckey, S. A. *Int. J. Mass Spectrom.* **2011**, *300*, 158-166.
(33) Merenbloom, S. I.; Flick, T. G.; Daly, M. P.; Williams, E. R. *J. Am. Soc. Mass Spectrom.* **2011**, *22*, 1978-1990.
(34) Han, L. J.; Hyung, S. J.; Mayers, J. J. S.; Ruotolo, B. T. *J. Am. Chem. Soc.* **2011**, *133*, 11358-11367.
(35) Freeke, J.; Robinson, C. V.; Ruotolo, B. T. *Int. J. Mass Spectrom.* **2010**, *298*, 91-98.
(36) Freeke, J.; Bush, M. F.; Robinson, C. V.; Ruotolo, B. T. *Chem. Phys. Lett.* **2012**, *524*, 1-9.
(37) Flick, T. G.; Merenbloom, S. I.; Williams, E. R. *J. Am. Soc. Mass Spectrom.* **2011**, *22*, 1968-1977.
(38) Stephenson, J. L.; McLuckey, S. A. *Anal. Chem.* **1997**, *69*, 281-285.
(39) Flick, T. G.; Merenbloom, S. I.; Williams, E. R. *Anal. Chem.* **2011**, *83*, 2210-2214.
(40) Robinson, E. W.; Williams, E. R. *J. Am. Soc. Mass Spectrom.* **2005**, *16*, 1427-1437.
(41) Krishnaswamy, S. R.; Williams, E. R.; Kirsch, J. F. *Protein Sci.* **2006**, *15*, 1465-1475.
(42) Shao, Y.; al., e. *Phys. Chem. Chem. Phys.* **2006**, *8*, 3172-3191.
(43) Gatlin, C. L.; Tureček, F. *Anal. Chem.* **1994**, *66*, 712-718.

6.6 Tables

Table 6.1. Relative abundances of the fully protonated and most abundant molecular ion and average # of sodium adducts for ubiquitin 5+ and 6+.

Ubiquitin 5+

Ammonium Additive	Relative Abundance of Protonated Molecular Ion	Relative Abundance of Most Abundant Ion	Average # of Sodium Adducts
No Additive	1 ± 1% (25)[a]	11 ± 1% (364)[a]	6.3 ± 1.4
1 M Ammonium Acetate	12 ± 3% (342)[a]	13 ± 5% (387)[a]	4.8 ± 1.4
25 mM Ammonium Iodide	48 ± 7% (1749)[a]	48 ± 7% (1749)[a]	1.5 ± 0.2
25 mM Ammonium Bromide	70 ± 12% (3211)[a]	70 ± 12% (3211)[a]	0.5 ± 0.2

Ubiquitin 6+

Ammonium Additive	Relative Abundance of Protonated Molecular Ion	Relative Abundance of Most Abundant Ion	Average # of Sodium Adducts
No Additive	2 ± 1% (17)[a]	13 ± 3% (100)[a]	5.8 ± 0.8
1 M Ammonium Acetate	44 ± 5% (443)[a]	44 ± 5% (443)[a]	1.3 ± 0.1
25 mM Ammonium Iodide	64 ± 3% (3044)[a]	64 ± 3% (3044)[a]	0.4 ± 0.2
25 mM Ammonium Bromide	74% ± 9% (6578)[a]	74 ± 9% (6578)[a]	0.4 ± 0.1

[a]Values in parentheses are the absolute S/N obtained from a single ESI capillary.

6.7 Figures

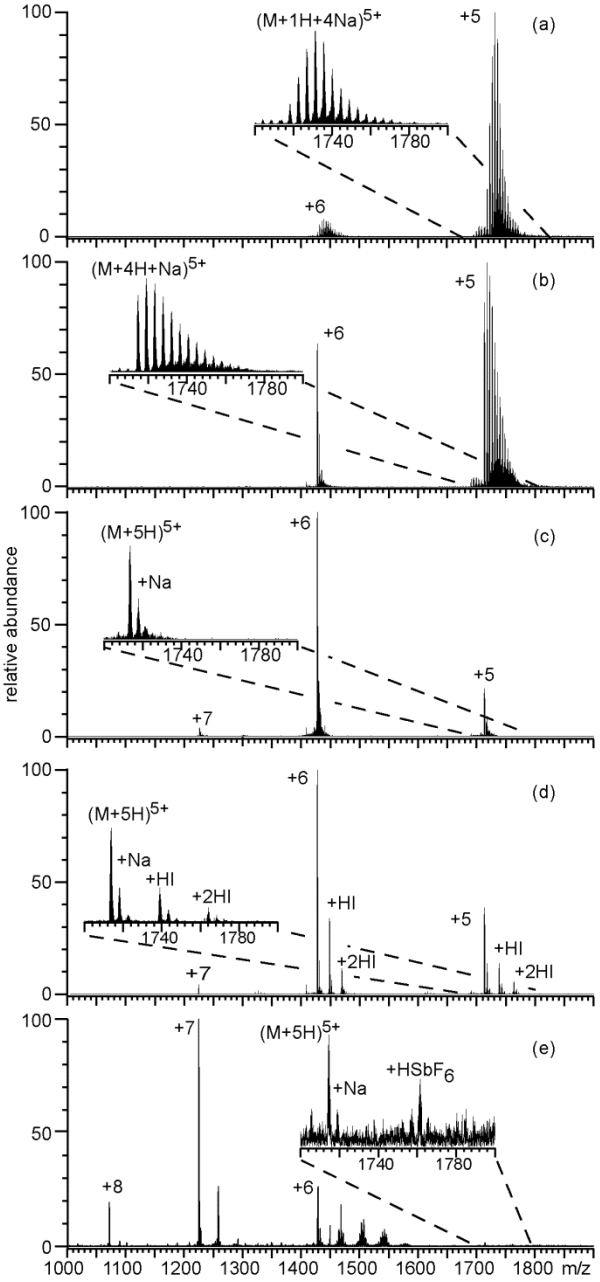

Figure 6.1. ESI mass spectra obtained from aqueous solutions containing 10 μM ubiquitin with 1.0 mM NaCl and (a) no additional additive, (b) 1.0 M ammonium acetate, (c) 25 mM ammonium bromide, (d) 25 mM ammonium iodide, or (e) 1.0 mM $NaSbF_6$. Insets show an expanded region of the 5+ charge state.

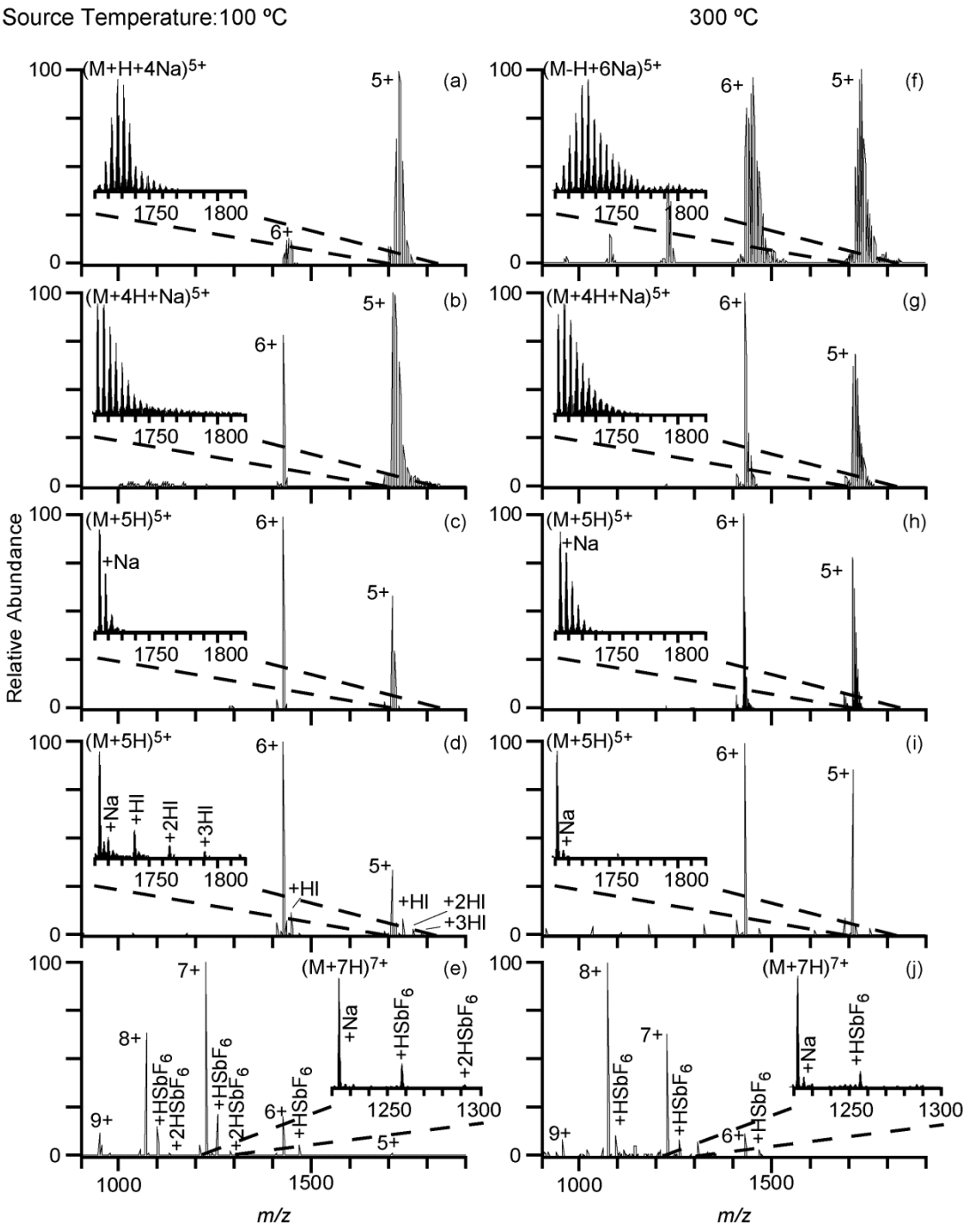

Figure 6.2. ESI mass spectra obtained on a LTQ-orbitrap mass spectrometer from aqueous solutions of 10 μM ubiquitin and 1.0 mM NaCl with (a),(f) no additional additives, (b),(g) 1.0 M ammonium acetate, (c),(h) 25 mM ammonium bromide, (d),(i) 25 mM ammonium iodide, and (e),(j) 1.0 mM $NaSbF_6$ using a capillary temperature of 100 ^oC or 300 ^oC, respectively.

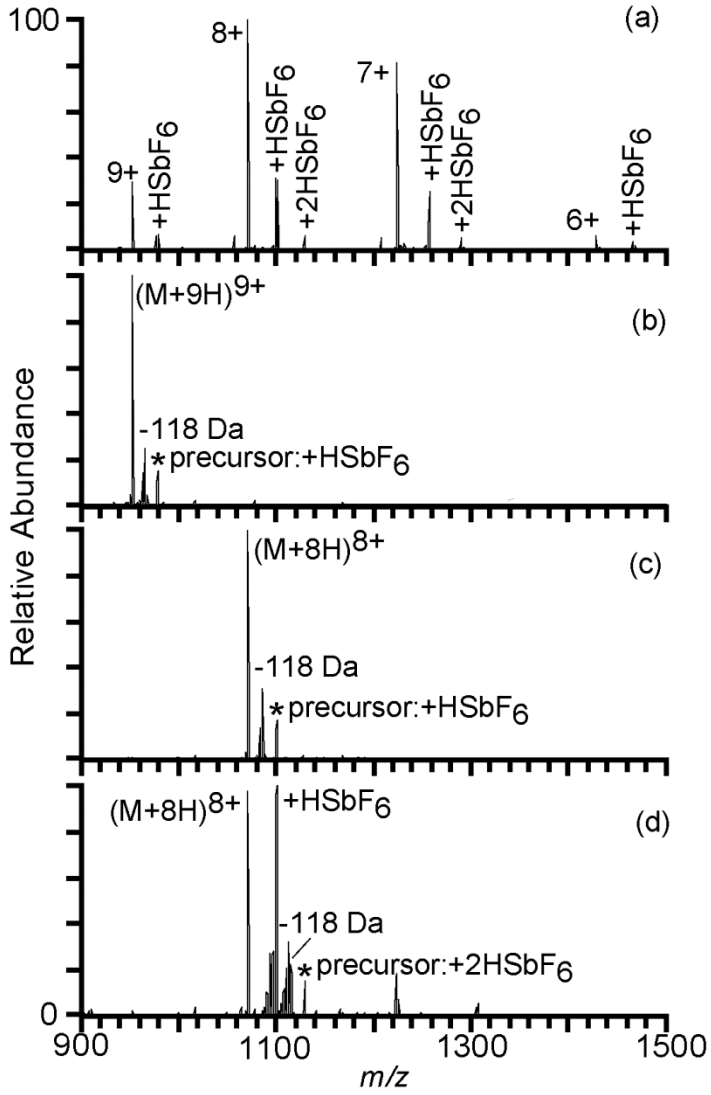

Figure 6.3. (a) ESI mass spectrum obtained on a LTQ-orbitrap mass spectrometer from an aqueous solution of 10 μM ubiquitin, 1.0 mM NaCl, and 1.0 mM $NaSbF_6$. Collision induced dissociation mass spectra of (b) (ubiquitin $+HSbF_6$ + 9H)$^{9+}$, (c) (ubiquitin + $HSbF_6$ + 8H)$^{8+}$, and (d) (ubiquitin + $2HSbF_6$ + 8H)$^{8+}$ using a normalized collision energy of 20%.

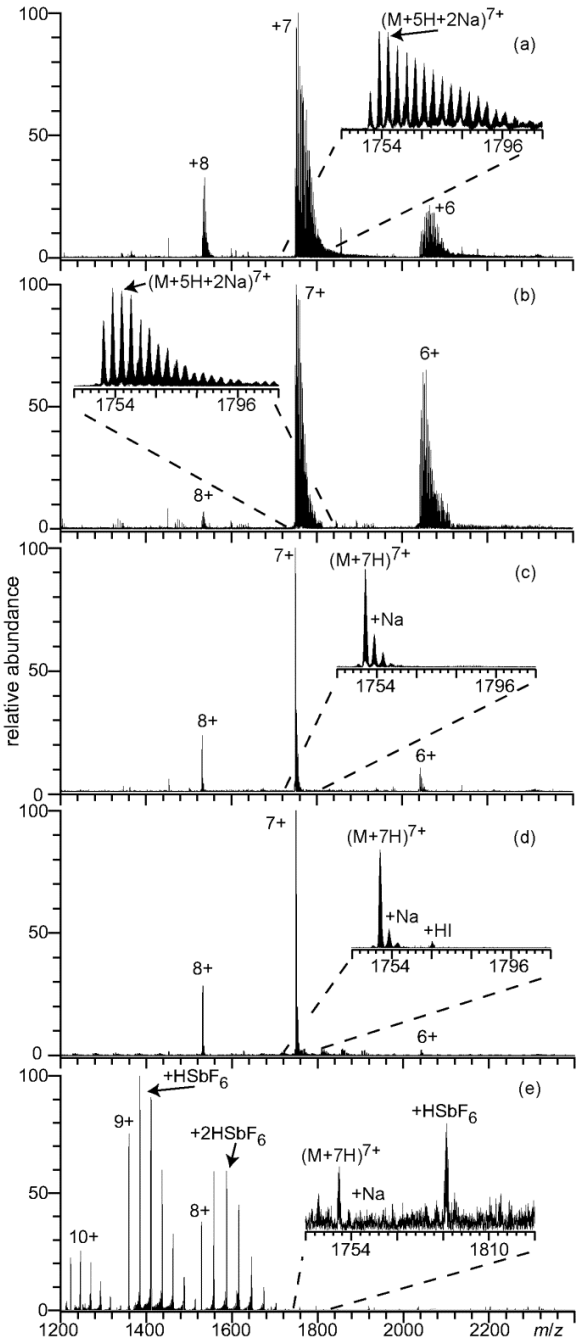

Figure 6.4. ESI mass spectra obtained from aqueous solutions containing 10 μM cytochrome *c* with 1.0 mM NaCl and (a) no additional additive, (b) 1.0 M ammonium acetate, (c) 25 mM ammonium bromide, (d) 25 mM ammonium iodide, or (e) 1.0 mM $NaSbF_6$. Insets show an expanded region of the 7+ charge state.

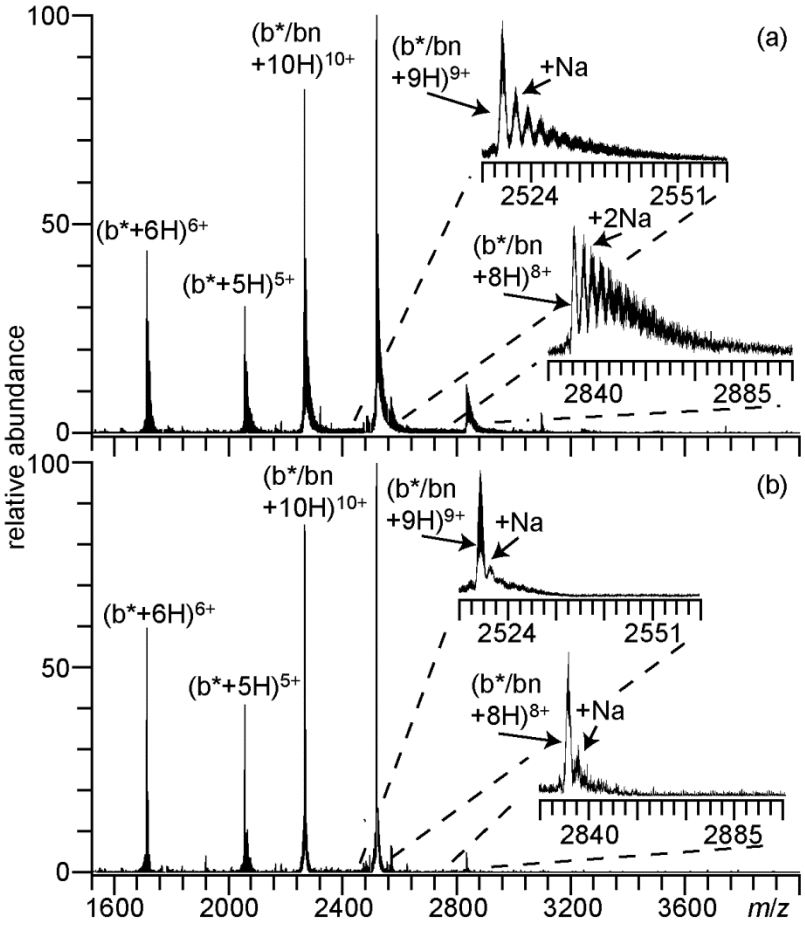

Figure 6.5. ESI mass spectra obtained from an aqueous solution of 5 μM barnase (bn) and 8 μM barstar (b*) containing 1.0 mM NaCl and (a) 1.0 M ammonium acetate or (b) 25 mM ammonium bromide.

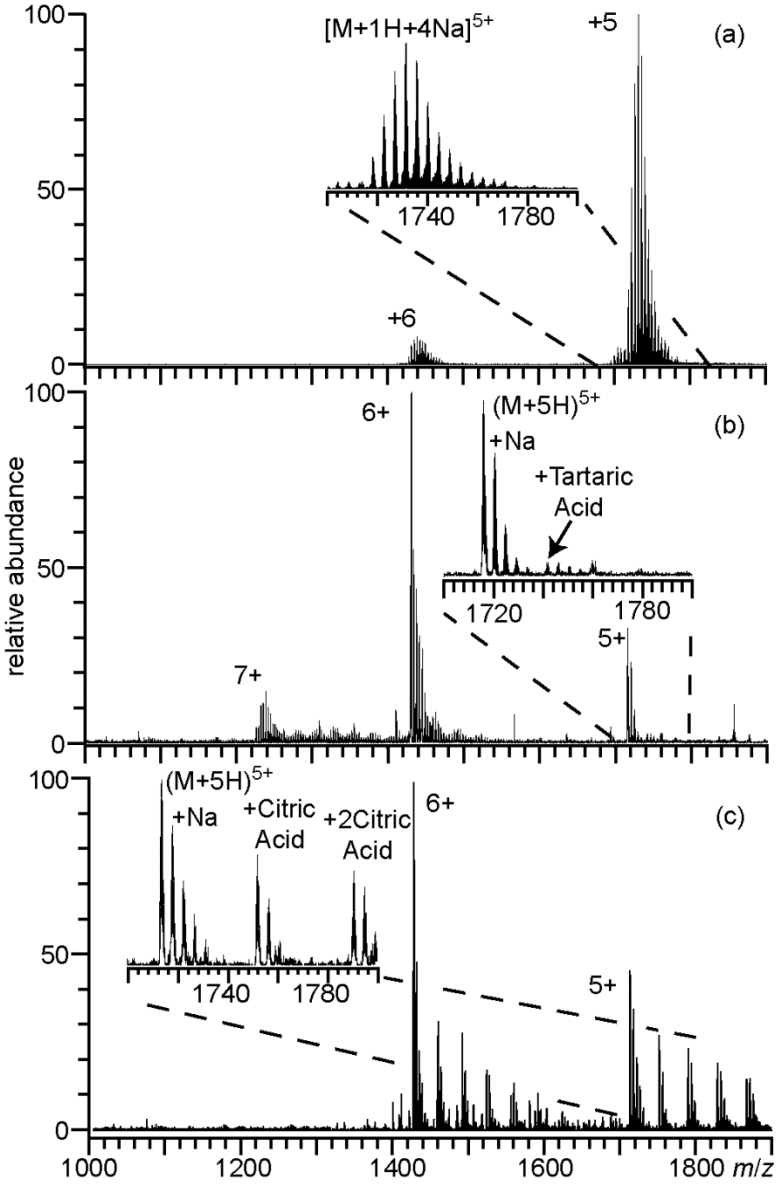

Figure 6.6. ESI mass spectra obtained from aqueous solutions containing 10 μM ubiquitin with 1.0 mM NaCl and (a) no additional additive, (b) 25 mM ammonium tartrate, or (c) 25 mM ammonium citrate.

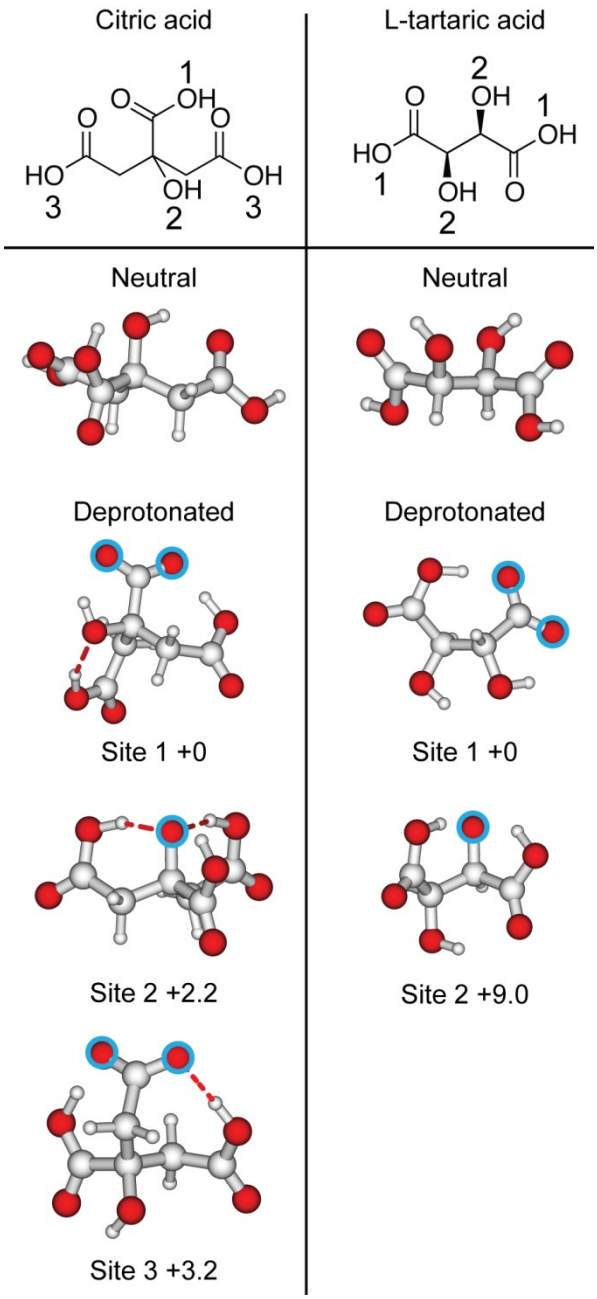

Figure 6.7. Calculated structures of lowest energy for citric acid and L-tartaric acid. Both the neutral and deprotonated forms are shown. The deprotonation site is indicated with a circle and relative Gibbs free energies are reported in kcal • mol^{-1}.

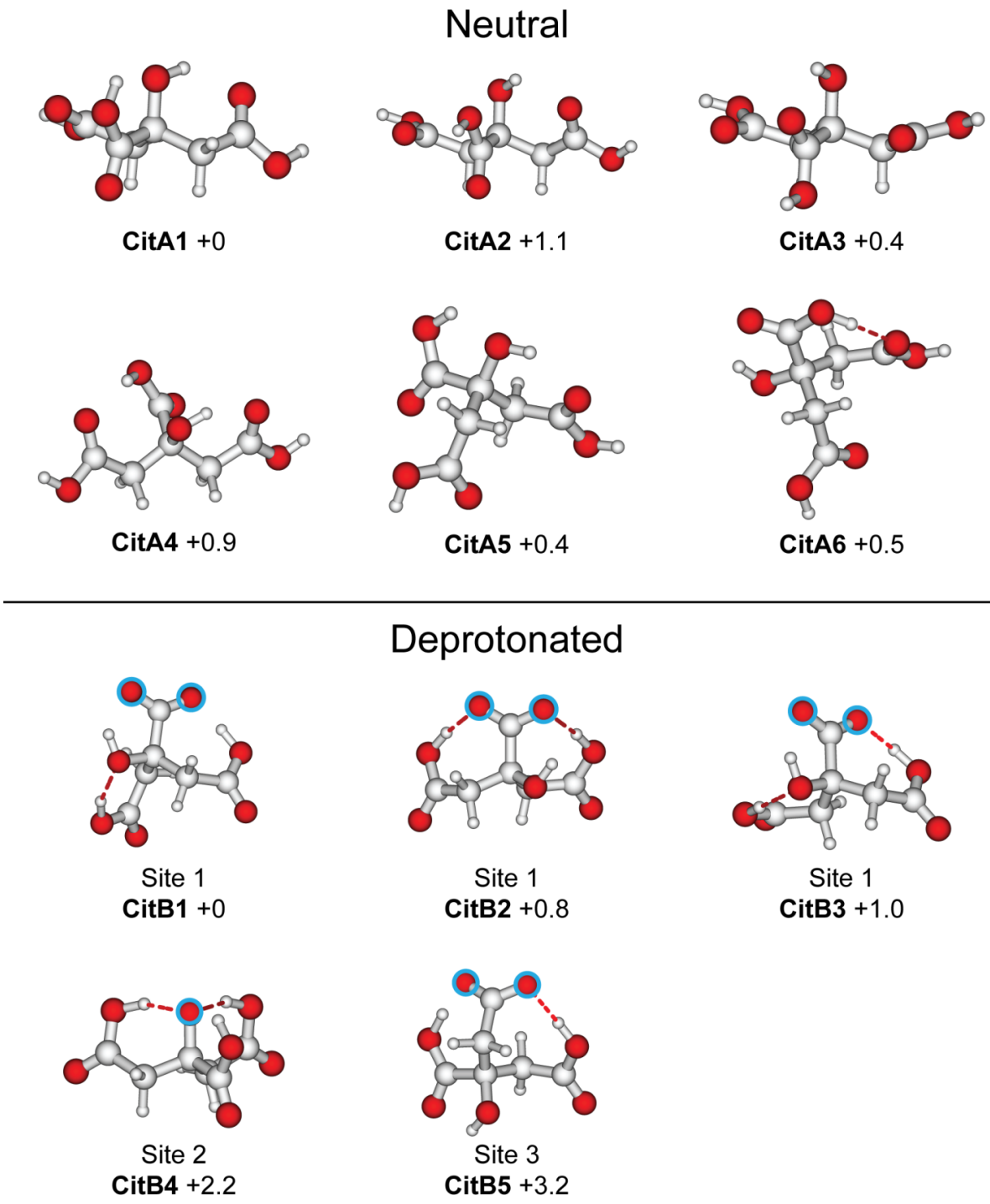

Figure 6.8. Calculated structures and relative Gibbs free energies (kcal • mol^{-1}) at 298 K for neutral (top) and singly deprotonated (bottom) citric acid. Relative energies are calculated at the B3LYP/6-311++G** level of theory.

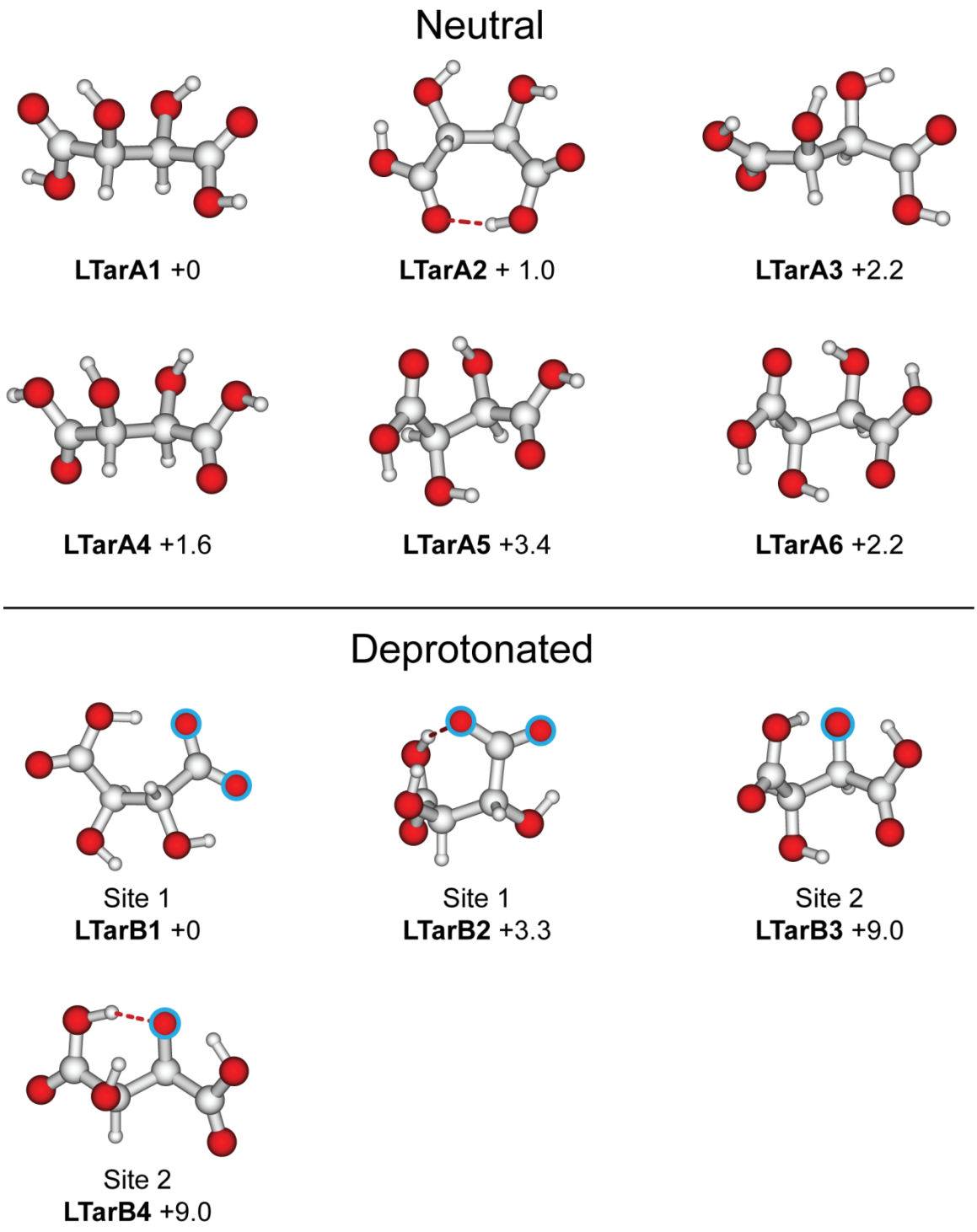

Figure 6.9. Calculated structures and relative Gibbs free energies (kcal • mol^{-1}) at 298 K for neutral (top) and singly deprotonated (bottom) L-tartaric acid. Relative energies are calculated at the B3LYP/6-311++G** level of theory.

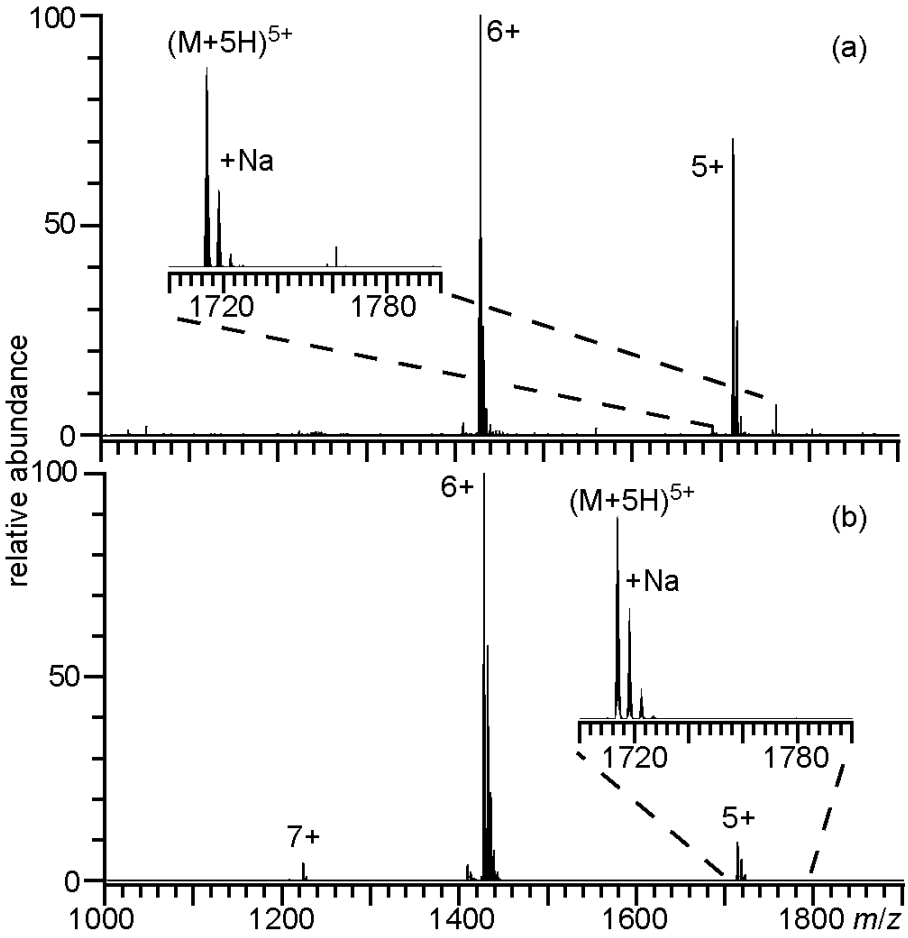

Figure 6.10. ESI mass spectra obtained on a LTQ-orbitrap mass spectrometer from aqueous solutions containing 10 μM ubiquitin with 1.0 mM NaCl and (a) 25 mM ammonium tartrate or (b) 25 mM ammonium citrate using a capillary temperature of 300 ^{o}C.

CHAPTER 7

Supercharging with Trivalent Metal Ions in Native Mass Spectrometry

(This chapter is reproduced with permission from Flick, T.G. and Williams, E.R. This chapter was submitted to the *Journal of American Society for Mass Spectrometry*.)

7.1 Introduction

Electrospray (ESI) ionization is widely used to generate intact multiply-charged ions of proteins and protein complexes from aqueous solutions, a technique often referred to as native mass spectrometry (MS).[1-4] The multiple charging of large molecules that typically occurs with ESI is advantageous for lowering m/z values into a range where high performance mass measurements can be made.[5,6] Increasing analyte charge also increases the sensitivity of mass spectrometers where the signal of an ion is proportional to it's charge, such as orbitrap and Fourier-transform ion cyclotron resonance (FT-ICR) instruments.[7,8]

Several factors affect the extent of analyte charging by ESI, including analyte conformation,[9-11] solvent and analyte basicity,[12-14] instrumental factors,[15,16] and solvent surface tension.[17-19] Broad charge state distributions of molecular ions centered about high charge are typically observed from solutions in which proteins are unfolded, whereas narrow distributions at low charge are obtained for proteins and protein complexes formed from solutions in which these molecules have native structures.[9-11] The solution-phase denaturation of proteins as a result of heating or acidifying the bulk ESI solution can be monitored by ESI-MS from shifts in the charge state distribution towards higher charge.[10,11] Complexation of multivalent metal ions can also increase the charge states of molecular ions formed by ESI,[20-23] and has been used effectively to obtain electron capture dissociation (ECD) spectra of small peptides for which multiply protonated ions are not typically formed.[21-23]

An effective method to increase the charging observed for many biomolecules is the use of supercharging reagents, such as *m*-nitrobenzyl alcohol (*m*-NBA).[17-19,24-37] Originally demonstrated for protein ions formed from denaturing solutions,[17-19] this supercharging method is also effective at increasing the charge states of protein and protein complex ions formed from native solutions.[24-31] Supercharging reagents have high boiling points and the concentrations of these reagents increases as ESI droplet evaporation occurs.[31,32] Enrichment of the supercharging reagent affects many physical properties of the ESI droplet, including the surface tension, temperature, propensities to proton transfer, etc. Results from circular dichroism spectroscopy[29-31] and hydrogen-deuterium exchange MS[30,31] indicate the supercharging reagents do not effect protein conformation at the low concentrations typically used in the initial solutions, but can cause chemical and/or thermal denaturation of the protein in the ESI droplet as the concentration of these reagents is increased. Proteins that have lost some or all of their native structures can carry away more charge and the charge enhancement from the denaturing effect is greater than the effect of the lower surface tension.[28]

The charge states of proteins generated by ESI from unbuffered aqueous solutions can also be increased by introducing acid vapor into the drying gas of an ESI interface.[38] Addition of HCl acid vapor into the drying gas resulted in an increase in the maximum charge state of cytochrome *c* by 10 and a shift in the average state from 8.9 to 15.4 compared to when no acid vapor was introduced.[38] The acid vapor lowers the pH of the ESI droplet and acid denaturation of the protein occurs, resulting in higher ion charge states in the mass spectrum.[38] An electrothermal supercharging method to generate high charge state protein ions with ESI from buffered aqueous solutions in which the proteins have native structures was recently introduced.[39] ESI mass spectra resembling those obtained from denaturing solutions, where the maximum extent of charging can exceed the number of basic sites in the molecule can be obtained with this method.[39] The effectiveness depends on a number of different factors, but ESI mass spectra resembling those measured from standard native or denatured solutions can be reversibly obtained simply by toggling the electrospray voltage between low and high values.[39] This method has the advantages over acidification of the ESI droplets in that it can be used with aqueous solutions with high buffer capacity.[39]

Here, addition of millimolar concentrations of La^{3+} to aqueous protein-containing solutions is shown to increase the extent of protein charging by ESI as a result of La^{3+} adduction onto native protein conformers. The enhanced protein charging via La^{3+} adduction is slightly lower than that obtained from aqueous ammonium acetate solutions that contain the supercharging reagent *m*-NBA, but both *m*-NBA and $LaCl_3$ can be used in combination to readily form charge states in excess of the number of basic sites in the protein. ECD of high charge states generated by trivalent metal ion supercharging from aqueous solutions results in improved fragmentation efficiency and sequence coverage compared to that obtained from the highest charge state formed from aqueous solutions without La^{3+}.

7.2 Experimental

7.2.1 Mass Spectrometry. Experiments were performed using a 9.4 T FT-ICR mass spectrometer equipped with an external ESI source.[40] Bovine ubiquitin, bovine cytochrome *c*, chicken egg white lysozyme, $LaCl_3$, *m*-nitrobenzyl alcohol (*m*-NBA), methanol, acetic acid, and ammonium acetate were all purchased from Sigma Aldrich (St. Louis, MO). Stock solutions containing 10 μM protein were prepared in either water with 5 mM ammonium acetate or with 48.5/48.5/3.0 methanol/water/acetic acid (v/v/v). A small volume of sample solution (~2-10 μL) is loaded into a borosilicate capillary (1.0 mm o.d./0.78 mm i.d.; Sutter Instruments, Novato, CA, USA) that is pulled to a tip with an inner diameter of ~2 μm (model P-87 capillary puller; Sutter Instruments, Novato, CA). A grounded platinum wire is inserted into the solution and the capillary is positioned ~2 mm away from the source inlet capillary to which a potential of -800 to -1200 V is applied, and the resulting ions that are formed by ESI are trapped in the ion cell. For ECD experiments, the precursor ion of interest is isolated using stored waveform inverse Fourier transforms (SWIFTs) with a 2 kHz or wider window around the precursor. Electrons from a heated dispenser cathode (Heatwave Labs, Watsonville, CA) that is mounted axially from the cell center are introduced into the ion

cell 100 ms after ion isolation by changing the cathode housing potential from +10 V to either -0.40 or -0.65 V for 100 ms. Ions are detected 1.0 s after electron irradiation.

EC efficiency (Eff_{EC}) is calculated using equation 1

$$Eff_{EC} = \frac{\sum I_{fragment} + \sum I_{reduced}}{I_{precursor} + \sum I_{reduced} + \sum I_{fragment}} \times 100 \quad \text{(eq. 1)}$$

where $I_{precursor}$, $I_{fragment}$, and $I_{reduced}$ are ion abundances of the precursor, the fragments, and the reduced precursors, respectively. Fragmentation efficiency (Eff_{frag}) is calculated using equation 2

$$Eff_{EC} = \frac{\sum I_{fragment}}{I_{precursor} + \sum I_{reduced} + \sum I_{fragment}} \times 100 \quad \text{(eq. 2)}$$

and the measured ion abundances were normalized for charge. Uncertainties for electron capture and fragmentation efficiencies are reported as ± one standard deviation of three replicate measurements. Each measurement was repeated with a different SWIFT for isolation with a window between two to four kHz around the precursor. Changing the SWIFT window between these values did not have a significant effect on electron capture and fragmentation efficiencies, indicating that the overlap of the precursor ions and electrons was not measurably perturbed by the isolation.

7.2.2 Circular Dichroism. Circular dichroism (CD) spectra were acquired on a Jasco model 810 spectropolarimeter (JASCO, Inc., Easton, MD, USA) from solutions containing 20 μM ubiquitin in denaturing solution conditions (48.5/48.5/3 methanol/water/acetic acid) or water with 5.0 mM ammonium acetate either with no additional additive or 1.0 mM to 5.0 M $LaCl_3$. Samples were transferred to a 1.0 cm quartz cuvette with constant mixing using a Teflon stir bar while performing a wavelength scan analysis from 210 to 250 nm.

7.2.3 Ion Mobility. Ion mobility experiments were performed using a Synapt G2 High Definition MS (Waters, Milford, MA, USA) equipped with a Z-spray ion source. Ions are formed by ESI as described above using a platinum wire potential of 1.0 to 1.5 kV. The sample and extraction cone potentials were 40 V and 3 V, respectively. The travelling wave ion mobility spectrometer mobility cell was operated with a constant wave velocity of 700 m/s, wave height of 40 V, helium flow rate of 180 mL/min, and IMS (N_2) flow rate of 90 mL/min. The time of flight mass analyzer was operated in sensitivity mode ("V"). Drift times were converted to a collision cross section (ccs) scale using the procedure outlined by Robinson and coworkers[41,42] with ubiquitin (9+ through 13+), cytochrome *c* (13+ through 18+), and myoglobin (16+ through 22+) formed from denaturing solutions as calibrant ions. An average ccs was obtained for a given charge state of ubiquitin by weighting the ccs for each conformation by peak area.

7.3 Results and Discussion

7.3.1 Trivalent Metal Ion Supercharging in Aqueous Solutions. The 5+ charge state of ubiquitin is the most abundant ion produced by ESI (aqueous 5.0 mM ammonium acetate), and the average and maximum charge states are 5.2 and 7, respectively (Figure 7.1a). With 1.0 mM $LaCl_3$ added to this solution, the average (7.6) and maximum (11) charge states are significantly higher (Figure 7.1b). More La^{3+} ions

adduct to the higher charge state ions. The average number of La^{3+} adducts increases from 1.7 to 3 for the 6+ and 11+ charge states, respectively. About 12% of the 6+ molecular ions are fully protonated whereas all ions of the 11+ charge state have La^{3+} bound. Similar results were also obtained from ESI of an aqueous solution containing 1.0 mM $EuCl_3$ (data not shown), suggesting that the binding of these metal ions is not specific. In contrast, ESI of an aqueous solution of ubiquitin containing 1.0 mM NaCl results in no significant change to the average charge state (5.0), and Na^+ adduction occurs more substantially to the lower charge state ions (data not shown), a result consistent with previous reports.[43,44] The greater adduction of La^{3+} to higher charge states of ubiquitin suggests that the increased charging observed with $LaCl_3$ is due to adduction of multiple La^{3+} ions to ubiquitin which is folded in solution.

To compare the extent of charge enhancement obtained from native solutions with $LaCl_3$ to conventional supercharging reagents,[24-31] an ESI mass spectrum of an aqueous solution of ubiquitin with 1.0% *m*-NBA was obtained under identical conditions (Figure 7.1c). The charge state distribution is slightly broader than that obtained with $LaCl_3$ and it is centered about 9+ with an average charge state of 8.5. The maximum charge state (11) that is formed is the same for both *m*-NBA or $LaCl_3$, but with *m*-NBA, the average charge state is one higher and the abundance of the maximum charge state is greater.

To determine whether the combination of trivalent metal ion adduction and *m*-NBA results in more charging than either reagent individually, an ESI mass spectrum of ubiquitin from an aqueous solution containing both 1.0% *m*-NBA and 1.0 mM $LaCl_3$ was obtained (Figure 7.1d). The average (9.8) and maximum (14) charge states are greater than those obtained with either $LaCl_3$ or *m*-NBA alone. Higher charge states have more La^{3+} adduction, as occurred without *m*-NBA. The 12+ - 14+ charge states all have La^{3+} bound, whereas La^{3+} is adducted to only 9.5% of the 7+ charge state ions. Ubiquitin has 13 basic sites consisting of 12 basic amino acids (H, R, and K) and the N-terminus. Thus, formation of the 14+ charge state corresponds to charging greater than the number of basic sites in the protein despite formation of these ions from an aqueous solution in which ubiquitin has a folded structure.

Similar results were obtained for bovine cytochrome *c*, a larger protein with a higher isoelectric point than ubiquitin. The average and maximum charge states of cytochrome *c* in an ESI mass spectrum from an aqueous solution with 5.0 mM ammonium acetate are 6.9 and 8, respectively (Figure 7.1e). With 1.0 mM $LaCl_3$, the average and maximum charge states in the ESI mass spectrum increase to 8.9 and 13, respectively (Figure 7.1f). The average (10.3) and maximum (14) charge states with 1.0% *m*-NBA are slightly higher than those obtained with 1.0 mM $LaCl_3$ (Figure 7.1g). With both *m*-NBA and $LaCl_3$, the average (12.5) and maximum (17) charge states are 5.6 and 9 more charges, respectively, than those formed from ammonium acetate alone (Figure 7.1h).

To determine the extent to which intramolecular disulfide bridges, which reduce the conformational flexibility of a protein, can affect the charge enhancement by $LaCl_3$, an ESI mass spectrum of an aqueous solution (5.0 mM ammonium acetate) containing 10 μM lysozyme and 1.0 mM $LaCl_3$ was obtained (Figure 7.2). With 1.0 mM $LaCl_3$, the average and maximum charge states increase from 8.0 to 9.7 and 10 to 12,

respectively, compared with those obtained from the solution containing ammonium acetate alone. An aqueous solution containing both 1.0 mM $LaCl_3$ and 1.0% *m*-NBA results in average and maximum charge states of 11.8 and 20, respectively. Lysozyme has 19 basic sites, and the formation of the 20+ charge state indicates that charge states greater than the number of basic sites can be generated from a native solution even for a protein that is conformationally constrained by disulfide bonds.

7.3.2 Effect of Supercharging Additives on S/N. The effects of $LaCl_3$ and *m*-NBA, individually and combined, on the signal-to-noise ratios (S/N) of the most abundant ion and total ion abundance for ubiquitin, cytochrome *c*, and lysozyme are shown in Table 7.1. There is little to no adverse affect on ESI signal for any of these proteins with 1.0% *m*-NBA, consistent with previous results.[18] Similarly, 1.0 mM $LaCl_3$ has little effect on the total ion abundance, but does lower the S/N for the most abundant ion slightly. The S/N of the most abundant ion is 39%, 13%, and 37% lower for ubiquitin, cytochrome *c*, and lysozyme, respectively, with 1.0 mM $LaCl_3$ compared to ammonium acetate alone, as a result of ion abundance being distributed into multiple peaks with varying numbers of La^{3+} adducts. With both *m*-NBA and $LaCl_3$, the total ion abundance for all three proteins is reduced compared with ammonium acetate alone. Similar to results with just $LaCl_3$, the S/N of the most abundant ion is significantly reduced (~2 - 9×) because ion abundance is distributed over varying numbers of La^{3+} adducts.

7.3.3 Effect of La^{3+} on Protein Conformation. High charge state protein ions can be formed by ESI from solutions in which the protein is unfolded, or when protein unfolding occurs in the ESI droplet.[26-31,38] The effect of $LaCl_3$ on protein conformation in solution was investigated using circular dichroism (CD). Far-UV CD spectra (210-250 nm), which probes the α-helical and β-sheet content of a protein, were acquired for ubiquitin in a denaturing solution, 5.0 mM ammonium acetate solution, and 5.0 mM ammonium acetate solution containing between 1.0 mM to 5.0 M $LaCl_3$ (Figure 7.3a). The CD signal in this spectral region is the same with and without $LaCl_3$ for concentrations up to 1.0 M, indicating that there is no measurable change in the secondary structure of ubiquitin. With 5.0 M $LaCl_3$, the CD spectrum is distinctly different, indicating that the secondary structure changes at this high salt concentration. The CD spectrum of denatured ubiquitin has a notable decrease in ellipticity at 220 nm compared to that obtained for the folded form from native solutions, which is consistent with an increase in α-helical content characteristic of the denatured A-state form of ubiquitin.[45]

Ion mobility experiments were performed to investigate how La^{3+} adduction affects the conformations of the resulting gaseous ubiquitin ions. There are multiple conformers for many charge states of ubiquitin (Figure 7.4), consistent with previous studies.[46,47] To simplify comparisons, the average ccs for each charge state was determined by weighting each feature in the drift profile by peak area. The average ccs as a function of the charge state of ubiquitin for fully protonated ions generated from native and denaturing solutions, and for ions with two or three La^{3+} adducts formed from aqueous solutions containing $LaCl_3$ is shown in Figure 7.3b. For the fully protonated ions generated from a denaturing solution, the average ccs increases with increasing charge, as previously reported.[46,47] For aqueous solutions containing 1.0 mM $LaCl_3$, the

average ccs of ubiquitin ions with two or three La^{3+} adducts also increases with increasing charge state, and the 8+ - 14+ La^{3+} adducted ubiquitin ions have more elongated conformations compared to the fully protonated 5+ and 6+ charge states formed from ammonium acetate alone. However, the average ccs of the La^{3+} adducted ions is consistently smaller than the corresponding protonated form with the same charge state generated from either a native or denaturing solution. The CD data indicate that the 1.0 mM $LaCl_3$ does not denature ubiquitin in the initial solution, but the ion mobility experiments show that La^{3+}-bound high charge state ions (8+ - 14+) formed from this solution have more elongated conformations than the 5+ and 6+ charge states formed without $LaCl_3$. This indicates that the presence of La^{3+} causes ubiquitin to unfold during the late stages of the electrospray process or in the gas phase.

7.3.4 Effects of Trivalent Metal Ion Supercharging on ECD. High charge state ions typically dissociate more readily, which can increase the structural information obtained in tandem MS experiments.[30,48-51] To determine how ECD sequence coverage is affected by supercharging with either La^{3+} adduction, *m*-NBA, or a combination of both, ECD spectra of the highest charge state of ubiquitin that could be isolated with sufficient S/N to observe most fragments were obtained from an ammonium acetate solution (6+) and ammonium acetate solutions containing $LaCl_3$ (9+), *m*-NBA (10+), or both supercharging additives (12+). ECD of $(ubiquitin + 6H)^{6+}$ formed from a 5 mM ammonium acetate aqueous solution results primarily in the formation of the 5+ and 4+ reduced precursors. Fragmentation occurs close to the N- and C-termini (Figure 7.5a) with no fragmentation between residues 23 and 59, suggesting that residues within this region are involved in extensive noncovalent interactions.[48,49] ECD of $(ubiquitin + 3La)^{9+}$ results in additional fragmentation in the middle of the protein (Figure 7.5b). The electron capture and fragmentation efficiencies for $(ubiquitin + 3La)^{9+}$ are 9% and 21%, respectively, higher than the values obtained for the fully protonated 6+ ion (Table 2). The sequence coverage obtained from the ECD spectrum of $(ubiquitin + 6H)^{6+}$ is 33%, whereas that for $(ubiquitin + 3La)^{9+}$ is 63%. These results indicate the significant advantage in using $LaCl_3$ to increase the charge state of protein ions to obtain enhanced sequence coverage and electron capture efficiency for ECD of protein ions formed from native solutions.

Extensive fragmentation occurs throughout the protein from ECD of $(ubiquitin + 10H)^{10+}$ formed from an aqueous solution containing 1.0% *m*-NBA (Figure 7.5c), and 55% sequence coverage is obtained. $(ubiquitin + 3La)^{9+}$ has both an ~11% smaller average ccs and lower charge state than $(ubiquitin + 10H)^{10+}$, yet greater sequence coverage is obtained for the La^{3+} adducted ion. ECD of $(ubiquitin + 9H + La)^{12+}$ formed from a solution with both 1.0% *m*-NBA and 1.0 mM $LaCl_3$ results in even more extensive fragmentation along the backbone of the protein (Figure 7.5d), from which 76% sequence coverage is obtained. Thus, a 2.3 fold increase in sequence coverage is obtained from the high charge state ion that is formed with both supercharging reagents compared to the ion formed from native solutions that do not contain these reagents. ECD data of $(ubiquitin + 6H)^{6+}$, $(ubiquitin + 3La)^{9+}$, $(ubiquitin + 10H)^{10+}$, and $(ubiquitin + 9H + La)^{12+}$ combined results in 89% sequence coverage for these ions that are formed from native solutions.

Similar improvements in sequence coverage occurred from ECD of high charge state ions of cytochrome *c* formed from ammonium acetate solutions containing either *m*-NBA, $LaCl_3$ or both compared to data obtained without supercharging additives. The 7+ and 6+ reduced precursors are predominantly produced by ECD of (cytochrome *c* + 8H)$^{8+}$ formed from an ammonium acetate solution, and 30% sequence coverage is obtained (Figure 7.6a). ECD of (cytochrome *c* + 7H + La)$^{10+}$ formed from an aqueous solution containing 1.0 mM $LaCl_3$ results in more extensive fragmentation throughout the protein (Figure 7.6b). 53% sequence coverage is obtained, whereas only 43% sequence coverage is obtained from ECD of (cytochrome *c* + 12H)$^{12+}$ generated from an aqueous solution containing 1.0% *m*-NBA (Figure 7.6c). Using both *m*-NBA and $LaCl_3$, ECD of (cytochrome *c* + 11H + La)$^{14+}$ results in 56% sequence coverage (Figure 7.6d). The sequence coverage from the combined ECD data for all four of these protein ions formed from native solutions is 76%, more than double the sequence coverage obtained without these reagents.

7.3.5 Effect of Cross Section and Trivalent Metal Ion on ECD. Results presented here and from earlier studies[30,48-51] show that greater sequence coverage is often obtained from dissociation of high charge state protein ions, which tend to have elongated conformations, than low charge state protein ions with compact structures. (ubiquitin + 2La)$^{6+}$ has an ~14% smaller average ccs than that of (ubiquitin + 6H)$^{6+}$, and the EC efficiency, fragmentation efficiency, and sequence coverage are 7%, 19%, and 8% lower, respectively, for (ubiquitin + 2La)$^{6+}$ compared to (ubiquitin + 6H)$^{6+}$ (Table 7.2). However, greater sequence coverage was not always obtained from ECD of a protein ion with a higher charge state and larger ccs. For example, ECD of (ubiquitin + 3La)$^{9+}$ results in 8% higher sequence coverage than (ubiquitin + 10H)$^{10+}$, even though the 9+ ion has one less charge and ~11% smaller average ccs. Similarly, (cytochrome *c* + La + 3H)$^{10+}$ has a ~9% smaller average ccs than (cytochrome *c* + 12H)$^{12+}$, yet ECD of the smaller, less highly charged La^{3+} bound ion results in 10% higher sequence coverage. These results indicate that the ccs and charge state of an ion are not the only factors in determining the extent of sequence coverage, and other characteristics[52] must play a significant role.

7.3.6 Trivalent Metal Ion Supercharging with Denaturing Solution. To determine the extent to which La^{3+} adducts to denatured proteins in solution, an ESI mass spectrum of ubiquitin from a denaturing solution (48.5/48.5/3 methanol/water/acetic acid) containing 1.0 mM $LaCl_3$ was obtained (Figure 7.7b). Both the average (10.3) and maximum (13) charge states are essentially the same for the solutions with and without $LaCl_3$ (Figure 7.7a). More La^{3+} adduction to lower charge state ions occurs, which is in striking contrast to results for aqueous solutions where La^{3+} adduction increases with increasing charge state. The percentage of the 7+ and 12+ charge states that have La^{3+} adducted are 79% and 32%, respectively. With 1.0% *m*-NBA, the average charge state increases from 10.1 to 11.8 (Figure 7.7c) and the maximum charge state formed is 14+. With both 1.0% *m*-NBA and 1.0 mM $LaCl_3$, the 16+ charge state is formed, which is three more charges than the total number of basic sites in this protein (Figure 7.7d). The charge state distribution is centered about the 13+ and the average charge state is 13.4. These results demonstrate that trivalent

metal ion supercharging in denaturing solutions using ESI can be used to produce higher charge states of proteins than have previously been observed.

An ECD mass spectrum of (ubiquitin + 11H +La)$^{14+}$ formed from a denaturing solution containing 1.0% *m*-NBA and 1.0 mM $LaCl_3$ was acquired and the resulting fragments are shown in Figure 7.8b. The low S/N of (ubiquitin + 14H)$^{14+}$ (~20) formed from the denaturing solution with 1.0% *m*-NBA precludes a direct comparison to ECD of the fully protonated 14+ charge state, but fragments formed by ECD of (ubiquitin + 13H)$^{13+}$ are shown in Figure 7.8a. The electron capture and fragmentation efficiencies of (ubiquitin + 11H + La)$^{14+}$ are only slightly greater, 5% and 4%, respectively, than for (ubiquitin + 13H)$^{13+}$. The sequence coverage obtained under these conditions for both ions was 68%. However, many of the ECD fragments formed from both ions are unique, resulting in 85% sequence coverage when the data from both ions are combined. These data indicate that ECD of high charge states formed from denaturing solutions containing both *m*-NBA and $LaCl_3$ can significantly improve the sequence coverage.

7.3.7 Mechanism of Charging via La^{3+} Adduction. The CD results show that the secondary structure content of ubiquitin is not affected in solutions with up to 1.0 M $LaCl_3$, but denaturation occurs with 5.0 M $LaCl_3$. For denaturation to occur in the ESI droplet, the $LaCl_3$ concentration must increase by more than a 1,000-fold. By comparison, a ~×5 enrichment of the supercharging reagent dimethyl sulfoxide occurs in the ESI droplet to produce supercharging.[31] Minimal La^{3+} adduction occurs for protein ions formed from denaturing solutions, and more La^{3+} adducts to lower charge state ions. In striking contrast, significant La^{3+} adduction to protein ions generated from native solutions occurs, and more La^{3+} adducts to higher charge state ions. These results suggest that La^{3+} preferentially adducts to native or native-like protein conformers during ESI. The higher charge state La^{3+} bound ubiquitin ions (8+ - 14+) have more elongated conformations than low charge state ions (5+ and 6+) formed from native solutions without $LaCl_3$. These results suggest that substantial adduction of La^{3+} onto compact conformers of ubiquitin during ESI results in protein ions with higher charge, which subsequently adopt more unfolded gas-phase conformations, presumably due to higher Coulombic repulsion.

7.4 Conclusions

$LaCl_3$ can significantly increase the average and maximum charge states of protein ions formed by ESI from native solutions. Charge states greater than the number of basic sites in the protein can be produced from either aqueous solutions in which the protein has a native folded structure, or denaturing solutions that contain both La^{3+} and *m*-NBA, even for a protein that is conformationally constrained due to native disulfide bonds. Better ECD sequence coverage can be obtained from the high charge state protein ions formed as a result of La^{3+} adduction, making the information content of ECD of protein ions formed from native solutions comparable to that obtained from denaturing solutions. Addition of 1.0 mM $LaCl_3$ to aqueous solutions does not adversely affect the total protein ion abundance generated by ESI, but can lower the S/N of the most abundant ion owing to the distribution of signal into ions with various numbers of La^{3+} adducts. However, the improved fragmentation efficiency and sequence coverage

obtained for the high charge state La^{3+} adducted ions more than compensates for the reduced precursor abundance. These results indicate that trivalent metal ion supercharging can substantially increase the fragmentation of protein ions formed from native solutions, and should reduce the need to denature proteins prior to tandem MS analysis.

7.5 References

(1) van den Heuvel, R.H.; Heck, A.J.R. *Curr. Opin. Chem. Biol.* **2004**, *8*, 519-526.
(2) Heck, A.J.R. *Nat. Methods* **2008**, *5*, 927-933.
(3) Kaddis, C.S.; Loo, J.A. *Anal. Chem.* **2007**, *79*, 1778-1784.
(4) Barrera, N.P.; Robinson, C.V. *Annu. Rev. Biochem.* **2011**, *80*, 247-271.
(5) Loo, J.A.; Quinn, J.P.; Ryu, S.I.; Henry, K.D.; Senko, M.W.; McLafferty, F.W. *Proc. Natl. Acad. Sci. U. S. A.* **1992**, *89*, 286-289.
(6) Marshall, A.G.; Hendrickson, C.L. *Rapid Commun. Mass Spectrom.* **2001**, *15*, 232-235.
(7) Marshall, A.G.; Hendrickson, C.L. *Annu. Rev. Anal. Chem.* **2008**, *1*, 579-599.
(8) Perry, R.H.; Cooks, R.G.; Noll, R.J. *Mass Spectrom. Rev.* **2008**, *27*, 661-699.
(9) Testa, L.; Brocca, S.; Grandori, R. *Anal. Chem.* **2011**, *83*, 6459-6463.
(10) Chowdhury, S.K.; Katta, V.; Chait, B.T. *J. Am. Chem. Soc.* **1990**, *112*, 9012-9013.
(11) Wang, G.B.; Abzalimov, R.R.; Kaltashov, I.A. *Anal. Chem.* **2011**, *83*, 2870-2876.
(12) Williams, E.R. *J. Mass Spectrom.* **1996**, *31*, 831-842.
(13) Loo, R.R.O.; Smith, R.D. *J. Mass Spectrom.* **1995**, *30*, 339-347.
(14) Iavarone, A.T.; Jurchen, J.C.; Williams, E.R. *J. Am. Soc. Mass Spectrom.* **2000**, *11*, 976-985.
(15) Thomson, B.A. *J. Am. Soc. Mass Spectrom.* **1997**, *8*, 1053-1058.
(16) Benkestock, K.; Sundqvist, G.; Edlund, P.O.; Roeraade, J. *J. Mass Spectrom.* **2004**, *39*, 1059-1067.
(17) Iavarone, A.T.; Jurchen, J.C.; Williams, E.R. *Anal. Chem.* **2001**, *73*, 1455-1460.
(18) Iavarone, A.T.; Williams, E.R. *Int. J. Mass Spectrom.* **2002**, *219*, 63-72.
(19) Iavarone, A.T.; Williams, E.R. *J. Am. Chem. Soc.* **2003**, *125*, 2319-2327.
(20) Shvartsburg, A.A.; Jones, R.C. *J. Am. Soc. Mass Spectrom.* **2004**, *15*, 406-408.
(21) Liu, H.C.; Hakansson, K. *J. Am. Soc. Mass Spectrom.* **2006**, *17*, 1731-1741.
(22) Chen, X.F.; Fung, Y.M.E.; Chan, W.Y.K.; Wong, P.S.; Yeung, H.S.; Chan, T.W.D. *J. Am. Soc. Mass Spectrom.* **2011**, *22*, 2232-2245.
(23) Mosely, J.A.; Murray, B.S.; Parker, D. *Eur. J. Mass Spectrom.* **2009**, *15*, 145-155.
(24) Lomeli, S.H.; Yin, S.; Loo, R.R.O.; Loo, J.A. *J. Am. Soc. Mass Spectrom.* **2009**, *20*, 593-596.
(25) Lomeli, S.H.; Peng, I.X.; Yin, S.; Loo, R.R.O.; Loo, J.A. *J. Am. Soc. Mass Spectrom.* **2010**, *21*, 127-131.
(26) Sterling, H.J.; Williams, E.R. *J. Am. Soc. Mass Spectrom.* **2009**, *20*, 1933-1943.
(27) Sterling, H.J.; Kintzer, A.F.; Feld, G.K.; Cassou, C.A.; Krantz, B.A.; Williams, E.R. *J. Am. Soc. Mass Spectrom.* **2012**, *23*, 191-200.
(28) Sterling, H.J.; Cassou, C.A.; Trnka, M.J.; Burlingame, A.L.; Krantz, B.A.; Williams, E.R. *Phys. Chem. Chem. Phys.* **2011**, *13*, 18288-18296.
(29) Sterling, H.J.; Daly, M.P.; Feld, G.K.; Thoren, K.L.; Kintzer, A.F.; Krantz, B.A.; Williams, E.R. *J. Am. Soc. Mass Spectrom.* **2010**, *21*, 1762-1774.
(30) Sterling, H.J.; Williams, E.R. *Anal. Chem.* **2010**, *82*, 9050-9057.
(31) Sterling, H.J.; Prell, J.S.; Cassou, C.A.; Williams, E.R. *J. Am. Soc. Mass Spectrom.* **2011**, *22*, 1178-1186.

(32) Grimm, R.L.; Beauchamp, J.L. *J. Phys. Chem. A* **2010**, *114*, 1411-1419.
(33) Douglass, K.A.; Venter, A.R. *J. Am. Soc. Mass Spectrom.* **2012**, *23*, 489-497.
(34) Hogan, C.J.; Loo, R.R.O.; Loo, J.A.; de la Mora, J.F. *Phys. Chem. Chem. Phys.* **2010**, *12* 13476-13483.
(35) Sze, S.K.; Ge, Y.; Oh, H.; McLafferty, F.W. *Proc. Natl. Acad. Sci. U. S. A.* **2002**, *99*, 1774-1779.
(36) Sheng, Y.; Loo, J.A. *Int. J. Mass Spectrom.* **2011**, *300*, 118-122.
(37) Valeja, S.G.; Tipton, J.D.; Emmett, M.R.; Marshall, A.G. *Anal. Chem.* **2010**, *82*, 7515-7519.
(38) Kharlamova, A.; Prentice, B.M.; Huang, T.Y.; McLuckey, S.A. *Anal. Chem.* **2010**, *82*, 7422-7429.
(39) Sterling, H.J.; Cassou, C.A.; Susa, A.C.; Williams, E.R. *Anal. Chem.* **2012**, *84*, 3795-3801.
(40) Jurchen, J.C.; Williams, E.R. *J. Am. Chem. Soc.* **2003**, *125*, 2817-2826.
(41) Bush, M.F.; Hall, Z.; Giles, K.; Hoyes, J.; Robinson, C.V.; Ruotolo, B.T. *Anal. Chem.* **2010**, *82*, 9557-9565.
(42) Ruotolo, B.T.; Benesch, J.L.P.; Sandercock, A.M.; Hyung, S.J.; Robinson, C.V. *Nat. Protoc.* **2008**, *3*, 1139-1152.
(43) Iavarone, A.T.; Udekwu, O.A.; Williams, E.R. *Anal. Chem.* **2004**, *76*, 3944-3950.
(44) Pan, P.; Gunawardena, H.P.; Xia, Y.; McLuckey, S.A. *Anal. Chem.* **2004**, *76*, 1165-1174.
(45) Brutscher, B.; Bruschweiler, R.; Ernst, R.R. *Biochemistry* **1997**, *36*, 13043-13053.
(46) Myung, S.; Badman, E.R.; Lee, Y.J.; Clemmer, D.E. *J. Phys. Chem. A* **2002**, *106*, 9976-9982.
(47) Hoaglund, C.S.; Valentine, S.J.; Sporleder, C.R.; Reilly, J.P.; Clemmer, D.E. *Anal. Chem.* **1998**, *70*, 2236-2242.
(48) Breuker, K.; Oh, H.B.; Horn, D.M.; Cerda, B.A.; McLafferty, F.W. *J. Am. Chem. Soc.* **2002**, *124*, 6407-6420.
(49) Breuker, K.; Oh, H.B.; Lin, C.; Carpenter, B.K.; McLafferty, F.W. *Proc. Natl. Acad. Sci. U. S. A.* **2004**, *101*, 14011-14016.
(50) Iavarone, A.T.; Williams, E.R. *Anal. Chem.* **2003**, *75*, 4525-4533.
(51) Madsen, J.A.; Brodbelt, J.S. *J. Am. Soc. Mass Spectrom.* **2009**, *20*, 349-358.
(52) Robinson, E.W.; Leib, R.D.; Williams, E.R. *J. Am. Soc. Mass Spectrom.* **2006**, *17*, 1469-1479.

7.6 Tables

Table 7.1. The most abundant ion S/N, and total ion abundance S/N of ubiquitin, cytochrome *c*, or lysozyme from the ESI mass spectra of aqueous solutions (5 mM ammonium acetate) with and without supercharging additives

Protein	Additive	Most Abundant Ion	Most Abundant Ion S/N	Total Ion Abundance S/N
ubiquitin	none	$(ubiquitin + 5H)^{5+}$	9,068	27,256
	1.0% *m*-NBA	$(ubiquitin + 9H)^{9+}$	8,380	25,524
	1.0 mM $LaCl_3$	$(ubiquitin + H + 2La)^{7+}$	5,487	23,713
	1.0% m-NBA & 1.0 mM $LaCl_3$	$(ubiquitin + 4H + 2La)^{10+}$	955	9,734
cytochrome *c* (cyt *c*)	none	$(cyt\ c + 7H)^{7+}$	7,943	17,475
	1.0% *m*-NBA	$(cyt\ c + 10H)^{10+}$	8,332	23,330
	1.0 mM $LaCl_3$	$(cyt\ c + 6H + La)^{9+}$	6,896	17,930
	1.0% m-NBA & 1.0 mM $LaCl_3$	$(cyt\ c + 7H + 2La)^{13+}$	2,786	7,244
lysozyme (lys)	none	$(lys + 8H)^{8+}$	12,345	17,283
	1.0% *m*-NBA	$(lys + 11H)^{11+}$	10,452	24,040
	1.0 mM $LaCl_3$	$(lys + 7H + La)^{10+}$	7,782	17,439
	1.0% m-NBA & 1.0 mM $LaCl_3$	$(lys + 11H)^{11+}$	5,481	13,703

Table 7.2. Average collision cross section (Å^2), % sequence coverage, electron capture efficiency and fragmentation efficiency for ions of ubiquitin, cytochrome *c*, and lysozyme

protein	precursor	avg. ccs (Å^2)	% Sequence Coverage	% Eff_{EC}	% Eff_{frag}
ubiquitin	$(ubq + 6H)^{6+}$	1776	33%	84.3% ± 0.3%	64.7% ± 1.1%
	$(ubq + 2La)^{6+}$	1527	25%	77.2% ± 0.7%	45.9% ± 0.8%
	$(ubq + 9H)^{9+}$	2108	59%	91.9% ± 0.6%	89.5% ± 0.6%
	$(ubq + 3La)^{9+}$	2014	63%	93.2% ± 0.9%	85.8% ± 1.7%
	$(ubq + 10H)^{10+}$	2263	55%	92.4%	89.8%
	$(ubq + 9H + La)^{12+}$	2526	76%	93.9%	87.5%
cytochrome *c*	$(cyt\ c + 8H)^{8+}$	2472	30%	87.4%	56.9%
	$(cyt\ c + La + 7H)^{10+}$	2718	53%	88.4%	66.9%
	$(cyt\ c + 12H)^{12+}$	3000	43%	89.8%	71.8%
	$(cyt\ c + La + 11H)^{14+}$	3194	56%	94.5%	87.7%
lysozyme	$(lys + 10H)^{10+}$	2692	-	72.7% ± 0.6%	-
	$(lys + La + 7H)^{10+}$	2692	-	74.8% ± 0.8%	-

7.7 Figures

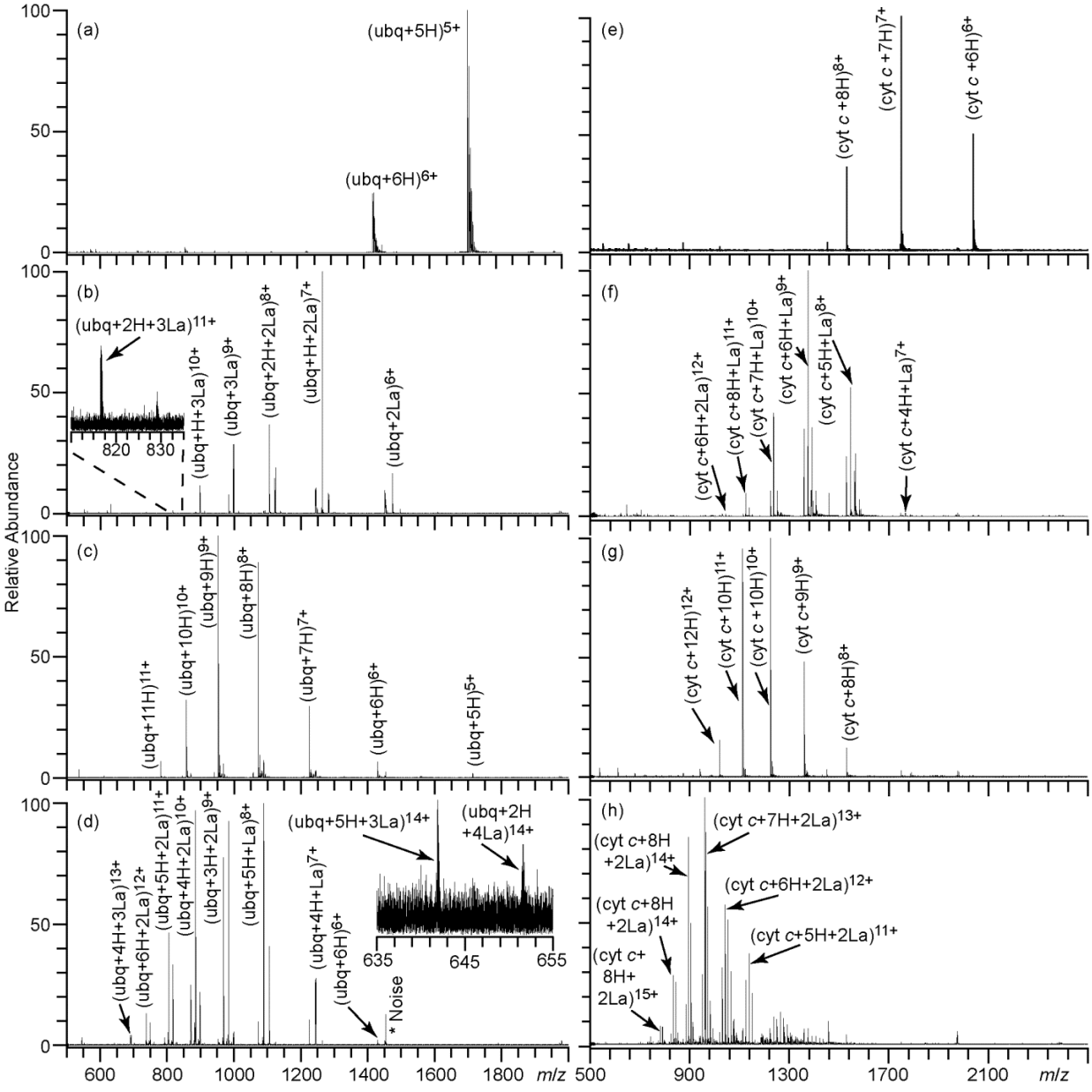

Figure 7.1. ESI mass spectra of aqueous solutions of 10 μM ubiquitin or cytochrome *c* in 5 mM ammonium acetate containing (a and e) no additives, (b and f) 1.0 mM $LaCl_3$, (c and g) 1.0% *m*-NBA, or (d and h) 1.0 mM $LaCl_3$ and 1.0% *m*-NBA, respectively.

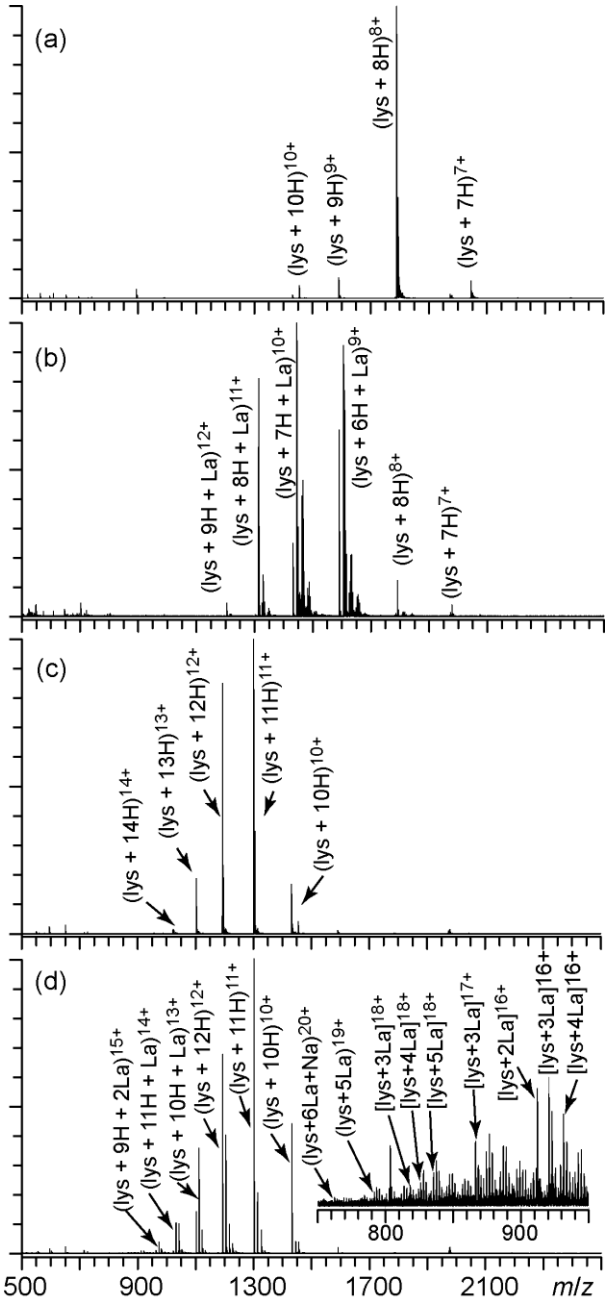

Figure 7.2. ESI mass spectra of aqueous solutions of 10 μM lysozyme (lys) with 1.0 mM NaCl ammonium acetate containing (1) no additives, (b) 1.0 mM $LaCl_3$, (c) 1.0% *m*-NBA, or (d) 1.0 mM $LaCl_3$ and 1.0% *m*-NBA.

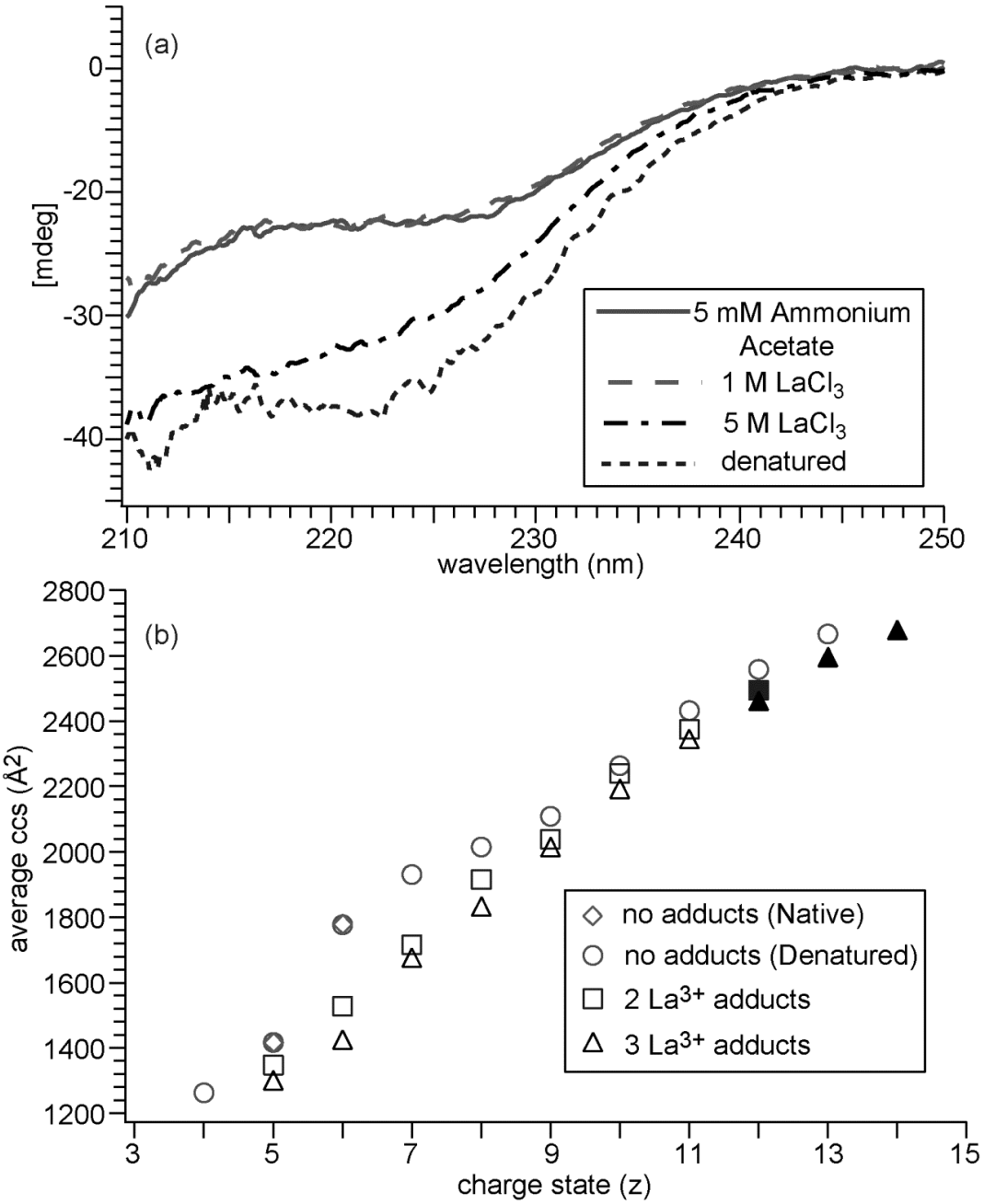

Figure 7.3. (a) Circular dichroism spectra between 210 to 250 nm for 20 μM ubiquitin in 5 mM ammonium acetate, 1 M $LaCl_3$ (5 mM ammonium acetate), 5 M $LaCl_3$ (5 mM ammonium acetate), or 48.5/48.5/3.0 methanol/water/acetic acid (v/v/v) (denatured). (b) Average collision cross sections as a function of ion charge state for ubiquitin with no adducts from a denatured solution (o) and from an aqueous ammonium acetate solution (◊) without $LaCl_3$, and with two (□) or three (△) La^{3+} adducts from an aqueous ammonium acetate solution containing 1.0 mM $LaCl_3$. Filled symbols are ubiquitin ions formed from an aqueous ammonium acetate solution containing $LaCl_3$ and *m*-NBA.

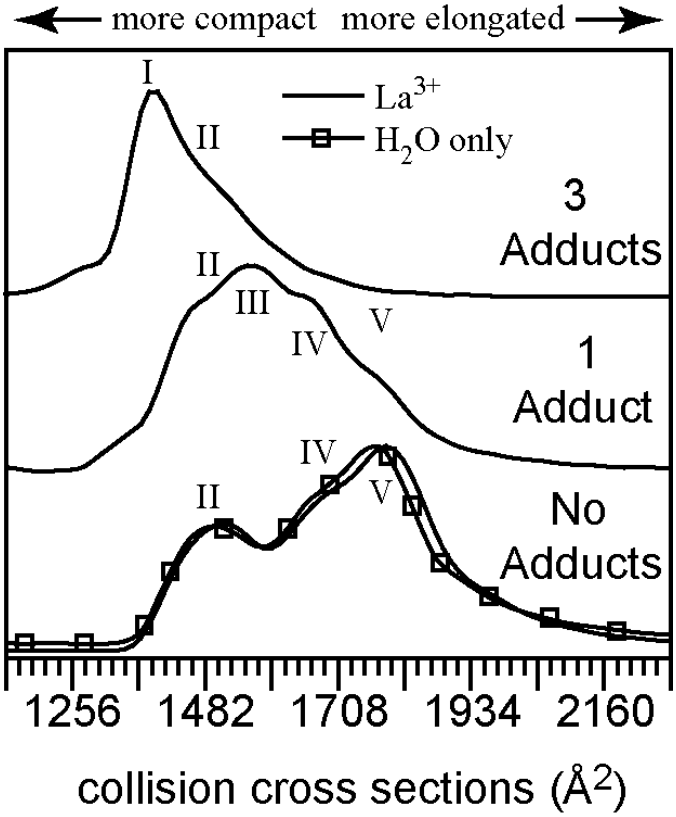

Figure 7.4. Drift profiles of 6+ ions of ubquitin formed from aqueous solutions containing no additional additive (squares) or 1 mM $LaCl_3$ (solid line). Distributions are shown for ions with no adducts (bottom) and up to three adducts (top), and were obtained by integrating the area across *m*/*z* values corresponding to each addition from the two-dimensional dataset.

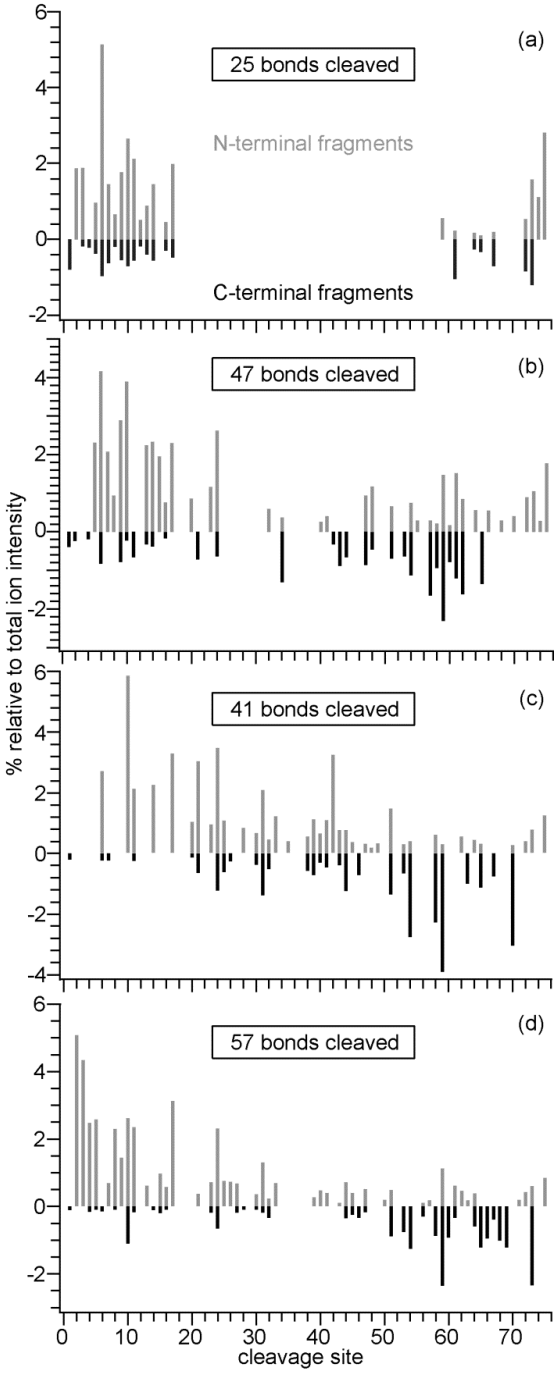

Figure 7.5. Relative ECD fragment ion abundances at each cleavage site for (a) (ubiquitin + 6H)$^{6+}$, (b) (ubiquitin + 3La)$^{9+}$, (c) (ubiquitin + 10H)$^{10+}$, and (d) (ubiquitin + 9H + La)$^{12+}$; N-terminal and C-terminal fragments are represented as positive (grey) and negative (black) values, respectively.

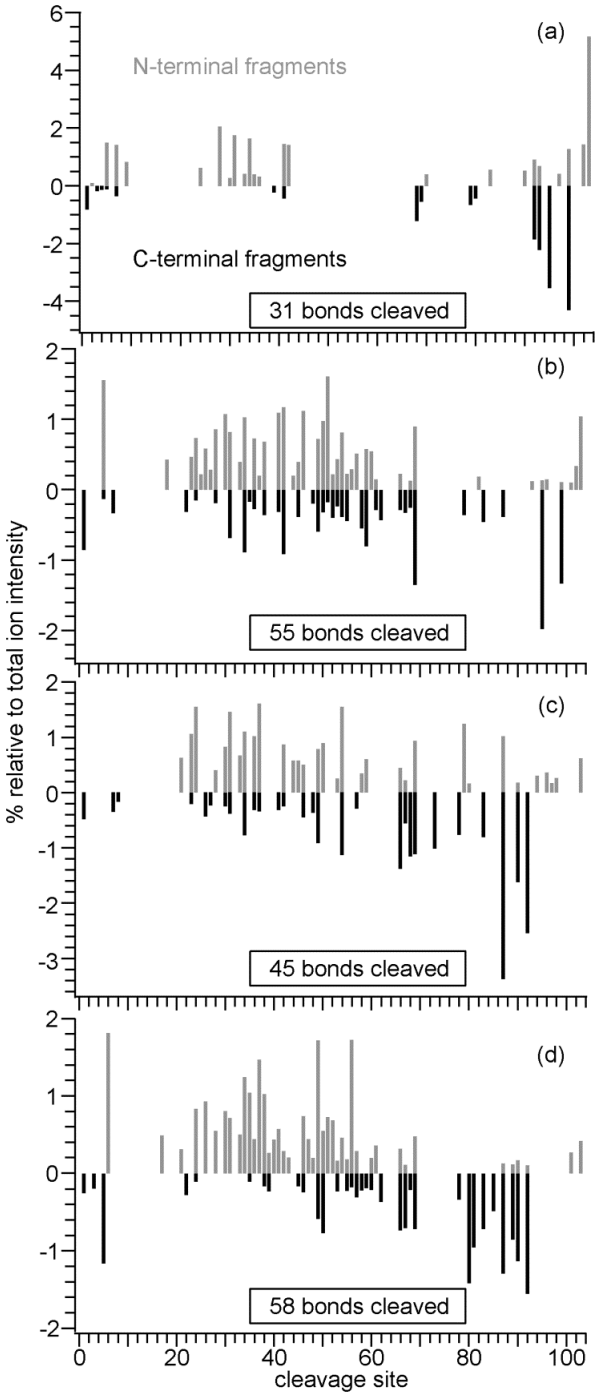

Figure 7.6. Relative ECD fragment ion abundances at each cleavage site for (a) (cytochrome *c* + 8H)$^{8+}$, (b) (cytochrome *c* + 7H + La)$^{10+}$, (c) (cytochrome *c* + 12H)$^{12+}$, and (d) (ubiquitin + 11H + La)$^{14+}$; N-terminal and C-terminal fragments are represented as positive (grey) and negative (black) values, respectively.

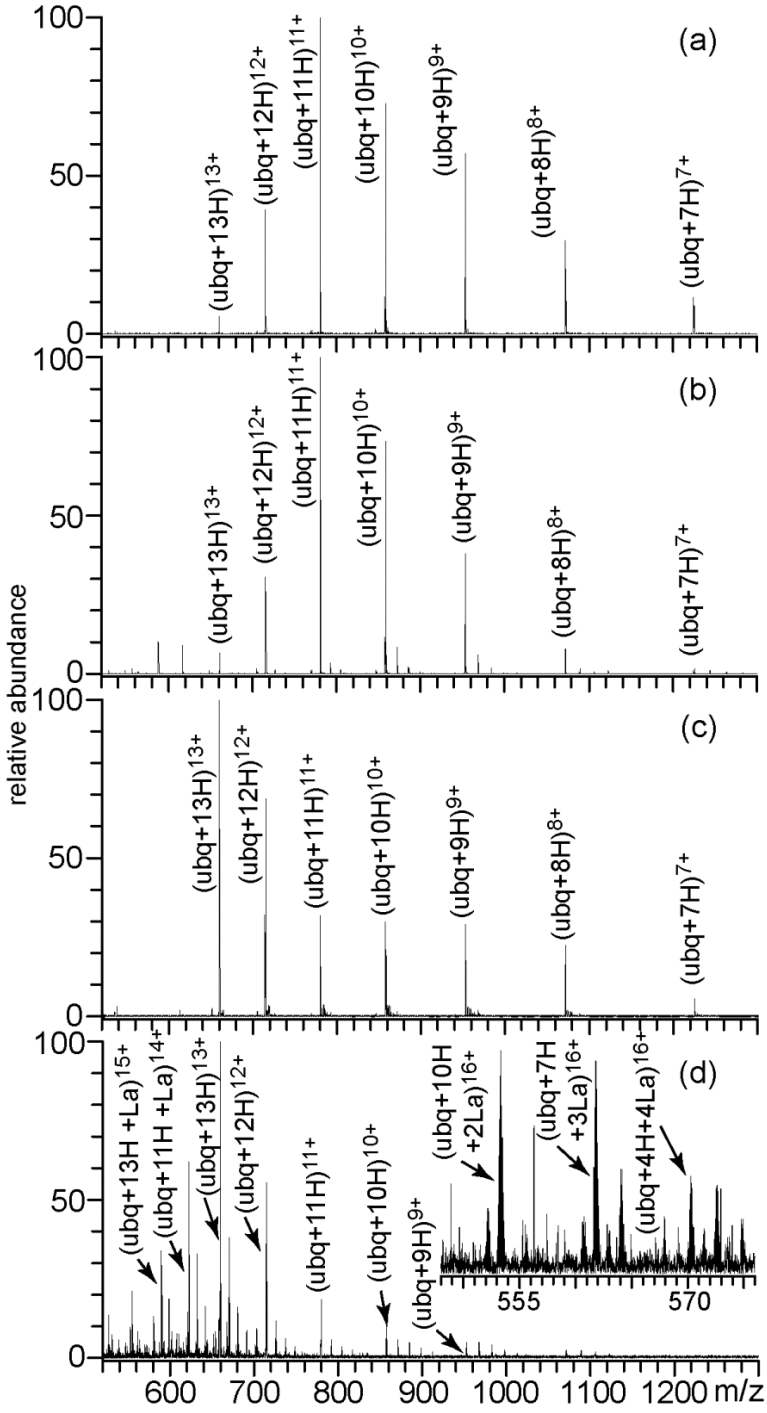

Figure 7.7. ESI mass spectra of 10 μM ubiquitin in 48.5/48.5/3.0 methanol/water/acetic acid (v/v/v) containing (a) no additives, (b) 1.0 mM $LaCl_3$, (c) 1.0% *m*-NBA, or (d) 1.0 mM $LaCl_3$ and 1.0% *m*-NBA.

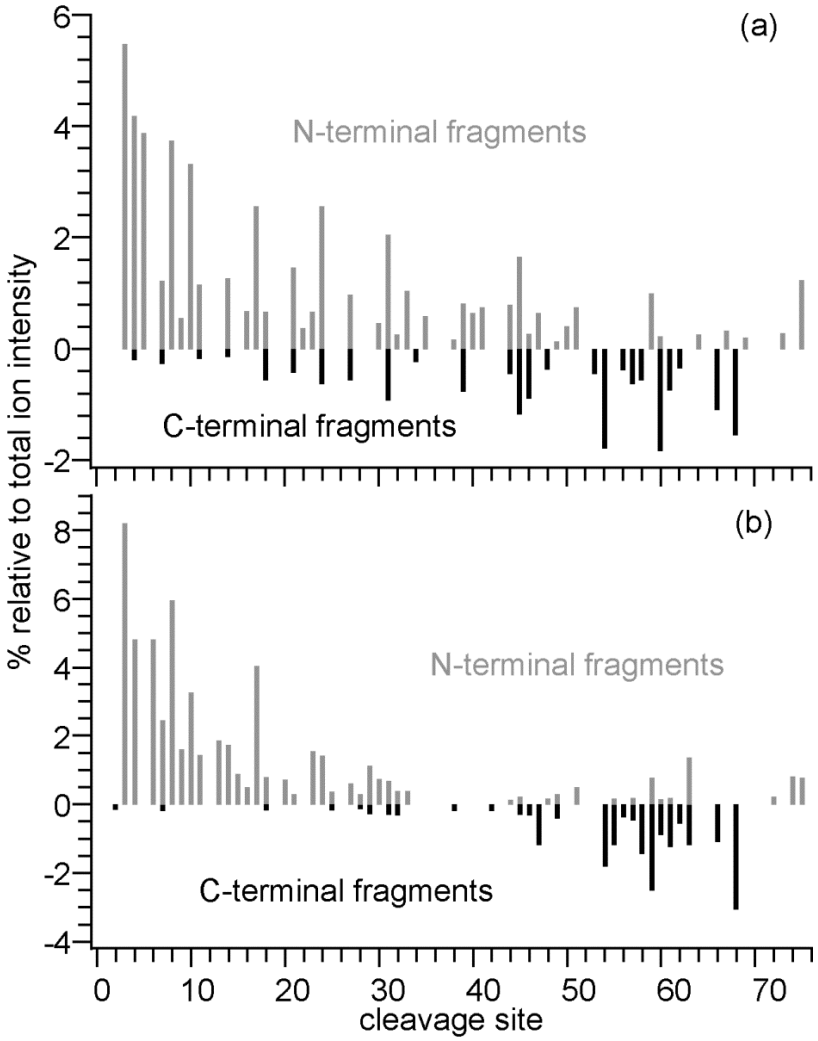

Figure 7.8. Relative ECD fragment ion abundances at each cleavage site for (a) $(\text{ubiquitin} + 13\text{H})^{13+}$ and (b) $(\text{ubiquitin} + 11\text{H} + \text{La})^{14+}$; N-terminal and C-terminal fragments are represented as positive (grey) and negative (black) values, respectively.

CHAPTER 8

Electron Capture Dissociation of Trivalent Metal Ion-Peptide Complexes

(This chapter is reproduced with permission from Flick, T.G.; Donald, W.A.; Williams, E.R. This chapter was submitted to the Journal of American Society for Mass Spectrometry)

8.1 Introduction

Peptide sequencing by tandem mass spectrometry is widely used to identify proteins and locate sites of post-translational modifications.[1-15] Dissociation by electron-ion recombination methods, whether by capture of a free electron (electron capture dissociation; ECD)[4-7] or transfer of an electron from an anion (electron transfer dissociation; ETD)[8-11] or from an atom (electron capture induced dissociation; ECID)[16-18] produces characteristic *c* and *z* ion fragments and can often result in minimal loss of labile posttranslational modifications, such as phosphorylation,[4] making these attractive methods for determining the locations of such chemically modified sites. The extent of fragmentation, electron capture efficiency, and recombination energy significantly increase with increasing ion charge state.[19-25] For example, at least 36% more unique peptides could be identified with ETD than collisional dissociation methods for both tryptic and Lys-C peptides with charge states greater than two.[21]

One significant disadvantage of these ion-electron recombination methods for small peptides is that the charge state is reduced, making it challenging to apply these methods when only singly protonated ions are formed by electrospray ionization. With ECID, the reduced precursor of a singly protonated peptide can be reionized in a second atomic collision and the fragmentation induced by the neutralization step can be readily analyzed.[16] Electron detachment dissociation (EDD), where excited radical cations with one higher charge or anions with one lower charge are produced by irradiating trapped ions with electrons that have 10 eV or higher kinetic energy, results in similar fragmentation pathways as those obtained with ECD.[26-29] Although fragmentation can be more extensive with EDD than with ETD, the efficiency of the EDD process is relatively low.[26-29]

Complexation of a divalent metal ion, M_D, to a small peptide can result in divalent ions that can readily dissociate upon ion-electron recombination.[20,30-40] Håkansson and coworkers found that ECD of (substance P + H + M_D)$^{3+}$, where M_D = different alkaline earth metal ions, Mn, Fe, or Zn, results in similar sequence coverage to that obtained from ECD of (substance P + 3H)$^{3+}$.[30] Protonated *c* ions and complementary metal containing *z* ions are formed, which was attributed to the metal ion binding close to the C-terminus.[30] In contrast, ECD of Co^{2+} and Ni^{2+}-bound peptides predominately cleaves C-terminal to methionine, the likely metal binding site, and lower sequence coverage than that from ECD of (substance P + 3H)$^{3+}$ is obtained.[30] Zubarev and coworkers found fewer fragment ions are produced by ECD of (angiotensin II + Zn)$^{2+}$ compared to

ECD of the diprotonated ion, but the fragments provide complementary sequence information.[20]

ECD of Cu^{2+}-bound peptides results in mostly *b*/*y* fragments and few or no *c*/*z* ions are typically formed.[30-34] However, *c*/*z* ions are formed by ECD of Cu^{2+}-bound peptides when there are a sufficient number of coordinating residues,[35,36] an effect attributed to a lowering of the electron-metal ion recombination energy making electron capture at a metal remote site more favorable.[35] The electronic configuration of metal ions has also been reported to play a role in whether metal ion reduction occurs.[34] Chan and coworkers have investigated ECD of many different metal ion-peptide complexes.[34,37,38] For alkali earth metals and some transition metals, ECD results in metallated and non-metallated *c*/*z* fragment ions, a result attributed to a zwitterionic peptide structure in which a carboxylate group is deprotonated and fragmentation is driven by a remote protonation site.[34,37,38] For other transition metal ions, *a*/*b*/*y* ions were formed, which was attributed to reduction of the metal ion in a charge-solvated structure.[34,37,38]

Trivalent metal ion (M_T)-peptide complexes can be readily formed by electrospray ionization (ESI), and complexation of metal ions to small peptides can increase the charge state of the molecular ions.[41-47] Attachment of trivalent metal ions to small peptides for which singly protonated ions would typically be formed resulted in deprotonated, doubly charged ions, where the metal ion displaces a proton at an acidic site to form a salt-bridge structure.[41-43] Results from infrared multiphoton dissociation spectroscopy of M_T-polyalanine complexes, $(Ala_n - H + M_T)^{2+}$, $n = 2 - 5$, indicate that these ions exists in compact salt-bridge conformations in which all carbonyl oxygen atoms of the peptide backbone coordinate to M_T, but coordination to other side chains, such as the Tyr or Phe aromatic rings, is favorable for other peptides.[41] For larger peptides, $(peptide + M_T)^{3+}$ is primarily formed, even for peptides for which only doubly protonated ions are typically formed by ESI.[43-45] ECD of lanthanide metal-heptadentate ligands complexed with phosphopeptides resulted in extensive fragmentation of the peptide backbone and the phosphorylation site could be readily identified.[47]

Here, results for ECD of peptides complexed with lanthanide ions are reported for peptides with molecular weights below ~2,000 Da and are compared to those for the multiply protonated ions formed directly by ESI. These results indicate that cationization of peptides with trivalent metal ions can lead to significant increases in both the fragmentation and electron capture efficiency for small peptides, but is not so advantageous for larger peptides for which triply protonated ions can be formed. These results also indicate that the metal ion solvation by the peptide is extensive in the larger peptides, resulting in similar electrochemical properties of these metal ions in both the peptide environment and in aqueous solution.

8.2 Experimental

All experiments were performed using a 9.4 T Fourier-transform ion cyclotron resonance mass spectrometer that is described elsewhere.[48] Ions are generated by nanoESI using borosilicate capillaries that are pulled so that the tips have a ~2 μm inner diameter (model P-87 capillary puller, Sutter Instruments, Novato, CA). Approximately 2 to 10 μL of sample is loaded into the capillary, and a platinum wire is inserted into the

solution. The capillary is positioned ~2 mm from the source inlet, and a potential difference of 800 to 1200 V between the platinum wire and source inlet is applied. Ions are accumulated in an external hexapole ion trap for 0.5 to 4.0 s, and are subsequently injected into the ion cell. For tandem MS experiments, the precursor ion of interest is isolated using stored waveform inverse Fourier transforms (SWIFTs) followed by a 100 ms delay. For ECD, electrons from a heated dispenser cathode (Heatwave Labs, Watsonville, CA) that is mounted axially from the cell center are introduced into the ion cell by changing the cathode housing potential from +10 V to -1.4 V for 100 ms. Ions are detected 1.0 s after electron irradiation. For sustained off-resonance irradiation collisionally activated dissociation (SORI-CAD), the precursor is excited using a single frequency waveform (4.0 $V_{peak\text{-}to\text{-}peak}$, 2500 Hz offset) for 0.5 s, resulting in a maximum lab-frame translational energy of 0.5 eV, and collided with N_2 gas that is introduced to a pressure of ~10^{-6} Torr using a pulsed piezoelectric valve. All peptides and salts were obtained from Sigma Aldrich (St. Louis, MO). Solutions were prepared at a concentration of 10 to 100 μM peptide with 100 μM to 1 mM metal salt using 18 MΩ water (Milli-Q, Millipore, Billerica, MA) with a peptide to metal ratio of 1:10 for all solutions. A pH of ~7 was measured for all sample solutions using pH indicator strips.

8.3 Results and Discussion

8.3.1 Attachment of Trivalent Metal Ions. ESI of an aqueous solution of 10 μM leucine enkephalin (LeEnk) with 100 μM $LaCl_3$ results in the formation of both $(LeEnk + H)^+$ and $(LeEnk - H + La)^{2+}$ (Figure 8.1a). Only protonated amidated LeEnk, $(LeEnk\text{-}NH_2 + H)^+$, is formed with these same conditions; no (<0.004%) cationization by La^{3+} occurs (Figure 8.1a, inset). This indicates that La^{3+} binds to the carboxylate group of LeEnk, consistent with a salt-bridge structure identified for this ion by IRPD spectroscopy.[40] In contrast, cationization of substance P (SP), which has an amidated C-terminus and no acidic residues, with La^{3+} readily occurs, and the abundance of $(SP + La)^{3+}$ is a factor of 3× greater than that of $(SP + 3H)^{3+}$. These results indicate that a salt-bridge structure is not essential for La^{3+} adduction to all peptides. Stabilization of La^{3+} can also occur through interactions with polarizable atoms, such as carbonyl oxygen atoms on the peptide backbone or side-chain hetero atoms or phenyl groups, resulting in a charge-solvated structure.

The relative abundances of $(peptide + M_T - H)^{2+}$ and $(peptide + M_T)^{3+}$ depend predominantly on peptide size. For example, in contrast to the results for leucine enkephalin, $(peptide + La)^{3+}$ is the most abundant form of SFLLRNPNDKYEPF (SFLLR), and this ion is ~8× more abundant than $(peptide + 3H)^{3+}$ (Figure 8.1b). Both $(SFLLR - H + La)^{2+}$ and $(SFLLR - 3H + 2La)^{3+}$ are also formed, but are approximately a factor of 70 and 3 less abundant, respectively, than $(SFLLR + La)^{3+}$. The relative abundances of $(peptide + M_T - H)^{2+}$ and $(peptide + M_T)^{3+}$ as a function of molecular weight (MW) for various peptides complexed to La^{3+} are shown in Figure 8.1c. For peptides with MW's below ~1,000 Da, $(peptide - H + La)^{2+}$ is preferentially formed, whereas $(peptide + La)^{3+}$ is the most abundant ion for peptides with MW > 1,000 Da. There is no significant dependence of the abundance of $(peptide + M_T)^{3+}$ on the 3rd ionization energy of the trivalent metal for any of the peptides or metal ions investigated here. The transition to $(peptide + La)^{3+}$ becoming the most abundant form of the

molecular ion above ~1,000 Da (or more than approximately eight residues) indicates that there is a critical peptide size where charge-solvation structures, or salt-bridge structures in which a proton is displaced to another residue, become most stable.

8.3.2 ECD of (peptide – H + M_T)$^{2+}$. ESI of an aqueous solution that contains a trivalent metal ion and small peptide (MW < 800 Da) for which multiply protonated ions are not typically formed results in the formation of (peptide – H + M_T)$^{2+}$ for peptides with an acidic site. The same charge state can also be formed by attachment of divalent metal ions. To compare dissociation of divalent peptide ions formed by attachment of trivalent metal ions and divalent metal ions, ECD spectra of the small peptides LeEnk, Ala_6, and FLEEL were acquired for (peptide – H + M_T)$^{2+}$, where M_T = La^{3+}, Tm^{3+}, Eu^{3+}, or Yb^{3+}, and compared to ECD results for divalent metal ion-peptide complexes, (peptide + M_D)$^{2+}$, where M_D = Mg^{2+}, Ca^{2+}, Ba^{2+}, or Sr^{2+}. In general, the electron capture (EC) efficiency and sequence coverage is greater (by more than 6% and 25%, respectively) for (peptide – H + M_T)$^{2+}$ compared to (peptide + M_D)$^{2+}$. Representative ECD spectra for both (LeEnk + Ca)$^{2+}$ and (LeEnk – H + La)$^{2+}$ are shown in Figure 8.2 with the relative fragment abundances as a function of cleavage site inset. All fragments retain the metal ion for both precursors, but the sequence coverage and EC efficiency is 2× and ~6% greater, respectively, for (LeEnk – H + La)$^{2+}$, for which complete sequence coverage is obtained. Complete sequence coverage is also obtained for Yb^{3+} and Tm^{3+}, whereas the maximum sequence coverage obtained with the divalent metal ions was only 75% for (LeEnk + Mg)$^{2+}$ (Table 8.1). Similarly, sequence coverage is 40 to 50% greater for ECD of (peptide – H + M_T)$^{2+}$ (peptide = FLEEL and Ala_6) for all trivalent metal ions, except for Eu^{3+}, compared to results for (peptide + M_D)$^{2+}$ (Figures 8.3 and 8.4). ECD of (peptide – H + Eu)$^{3+}$ also results in *c*/*z* fragment ions, but a minimum of 25% lower sequence coverage is obtained for all peptides than with the other trivalent metal ions. The EC efficiency was 6 to 39% greater for (peptide – H + M_T)$^{2+}$ compared to (peptide + M_D)$^{2+}$ for all trivalent metal ions, even Eu^{3+}, a result that may be attributed to higher localized charge on the peptide with the trivalent metal ion. These results indicate that formation of (peptide – H + M_T)$^{2+}$ for small peptides substantially increase the EC efficiency and the structural information obtained with ECD.

8.3.3 ECD of (peptide + M)$^{3+}$. ECD spectra were also acquired for (peptide + M_T)$^{3+}$, where M_T = La^{3+}, Eu^{3+}, Yb^{3+}, Pm^{3+}, Tb^{3+}, Sm^{3+}, Tm^{3+}, Ho^{3+}, or Lu^{3+}, for seven peptides with MW's > 900 Da, and these results are compared to ECD data for the fully protonated ion with the highest charge state formed by ESI from a purely aqueous solution. ECD of (peptide + M_T)$^{3+}$ typically results in similar or lower sequence coverage compared to ECD of (peptide + 3H)$^{3+}$ or (peptide + 2H)$^{2+}$. For example, the ECD products for (ranakinin + 3H)$^{3+}$ and (ranakinin + M_T)$^{3+}$ where M_T = La^{3+}, Eu^{3+}, or Yb^{3+} are shown in Figure 8.5. These trivalent metal ions span the lowest (La^{3+}) and highest (Eu^{3+} and Yb^{3+}) 3rd ionization energies of the lanthanides investigated. The same sequence coverage (100%) and similar EC efficiency (~65%) was obtained from ECD of (ranakinin + M_T)$^{3+}$ with La^{3+} and Yb^{3+} compared to (ranakinin + 3H)$^{3+}$, whereas (ranakinin + Eu)$^{3+}$ resulted in only 50% sequence coverage. Cleavage at the N-C_α peptide bond N-terminal to proline is not detected either because it does not occur or because the N and C_α atoms in the proline residue remain linked by the side chain

methylene units after cleavage of the N- C_α bond. However, *b*/*y* ions are formed due to amide bond cleavage N-terminal to the proline residue, likely a result of vibrational excitation of the charge reduced precursor or ECD fragment ions.[49,50] As was the case for smaller peptides, the results for Eu^{3+} are significantly different than those obtained for the other trivalent metal ions.

ECD data for (peptide + $La)^{3+}$ where the peptide is SFLLR, neurotensin, neurokinin, or histatin 8 resulted in 23 – 33% lower sequence coverage than (peptide + $3H)^{3+}$. (SP + $La)^{3+}$ was the only ion where higher sequence coverage (by 10%) was obtained for (peptide + $M_T)^{3+}$ vs. (peptide + $3H)^{3+}$. For both angiotensin II and bradykinin 2 - 9, (peptide + $3H)^{3+}$ could not be formed, so ECD data of (peptide + $M_T)^{3+}$ is compared to that for (peptide + $2H)^{2+}$. The EC efficiency was 19 to 44% higher for the (peptide + $M_T)^{3+}$ for both angiotensin II and bradykinin 2-9 compared to (peptide + $2H)^{2+}$, but the sequence coverage was the same for all trivalent metal ions, except for Eu^{3+}, compared to the protonated ions. These results indicate that ECD of (peptide + $M_T)^{3+}$ does not improve the sequence coverage compared to (peptide + $2H)^{2+}$ or (peptide + $3H)^{3+}$, but can result in a significant improvement in the EC efficiency if complexation of the trivalent metal ion to the peptide results in an increase in the charge state compared to the fully protonated form.

8.3.4 Metal Binding to Acidic Sites. ECD of (peptide + $M_T)^{3+}$ results in both metal-attached fragment ions as well as fragments that do not bind the metal ion. Metal attached fragment ions formed by ECD of (ranakinin + $M_T)^{3+}$ all contain the glutamic acid residue, whereas no protonated fragments with this residue are formed (Figure 8.5), indicating that the metal ion binds to glutamic acid in this peptide. Similar results were obtained for other peptides with acidic sites. ECD fragmentation of (neurokinin + $La)^{3+}$, (SFLLR + $La)^{3+}$, and (angiotensin II + $La)^{3+}$ are shown in Figure 8.6. Neurokinin is amidated on the C-terminus, and has one acidic residue, D4. All metal containing fragments include D4, and those that do not contain this residue do not have the metal ion. Similar results are also obtained when the trivalent metal ion is Eu^{3+} or Yb^{3+} (Figure 8.7). All ECD fragments of (SFLLR + $La)^{3+}$ that retain La^{3+} contain both D9 and E12 (Figure 8.6b). No fragments between these residues are formed, suggesting that the metal ion may coordinate to both acidic residues. Similar results are obtained when the trivalent metal ion is Yb^{3+}, Lu^{3+}, Ho^{3+}, Sm^{3+}, Tm^{3+}, Tb^{3+}, or Pm^{3+} (Figure 8.8). For (angiotensin II + $La)^{3+}$ (Figure 8.6c), there are two acidic sites, the C-terminus and D9. Both N- and C-terminal fragments retain La^{3+}, indicating that either site likely coordinates to La^{3+} and both forms of these adducted ions are present.

These data indicate that for peptides with acidic sites, the trivalent metals ions coordinate specifically to these sites, and that the salt-bridge form of the trivalent ion in which the metal ion is bound to a carboxylate group and a proton is bound elsewhere in the peptide is more stable than the entirely charge-solvated form. In contrast, other studies indicate divalent metal ions bind to locations other than acidic sites in the peptide depending on metal ion identity.[30] The propensity for trivalent metal binding at acidic sites should make it possible to more readily determine the position of acidic residues in small peptides even when fragmentation is incomplete. Sequence information can also be obtained from the accurate mass, but there are instances where isobaric fragments cannot be determined from accurate mass alone at a given mass

measuring accuracy.[51] The most common nominal isobar arises from the difference between CH_4 and O (36 mDa). For example, the combined residue mass of Tyr and Leu is only 36 mDa higher than the combined residue mass of Phe and Glu.[51] In these instances, this method could be used to provide additional sequence information to aid peptide identification.

8.3.5 Eu^{3+} as an Electron Trap. ECD of (peptide + $Eu)^{3+}$ generally resulted in less than half the sequence coverage compared to the other trivalent metal ions and the extent of fragmentation decreases with increasing peptide size. For example, there are no *c*/*z* fragments in the ECD spectra of (angiotensin II + $Eu)^{3+}$; *b*/*y* ions and ions corresponding to small neutral losses from the charge reduced precursor are formed instead (Figure 8.9). The sequence coverage obtained from the ECD spectrum of (angiotensin II + $Eu)^{3+}$ is only 29%, whereas that for (angiotensin II + $2H)^{2+}$ and (angiotensin II + $M_T)^{3+}$, where M_T = La^{3+} or Yb^{3+}, is 100%.

For even larger peptides, i.e., > ~1560 Da (histatin 8, neurotensin, and SFLLR), the charge reduced precursor, (peptide + $Eu)^{2+}$, accounts for >93% of the total product ions formed from ECD, and predominantly small neutral loss products or *b*/*y* ions are formed. For example, the electron capture dissociation spectra for (SFLLR + $La)^{3+}$ and (SFLLR + $Eu)^{3+}$ are shown in Figure 8.10a-b. Whereas, electron capture by (SFLLR + $La)^{3+}$ results mostly in the formation *c*/*z* ions (69% sequence coverage) and the charged reduced precursor accounts for only 7% of the total product ions (Figure 8.10a), for (SFLLR + $Eu)^{3+}$, the charge reduced precursor accounts for 96% of the total product ions (no sequence coverage), and only a small neutral loss and a *b* fragment is observed (Figure 8.10b). Significantly more extensive fragmentation occurs for many lanthanides (e.g., La, Lu, Sm, Ho, Pm, and Tb) that have lower 3rd ionization energies than Eu, which has one of the highest. Despite the significantly different fragmentation, there is essentially no difference (<2%) in the ECD efficiency for these two ions. To determine if *c*/*z* ions are formed from ECD of (SFLLR + $Eu)^{3+}$, but remain noncovalently bound in the reduced precursor, the charge reduced precursor, (SFLLR + $Eu)^{2+}$, was activated by SORI-CAD (Figure 8.10c). Only *b*/*y* fragments, and no *c*/*z* ions, are formed.

The absence of *c*/*z* fragments formed from ECD of (peptide + $Eu)^{3+}$ or by SORI-CAD of the reduced precursor for larger peptides indicates that a direct one-electron reduction of Eu^{3+} occurs to form an ion where there is no radical site, (peptide + $Eu)^{2+}$ (Scheme 1; Site A). In contrast, electron capture is directed by the protonation site for the other trivalent metal ion-peptide complexes to form a more conventional odd electron ECD product ion, (peptide + $M_T)^{2+\bullet}$, that dissociates through typical ECD pathways (Scheme 1; Site B). The recombination enthalpy of direct trivalent metal ion reduction, ΔH_{red}, depends on the 3rd ionization energy of the metal ion, ΔH(III), and the difference in solvation energies of the trivalent, ΔH_{solv}(3+), and divalent metal ion, ΔH_{solv}(2+), that correspond to the enthalpy change upon solvation of the respective metal ions by the peptide, eq. 1.[24]

$$\Delta H_{red} = -\Delta H(\mathrm{III}) - \Delta H_{solv}(3+) + \Delta H_{solv}(2+) \quad (1)$$

The complete absence of *c*/*z* fragments from ECD of (peptide + $Eu)^{3+}$ for large peptides indicates that the 3rd ionization energy of Eu^{3+} is sufficiently large to overcome both the

change in solvation energy that results when the metal ion is reduced and the reduction energy at a site remote from the metal ion, resulting in direct reduction of Eu^{3+}. The *b*/*y* fragments and small neutral losses from the charge reduced precursor that are formed from ECD of (peptide + Eu)$^{3+}$ are a result of the recombination energy associated with reduction of Eu^{3+} to Eu^{2+} being redistributed throughout the peptide, and subsequent fragmentation of the even electron peptide ion. The decrease in these fragments with increasing peptide size is attributable to a degrees of freedom effect. These results are consistent with results for electron capture by $Eu(H_2O)_n^{3+}$ that show direct reduction of Eu^{3+} occurs, whereas ion-electron pairs are formed for the other solvated trivalent metal ions (and some divalent metal ions) at large cluster size.[24,52-55] One electron reduction of Eu^{3+} occurs in aqueous solution, but not for the other trivalent metal ions investigated here, with the exception of Yb^{3+} which has a significantly lower reduction potential.

Similar results are obtained for most other triply charged ions where 3+ to 2+ reduction occurs in aqueous solution. ECD spectra of (SFLLR + $Co(NH_3)_6$)$^{3+}$ and (SFLLR + $Ru(NH_3)_6$)$^{3+}$ were measured (Figure 8.11), and the primary product ion is the reduced precursor that has lost six NH_3 molecules. No *c*/*z* ions are formed. These results indicate that electron capture reduces the metal complex to its 2+ form, as occurs upon electron capture by these same metal ion complexes in aqueous nanodrops.[56] Part of the recombination energy goes into the expulsion of the six NH_3 molecules located at the site of electron capture.

It is interested that for Yb, which has the highest third ionization energy of the lanthanides investigated here, ECD of peptides complexed to Yb^{3+} results in *c*/*z* ion formation. These results indicate that Yb^{3+} is not directly reduced in these experiments. In aqueous solution, the one-electron reduction potential of Yb^{3+} is lower than that of Eu^{3+}, $Ru(NH_3)_6^{3+}$, and $Co(NH_3)^{3+}$ by at least 0.8 V (0.8 eV).[57-61] Thus, Eu^{3+}, $Ru(NH_3)_6^{3+}$, and $Co(NH_3)^{3+}$ are significantly more readily reduced than Yb^{3+} in water, despite Yb having a higher third ionization energy than Eu in isolation. Thus, solvation can profoundly affect the relative reduction energies of metals. For ECD of metalated peptides, the reduction enthalpy of Yb^{3+} is not sufficiently high to overcome the solvation enthalpy difference of the corresponding 3+ and 2+ ions to reduce the metal ion directly and suppress radical directed fragmentation of the peptide (eq. 1), which is consistent with the results for these ions when fully solvated in solution. These results indicate that the electrochemical properties of the metal ions when solvated by larger peptides are more similar to those of the same ions in solution than those of the metal ions in isolation.

Recent studies indicate that electron capture by Cd^{2+} and Hg^{2+} adducted peptides results in mostly *a*-type fragment ions and small neutral side chain losses from the reduced precursor, whereas typical *c*/*z* ions are formed for Zn^{2+} adducted peptides.[38] These results were attributed to Cd^{2+} and Hg^{2+}-peptide complexes adopting a charge-solvated structure, and Zn^{2+} adducted peptides forming salt-bridge structures.[38] Our results indicate that the electrochemical properties of the metal ions in the peptide environment determine whether or not electron capture occurs at the metal ion or at a remote protonation site in the peptide.

8.4 Conclusions

Attachment of trivalent metal ions to small peptides for which only singly protonated ions are formed by ESI can result in higher charge state ions, making this method to increase charge effective for peptide sequencing with electron capture methods. Divalent ions, $(\text{peptide} - H + M_T)^{2+}$, are formed for small peptides with acidic sites, whereas $(\text{peptide} + M_T)^{3+}$ are formed for larger peptides. The trivalent metal ions preferentially bind to acidic sites resulting in salt-bridge structures, although entirely charge-solvated structures can be formed for large peptides without acidic sites. For the larger peptides, electron capture does not result in the direct reduction of the trivalent metal ion for all the lanthanide metals investigated except Eu. Reduction is driven by the protonation site located remotely from metal ion binding and results in *c*/*z* ions. In contrast, Eu^{3+} is directly reduced and *b*/*y* ions are formed instead. The electrochemical properties of these metal ions bound to the larger peptides is the same as that observed for these same ions in large aqueous nanodrops and in solution. This indicates that the solvation environment provided by these gaseous peptides results in high solvation energies comparable to those in water, which produces similar electrochemical properties of these ions both in the gas phase and in solution.

8.5 References

(1) Bogdanov, B.; Smith, R.D. *Mass Spectrom. Rev.* **2005,** *24*, 168-200.
(2) Mann, M.; Jensen, O.N. *Nature Biotech.* **2003**, *21*, 255-261.
(3) Siuti, N.; Kelleher, N.L. *Nature Methods* **2007**, *4*, 817-821.
(4) Shi, S.D.H.; Hemling, M.E.; Carr, S.A.; Horn, D.M.; Lindh, I.; McLafferty, F.W. *Anal. Chem.* **2001**, *73*, 19-22.
(5) Mirgorodskaya, E.; Roepstorff, P.; Zubarev, R.A. *Anal. Chem.* **1999**, *71*, 4431-4436.
(6) Cooper, H.J.; Håkansson, K.; Marshall, A.G. *Mass Spectrom. Rev.* **2005**, *24*, 201-222.
(7) Håkansson, K.; Cooper, H.J.; Emmett, M.R.; Costello, C.E.; Marshall, A.G.; Nilsson, C.L. *Anal. Chem.* **2001**, *73*, 4530-4536.
(8) Syka, J.E.P.; Coon, J.J.; Schroeder, M.J.; Shabanowitz, J.; Hunt, D.F. *Proc. Natl. Acad. Sci. U. S. A.* **2004**, *101*, 9528-9533.
(9) Hogan, J.M.; Pitteri, S.J.; Chrisman, P.A.; McLuckey, S.A. *J. Proteome Res.* **2005**, *4*, 628-632.
(10) Mikesh, L.M.; Ueberheide, B.; Chi, A.; Coon, J.J.; Syka, J.E.P.; Shabanowitz, J.; Hunt, D.F. *Biochim. Biophys. Acta.* **2006**, *1764*, 1811-1822.
(11) Medzihradszky, K.F.; Guan, S.; Maltby, D.A.; Burlingame, A.L. *J. Am. Soc. Mass Spectrom.* **2007**, *18*, 1617-1624.
(12) Han, X.M.; Aslanian, A.; Yates, J.R. *Curr. Opin. Chem. Biol.* **2008**, *12*, 483-490.
(13) Coon, J.J. *Anal. Chem.* **2009**, *81*, 3208-3215.
(14) McLachlin, D.T.; Chait, B.T. *Curr. Opin. Chem. Biol.* **2001**, *5*, 591-602.
(15) Kaltashov, I.A.; Bobst, C.E.; Abzalimov, R.R. *Anal. Chem.* **2009**, *81,* 7892-7899.
(16) Hvelplund, P.; Liu, B.; Nielsen, S.B.; Panja, S.; Poully, J.C.; Stochkel, K. *Int. J. Mass Spectrom.* **2007**, *263*, 66-70.
(17) Jensen, C.S.; Wyer, J.A.; Houmoller, J.; Hvelplund, P.; Nielsen, S.B. *Phys. Chem. Chem. Phys.* **2011**, *13*, 18373-18378.
(18) Hvelplund, P.; Liu, B.; Nielsen, S.B.; Tomita, S. *Int. J. Mass Spectrom.* **2003**, *225*, 83-87.
(19) Zubarev, R.A.; Kelleher, N.L.; McLafferty, F.W. *J. Am. Chem. Soc.* **1998**, *120*, 3265-3266.
(20) Zubarev, R.A.; Haselmann, K.F.; Budnik, B.; Kjeldsen, F.; Jensen, F. *Eur. J. Mass Spectrom.* **2002**, *8*, 337-349.
(21) Good, D.M.; Wirtala, M.; McAlister, G.C.; Coon, J.J. *Mol. Cell. Proteomics* **2007**, *6*, 1942-1951.
(22) Iavarone, A. T.; Paech, K.; Williams, E. R. *Anal. Chem.* **2004**, *76*, 2231-2238.
(23) Donald, W.A.; Williams, E.R. *J. Am. Soc. Mass Spectrom.* **2010**, *21*, 615-625.
(24) Donald, W.A.; Demireva, M.; Leib, R.D.; Aiken, M.J.; Williams, E.R. *J. Am. Chem. Soc.* **2010**, *132*, 4633-4640.
(25) Prell, J.S.; O'Brien, J.T.; Holm, A.I.S.; Leib, R.D.; Donald, W.A.; Williams, E.R. *J. Am. Chem. Soc.* **2008**, *130*, 12680-12689.
(26) Budnik, B.A.; Haselmann, K.F.; Zubarev, R.A. *Chem. Phys. Lett.* **2001**, *342*, 299-302.

(27) Yang, J.; Mo, J.J.; Adamson, J.T.; Håkansson, K. *Anal. Chem.* **2005**, *77*, 1876-1882.
(28) Haselmann, K.F.; Budnik, B.A.; Kjeldsen, F.; Nielsen, M.L.; Olsen, J.V.; Zubarev, R.A. *Eur. J. Mass Spectrom.* **2002**, *8*, 117-121.
(29) Fung, Y.M.E.; Adams, C.M.; Zubarev, R.A. *J. Am. Chem. Soc.* **1312009**, *131*, 9977-9985.
(30) Liu, H.C.; Håkansson, K. *J. Am. Soc. Mass Spectrom.* **2006**, *17*, 1731-1741.
(31) Turecek, F.; Jones, J.W.; Holm, A.I.S.; Panja, S.; Nielsen, S.B.; Hvelplund, P. *J. Mass Spectrom.* **2009**, *44*, 707-724.
(32) Kleinnijenhuis, A.J.; Mihalca, R.; Heeren, R.M.A.; Heck, A.J.R. *Int. J. Mass Spectrom.* **2006**, *253*, 217-224.
(33) van der Burgt, Y.E.M.; Palmblad, M.; Dalebout, H.; Heeren, R.M.A.; Deelder, A.M. *Rapid Commun. Mass Spectrom.* **2009**, *23*, 31-38.
(34) Chen, X.F.; Fung, Y.M.E.; Chan, W.Y.K.; Wong, P.S.; Yeung, H.S.; Chan, T.W.D. *J. Am. Soc. Mass Spectrom.* **2011**, *22*, 2232-2245.
(35) Dong, J.; Vachet, R.W. *J. Am. Soc. Mass Spectrom.* **2012**, *23*, 321-329.
(36) Alfonso, C.; Tabet, J.C.; Giorgi, G.; Tureček, F. *J. Mass Spectrom.* **2012**, *47*, 208-220.
(37) Fung, Y.M.E.; Liu, H.C.; Chan, T.W.D. *J. Am. Soc. Mass Spectrom.* **2006**, *17*, 757-771.
(38) Chen, X.F.; Chan, W.Y.K.; Wong, P.S.; Yeung, H.S.; Chan, T.W.D. *J. Am. Soc. Mass Spectrom.* **2011**, *22*, 233-244.
(39) Adamson, J.T.; Håkansson, K. *Anal. Chem.* **2007**, *79*, 2901-2910.
(40) Barr, J.M.; Van Stipdonk, M.J. *Rapid Commun. Mass Spectrom.* **2002**, *16*, 566-578.
(41) Prell, J.S.; Flick, T.G.; Oomens, J.; Berden, G.; Williams, E.R. *J. Phys. Chem. A* **2010**, *114*, 854-860.
(42) Shi, T.J.; Hopkinson, A.C.; Siu, K.W.M. *Chem. Eur. J.* **2007**, *13*, 1142-1151.
(43) Shi, T.J.; Siu, K.W.M.; Hopkinson, A.C. *J. Phys. Chem. A* **2007**, *111*, 11562-11571.
(44) Shvartsburg, A.A.; Jones, R.C. *J. Am. Soc. Mass Spectrom.* **2004**, *15*, 406-408.
(45) Shi, T., Siu, C.K., Siu, K.W.M., Hopkinson, A.C.: Dipositively Charged Protonated a(3) and a(2) Ions: Generation by Fragmentation of La(GGG)$(CH_3CN)_2^{3+}$. *Angew. Chem. Int. Ed.* **2008**, *47*, 8288-8291.
(46) Pu, D., Vincent, J.B., Cassady, C.J. *J. Mass Spectrom.* **2008**, *43*, 773-781.
(47) Mosely, J.A.; Murray, B.S.; Parker, D. *Eur. J. Mass Spectrom.* **2009**, *15*, 145-155.
(48) Jurchen, J.C.; Williams, E.R. *J. Am. Chem. Soc.* **2003**, *125*, 2817-2826.
(49) Han, H.L.; Xia, Y.; McLuckey, S.A. *J. Proteome Res.* **2007**, *6*, 3062-3069.
(50) Zhang, L.Y.; Reilly, J.P. *J. Am. Soc. Mass Spectrom.* **2009**, *20* 1378-1390.
(51) He, F.; Emmett, M.R.; Håkansson, K.; Hendrickson, C.L.; Marshall, A.G. *J. Proteome Res.* **2004**, *3*, 61-67.
(52) Donald, W.A.; Leib, R.D.; Demireva, M.; O'Brien, J.T.; Prell, J.S.; Williams, E.R. *J. Am. Chem. Soc.* **2009**, *131*, 13328-13337.
(53) Donald, W. A.; Leib, R. D.; O'Brien, J. T.; Holm, A. I. S.; Williams, E. R. *Proc. Natl. Acad. Sci. USA* **2008**, *105*, 18102-18107.

(54) Donald, W. A.; Leib, R. D.; O'Brien, J. T.; Williams, E. R. *Chem. Eur. J.* **2009**, *15*, 5926-5934.
(55) Donald, W. A.; Williams, E. R. *Pure Appl. Chem.* **2011**, *83*, 2129-2151.
(56) Donald, W. A.; Leib, R. D.; O'Brien, J. T.; Bush, M. F.; Williams, E. R. *J. Am. Chem. Soc.* **2008**, *130*, 3371-3381.
(57) Amorello, D.; Romano, V.; Zingales, R. *Annali di Chimica* **2003**, *94*.
(58) Walters, G.C.; Pearce, D.W. *J. Am. Chem. Soc.* **1940**, *62*, 3330-3332.
(59) Laitinen, H.A.; Taebel, W.A. *Ind. Chem. Eng.* **1941**, *13*, 825-829.
(60) Meyer, T.J.; Taube, H. *Inorg. Chem.* **1968**, *7*, 2369-2379.
(61) Curtis, N.J.; Lawrance, G.A.; Sargeson, A.M. *Aus. J. Chem.* **1983**, *36*, 1327-1339.

8.6 Tables

Table 8.1. ECD efficiency and sequence coverage obtained from ECD of various peptides complexed with different charge carriers.

Peptide	Peptide Molecular Weight	Charge Carrier	Charge State (z)	Sequence Coverage (%)	ECD Efficiency
AAAAAA	444	Ca	2	60	14
		La	2	100	22
		Eu	2	60	48
		Yb	2	100	38
Leucine Enkephalin (YGGFL)	555	Ca	2	50	11
		Mg	2	75	10
		Ba	2	50	10
		Sr	2	50	9
		La	2	100	17
		Eu	2	75	29
		Yb	2	100	26
		Tm	2	100	26
FLEEL	649	Ca	2	50	16
		La	2	100	29
		Eu	2	75	42
		Yb	2	100	50
Angiotensin II (DRVYIHPF)	1046	H	2	100	27
		La	2	57	14
		Eu	2	29	24
		Yb	2	86	18
		La	3	100	48
		Eu	3	29	52
		Yb	3	100	71
Bradykinin 2-9 (PPGFSPFR)	904	H	2	86	26
		La	3	86	45
		Eu	3	57	51
		Yb	3	86	67
Neurokinin ($HKTDSFVGLM\text{-}NH_2$)	1133	H	2	100	53
		La	3	67	18
		Eu	3	67	77
		Yb	3	100	64
		Eu	2	0	39
		Yb	2	44	14
LHRH (pEHWSYGLRPG)	1182	H	2	56	24
		La	2	56	26
		Eu	2	11	31
		Yb	2	56	26
Substance P (RPKPNNFFGLM)	1348	H	3	80	66
		La	3	90	36
		Eu	3	44	44
		Yb	3	67	43
Ranakinin ($KPNPERFYGLM\text{-}NH_2$)	1351	H	2	90	63
		H	3	100	67
		La	3	90	48
		Eu	3	50	70
		Yb	3	90	65
Histatin 8 (KFHEKHHSHRGY)	1563	H	3	91	74
		La	3	64	30
		Eu	3	0	35
		Yb	3	55	60
Neurotensin (pyroELYENKPRRPYIL)	1673	H	3	83	69
		La	3	58	32
		Eu	3	8	68
		Yb	3	50	48
SFLLRNPNDKYEPF	1739	H	3	92	33
		La	3	69	27
		Eu	3	8	29
		Yb	3	46	41
		Lu	3	54	23
		Sm	3	62	67
		Ho	3	54	42
		Pm	3	100	47
		Tb	3	100	48

8.7 Figures

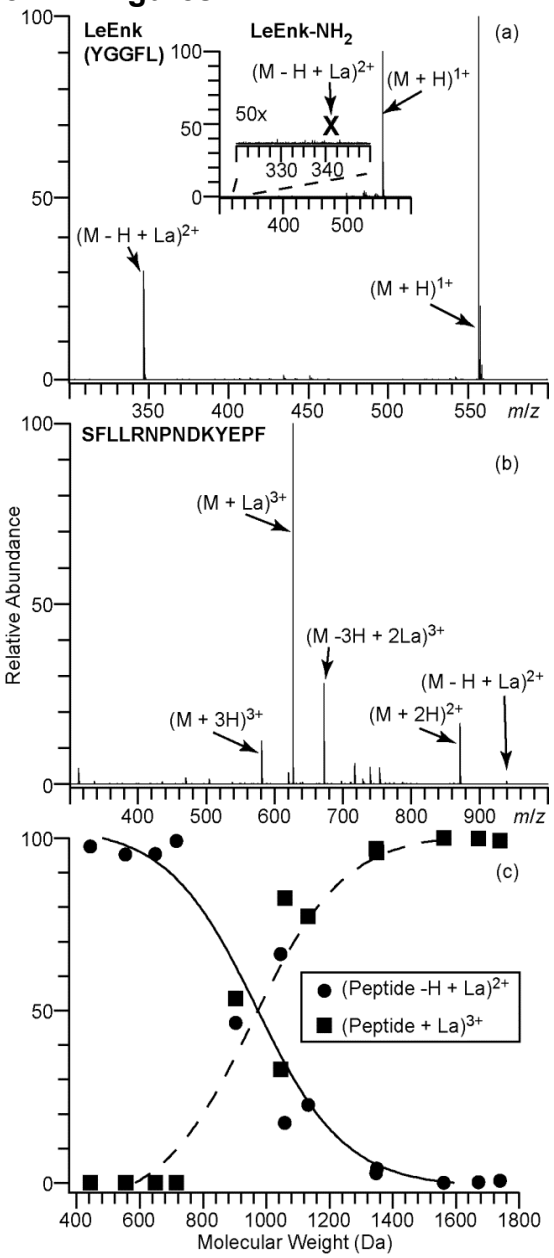

Figure 8.1. (a) ESI mass spectrum of an aqueous solution containing 10 μM leucine enkephalin (LeEnk) and 100 μM $LaCl_3$. Inset is an ESI mass spectrum of an aqueous solution containing 10 μM amidated leucine enkephalin (LeEnk-NH_2) and 100 μM $LaCl_3$ with a ×50 expansion of the spectral region where (LeEnk-NH_2 – H + $La)^{2+}$ would be located. (b) ESI mass spectrum of an aqueous solution containing 10 μM SFLLRNPNDKYEPF and 100 μM $LaCl_3$. (c) Relative ion abundances of (peptide – H + $La)^{2+}$ and (peptide + $La)^{3+}$ as a function of peptide molecular weight.

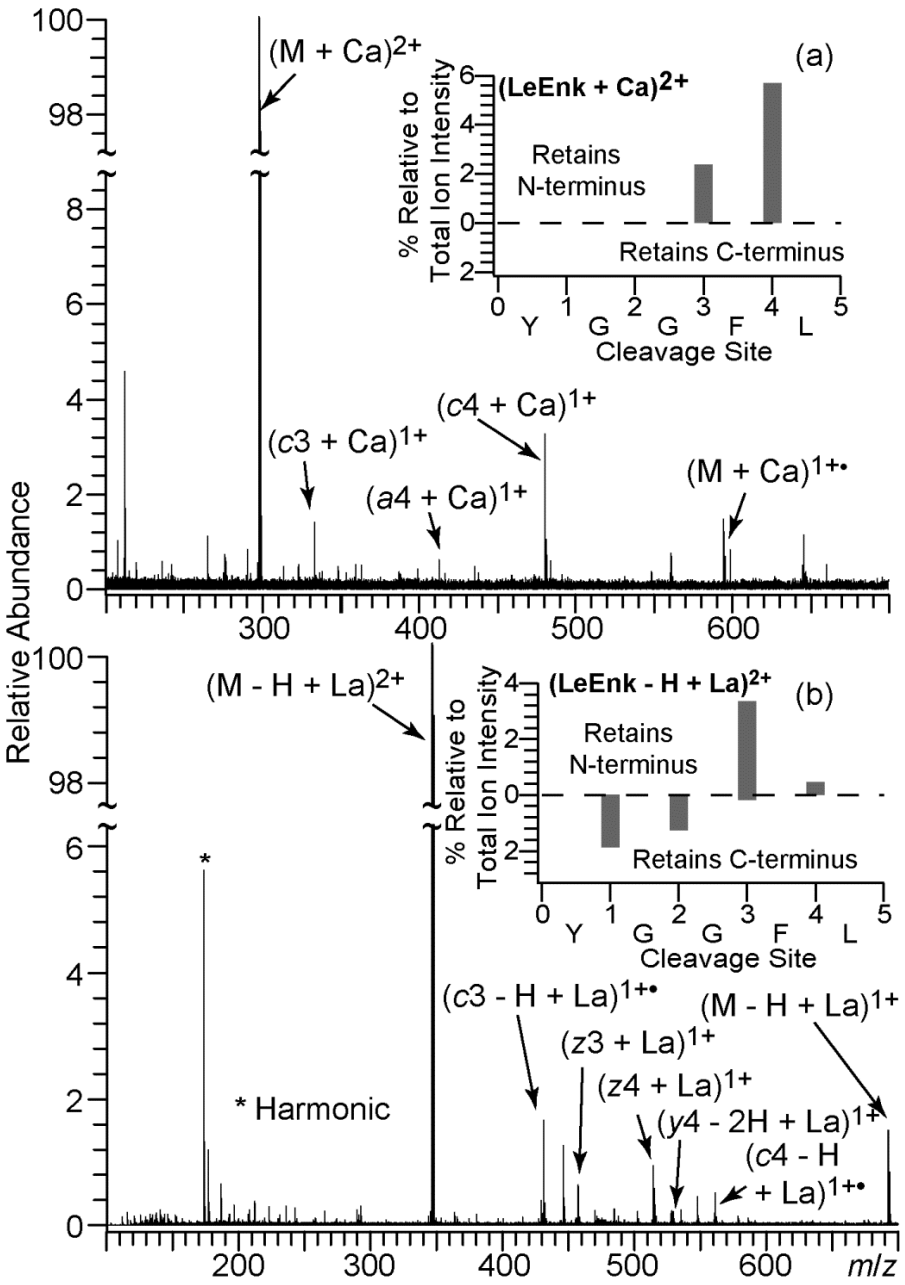

Figure 8.2. ECD spectra of $(LeEnk + Ca)^{2+}$ and (b) $(LeEnk – H + M)^{3+}$ with abundance of sequence-specific fragments inset.

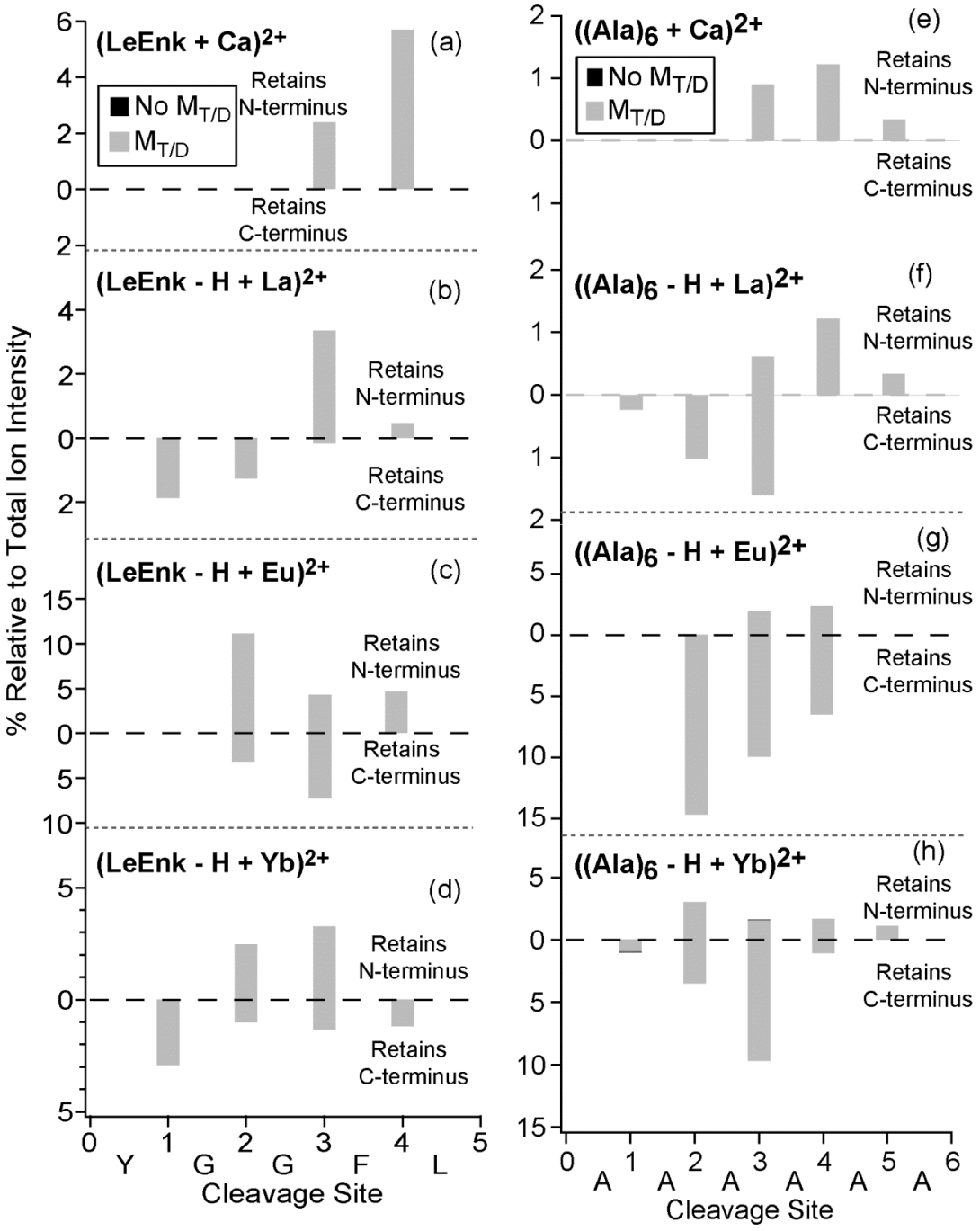

Figure 8.3. Relative ECD fragment ion abundances at each cleavage site for (a) (LeEnk + Ca)$^{2+}$ (b) (LeEnk – H + La)$^{2+}$, (c) (LeEnk – H + Eu)$^{2+}$, (d) (LeEnk – H + Yb)$^{2+}$, (e) (Ala_6 + Ca)$^{2+}$, (f) (Ala_6 – H + La)$^{2+}$, (g) (Ala_6 – H + Eu)$^{2+}$, and (h) (Ala_6 – H + Yb)$^{2+}$.

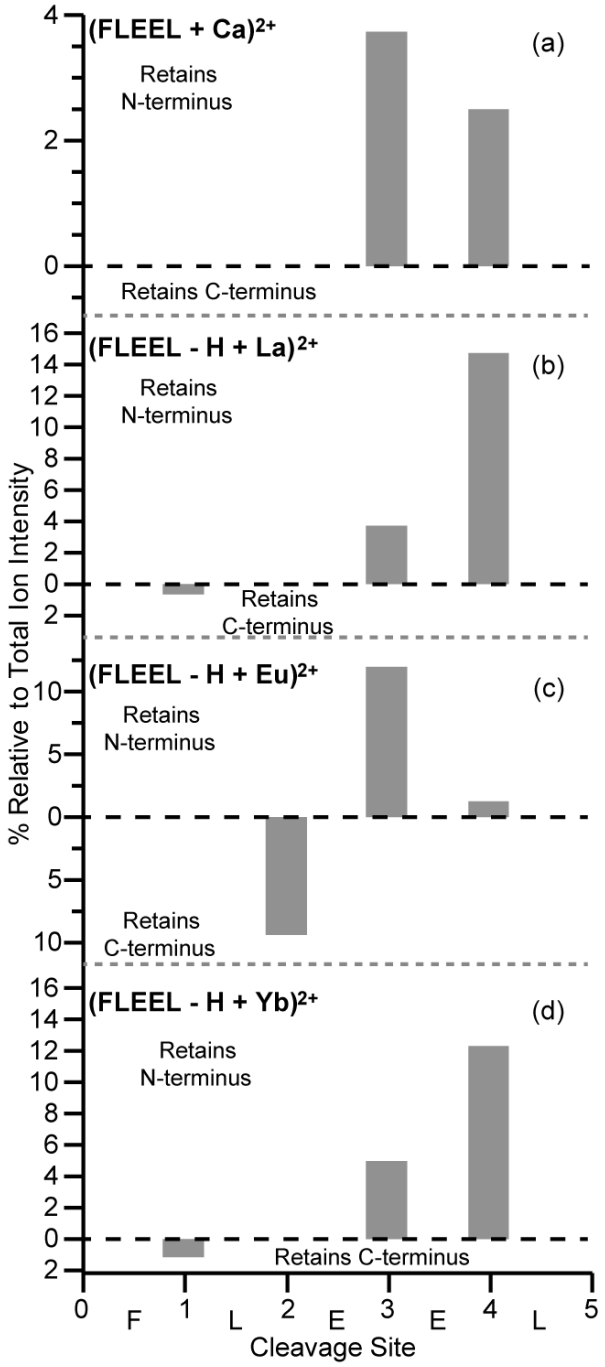

Figure 8.4. Relative ECD fragment ion abundances at each cleavage site for (a) $(FLEEL + Ca)^{2+}$ (b) $(FLEEL – H + La)^{2+}$, (c) $(FLEEL – H + Eu)^{2+}$, and (d) $(FLEEL – H + Yb)^{2+}$.

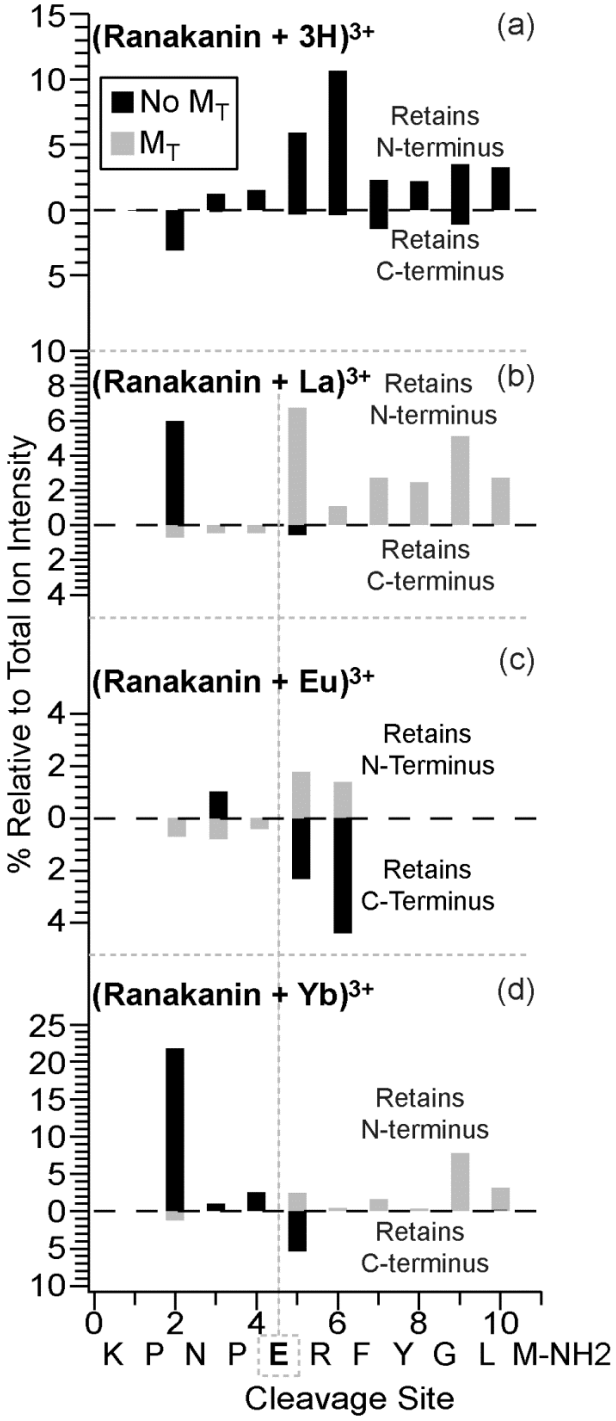

Figure 8.5. Relative ECD fragment ion abundances at each cleavage site for (a) (ranakinin + 3H)$^{3+}$, (b) (ranakinin + La)$^{3+}$, (c) (ranakinin + Eu)$^{3+}$, and (ranakinin + Yb)$^{3+}$. Grey bars correspond to fragments that retain M_T, whereas black bars correspond to non-metallated fragments.

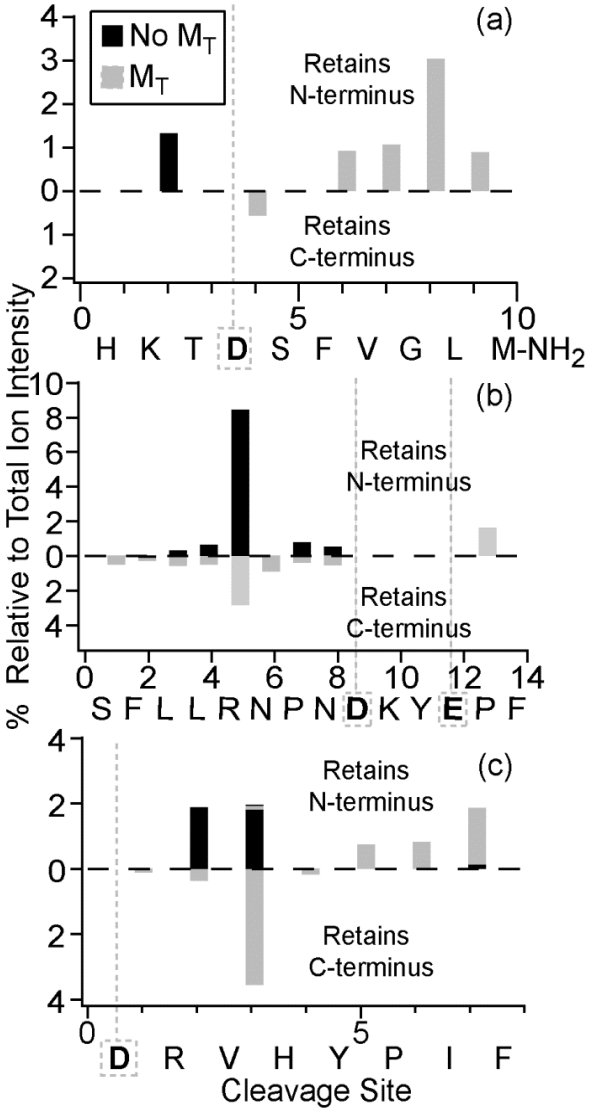

Figure 8.6. Relative ECD fragment ion abundances at each cleavage site for (a) (neurokinin + La)$^{3+}$, (b) (SFLLR + La)$^{3+}$, and (c) (angiotensin II + La)$^{3+}$. Grey bars correspond to fragments that retain M_T, whereas black bars correspond to non-metallated fragments

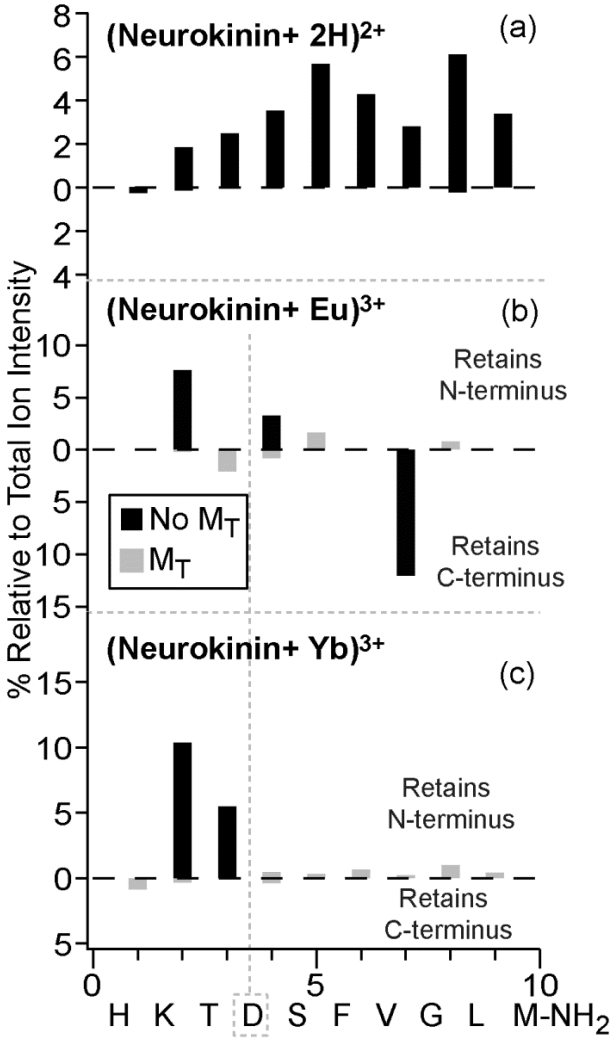

Figure 8.7. Relative ECD fragment ion abundances at each cleavage site for (a) (neurokinin + 2H)$^{2+}$ and (neurokinin + M_T)$^{3+}$, where M_T = (b) Eu^{3+} or (c) Yb^{3+}.

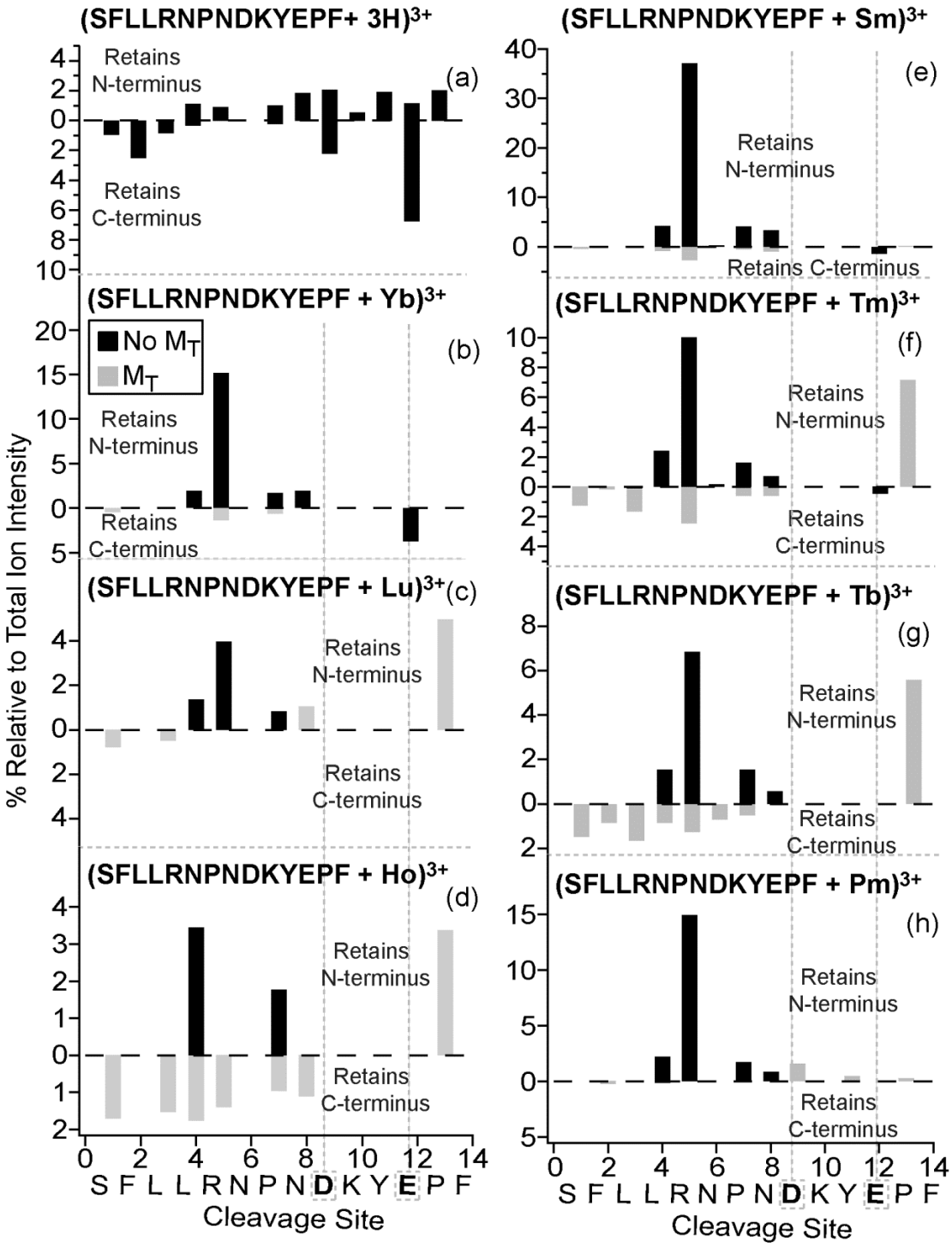

Figure 8.8. Relative ECD fragment ion abundances at each cleavage site for (a) $(SFLLRNPNDKYEPF + 3H)^{3+}$ and $(SFLLRNPNDKYEPF + M_T)^{3+}$, where M_T = (b) Yb^{3+}, (c) Lu^{3+}, (d) Ho^{3+}, (e) Sm^{3+}, (f) Tm^{3+}, (g) Tb^{3+}, or (h) Pm^{3+}.

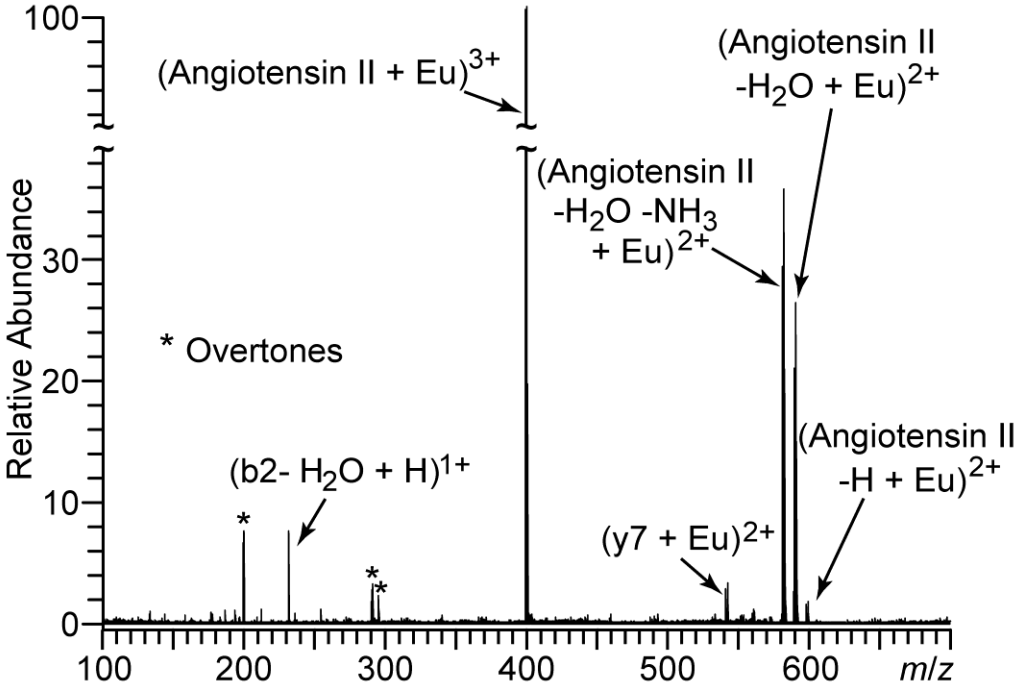

Figure 8.9. ECD spectrum of (angiotensin II + $Eu)^{3+}$.

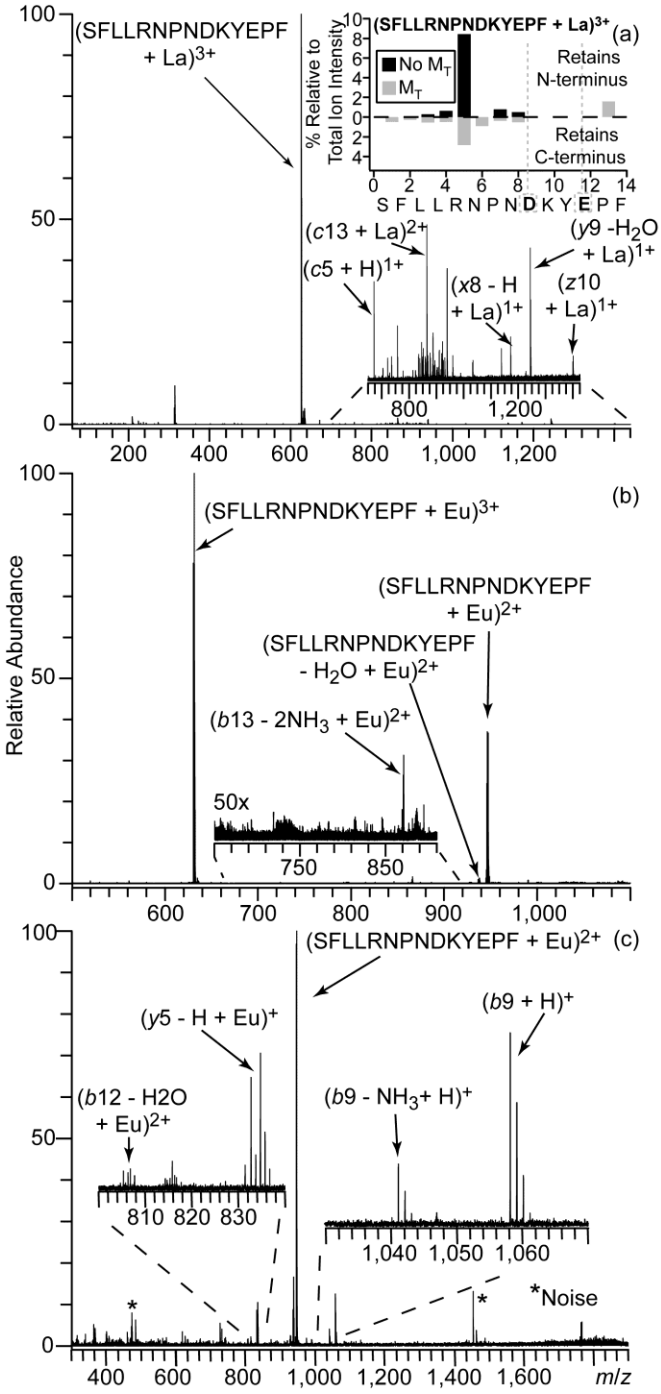

Figure 8.10. (a) ECD spectrum of (SFLLRNPNDKYEPF + La)$^{3+}$ with relative ECD fragment ion abundances at each cleavage site inset. (b) ECD spectrum of (SFLLRNPNDKYEPF + Eu)$^{3+}$. (c) SORI-CAD spectrum of the charge reduced precursor, (SFLLRNPNDKYEPF + Eu)$^{2+}$, generated from ECD of (SFLLRNPNDKYEPF + Eu)$^{3+}$.

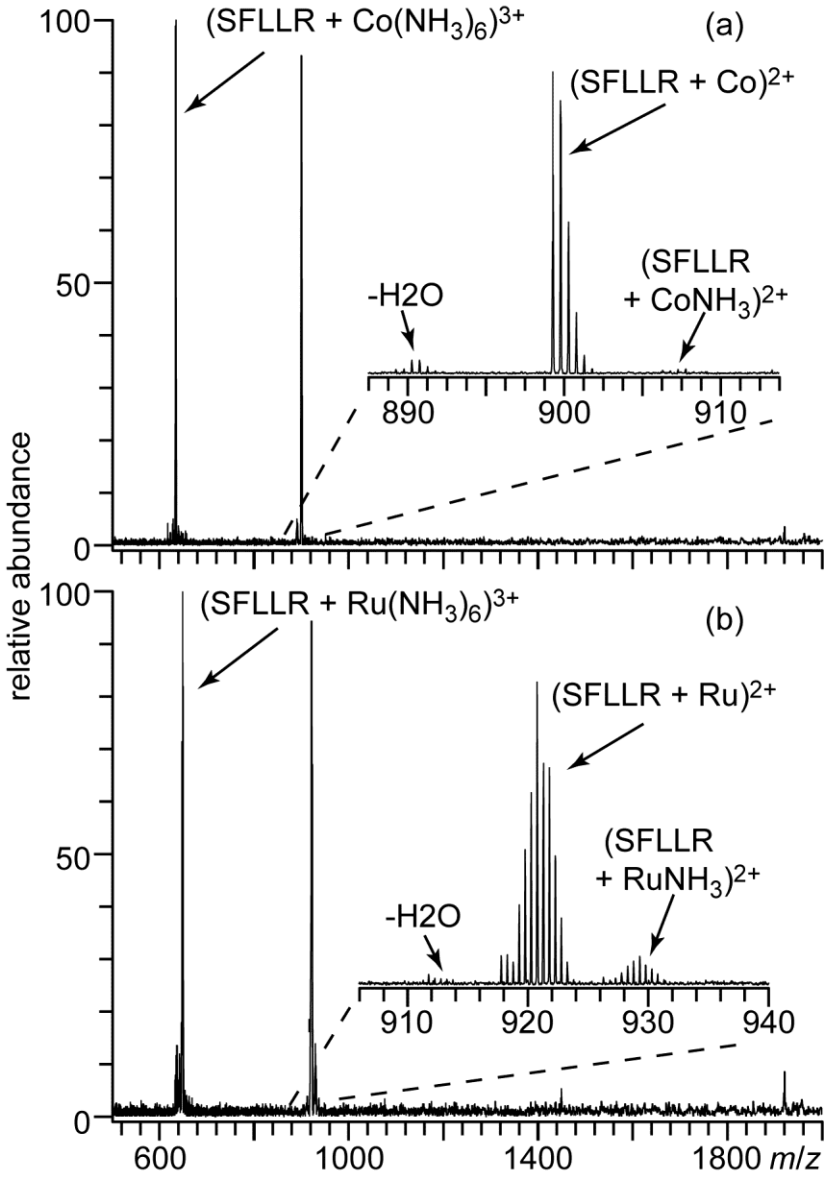

Figure 8.11. ECD mass spectra for (a) (SFLLRNPNDKYEPF + $Co(NH_3)_6)^{3+}$ and (b) (SFLLRNPNDKYEPF + $Ru(NH_3)_6)^{3+}$

Scheme 1.

For M^{3+} = La^{3+}, Yb^{3+}, Lu^{3+}, Ho^{3+}, Sm^{3+}, Tm^{3+}, Tb^{3+}, Pm^{3+}

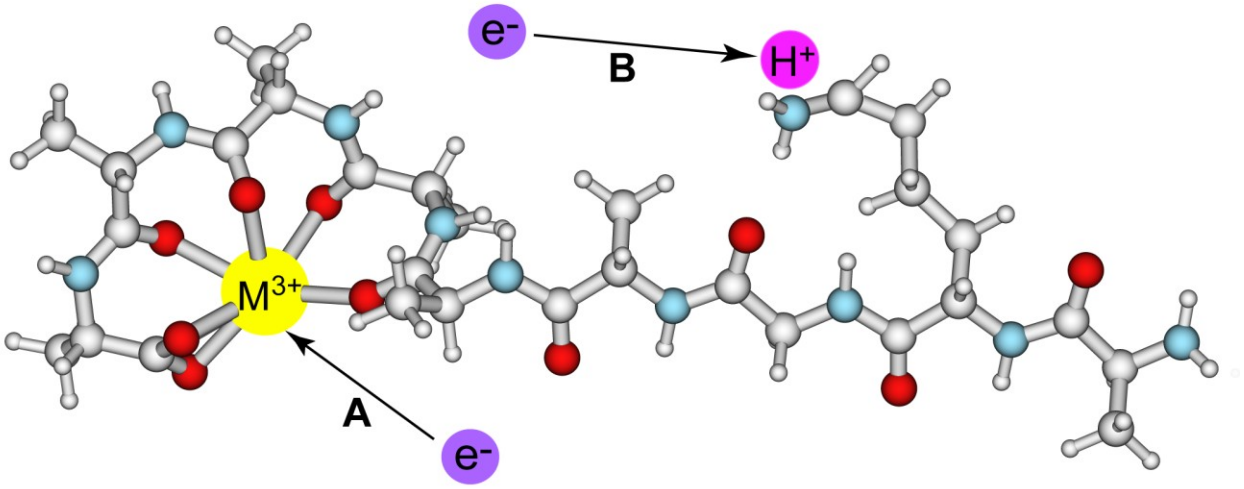

For M^{3+} = Eu^{3+}, $Ru(NH_3)_6^{3+}$, $Co(NH_3)_6^{3+}$

CHAPTER 9

Effects of Metal Ion Adduction on the Gas-Phase Conformations of Protein Ions

(This chapter is reproduced with permission from Flick, T.G.; Merenbloom, S.I.; Williams, E.R. This chapter was submitted to the Journal of American Society for Mass Spectrometry)

9.1 Introduction

Metal ion-biomolecule interactions are important in many different biological processes, including stabilizing macromolecular structure, storage and transfer of electrons, and catalytic activity.[1-3] It is estimated that one quarter to one third of all proteins require metals to function properly.[4,5] One of the most well known examples is hemoglobin, which has a central iron atom in the heme group, which is necessary for transportation of oxygen from the lungs to all other cells in the body.[6] EF-hand proteins, such as calmodulin, bind calcium ions in order to regulate a variety of functions, including inflammation, metabolism, skeletal- and smooth-muscle contraction, memory, and immune response.[7,8] Conformational changes in biomolecules that occur upon metal ion binding are typically investigated using X-ray crystallography[9-11] or nuclear magnetic resonance (NMR).[11,12] However, mass spectrometry (MS) has emerged as a rapid and sensitive analytical tool to investigate protein conformation and conformational changes from shifts in the charge-state distribution,[13,14] or in combination with hydrogen/deuterium (H/D) exchange,[15,16] chemical labeling and crosslinking,[17,18] or ion mobility spectrometry (IMS).[19-24]

Using H/D exchange, calmodulin was shown to adopt a structure with less solvent accessible surface area when the protein binds up to four Ca^{2+} adducts.[13] IMS measurements indicate two gas phase ion populations of calmodulin with the abundance of the compact conformer increasing relative to the elongated conformer with increasing numbers of Ca^{2+} adducts.[20] Metal cation adduction to heparin, a pharmaceutical drug that is an anticoagulant, also resulted in a smaller collisional cross section (ccs) of the octasaccharide anions compared to the ion with no metals bound, similar to conformational changes that occur in solution.[23]

The structures of small peptides bound to metal ions have been extensively studied.[19,21,22,25-34] Coordination of a metal ion often results in peptide ions adopting more compact structures compared to the fully protonated form. Infrared multiphoton dissociation spectra of polyalanine complexed to a trivalent metal ion, $((Ala)_n - H + M)^{2+}$, indicate that these ions have a compact conformation or conformations in which all carbonyl oxygen atoms coordinate to the metal ion, and interaction of the N-terminus with the metal ion is also favored.[32] Divalent metal ion adduction to insulin chain A anions stabilizes more compact conformations compared to the non-metalated or sodiated form that has the same net charge.[19] However, polyalanine peptide-divalent metal ion complexes can have more elongated conformations compared to the fully

protonated form, which has been attributed to the peptide adopting a helical conformation that is stabilized by coordination of the metal ion to the C-terminus.[21,22]

Although the presence of salts in solution can be essential to observe some macromolecular complexes in the gas phase,[35-37] there are relatively few studies about the effects of nonspecific ion-protein interactions on the structures of larger gaseous protein ions.[38,39] Nonspecific anion adduction to macromolecular complexes has recently been shown to preserve compact conformations of macromolecular complexes, and many of these anions can be readily removed by activating the ions without altering the conformation of these ions.[38] Recent experiments showed that acid adduction to cytochrome *c*, ubiquitin, and α-lactalbumin with partially-folded conformers results in these molecules adopting more compact conformations.[39]

Here, the effects of nonspecific metal ion adduction on the gas-phase conformations of various protein cations and anions are investigated using traveling wave ion mobility spectrometry (TWIMS) coupled to MS. These results show that nonspecific metal ion adduction to proteins typically result in ions that have more compact conformations than the non-metallated forms with the same charge state, and that this effect is the greatest for intermediate protein charge states and for increasing metal ion charge. These results suggest that a compaction of the gas-phase ion structure with metal ions attached may not be a reliable indicator of any conformational changes that occur in solution as a result of specific metal ion binding, whereas an increase in collisional cross section upon metal ion binding may be a more significant indicator of specific conformational changes that occur in solution.

9.2 Experimental

All experiments were performed using a Synapt G2 High Definition mass spectrometer (Waters, Milford, MA, USA). Ions are formed by nanoelectrospray (nanoESI) from borosilicate capillaries that are pulled to a tip i.d. of ~2 μm with a Flaming/Brown micropipette puller (Sutter Instruments, Novato, CA, USA). The capillary is loaded with ~2-10 μL of analyte solution, and a platinum wire is inserted into the solution. Electrospray is initiated by positioning the borosilicate capillary ~2 mm from the source inlet and applying a potential of 1.0-1.5 kV to the wire. The sampling and extraction cone potentials were 40 V and 3 V, respectively.

The TWIMS mobility cell was operated with a constant wave velocity of 700 m/s, wave height of 40 V, helium flow rate of 180 mL/min, IMS (N_2) flow rate of 90 mL/min. and measurements were made with the TOF analyzer in “V” (single reflectron) mode. Drift time distributions were smoothed twice using a Savitzky Golay algorithm with a one unit window. Drift times were converted to a ccs scale using the procedure outlined by Robinson and coworkers[38,39] with ions formed from denaturing solutions of ubiquitin (9+ through 13+), cytochrome *c* (13+ through 18+), and myoglobin (16+ through 22+) and the ccs values obtained for these ions from static-field drift tube experiments using N_2 as the drift gas carrier.[39] There is a 6.2% and 7.5% difference between the ccs calculated using this calibration procedure and values obtained using a static drift tube for cytochrome *c* 6+ and β-lactoglobulin 7+,[39] respectively, indicating the extent of the uncertainty associated with this calibration method. The calculated ccs using the exact

hard sphere (EHSS) and projection (Proj) method for the native conformation of ubiquitin and cytochrome *c* was obtained by converting the calculated ccs determined by Clemmer and coworkers[40-42] using He as the drift gas carrier to that expected if N_2 was used instead. This conversion factor was obtained by plotting the ccs values of ubiquitin 9+ to 11+, cytochrome *c* 14+ to 18+, and *apo*-myoglobin 19+ to 22+ obtained in static field IMS experiments using N_2 as the drift gas carrier against those when He is the drift gas.[39] The data was fit to a linear equation with an R^2 value of 0.998. For ubiquitin, the linear regression converted the Proj and EHSS values with He as the drift gas of 930 and 1162 $Å^2$ to values for N_2 of 1192 and 1492, respectively. Converting ccs values from He to N_2 has reported to introduce an error of at least 1.4%.[43]

All chemicals were purchased from Sigma Aldrich (St. Louis, MO) and used without further purification except for α-lactalbumin, which was desalted using a Bio-Rad Micro Bio Spin 6 column (Bio Rad Labs, Hercules, CA, USA). Solutions for analysis were prepared at a final concentration of 10 μM protein in denaturing solutions (48.5/48.5/3.0 methanol/water/acetic acid) and aqueous solutions with and without 1 mM of a chloride salt.

9.3 Results and Discussion

9.3.1 Metal Ion Adduction to Protein Cations. Under the conditions of these experiments, the 6+ charge state of ubiquitin is the most abundant ion produced by ESI from a 10 μM aqueous solution, and the average and maximum charge states are 5.6 and 7, respectively (Figure 9.1a). With 1.0 mM NaCl, the average (5.0) and maximum (6) charge states are slightly lower, and adduction of multiple sodium ions occurs, with more Na^+ adducting to lower charge state ions (Figure 9.1b), as has been previously reported.[44,45] Similar results were obtained from an aqueous solution containing KCl. In contrast, ESI of an aqueous solution of ubiquitin containing 1.0 mM $CaCl_2$ results in average (7.0) and maximum (8) charge states that are higher than that obtained from just water, and more extensive Ca^{2+} adduction occurs to higher charge state ions (Figure 9.1c). For example, up to 20 Ca^{2+} ions attach to the 8+ charge state, whereas a maximum of seven Ca^{2+} ions adduct to the 4+ charge state. Similar results were obtained from an aqueous solution containing $MgCl_2$. ESI of an aqueous solution of ubiquitin containing 1.0 mM $LaCl_3$ also produces significantly higher average (7.5) and maximum (10) charge states than those obtained from pure water (Figure 9.1d), and the charge enhancement is greater than that from the $CaCl_2$ solution. More La^{3+} ions adduct to higher charge state ions, with up to seven La^{3+} ions attached to the 9+ charge state. Similar results were obtained with an aqueous solution containing $EuCl_3$. The greater adduction of Ca^{2+} and La^{3+} to higher charge states of ubiquitin suggests that the higher charge state ions are a result of multiple Ca^{2+} or La^{3+} ions adducting to folded ubiquitin during electrospray.[46]

9.3.2 Effect of Cation Adduction on Protein Ion Conformation. Ion mobility experiments were performed to investigate the effects of nonspecific cation adduction on the resulting gaseous protein ion conformation. The drift profiles for ubiquitin 6+, a charge state common to the ESI mass spectra generated from aqueous solutions with and without 1.0 mM of the chloride salts of Na^+, K^+, Ca^{2+}, Mg^{2+}, La^{3+}, or Eu^{3+} are shown

in Figure 9.2. Features in the drift profiles are labeled with Roman numerals, with higher numbers corresponding to longer drift times and hence larger ccs values. The drift profiles show four main features at ~1424 $Å^2$ (I), ~1560 $Å^2$ (II), ~1725 $Å^2$ (III), and ~1800 $Å^2$ (IV). The drift distribution for $(ubiquitin + 6H)^{6+}$ has three features (II, III, and IV). The distributions for this ion formed from solutions containing each salt are similar, indicating that the presence of these salts at millimolar concentrations does not affect the conformation of this ion to an extent that can be measured using TWIMS-MS. The drift profile for $(ubiquitin + 6H)^{6+}$ is similar to that reported previously with TWIMS-MS,[37,47] but differs from results for this ion from static-field IMS experiments.[40,41] More elongated conformations are observed with TWIMS-MS, consistent with these ions being heated prior to or during the TWIMS separation.[47]

In contrast, the drift profiles of ubiquitin 6+ adducted with cations are significantly different than those obtained for $(ubiquitin + 6H)^{6+}$. Attachment of a single monovalent cation (M^+) to ubiquitin 6+ results in an increase in the abundance of conformer III and a decrease in the abundance of feature IV compared to the fully protonated ion. With three M^+ adducts, a new, more compact feature (I) appears. Features I and II are more abundant with five M^+ adducts, and the abundance of III and IV decrease with increasing numbers of M^+ adducts. With 13 Na^+ adducts, only feature I is observed.

A more significant change in the ccs of ubiquitin 6+ occurs with attachment of just one divalent (M^{2+}) or trivalent (M^{3+}) metal ion compared to adduction of three M^+. With one M^{2+} adduct, II is the most abundant feature (Figure 9.2, middle). Feature I increases and II decreases in abundance with increasing numbers of M^{2+} adducts. With one M^{3+} adduct, II is the most abundant feature, and I is the dominant feature with three M^{3+} adducts (Figure 9.2, right). There are only minor differences in the drift profile for cation adducts with the same charge state, i.e., Na^+ vs. K^+; Ca^{2+} vs. Mg^{2+}; or La^{3+} vs. Eu^{3+}, indicating that the metal ion charge state, and not the identity, is the most important factor which affects the conformation of the adducted protein ion.

To simplify comparisons between ions with different number of adducts and different charge states, an average ccs of ubiquitin 6+ was determined by weighting each feature in the drift profile by peak area to evaluate the overall effect of metal cation adduction on the gas-phase conformation of this charge state, and these values are shown as a function of the number of metal ion adducts in Figure 9.3a. Adduction of three M^{3+} to ubiquitin 6+ results in an average ccs that is ~19% lower than that of the fully protonated molecular ion. A similar reduction in the average ccs occurs with seven M^{2+} and 14 M^+ adducts. For a given numbers of adducts, the average ccs consistently follows the trend: $M^{3+} < M^{2+} < M^+$. The smaller average ccs with increasing charge of the metal ion is consistent with salt-bridge interactions between the metal ion and acidic sites in the protein as well as charge-solvation interactions between the metal ion and heteroatoms in the protein inducing the more compact conformers observed here. Attachment of $HClO_4$, HI, or H_2SO_4 to multiply protonated protein ions can also induce compact conformations as a result of ionic interactions between the acid molecule and basic sites in the protein.[37]

The 4+ is the lowest charge state generated by ESI from these aqueous solutions, and $(ubiquitin + 4H)^{4+}$ exists in a single, compact conformer with a ccs of

1262 Å^2 (Figure 9.3a), which is approximately 6% higher than the ccs of the single conformer of this ion that was reported previously,[40,41] and converted to nitrogen as the drift gas. This value is also ~6% greater than the calculated ccs of the crystal structure of native ubiquitin obtained using the Proj method calibrated for nitrogen as the drift gas (~1192 Å^2), which can be considered a lower limit to the actual ccs of native ubiquitin.[40,41] With increasing metal ion adduction, more elongated features of ubiquitin 6+ become more compact, and the maximally adducted ion for M^+, M^{2+}, and M^{3+} adopt primarily a single, compact conformation or family of conformers, with ccs values between 1398 to 1425 Å^2. These ccs values are at least 11% greater than that measured for (ubiquitin + 4H)$^{4+}$ and are bracketed between the calculated ccs of the native crystal structure obtained using the Proj and EHSS method. These results indicate that ionic interactions between the cations and the protein results in more compact conformations of ubiquitin 6+, but these conformations have larger ccs values than (ubiquitin + 4H)$^{4+}$ at these levels of adduction.

The 6+ ion is the lowest charge state generated by ESI from an aqueous solution containing cytochrome *c*, and the calculated average ccs for this ion lies between the calculated ccs obtained for the native crystal structure of cytochrome *c* calculated using the EHSS and Proj methods[43] (Figure 9.3b). The average ccs decreases from 2159 Å^2 for (cytochrome *c* + 7H)$^{7+}$ to 1805 Å^2 with three M^{3+} adducts, whereas 7 M^{2+} adducts are necessary to reach a similar ccs (1810 Å^2) (drift profiles shown in Figure 9.4). A similarly compact structure is not formed with up to 13 M^+ adducts. The average ccs of maximally adducted cytochrome *c* 7+ approaches that of (cytochrome *c* + 6H)$^{6+}$ and the calculated ccs(N_2) for the native protein structure, but does not reach this compact state, presumably owing to the higher charge, which results in greater Coloumbic repulsion in the ion, and can contribute to greater ion heating in TWIMS.[47] Similar to that observed for ubiquitin, the average ccs of the metallated protein ions with a given number of adducts is consistently smaller for metal ions with higher charge. Similar results were obtained for lysozyme 8+, α-lactalbumin 7+, and *holo*-myoglobin 9+ (drift profiles of these protein ion charge states with various extents of metal ion adduction and the fully protonated form are shown in Figure 9.5). These results indicate that nonspecific electrostatic interactions between the metal ion and protein result in more compact conformations of the metallated protein cations, that approach the most compact form of the protein in both the gas phase and solution.

9.3.3 Effect of Metal Ion Adducts and Protein Charge State on Conformation. The average ccs for fully protonated ions and ions with two Na^+, Ca^{2+}, or La^{3+} adducts for all charge states of ubiquitin and cytochrome *c* that are formed from aqueous solutions with and without each respective chloride salt are shown in Figure 9.6. The average ccs values for fully protonated ions formed from a denaturing solution for these charge states are within 8% of previously reported values[39] and are also shown for comparison. For all charge states, the metallated protein ions have smaller average ccs values than the fully protonated form with the same charge generated from either a purely aqueous or denaturing solution. Ubiquitin 6+ and cytochrome *c* 9+ ions with two metal ions attached have the greatest difference in ccs compared to the corresponding fully protonated form with the same charge state, with an approximately

14% and 16% smaller average ccs value with 2 La^{3+} ions adducted to these respective ions. The average ccs values of the protein ions with multivalent ions adducted are also a minimum of ~5% smaller than the fully protonated ion for other charge states of ubiquitin (5+, 7+ - 9+) and cytochrome *c* (7+, 8+, 10+, and 11+). In contrast, there is little difference (< 2%) between the average ccs of the fully protonated and metallated ions for the lowest charge states for both ubiquitin (4+) and cytochrome *c* (5+ and 6+).

High charge states of ubiquitin (8+ - 10+) and cytochrome *c* (9+ - 11+) are formed by ESI from aqueous solutions that contain 1.0 mM $CaCl_2$ or $LaCl_3$, and these charge states are not formed from the aqueous solutions without these salts. The 9+ and 10+ ubiquitin ions formed from the $LaCl_3$ solution have average ccs values that are at least 6% higher than the highest charge state (7+) formed from the purely aqueous solution, whereas ubiquitin 8+ with 2 La^{3+} or Ca^{2+} adducts have smaller average ccs values than $(ubiquitin + 7H)^{7+}$. The high charge state ions formed for cytochrome *c*, except for $(cytochrome\ c + 3H + 2Ca)^{9+}$, also have more than a 5% larger ccs than the highest charge state, $(cytochrome\ c + 8H)^{8+}$, formed from the water only solution. These results indicate that metal ion adduction to proteins during ESI can result in high charge state protein ions that can have more open conformations than the highest charge state formed from a purely aqueous solution, but all metallated ions are more compact than the fully protonated forms with the same charge generated from either aqueous or denaturing solutions. These high charge state metallated ions are advantageous because they dissociate more efficiently upon electron capture to provide significant sequence coverage even when these ions are formed from solutions in which the protein has a native structure.[46]

9.3.4 Cation Adduction to Protein Anions. Unlike results for protein cations, the presence of multivalent cations in an aqueous solution does not alter the anion charge states generated by ESI for α-lactalbumin, cytochrome *c*, and ubiquitin (data not shown), even though substantial metal ion adduction occurs. To determine how cation adduction affects protein anion conformation, drift time distributions were measured for these anions with various numbers of metal ions adducted. For both α-lactalbumin and cytochrome *c*, the metallated protein ions are more compact compared to the conformation of the non-metallated deprotonated ion for a given charge state with even more compact conformations observed for higher charge metal ions. For example, the drift profile of $(\alpha\text{-lactalbumin} + Ca - 9H)^{7-}$ and profiles for this ion with various extents of nonspecific Na^+, Ca^{2+}, and La^{3+} adducts are shown in Figure 9.7a. Drift times are not converted to collision cross sections because no calibrant ccs values for protein anions are available. There are two features for $(\alpha\text{-lactalbumin} + Ca - 9H)^{7-}$ with drift times of ~7.7 ms (I) and ~9.8 ms (II), and these profiles are identical for this ion formed from aqueous solutions with and without NaCl, $CaCl_2$ or $LaCl_3$. Feature I increases and II decreases in abundance with increasing numbers of metal ion adducts. For a given number of adducts, the relative abundance of feature I follows the trend $La^{3+} \geq Ca^{2+} \geq Na^+$. Similar results were also obtained for cation adduction to cytochrome *c* 6- (Figure 9.8). These results indicate that electrostatic interactions between metal ions and the protein can also stabilize compact conformers of gaseous protein anions. However, a more elongated conformation was observed for metallated ubiquitin 5- compared to the

non-metallated form (Figure 9.7b). There are two features in the drift profiles of ubiquitin 5- with drift times of ~7.5 ms (I) and ~9.2 ms (II). Adduction of just one La^{3+} ion results in feature II becoming the most abundant, and this feature also is the most abundant when the protein has adducted three Ca^{2+} or seven Na^{+} ions. These results indicate that nonspecific electrostatic interactions between the metal ion and the protein can stabilize more open conformations of the protein anion as well.

9.3.5 Specific Cation-Protein Interactions. For each protein and metal ion investigated here, nonspecific attachment of one or more metal ion results in more abundant compact forms of the protein cation. This indicates that a decrease in the ccs value upon specific metal ion binding may not necessarily indicate specific conformational changes have occurred in solution. However, an increase in the ccs value may be a more reliable indicator that such a change has occurred. This is illustrated with α-lactalbumin, which binds one Ca^{2+} specifically. An ESI mass spectrum of this protein from an aqueous solution containing 100 μM $CaCl_2$ results in an abundant ion corresponding to $(\alpha\text{-lactalbumin} + 5H + Ca)^{7+}$; only 2.4% of the total ion abundance of the 7+ charge state is the Ca^{2+}-free form (Figure 9.9a). The drift profile of $(\alpha\text{-lactalbumin} + 7H)^{7+}$ has an abundant feature with a ccs of ~1698 $Å^2$, and a low intensity feature at ~1990 $Å^2$. In striking contrast, the more elongated conformation at ~1990 $Å^2$ is the dominant feature for $(\alpha\text{-lactalbumin} + 5H + Ca)^{7+}$, and the more compact conformation at ~1698 $Å^2$ is significantly less abundant. *Apo*-α-lactalbumin exists in a molten globule state with a high degree of alpha-helical secondary content, and Ca^{2+} adduction to the molten globule form results in the folding and stabilization of the native structure of the protein.[48,49] The crystal structures of *holo*- and *apo*-α-lactalbumin forms indicate that the molten globule form has a ~5% smaller accessible surface area than the Ca^{2}-bound native form.[49] These results indicate that specific metal ion-protein interactions that result in an increase in the protein surface area in solution can result in a larger ccs in the gas phase. Because nonspecific metal ion adduction typically results in more compact gaseous cations, an increase in ccs values for protein ions that specifically bind a metal ion in solution may be a more reliable indicator of a specific conformational change that occurs in solution.

9.4 Conclusions

A reduction in the collisional cross section of a metal-bound gaseous protein ion upon specific binding of the metal to the protein has been used to infer a specific structural change to the protein has occurred in solution and that elements of this structure remain intact in the gas phase.[18,21] However, nonspecific metal ion binding to the proteins investigated here consistently results in a decrease in the collisional cross sections of the protein cations. Similar results are observed for metal adducted protein anions, but attachment of metal ions to some anions can result in more unfolded forms being preferentially stabilized. These results suggest that a decrease in the gas-phase collisional cross section of protein cations upon specific metal ion binding in solution may not be a reliable indicator of a specific conformational change that has occurred in solution and that is preserved in the gas phase. In contrast, nonspecific binding of metal ions rarely leads to more open forms of gaseous ions, and therefore, an increase

in collision cross section upon metal adduction may be a more reliable indicator of solution-phase conformational changes that occur upon specific metal ion binding in solution.

9.5 References

(1) Gray, H.B. and Winkler, J.R. *Annu. Rev. Biochem.* **1996**, *5*, 537-561.
(2) Browner, M.F.; Smith, W.W.; Castelhano, A.L. *Biochemistry* **1995**, *34*, 6602-6610.
(3) Klein, D.J.; Moore, P.B.; Steitz, T.A. *Publication of the RNA Society* **2004**, *10*, 1366-1379.
(4) Waldron, K.J. and Robinson, N.J. *Nat. Rev. Microbiol.* **2009**, *7*, 25-35.
(5) Andreini, C.; Bertini, I.; Rosato, A. *Bioinformatics* **2004**, *20*, 1373-1380.
(6) Antonini, E. *Physiol. Rev.* **1965**, *45*, 123-128.
(7) Crivici, A. and Ikura, M. *Ann. Rev. of Biophys. and Biomol. Struct.* **1995**, ***24***, 85-116.
(8) Ogawa, Y. *J. of Biochem.* **1985**, *97*, 1011-1023.
(9) Hardman, K.D.; Agarwal, R.C.; Freiser, M.J. *J. Mol. Biol.* **1982**, *157*, 69-86.
(10) Hasnain, S.S. and Hodgson, K.O. *J. Synch. Rad.* **1999**, *6*, 852-864.
(11) Braun, W.; Vasak, M.; Robbins, A.H.; Stout, C.D.; Wagner, G.; Kagi, J.H.R.; Wuthrich, K. *Proc. Natl. Acad. Sci. USA* **1992**, *89*, 10124-10128.
(12) Bertini, I.; Turano, P.; Vila, A.J. *Chem. Rev.* **1993**, *93*, 2833-2932.
(13) Pan, J.X. and Konermann, L. *Biochemistry* **2010**, *49*, 3477-3486.
(14) Veenstra, T.D.; Johnson, K.L.; Tomlinson, A.J.; Kumar, R.; Naylor, S. *Rapid Comm. in Mass Spectrom.* **1998**, *12*, 613-619.
(15) Nemirovskiy, O.; Giblin, D.E.; Gross, M.L. *J. Am. Soc. Mass Spectrom.* **1999**, *10*, 711-718.
(16) Zhu, M.M.; Rempel, D.L.; Zhao, J.; Giblin, D.E.; Gross, M.L. *Biochemistry* **2003**, *42*, 15388-15397.
(17) Novak, P.; Havlicek, V.; Derrick, P.J.; Beran, K.A.; Bashir, S.; Giannakopulos, A.E. *Eur. J. Mass Spectrom.* **2007**, *13*, 281-290.
(18) Ly, T. and Julian, R.R. *J. Am. Soc. Mass Spectrom.* **2008**, *19*, 1663-1672.
(19) Taraszka, J.A.; Li, J.W.; Clemmer, D.E. *J. Phys. Chem. B* **2000**, *104*, 4545-4551.
(20) Wyttenbach, T.; Grabenauer, M.; Thalassinos, K.; Scrivens, J.H.; Bowers, M.T. *J. Phys. Chem. B* **2010**, *114*, 437-447.
(21) Kohtani, M.; Jarrold, M.F.; Wee, S.; O'Hair, R.A.J. *J. Phys. Chem. B* **2004**, *108*, 6093-6097.
(22) Kohtani, M.; Kinnear, B.S.; Jarrold, M.F. *J. Am. Chem. Soc.* **2000**, *122*, 12377-12378.
(23) Seo, Y.J.; Schenauer, M.R.; Leary, J.A. *Int. J. Mass Spectrom.* **2011**, *303*, 191-198.
(24) Leavell, M.D.; Gaucher, S.P.; Leary, J.A.; Taraszka, J.A.; Clemmer, D.E. *J. Am. Soc. Mass Spectrom.* **2002**, *13*, 284-293.
(25) Prell, J.S.; Demireva, M.; Oomens, J.; Williams, E.R. *J. Am. Chem. Soc.* **2009**, *131*, 1232-1242.
(26) Prell, J.S.; Flick, T.G.; Oomens, J.; Berden, G.; Williams, E.R. *J. Phys. Chem. A* **2010**, *114*, 854-860.
(27) Rodgers, M.T. and Armentrout, P.B. *Acc. Chem. Research* **2004**, *37*, 989-998.

(28) Polfer, N.C.; Oomens, J.; Dunbar R.C. *Chem. Phys. Chem.* **2008**, *9*, 579-589.
(29) Ye, S.J. and Armentrout, P.B. *J. Phys. Chem. A* **2008**, *112*, 3587-3596.
(30) Loo, J.A.; Hu, P.; Smith, R.D. *J. Am. Soc. Mass Spectrom.* **1994**, *5*, 959-965.
(31) Wyttenbach, T.; von Helden, G.; Bowers, M.T. *J. Am. Chem. Soc.* **1996**, *118*, 8355-8364.
(32) Rodgers, M.T.; Armentrout, P.B.; Oomens, J.; Steill, J.D. *J. Phys. Chem A* **2008**, *112*, 2258-2267.
(33) Loo, J.A. *Int. J. Mass Spectrom.* **2000**, **200**, 175-186.
(34) Heck, A.J.R. and van den Heuvel, R.H.H. *Mass Spectrom. Rev.* **2004**, *23*, 368-389.
(35) Sterling, H.J.; Batchelor, J.D.; Wemmer, D.E.; Williams, E.R. *J. Am. Soc. Mass Spectrom.* **2010**, *21*, 1045-1049.
(36) Han, L.J.; Hyung, S.J.; Mayers, J.J.S.; Ruotolo, B.T. *J. Am. Chem. Soc.* **2011**, *133*, 11358-11367.
(37) Merenbloom, S.I.; Flick, T.G.; Daly, M.T.; Williams, E.R. *J. Am. Soc. Mass Spectrom.* **2011**, *22*, 1978-1990.
(38) Ruotolo, B.T.; Benesch, J.L.P.; Sandercock, A.M.; Hyung, S.J.; Robinson, C.V. *Nat. Prot.* **2008**, *3*, 1139-1152.
(39) Bush, M.F.; Hall, Z.; Giles, K.; Hoyes, J.; Robinson, C.V.; Ruotolo, B.T. *Anal. Chem.* **2010**, *82*, 9557-9565.
(40) Myung, S.; Badman, E.R.; Young Jin, L.; Clemmer, D.E. *J. of Phys. Chem. A* **2002**, *106*, 9976-9982.
(41) Hoaglund, C.S.; Valentine, S.J.; Sporleder, C.R.; Reilly, J.P.; Clemmer, D.E. *Anal. Chem.* **1998**, *70*, 2236-2242.
(42) Badman, E.R.; Hoaglund-Hyzer, C.S.; Clemmer, D.E. *Anal. Chem.* **2001**, *73*, 6000-6007.
(43) Bush, M.F.; Campuzano, I.D.G.; Robinson, C.V. *Anal. Chem.* **2012**, *84*, 7124-7130.
(44) Iavarone, A.T.; Udekwu, O.A.; Williams, E.R. *Anal. Chem.* **2004**, *76*, 3944-3950.
(45) Pan, P.; Gunawardena, H.P.; Xia, Y.; McLuckey, S.A. *Anal. Chem.* **2004**, *76*, 1165-1174.
(46) Flick, T.G.; Williams, E.R. *J. Am. Soc. Mass Spectrom.* **2012**, *23*, 1885-1895.
(47) Merenbloom, S.I.; Flick, T.G.; Williams, E.R. *J. Am. Soc. Mass Spectrom.* **2012**, *23*, 553-562.
(48) Griko, Y.V.; Remeta, D.P. *Protein Sci.* **1999**, *8*, 554-561.
(49) Chrysina, E.D.; Brew, K.; Acharya, K.R. *J. of Biol. Chem.* **2000**, *275*, 37021-37029.

9.6 Figures

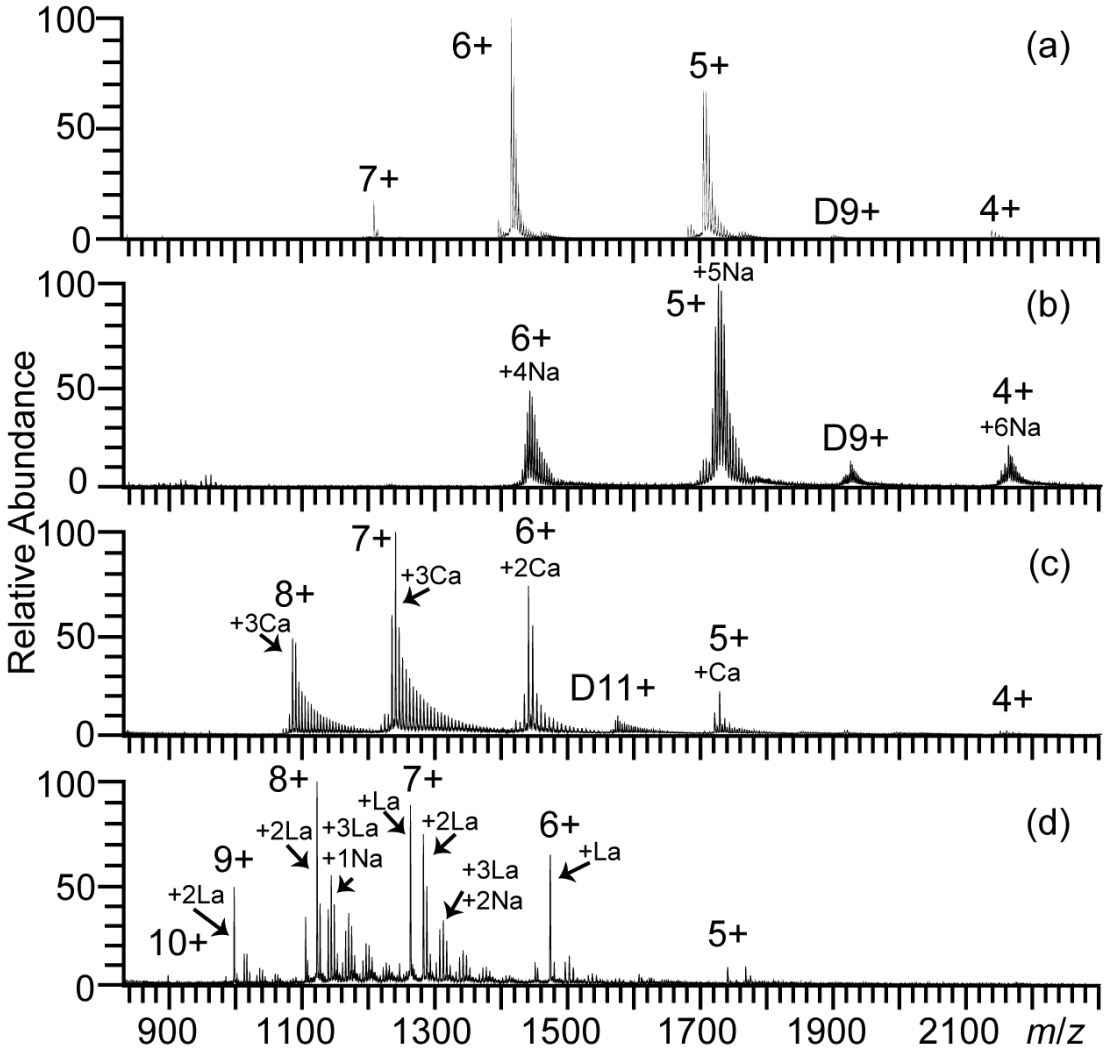

Figure 9.1. ESI mass spectra of aqueous solutions containing 10 μM ubiquitin in (a) pure water or aqueous solutions containing 1.0 mM (b) NaCl, (c) $CaCl_2$, or (d) $LaCl_3$.

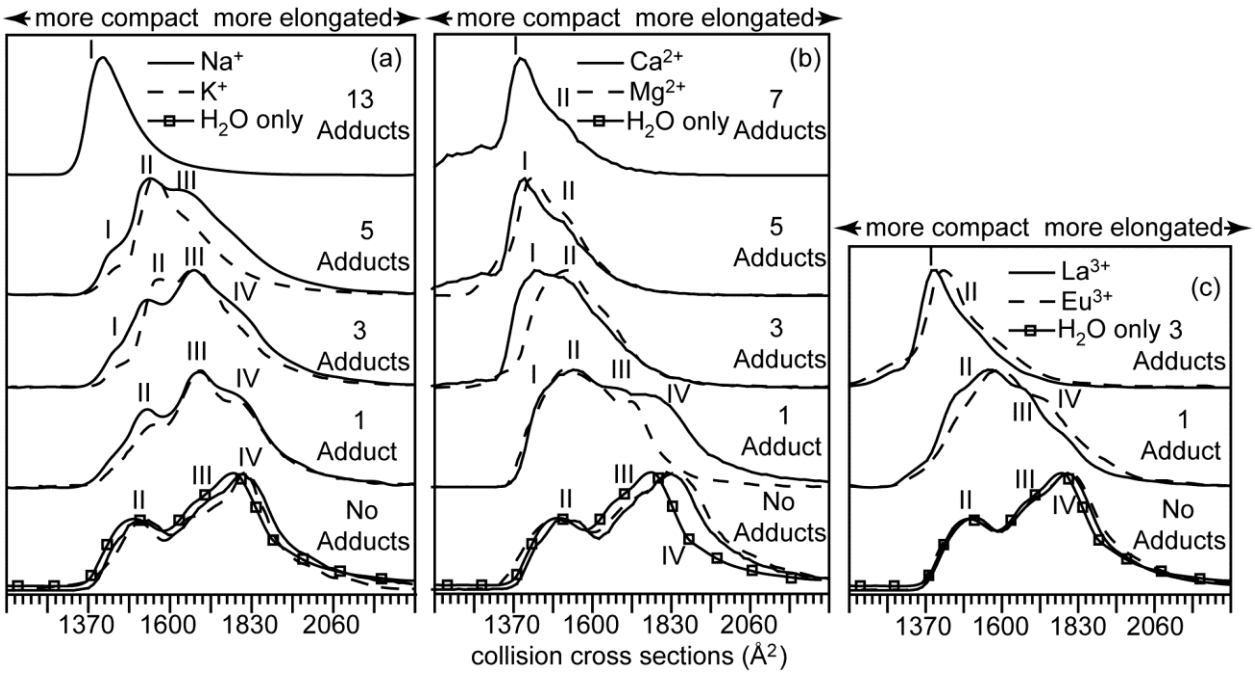

Figure 9.2. Drift profiles calibrated for collision cross sections in N_2 for fully protonated molecular ions and ions with various extents of metal ion adduction for ubiquitin 6+ formed from a purely aqueous solution (open squares) and aqueous solutions containing (a) 1.0 mM NaCl (solid line) or KCl (dashed line), (b) $CaCl_2$ (solid line) or $MgCl_2$ (dashed line), or (c) $LaCl_3$ (solid line) or $EuCl_3$ (dashed line).

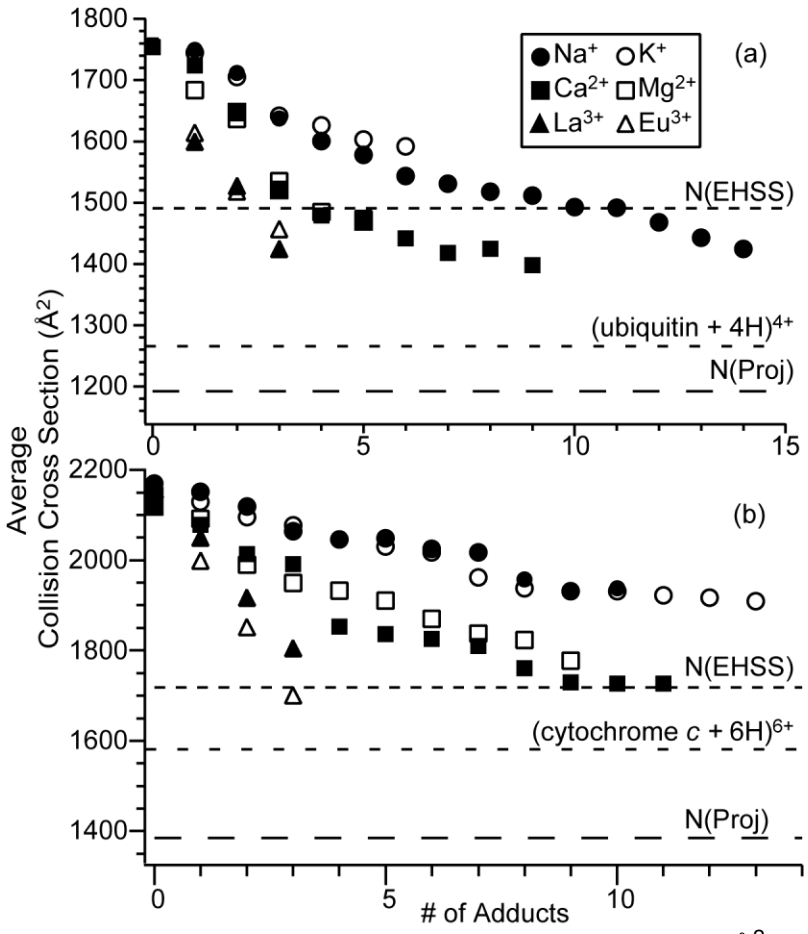

Figure 9.3. Average collision cross sections in N_2 (Å^2) for (a) ubiquitin 6+ and (b) cytochrome *c* 7+ as a function of the number of Na^+(●), K^+(○), Ca^{2+}(■), Mg^{2+}(□), La^{3+}(▲), or Eu^{3+}(△) adducts. N(EHSS) and N(Proj) are ccs values calculated by Clemmer and co-workers[40,42] for the native protein crystal structure using the projection method (Proj) and the exact hard-sphere scattering method (EHSS) for the native (N) conformations and converted for using N_2 as the drift gas.

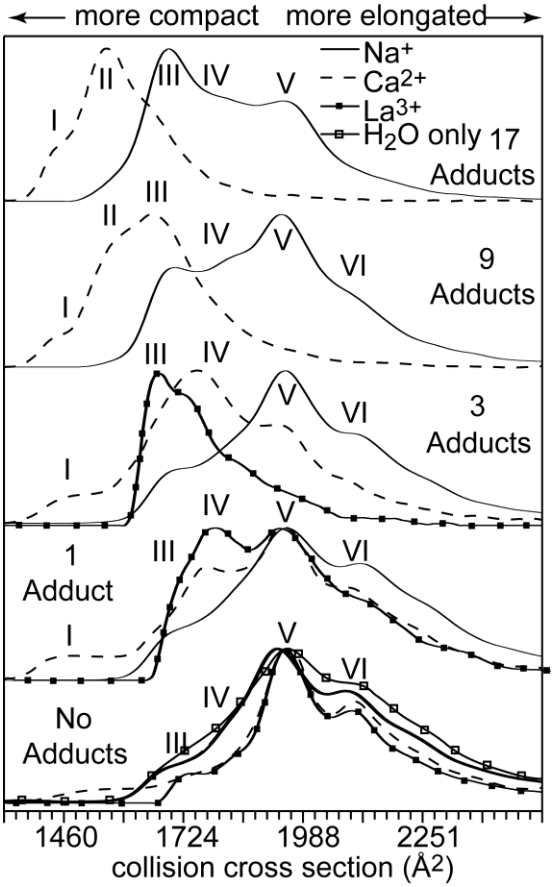

Figure 9.4. Drift profiles for fully protonated molecular ions and ions with various extents of metal ion adduction for cytochrome *c* 7+ formed from a purely aqueous solution (open squares) and aqueous solutions with 1 mM NaCl (solid line), $CaCl_2$ (dashed line), or $LaCl_3$ (solid squares).

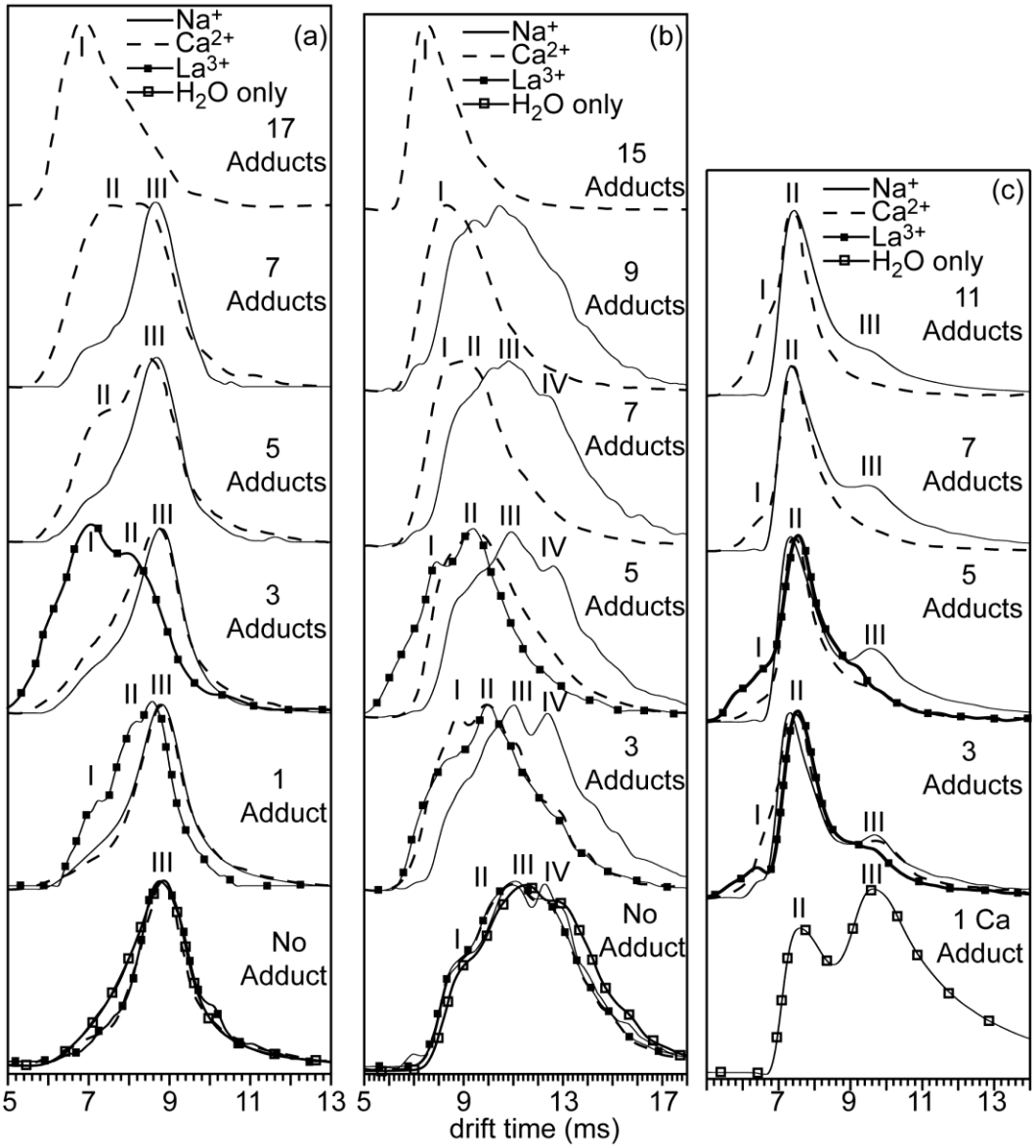

Figure 9.5. Drift profiles for fully protonated molecular ions and ions with various extents of metal ion adduction for (a) lysozyme 8+, (b) α-lactalbumin 7+, and (c) *holo*-myoglobin 9+ formed from a purely aqueous solution (open squares) and aqueous solutions with 1 mM NaCl (solid line), $CaCl_2$ (dashed line), or $LaCl_3$ (solid squares).

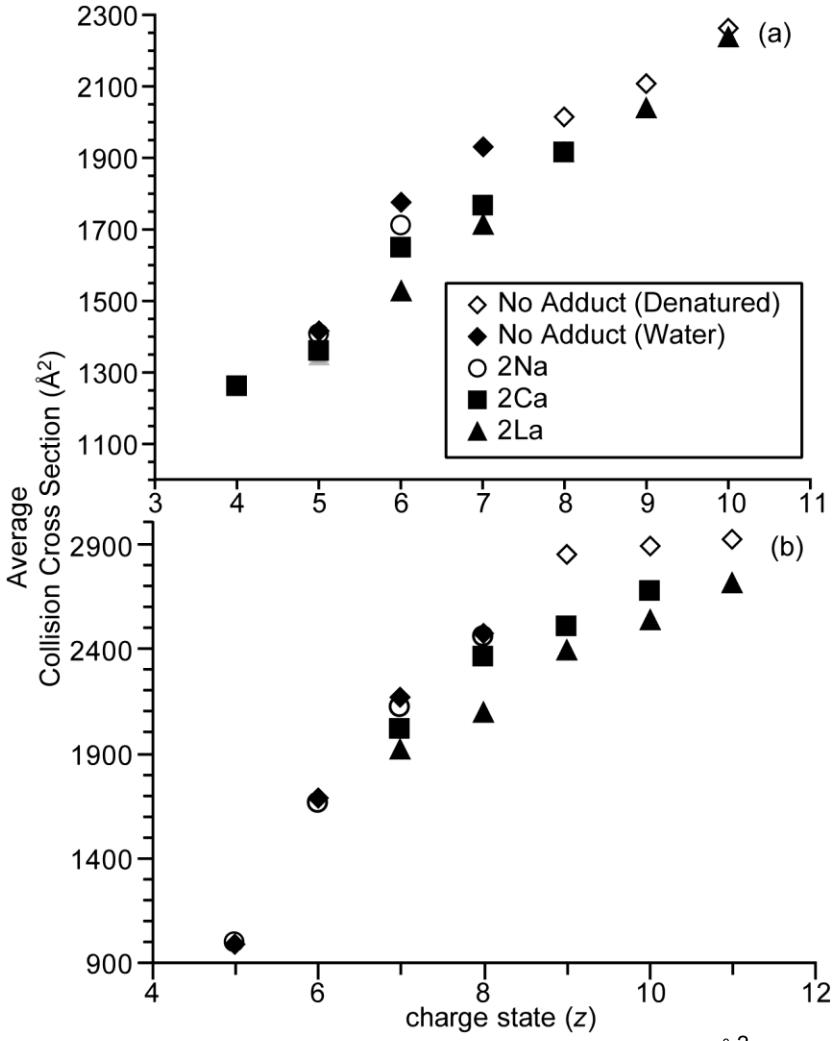

Figure 9.6. Average collision cross section in N_2 ($Å^2$) for the fully protonated molecular ions and ions with two Na^+, Ca^{2+}, or La^{3+} adducts for all charge states formed for (a) ubiquitin and (b) cytochrome *c* from aqueous solutions with and without the respective chloride salts. The average collision cross section of fully protonated molecular ions formed from denaturing solutions for these charge states are also shown for comparison.

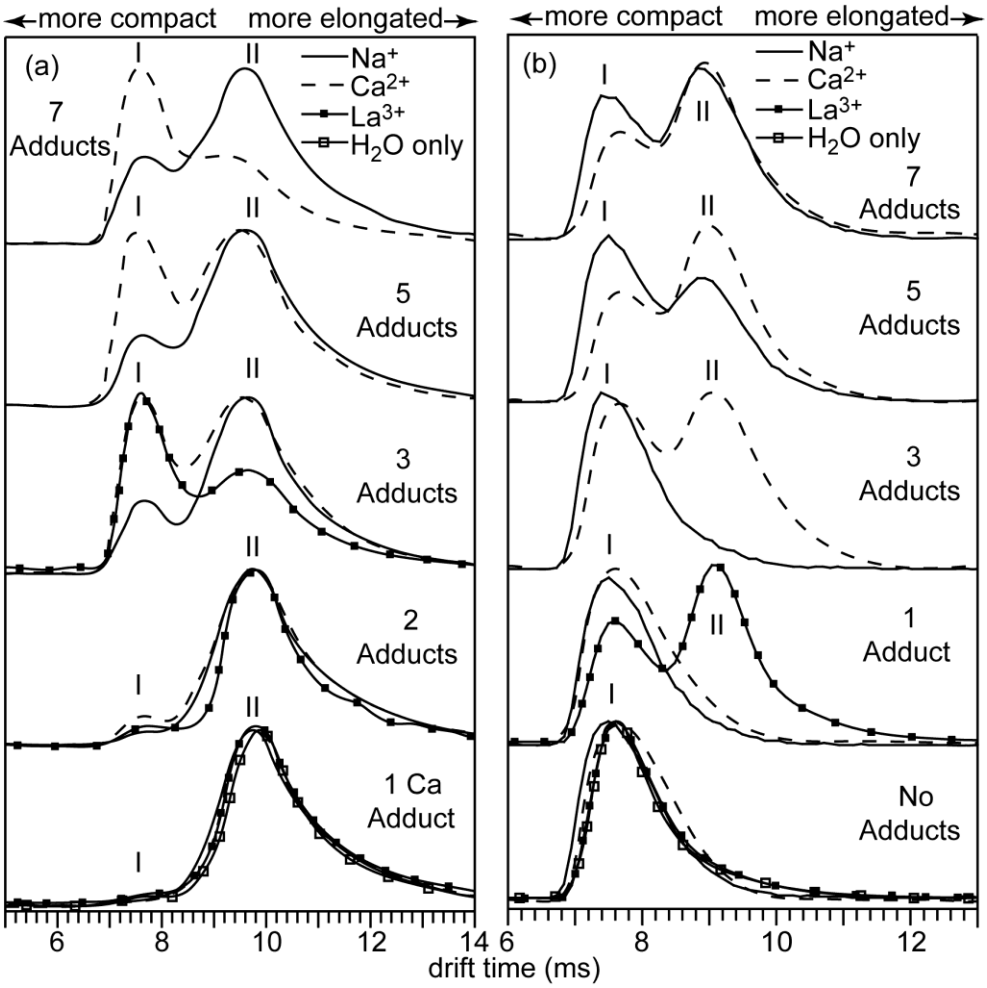

Figure 9.7. Drift profiles for fully protonated molecular ions and ions with various extents of metal ion adduction for (a) α-lactalbumin 7- and (c) ubiquitin 5- formed from a purely aqueous solution (open squares) and aqueous solutions with 1.0 mM NaCl (solid line), $CaCl_2$ (dashed line), or $LaCl_3$ (solid squares).

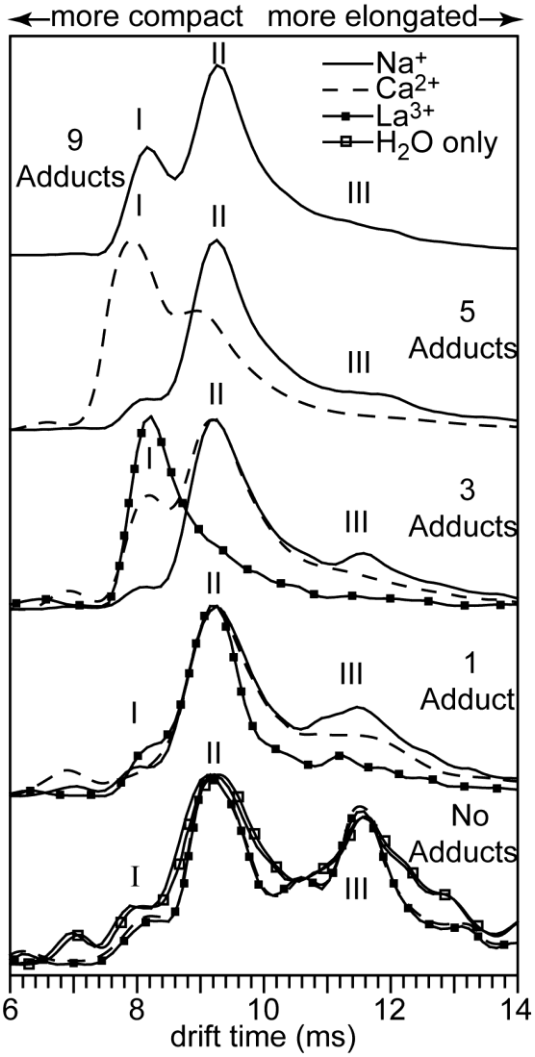

Figure 9.8. Drift profile for fully protonated molecular ions and ions with various extents of metal ion adduction for cytochrome *c* 6- formed from a purely aqueous solution (open squares) and aqueous solutions with 1 mM NaCl (solid line), $CaCl_2$ (dashed line), or $LaCl_3$ (solid squares).

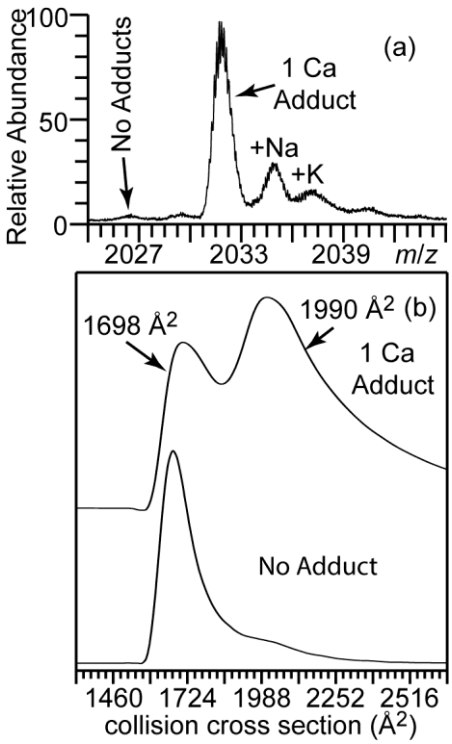

Figure 9.9. (a) Partial ESI positive ion mass spectrum from an aqueous solution containing 10 μM α-lactalbumin and 100 μM $CaCl_2$; (b) drift profiles in N_2 of α-lactalbumin 7+ with no adducts (bottom) and one Ca^{2+} adduct (top).